PROCESSING OF ELT SIGNALS FOR SEARCH AND RESCUE SATELLITE-AIDED TRACKING (SARSAT) USING THE MEM AND FFT

by

© AL-NASIR PREMJI, B.A.Sc.

A Thesis

Submitted to the Faculty of Graduate Studies

In Partial Fulfilment of the Requirements

for the Degree

Master of Engineering

McMaster University

March, 1982

PROCESSING OF SARSAT SIGNALS

MASTER OF ENGINEERING (1982)
(Electrical Engineering)

McMaster University
Hamilton, Ontario

TITLE: Processing of ELT Signals for Search and Rescue Satellite Aided Tracking (SARSAT) using the MEM and FFT.

AUTHOR: AL-NASIR PREMJI, B.A.Sc. (McMaster University)

SUPERVISOR: Dr. C.R. Carter
Department of Electrical and Computer Engineering

NUMBER OF PAGES: xvi, 175

ABSTRACT

The proposed methods of search and rescue (SAR) of mobile platforms use low altitude polar orbiting satellites to detect signals emanating from emergency locator transmitter (ELT) systems on board the distress platform. The uplink transmission receives a doppler shift due to the radial velocity of the satellite. Extracting the doppler from the signal is necessary for calculating the position of the ELT system. These ELT units were originally designed for reception by ordinary hand held receivers and detection by the human ear. For this reason the transmitters employ a distinct type of modulation often referred to as a chirp. Detection and estimation of the doppler by signal processing is complicated by this swept modulation. This dissertation compares two methods of spectral estimation, namely, Fourier analysis (in the form of an FFT algorithm) and the maximum entropy method (MEM) for application to ELT signals. The signals to be processed are divided into two categories, single and multiple signals. Multiple signal processing is necessary when two or more ELT systems are transmitting simultaneously and the time separation between transmissions is small enough to cause overlapping of signals in time. Results indicate that the enhanced detection capability by using the MEM offers a significant improvement in processing signals from an ELT.

ACKNOWLEDGEMENTS

It is with pleasure that I acknowledge the suggestions, contributions and encouragement of my supervisor, Dr. C.R. Carter, towards this thesis. I would also like to thank Dr. S. Kesler for discussions which aided my understanding of signal processing methods.

Finally, I would like to thank my fellow graduate students for debates which were both constructive and inspiring.

TABLE OF CONTENTS

TABLE OF CONTENTS (continued)

TABLE OF CONTENTS (continued) Page

LIST OF ILLUSTRATIONS

LIST OF ILLUSTRATIONS (continued)

LIST OF ILLUSTRATIONS (continued)

LIST OF ILLUSTRATIONS (continued) Page

LIST OF ILLUSTRATIONS (continued) Page

LIST OF ILLUSTRATIONS (continued) Page

LIST OF ILLUSTRATIONS (continued) Page

LIST OF ILLUSTRATIONS (continued) Page

LIST OF ILLUSTRATIONS (continued) Page

CHAPTER 1

INTRODUCTION

Research in Search and Rescue (SAR) has gained tremendous impetus in recent years. Countries presently actively involved in SAR research include Canada, the United States, France and Russia. This surge in interest was prompted by the cost of accidents in terms of loss of life and property. As an example, the American National Transportation Safety Board's (NTSB) figures for 1969 [1] indicate that reported marine and air accidents for that year reached a rate just under 50,000 per year and involved 170,000 people, 2,000 of whom were classified as saves (that is people who would have been fatalities if no rescue had been attempted). The figures for fatalities and seriously injured are 3,700 and 18,000, respectively. In a country such as Canada with vast remote expanses, the SAR problem becomes even more significant. Figure 1.1 [1] shows the probability of survival in a serious accident as a function of time to provide medical aid. Once again, the extreme weather conditions experienced in Canada lead to a reduction in the probability of survivial. From Fig. 1.1, it is evident that in order to improve the efficiency of the SAR program, the delay in rescue must be kept to a minimum.

This delay stems from two sources:

1) Excessive delay in alert notification or no notification at all.
2) Long search times caused by inaccurate position information.

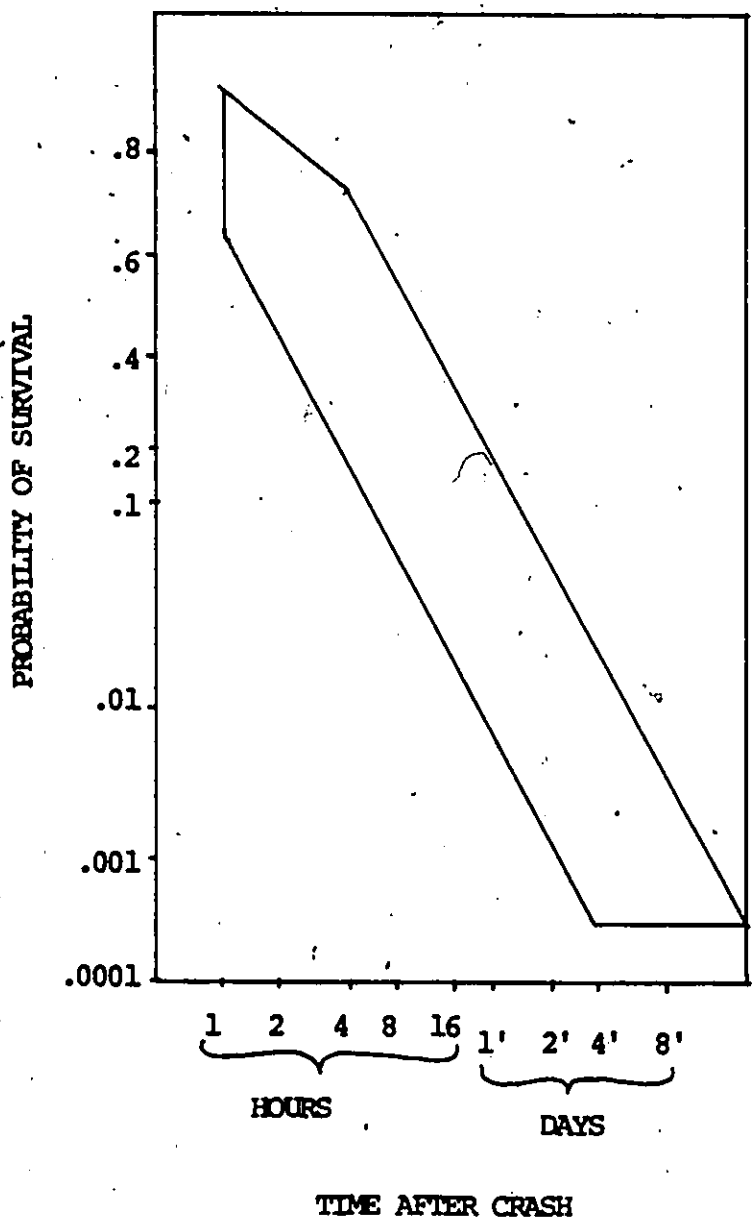

Fig. 1.1: Probability of survival in a serious accident as a function of time to provide medical aid.

In order to improve the chances of detection of a distress situation, Canadian regulations, as of January 1975, require every aircraft in Canada to carry an emergency locator transmitter (ELT) which emits a predefined signal in the event of an emergency. Currently the SAR program uses aircraft to detect the emergency signal. However, line of sight and terrain effects severely limit the range of reception of the ELT signal. For this reason the proposed SAR system incorporates dedicated low-altitude polar arbiting satellites (LAPOS) to provide coverage of the entire area of interest.

The proposed SAR system, scheduled to be deployed in June 1982, is shown in Fig. 1.2 [2,3]. As the satellite orbits the earth, it sweeps out paths over the region of interest. A repeater on board the satellite relays the ELT signals to a ground station. Lack of facilities for storage of data at the satellite requires that both ELT and ground station be visible to the satellite simultaneously. Although this limits coverage to areas of radius approximately 1000 km around the earth stations, it provides adequate local coverage. An updated system will incorporate storage facilities on board the satellite that will allow complete earth coverage, even over areas where no earth station is visible. At the ground station the received signal is processed to extract information regarding the location of the platform in distress. Once an estimate of the crash position is available, the SAR forces are deployed to the location to carry out the rescue.

The accuracy of the estimated position is largely dependent on the method used for processing the ELT signals. These signals consist of a

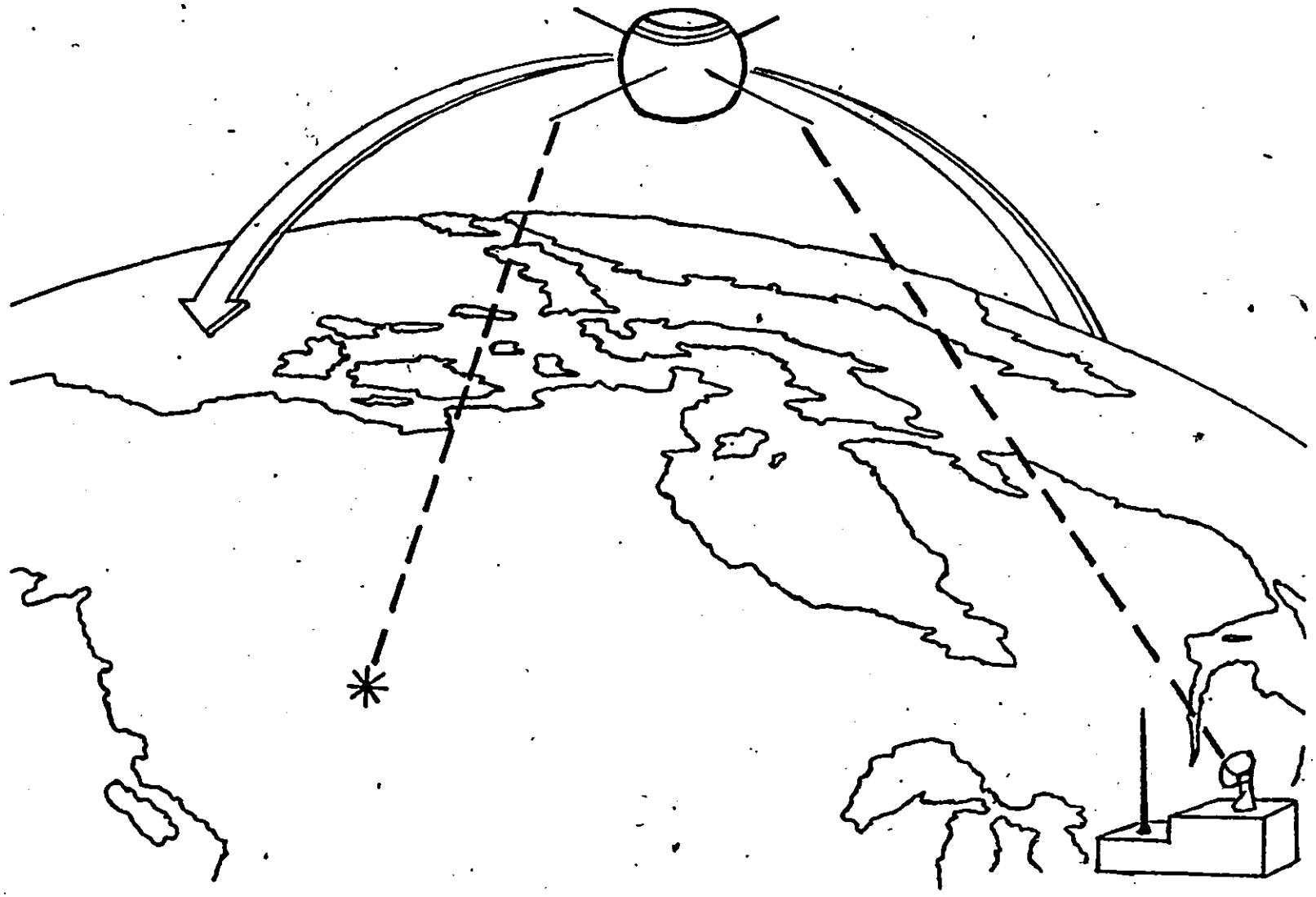

Fig. 1.2: Proposed SARSAT system.

continuous wave modulated by a swept audio tone. Figures 1.3 and 1.4 show 25 ms of two typical kinds of transmitted signals (employing square and sinusoidal modulating signals, respectively). At present, the received signals are processed using Fourier analysis in the form of the Fast Fourier transform algorithm. Some of the problems associated with the FFT, which are discussed in Chapter 3, lead to difficulties in the processing of these signals. It is with these problems in mind that we look to the Maximum Entropy Method (MEM) which may offer considerable improvements.

1.1 The ELT Signal

The ELT signal comprises a carrier modulated by a time function. This time function or modulating term can be sinusoidal or square with a period (1/f(t)) that increases with time. A signal of the form of the modulating term is often referred to as a chirp. The frequency f(t) is within the audio range allowing for reception of the signal on an ordinary communications receiver for detection by the human ear. It is also intended that the signal be suitable for homing by standard direction finding techniques. However, the ELT's have a fairly low radiating power, of the order of 100 mW, and poor spectral characteristics, i.e. the carrier component is not very well defined. It is these confining characteristics that make current signal processing techniques quite inadequate for detection of the ELT signal. Furthermore, as we shall show in Chapter 2, the diversity of signal formats used by different manufacturers makes matched filtering or

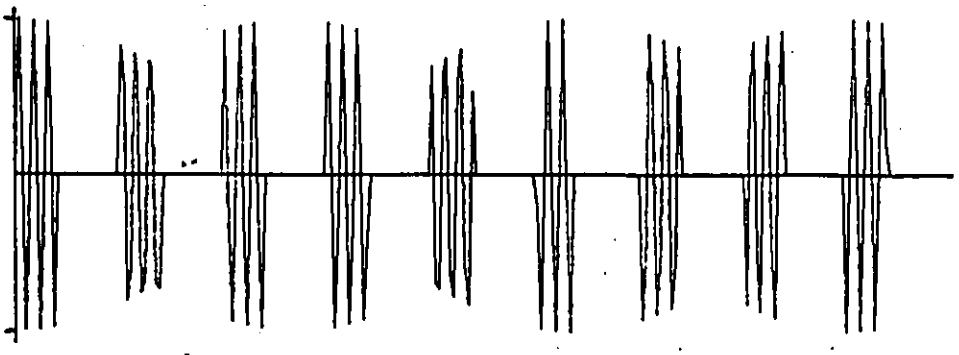

Fig. 1.3: 25 ms of a typical ELT signal employing square modulation.

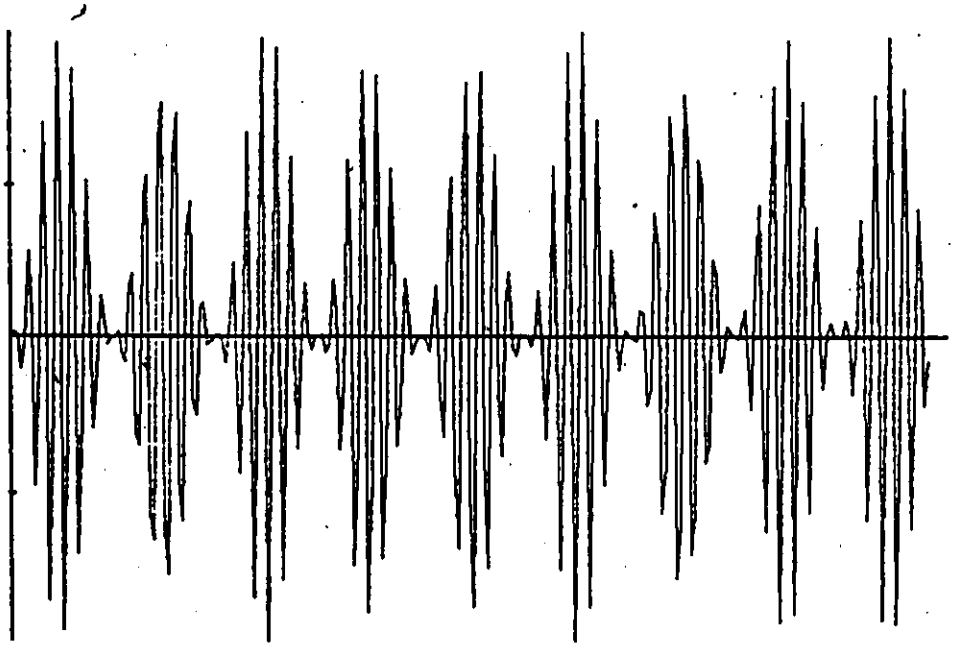

Fig. 1.4: 25 ms of a typical ELT signal employing sinusoidal modulation.

replica correlating very complex and expensive since each signal, would require a separate bank of matched filters. Another problem that appears to be a major one is the frequency drift associated with the oscillator in the ELT. This would result in an unknown bias in the doppler estimate if the oscillator frequency is assumed to be stable. As will be shown in the next section, this can be counteracted by extracting information from the doppler curve using a form of steepest slope measurement rather than an absolute zero-doppler frequency measurement.

1.2 The Doppler-Curve

The estimate of ELT position is based on information extracted from the doppler-time curve in conjunction with the spacecraft ephemeris. Movement of the satellite over the face of the earth affects a change in the radial velocity along the line joining the satellite and the ELT as shown in Fig. 1.5. This velocity varies from a positive value as the distance between satellite and ELT decreases, though a point of zero velocity when the velocity vector is perpendicular to the radial line, to a negative value as the satellite moves away where we have assumed direction toward the ELT to be positive. The radial velocity has an effect of introducing a doppler-shift to the ELT signal as received by the satellite. Equation 1.1 gives this doppler-frequency as a function of carrier frequency and doppler velocity.

$$f_d = \frac{v_r}{c} f_c \qquad (1.1)$$

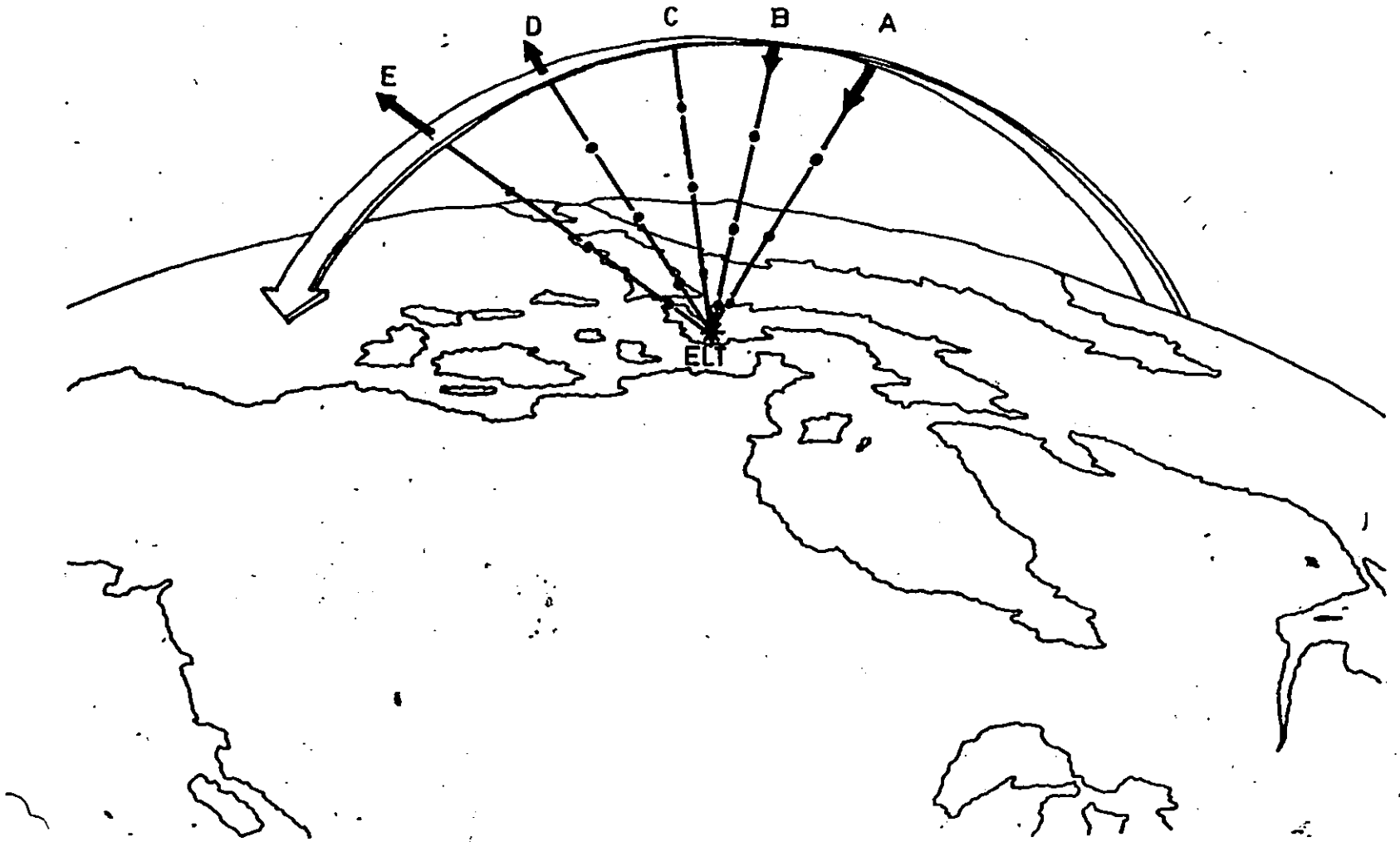

Fig. 1.5: Movement of the satellite over the face of the earth causes a change in radial velocity along the line joining satellite and ELT.

where

f_d = doppler frequency,

f_c = carrier frequency,

v_r = radial velocity, and

c = speed of light.

A plot of doppler versus time yields a curve of the shape shown by curve A of Fig. 1.6. However, this assumes the ideal situation of a stable oscillator in the ELT. In practice, the oscillators suffer a long term frequency drift. Because the effect is long term it merely causes the doppler curve to be shifted up or down (biased) as in curves B and C. In the curve fitting procedure, the bias appears as a constant term. By dropping this constant term the oscillator instability can be compensated. The resulting doppler-time curve is unique to a particular ELT position, with the point of maximum negative slope indicating the time at which the satellite is closest to the transmitter. If the spacecraft ephemeris is known, this position can be calculated. Assuming an accurate satellite orbit model, the accuracy of the estimated position is mainly dependent on the accuracy of the estimated doppler and hence on the choice of signal processing method.

1.3 Scope of Thesis

As explained, the choice of a suitable method of signal processing is of paramount importance to obtaining an accurate doppler estimate. At present, the processing is performed using Fourier analysis in the form of the Fast Fourier Transform (FFT). A method that appears to

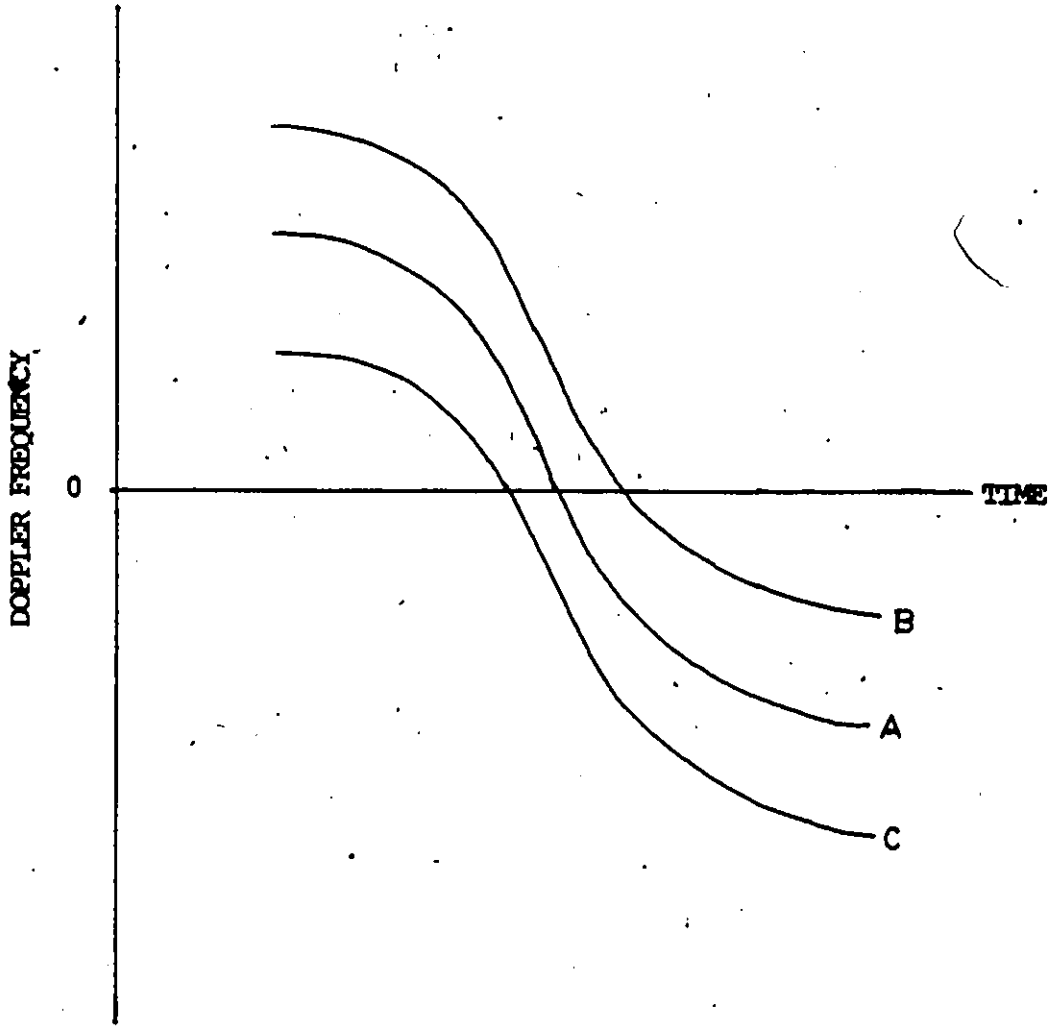

Fig. 1.6: Doppler versus time curves showing the effect of long term frequency drift in the oscillator.

offer better results is the Maximum Entropy Method (MEM) [4-7]. This method adapts itself to the input data. Since the signal can be any one of the many possibilities, a method such as the MEM can offer significant advantages.

A detailed description of the ELT signal together with noise considerations and signal to noise ratio definitions is presented in Chapter 2. Chapter 3 discusses various methods of signal processing including the MEM and the FFT. Advantages and problems with each method are discussed. Results of the computer simulation for single and multiple signals are presented in Chapters 4 and 5, respectively. A thorough comparison is made of the results for the MEM and the FFT.

Finally, Chapter 6 provides conclusions and indicates possible areas of further research relevant to the material in this thesis.

CHAPTER 2

THE RECEIVED ELT SIGNAL

In this Chapter we present a thorough description of the ELT signals including noise considerations and signal to noise ratio (SNR) definitions. The ELT signals considered are the 121.5/243 MHz type. A new type of ELT which transmits a burst of a continuous wave followed by additional information phase modulated onto the 406 MHz carrier is discussed toward the end of the Chapter. This ELT which is still in the experimental stages should offer many advantages over existing ELT's.

2.1 The ELT and its Transmission

Before explaining the ELT structure we consider a mathemtical representation of the transmitted signals. These signals are amplitude modulated signals of the form of eq. (2.1)

$$S(t) = A_c[1 + m(t)] \sin \omega_c t \qquad (2.1)$$

where A_c, the peak value of the carrier, can be assumed to be unity, $m(t)$ is the modulating signal and ω_c is the carrier frequency in radians per second. $S(t)$ can be divided into two categories according to the modulation, $m(t)$, which can be square or sinusoidal. Consider first the case of a sinusoidal modulation which can be written as [8]

$$m(t) = \mu \sin[\theta_i(t)] \qquad (2.2)$$

where the modulation factor μ has a value bounded by $0.85 \leq \mu \leq 1.0$ and $\theta_i(t)$ is given by

$$\theta_i(t) = 2\pi \int f_i(t)\, dt \tag{2.3}$$

The instantaneous frequency $f_i(t)$ can be a linear or quadratic function of time. Examples of each kind of sweep are given by eqs. (2.4) and (2.5), [2,9],

$$f_i(t) = 1400.0 - 700.0 \frac{t}{T_r} \tag{2.4}$$

$$f_i(t) = 1930.8 - 1784.8 \frac{t}{T_r} + 870.82 \frac{t^2}{T_r^2} \tag{2.5}$$

where T_r is the repetition time such that the sweep is modulo T_r

$$f_i(t) = f_i(t + nT_r) \quad n \text{ is an integer} \tag{2.6}$$

Typically this repetition time is in the region of a quarter of a second. Figure 1.3 shows 25 ms of an ELT signal of the form of eq. (2.1) with a sinusoidal modulation given by eqs. (2.2), (2.3) and (2.4). In this particular case the modulation factor is 1.0 and T_r is 0.25 s. Generation of such a signal involves the use of standard amplitude modulation techniques namely the square-law modulator or the switching modulator followed by suitable filters to remove unwanted components. These methods are well documented in the literature [8] and will not be detailed here.

Another type of signal, that is more popular because of the simplicity with which it can be generated, results by modulating a carrier with a string of pulses of durations that vary with time. As before, the signal is given by eq. (2.1) except that its modulation, m(t), now takes the form of Fig. 2.1. In order to define m(t) we need to specify the rising and falling edges of the pulses (times t_j and p_j

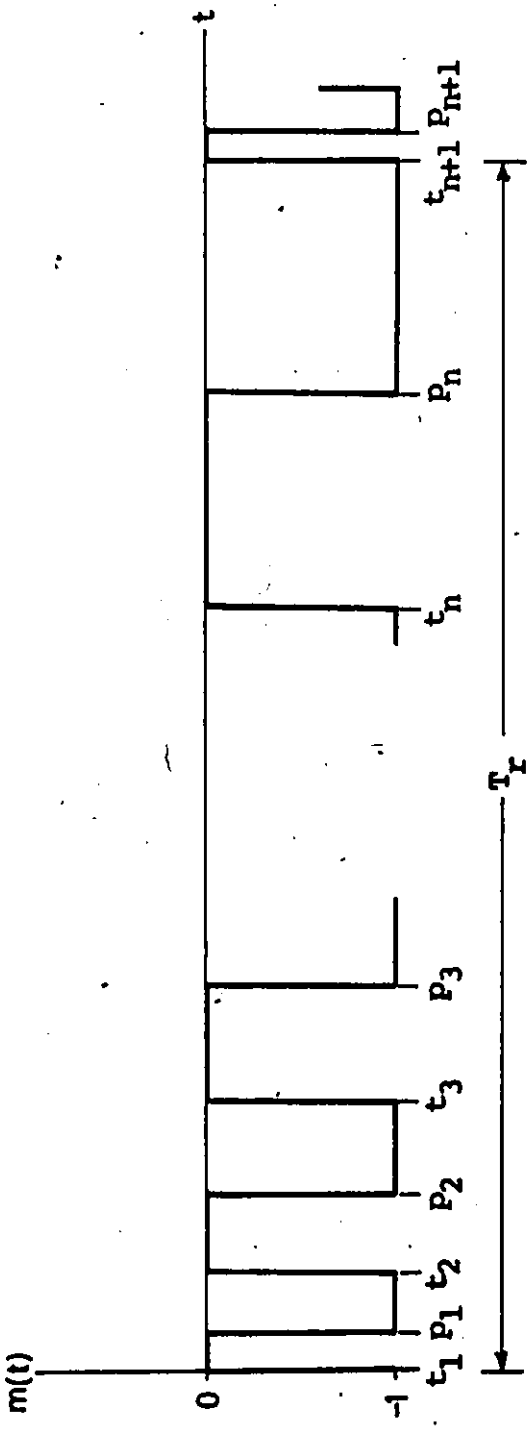

Fig. 2.1: A square modulation showing the increase in pulse duration with time.

respectively). These transition times ane calculated by solving the equations

$$\int_0^{t_j} f_i(t)\, dt = j-1 \tag{2.7}$$

$$\int_0^{p_j} f_i(t)\, dt = j-1+d \tag{2.8}$$

where the index j refers to the j^{th} pulse and the duty cycle d is restricted to the interval $0.3 \leq d \leq 0.5$. We note that repetition of the sweep frequency, as indicated by eq. (2.6), implies that the j^{th} pulse is identical to the $(j+k)^{th}$ pulse where k is the number of pulses in the time interval T_r. The nature of this signal can be better comprehended by an illustration. Figure 1.4 depicts 25 ms of a signal resulting from pulse modulating a carrier using a linear frequency sweep, eq. (2.4), and a duty cycle of 0.36. An ELT suitable for generating this type of signal is shown in Fig. 2.2 [9], where the frequency sweep and the repetition time are dependent on the sweep oscillator. The multivibrator output consists of a series of pulses as in Fig. 2.1. This output is applied to an amplifier, turning it on and off (much like on-off keying), to gate the carrier to the power amplifier. It is this gating that gives rise to the required signal.

A slight variation of this type of ELT is also available on the market. The signal emanating from this ELT is best described with reference to the diagram for the 121.5 MHz ELT using pulse modulation. In Fig. 2.2 if the output from the audio section is used to turn the oscillator on and off, rather than using it to gate the oscillator to

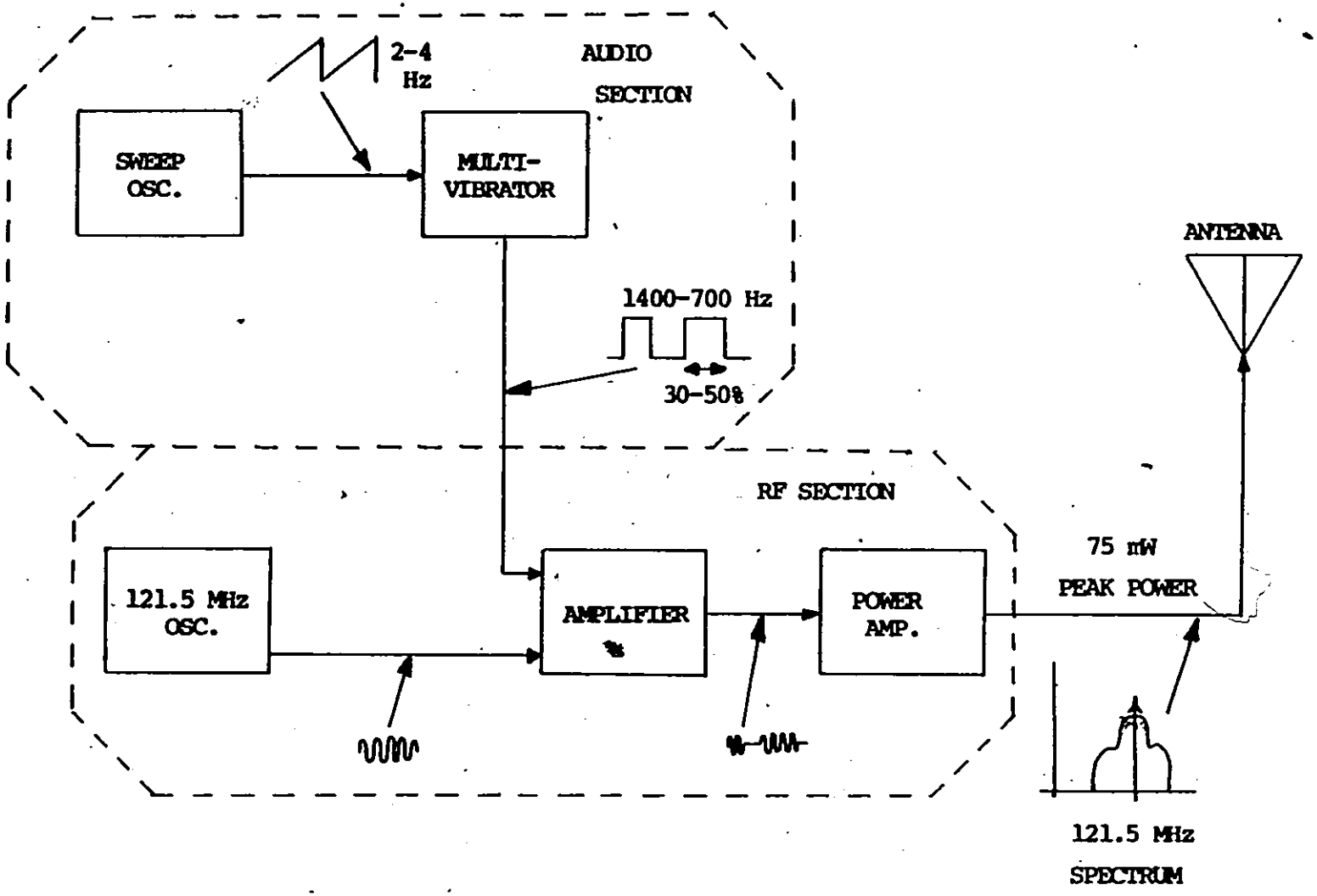

Fig. 2.2: Existing 121.5 MHz ELT employing square modulation.

the power amplifier, the phase at each time t_i will take on some arbitrary value. In our model for such a "phase randomized signal" we shall assume that the phase at time t_i is a uniform random variable distributed on $[0,2\pi]$.

We stated in Chapter 1 that these signals were designed for reception by ordinary communications receivers employing detection by the human ear. In view of this, modulation of the carrier using a swept audio frequency is ideal because of its unique sound. However, the sweep tends to complicate detection of the carrier, which contains doppler information, by spectral analysis because it has an effect of smearing the spectrum. In an effort to combat this situation where the signal is rather ill suited for processing methods a new type of ELT is being developed. Its continuous wave format and higher output power result in a well defined carrier. Section 2.3 presents an outline of such a transmitter. Thus far, no mention has been made of the signal received by the satellite which consists of the ELT signal corrupted by noise. In the next section, consideration is given to the effect of noise on the signal with the intension of formulating a definition for the signal to noise ratio (SNR).

2.2 Noise Considerations

The received signal can be written as a sum of the ELT signal and noise. Sources of noise include atmospheric noise and receiver noise. These random processes can be lumped together and the received signal written as

$$y(t) = S_d(t) + n(t) \tag{2.9}$$

where $S_d(t)$ is the doppler shifted ELT signal, n(t) is the combined noise process and y(t) is the received signal. In order to simulate the signal y(t), we define n(t) in a statistical sense. A random variable that models n(t) quite adequately is the Gaussian random variable. For this reason, the computer simulation of the received signal combines samples of the doppler shifted ELT signal and Gaussian noise. To measure the performance of the signal processor at various noise levels we define a ratio of the signal power to noise power (SNR).

$$SNR = P_s/\sigma^2 \tag{2.10}$$

where the noise power is equal to the variance (σ^2) of the Gaussian process and P_s is the signal power. Calculation of P_s involves making various approximations which are outlined below.

We consider the case of a square modulating signal first because of the simplicity with which its power can be calculated. In general, P_s is given by

$$P_s = \frac{1}{T_r} \int_0^{T_r} S_d^2(t)\, dt \tag{2.11}$$

where the power is calculated over the duration of a complete sweep (T_r). Before processing, the received signal is mixed down to some intermediate frequency (IF) and bandlimited. Assuming the filter bandwidth is sufficiently larger then the IF, the filtering operation will have negligible distorting effects on the signal. Using eqs. 2.1, 2.7, 2.8 and Fig. 2.1, we can write eq. 2.11 as

$$P_s = \frac{A_c^2}{2T_r} \sum_{i=1}^{n} \left[t - \frac{1}{2\omega_1} \sin(2\omega_1 t)\right]_{t_i}^{p_i} \qquad (2.12)$$

where ω_1 is the sum of the IF and the doppler frequency. Depending on the frequency sweep used, the number of pulses can be as large as 341. Since the doppler frequency can take on any value within a band approximately 6 KHz wide and signal power has to be recalculated each time the program is run. An approximation that leads to an acceptable degree of accuracy involves calculating the power using

$$P_s \approx \frac{A_c^2}{2T_r} \sum_{i=1}^{n} (p_i - t_i) \qquad (2.13)$$

where we have used the fact that the terms arising from the sinusoidal function of eq. (2.12) are small in comparison with $(p_i - t_i)$ and indeed a great number of the sinusoidal terms will cancel each other. Moreover, using the approximation

$$\sum_{i=1}^{n} (p_i - t_i) \approx dT_r \qquad (2.14)$$

where d is the duty cycle, we can write the power as

$$P_s \approx \frac{1}{2} A_c^2 d \qquad (2.15)$$

We now have a very simple expression which approximates the power quite adequately.

For a sinusoidal modulation with a linear frequency sweep the signal can be represented as

$$S_d(t) = A_c [1 + \mu \sin(\theta_i(t))] \sin \omega_1 t \qquad (2.16)$$

Integration of the square of this function is rather cumbersome, we

therefore resort to an approximation technique. Since the IF is a factor of ten greater than the average frequency of the modulation, the signal power can be approximated as half the power in the envelope, i.e.

$$P_s \propto \frac{1}{2}\frac{A_c^2}{T_r}\int_0^{T_r} [1 + \mu \sin(\theta_i(t))]\, dt \tag{2.17}$$

where

$$\theta_i(t) = 2\pi(-1400\, t^2 + 1400\, t + 0.75) \tag{2.18}$$

This instantaneous phase is found using eqs. (2.3) and (2.4) together with the initial condition

$[1 + \mu \sin(\theta_i(t))]$ a minimum at $t = 0$

The expression for P_s is found to be

$$P_s = \frac{1}{2T_r}\{[A_c^2 t + \frac{1}{2}\mu^2 A_c^2 t]_0^{T_r} + 2\mu A_c^2 \int_0^{T_r} \sin\theta_i(t)\, dt - \frac{1}{2}\mu^2 A_c^2 \int_0^{T_r} \cos[2\theta_i(t)]\, dt\} \tag{2.19}$$

Let the instantaneous phase be given by

$$\theta_i(t) = -at^2 + bt + c \tag{2.20}$$

Then the integrals of eq. (2.19) can be written

$$I_1 = \int_0^{T_r} \sin\theta_i(t)\, dt = \mathrm{Im}\left[\int_0^{T_r} \exp(-j\,[-\theta_i(t)])\, dt\right] \tag{2.21}$$

$$I_2 = \int_0^{T_r} \cos[2\theta_i(t)]dt = \mathrm{Re}\left[\int_0^{T_r} \exp(-j\,[-2\theta_i(t)])\, dt\right] \tag{2.22}$$

By completing the square of the quadratic function in the exponentials and performing a change of variable, we can write I_1 and I_2 in terms of

the Fresnal integrals

$$\int \cos(\tfrac{\pi}{2} z^2)\, dz \quad \text{and} \quad \int \sin(\tfrac{\pi}{2} z^2)\, dz$$

which are adequately tabulated [10]. Using the values of a, b and c in eq. (2.18) and $T_r = 0.25$ s the power is found to be

$$P_s \approx \frac{1}{2} A_c^2 + \frac{1}{4} \mu^2 A_c^2 + 4 \mu A_c^2 I_1 - \mu^2 A_c^2 I_2 \tag{2.23}$$

where

$$I_1 = 4.3056801 \times 10^{-7} \qquad I_2 = -5.8011508 \times 10^{-8}$$

A quadratic frequency sweep (eq. (2.5)) leads to an even more complex integration when we try to find the power. Terms appearing in the integration include sines and cosines with cubic arguments. It would seem that the best way to tackle such an integration is to use a numerical technique. However, an approximation that at first sight appears to be rather coarse but yields a good degree of accuracy involves using the two most significant terms

$$P_s \approx \frac{1}{2} A_c^2 + \frac{1}{4} \mu^2 A_c^2 \tag{2.24}$$

Comparing this estimate with a method using Simpson's formula indicates that the discrepancy is less than one percent. It is quite apparent that eq. (2.24) is adequate for our purposes and as such it will henceforth be used to estimate the power of a signal utilizing a sinusoidal modulation with a quadratic frequency sweep. As an illustration of our definition of SNR, the signals of Figs. 1.3 and 1.4 are plotted in Figs. 2.3 and 2.4 for a signal to noise ratio of 10 dB.

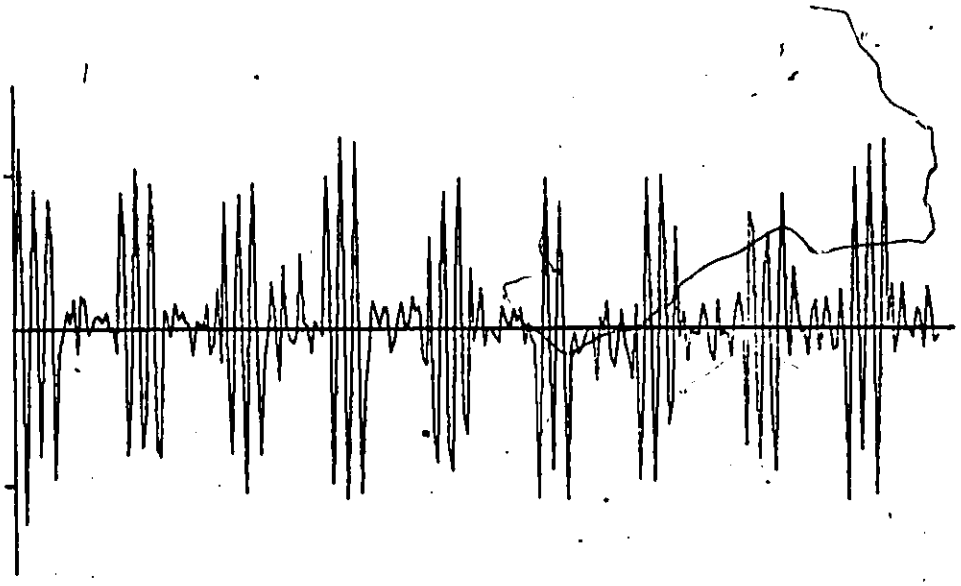

Fig. 2.3: 25 ms of a typical ELT signal employing square modulation at an SNR of 10 dB.

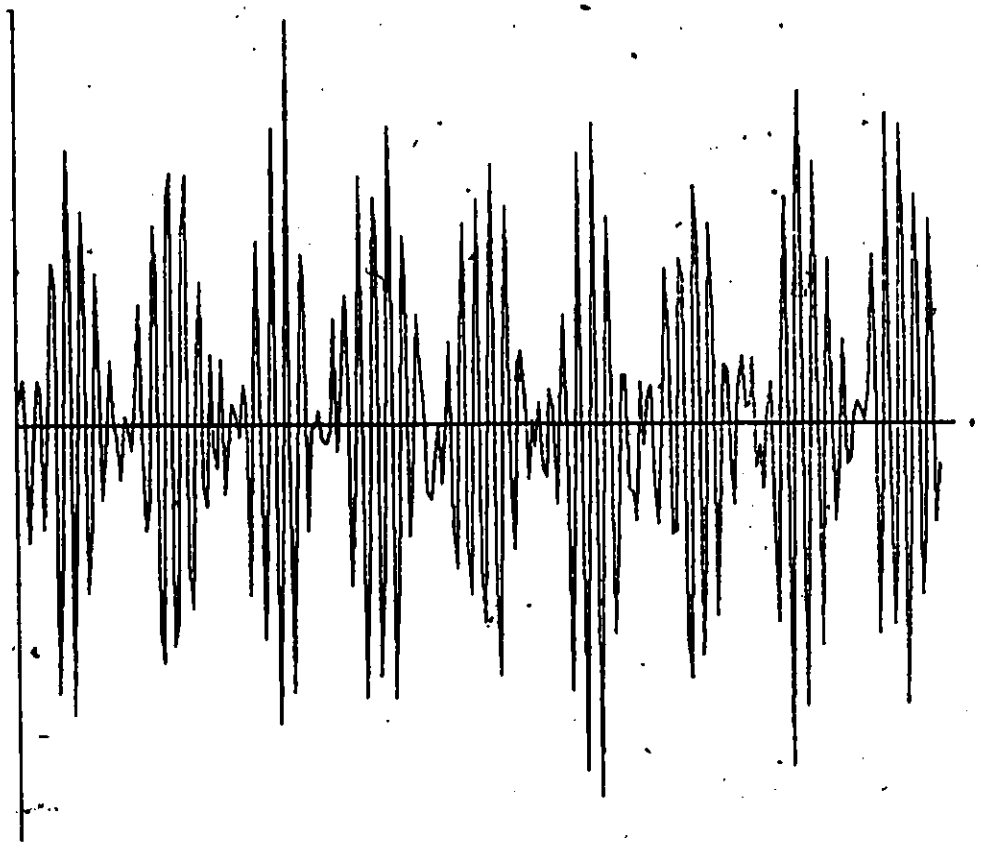

Fig. 2.4: 25 ms of a typical ELT signal employing sinusoidal modulation at an SNR of 10 dB.

We thus have a means of specifying the signal power for any one of the signals we will be considering. Using the appropriate equation for signal power and generating noise samples with required variance, eq. (2.10) can be used to specify the signal to noise ratio.

2.3 The 406 MHz ELT

Signals from the 121.5 and 243 MHz ELT's result in a spectrum that has a rather ill-defined carrier component. In order to overcome this problem, a new type of ELT is being developed which transmits at 406 MHz. Fig. 2.5 [9] shows the structure of such an ELT. The 406 MHz signals from this transmitter are 440 ms in duration and have a repetition time of 50 seconds. In between these signals the ELT transmits 121.5 or 243 MHz signals so that aircraft with detection equipment used at present can still aid in the final stages of the rescue. A description of the 406 MHz signal format is given in Fig. 2.6 [9]. An optional long message format provides 32 additional bits of data. From the short message format we see that the signal can be divided into two parts: the continuous wave (CW) preamble and the modulated message following it. The CW preamble is at a frequency of 406 MHz and has a duration of 160 ms. At the receiver it is this preamble that is processed to extract the doppler frequency. Information related to the distress situation is digitally encoded using bi-phase L encoding and then phase modulated onto the carrier to give the digital message which has a duration of 280 ms. It is intended that the 406 MHz signals be processed on board the spacecraft, time tagged

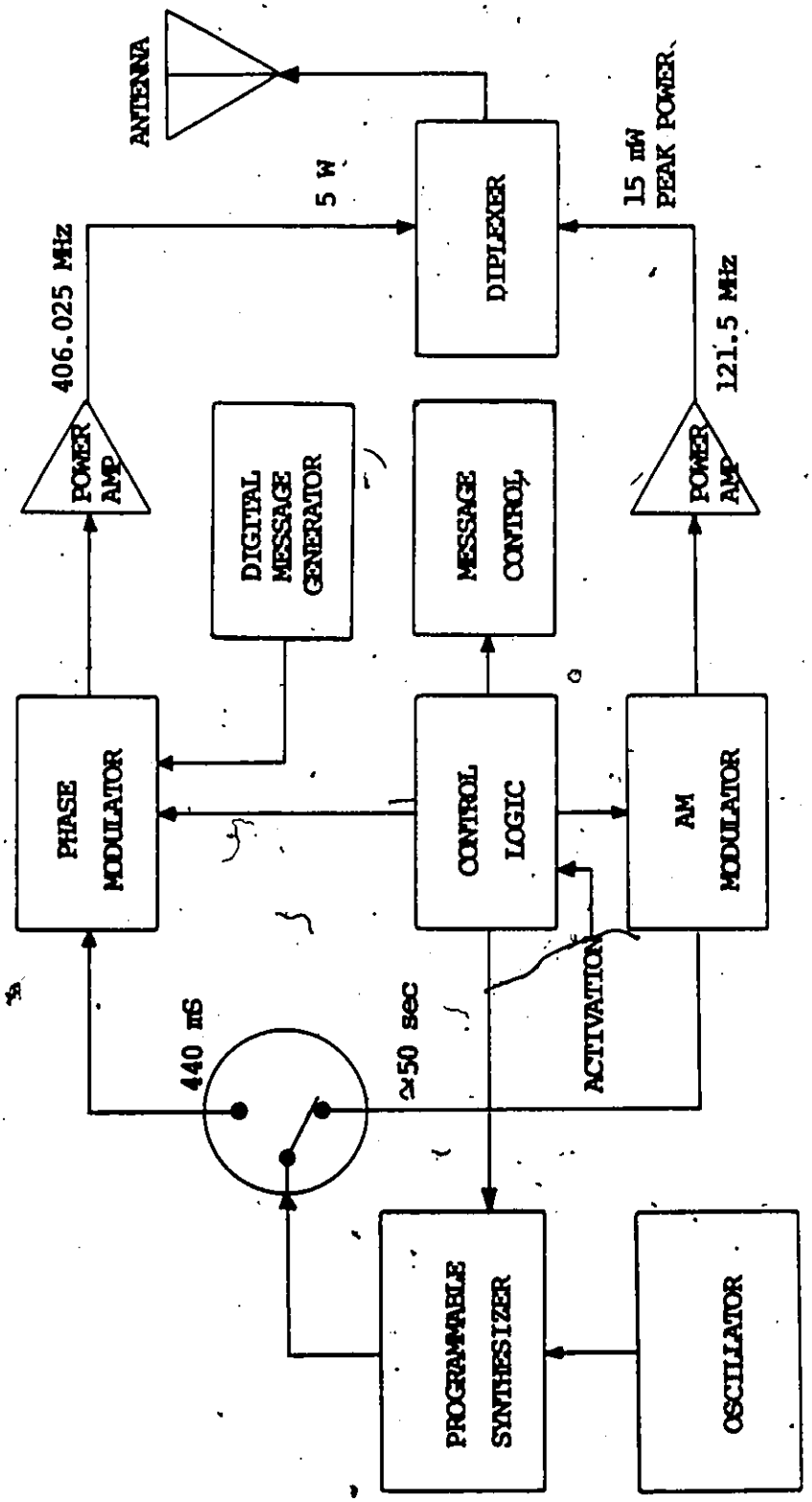

Fig. 2.5: Experimental 406 MHz ELT block diagram.

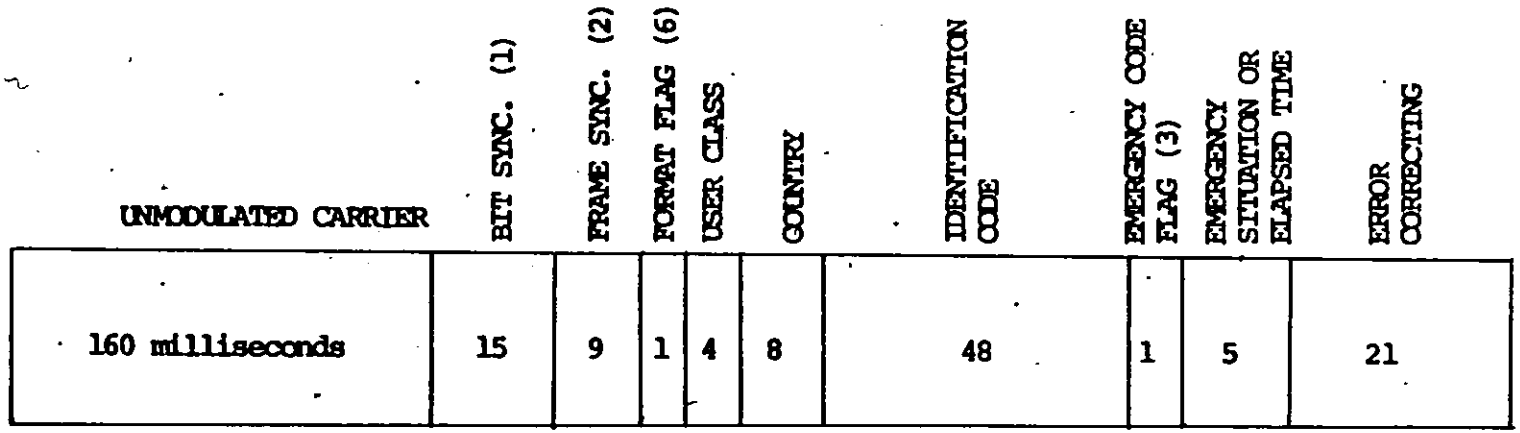

NOTES:
1) BIT SYNC - 15 "1" BITS
2) FRAME SYNC - 0001011[illegible]1
3) "1" BIT INDICATES EMERGENCY CODE, "0" BIT INDICATES ELAPSED TIME
4) ELAPSED TIME IN ONE HOUR INCREMENTS; COUNT HELD AT 32 HOURS
5) TOTAL MESSAGE DURATION 440 MILLISECONDS
6) "1" BIT INDICATES LONG MESSAGE FORMAT
"0" BIT INDICATES SHORT MESSAGE FORMAT

Fig. 2.6: 406 MHz ELT short message format.

and relayed to an earth station or Local User Terminal (LUT) when one is in view. to provide global coverage (including areas which do not have an LUT in the vicinity), the new system will incorporate the capability of storing the processed signals, until an LUT is in view. In Chapter 4 consideration is also given to processing signals from the new ELT's and comparisons made between results from the MEM and FFT.

CHAPTER 3

SIGNAL PROCESSING METHODS

It has been shown that ELT units in use at present transmit signals that are not very suitable for signal processing methods. Moreover, the received signal can be any one of a variety of different possibilities. the result of this is to severely limit the number of effective methods of processing these signals. Methods that at first appear to be suitable are matched filtering, spectral analysis using the Fast Fourier Transform (FFT) and a novel method called Maximum Entropy Spectral Analysis (MESA). This Chapter is concerned with describing each Method, exploring its applicability and pointing out its advantages and problems. Because the Maximum Entropy Method (MEM) is relatively new, it will be discussed in greater detail than the other two methods.

3.1 Matched Filtering

Matched filtering is the optimum form of receiver realization. In order to explain this form of detection, we tackle an example requiring the formulation of a matched filter. Consider the situation where we have a transmitted signal $S_i(t)$ $(i = 0, 1, \ldots, M-1)$ corresponding to a message M_i $(i = 0, 1, \ldots, M-1)$ which occurs with probability $P[m_i]$. Let the signal $S_i(t)$ be defined by

$$S_i(t) = \begin{cases} A\cos(2 f_i t) & ; \quad 0 \leq t \leq T \\ 0 & ; \quad \text{elsewhere} \end{cases} \tag{3.1}$$

It can be shown [10] that the optimum receiver is realized in the form of Fig. 3.1 where $S_i(T-t)$ is a filter whose impulse response is a delayed, time reversed version of the signal $S_i(t)$. The filters $S_i(T-t)$ are said to be matched to the original signal $S_i(t)$. If the received signal is given by

$$r(t) = S(t) + n(t) \tag{3.2}$$

then the input to the decision box is

$$\int_{-\infty}^{\infty} r(t)\, S_i(t)\, dt + C_i \tag{3.3}$$

where the term independent of time is dependent on the variance of the noise process ($N_o/2$), the a-priori probabilities $P[m_i]$ and the energy of the i^{th} signal E_i

$$C_i = \frac{1}{2} [N_o \ln P[m_i] - E_i) \tag{3.4}$$

The biggest drawback with this method is that each type of ELT signal would require a receiver with the set of filters $S_i(T-t)$ matched to that signal at frequencies f_i. Considering the variety of ELT's in use at present, with each type transmitting a different kind of signal, the required receiver structure would be very complex and expensive. For this reason we consider alternative methods for detecting the signals. At present the doppler frequency is estimated by using Fourier spectral analysis in the form of Fast Fourier Transform algorithms implemented on a digital computer. This method is discussed in the next section.

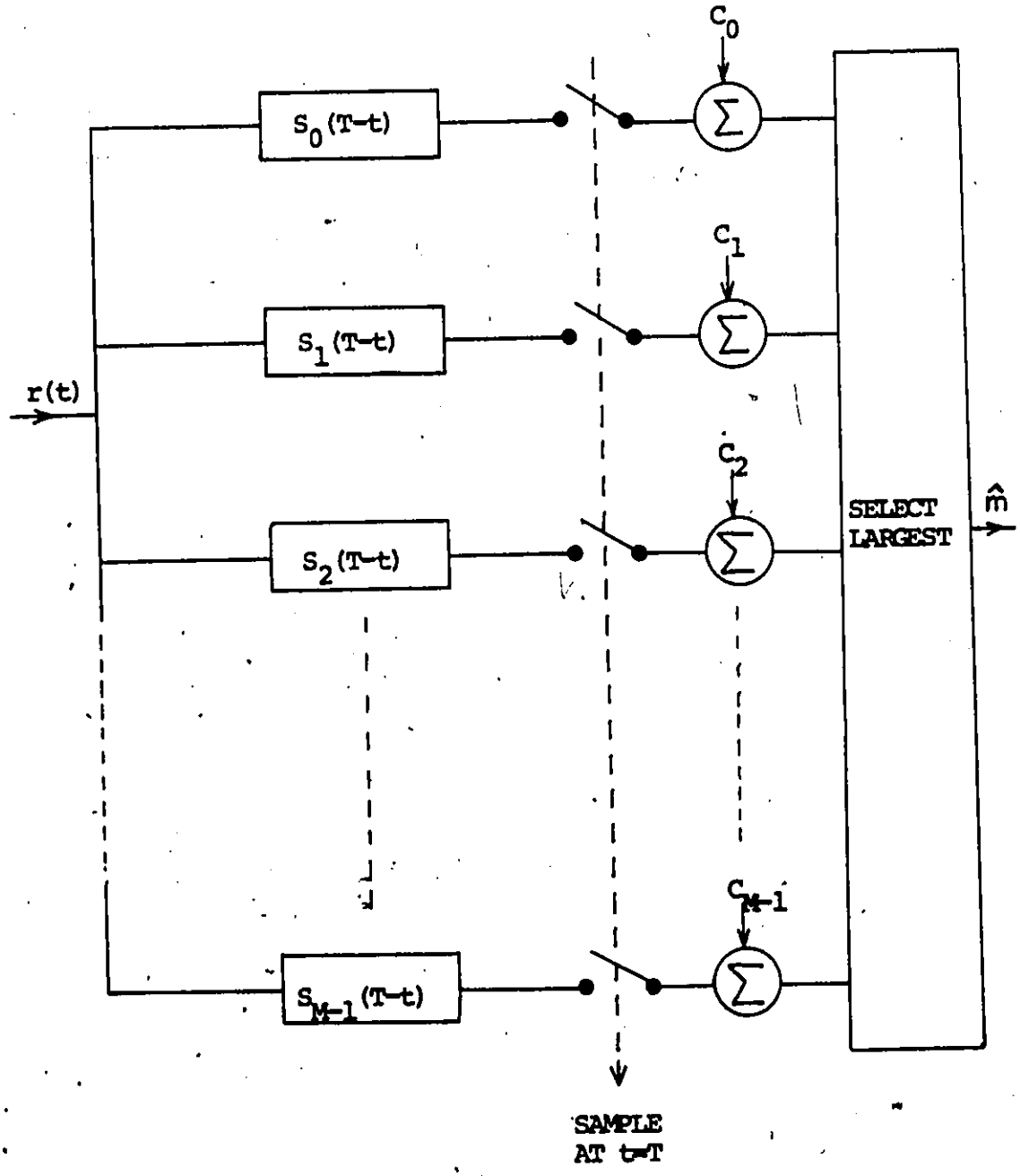

Fig. 3.1: An optimum receiver with M matched filters matched to a set of transmitted signals $\{S_i(t)\}$.

3.2 The Fast Fourier Transform

Because the Fast Fourier Transform is nothing more than an efficient implementation of the Discrete Fourier Transform (DFT), any discussion of the FFT must necessarily start with a description of the DFT. The discrete Fourier transform can be described as a Fourier representation of a finite duration sequence. In mathematical terms the DFT of a finite length sequence $\{x(n)\}$, $0 \leq n \leq N-1$ is defined as

$$X(k) = \sum_{n=0}^{N-1} x(n)\, e^{-j(2\pi/N)nk} \qquad k = 0, 1, \ldots, N-1 \tag{3.5}$$

If we replace the exponential term with

$$W_N = e^{-j(2\pi/N)} \tag{3.6}$$

eq. (3.5) can be written as

$$X(k) = \sum_{n=0}^{N-1} x(n)\, W_N^{nk} \tag{3.7}$$

Evaluation of the DFT using eq. (3.7) directly requires $(N-1)^2$ complex multiplications. Thus, for reasonably large values of N, evaluation of the DFT requires a large amount of computation. Consider the situation when N is even. We can write

$$X(k) = \sum_{\substack{n=0 \\ n \text{ even}}}^{N-1} x(n)\, W_N^{nk} + \sum_{\substack{n=0 \\ n \text{ odd}}}^{N-1} x(n)\, W_N^{nk} \tag{3.8}$$

It can be shown [13] that eq. (3.8) can be expressed in the form

$$X_1(k) + W_N^k X_2(k) \quad ; 0 \leq k \leq \frac{N}{2} - 1 \tag{3.9a}$$

$$X(k) =$$

$$X_1(k-\tfrac{N}{2}) + W_N^k X_2(k-\tfrac{N}{2}) \; ; \; \tfrac{N}{2} \leq k \leq N-1 \tag{3.9b}$$

where

$$X_1(k) = \sum_{n=0}^{N/2-1} x(2n) \, W_{N/2}^{nk}$$

$$X_1(k) = \sum_{n=0}^{N/2-1} x(2n+1) \, W_{N/2}^{nk}$$

and

$$W_{N/2}^{nk} = e^{-j[2\pi/(N/2)]}$$

Moreover, eq. (3.9b) can be written as eq. (3.9a) with the addition replaced by a subtraction. Thus, the number of complex multiplications involved equals the number of multiplications in (3.9a), i.e. ($N^2/2$ + N). By further decimation in time, division of the input sequence {x(n)}, the number of computations can be reduced to N/2 $\log_2$ N. Such methods that compute the DFT in an efficient manner are called Fast Fourier Transform algorithms. For a thorough understanding of the FFT the reader is referred to [11,12]. The algorithm implemented is termed a radix 2 FFT because it is based on the assumption that the number of samples is an integer power of 2 ($N = 2^L$; L integer).

Having established the derivation of the FFT algorithm, we now turn our attention to discussing some of the problems associated with its use. In Chapter 1 we pointed out the need for accurate doppler

estimates and the ability to resolve multiple ELT signals. The latter situation could arise as a result of multiple platforms in distress or due to transmitters being inadvertantly turned on through malfunction or oversight. In any case, the source of the transmission must be located. Some of the shortcomings of the FFT are in direct conflict with the need to fulfill the above requirements. It is these drawbacks which are explained below.

In the course of processing any data we must necessarily limit the data sequence to a finite length. Computer costs further restrict this length to a "reasonable" size in an effort to reduce processing time. This restriction is tentamount to multiplying the data by a rectangular pulse (window) of finite duration. An operation such as this results in an abrupt change at the endpoints of the data and introduces sidelobes (due to a sin x/x type response) in the Fourier spectrum. Furthermore, for the type of signals being considered, a carrier modulated by a string of pulses, the abrupt transitions due to the modulating pulses give rise to these high sidelobes. This can be seen in Fig. 3.2 which shows an FFT of the signal of Fig. 1.3. If these sidelobes are of sufficient magnitude, as compared to the main lobe, the resulting spectrum could lead to false alarms due to one or more sidelobes being mistaken for additional doppler components (due to multiple signals). On the other hand if a second doppler component does actually exist, it could be masked by the sidelobes resulting in a failure to detect. A solution to the problem of high sidelobes is to use a tapered window

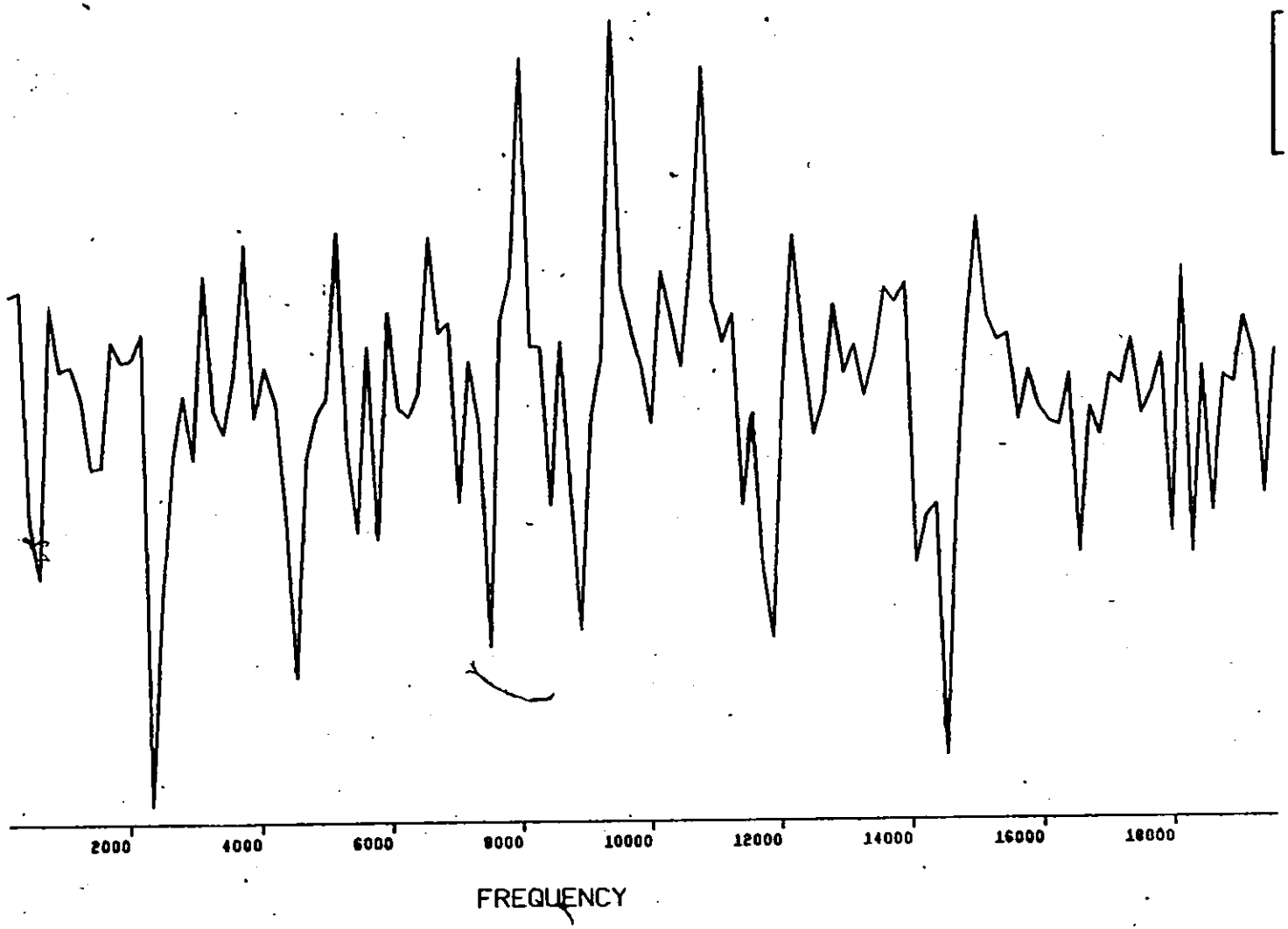

Fig. 3.2: Processing square modulated signals results in high FFT sidelobes.

function such that the amplitude of the data is gradually reduced at the endpoints. Such a modification of the data, however, leads to a reduction in sidelobe levels at the expense of a broadening (or smearing) of the main lobe and hence a decrease in resolution. The resulting increase in ambiguity of the location of the peak is in direct conflict with the need for accurate doppler estimates. It is with these drawbacks in mind that in Section 3.3 we look to a different method of signal processing, namely, the maximum entropy method. However, before proceeding to examine the MEM we need to verify the FFT algorithm that is implemented.

3.2.1 Verification of FFT Algorithm

In order to ensure that the algorithm does indeed yield correct results we use it to process two well known types of signals and compare the resulting spectra with the theoretical spectra. The signals we choose to process are a single baseband pulse and an RF pulse. It can be shown that the amplitude spectrum of a pulse is the squared magnitude of a sinc function. Moreover, the sidelobes are 13 dB down from the main lobe and the spectral nulls occur at frequencies n/T where n is an integer and T is the duration of the pulse. For reasons given in Chapter 4 we shall use a sampling rate of 40 KHz and process blocks of 256 data samples.

Consider processing the baseband pulse of Fig. 3.3 such that the duration T is 3.2 mS. We would expect the squared magnitude of the FFT to yield a $|(\sin x)/x|^2$ type result. Figure 3.4 shows the amplitude

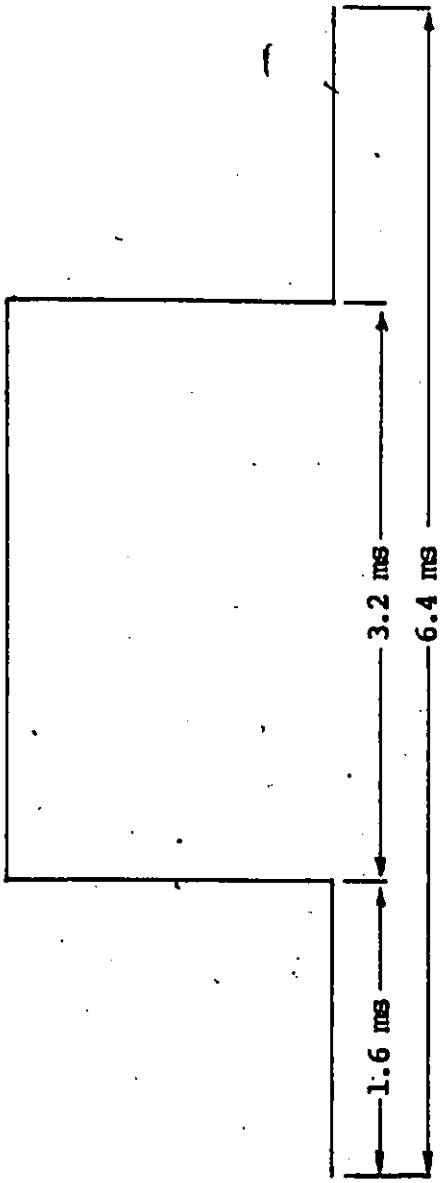

Fig. 3.3: A baseband pulse of duration T = 3.2 ms.

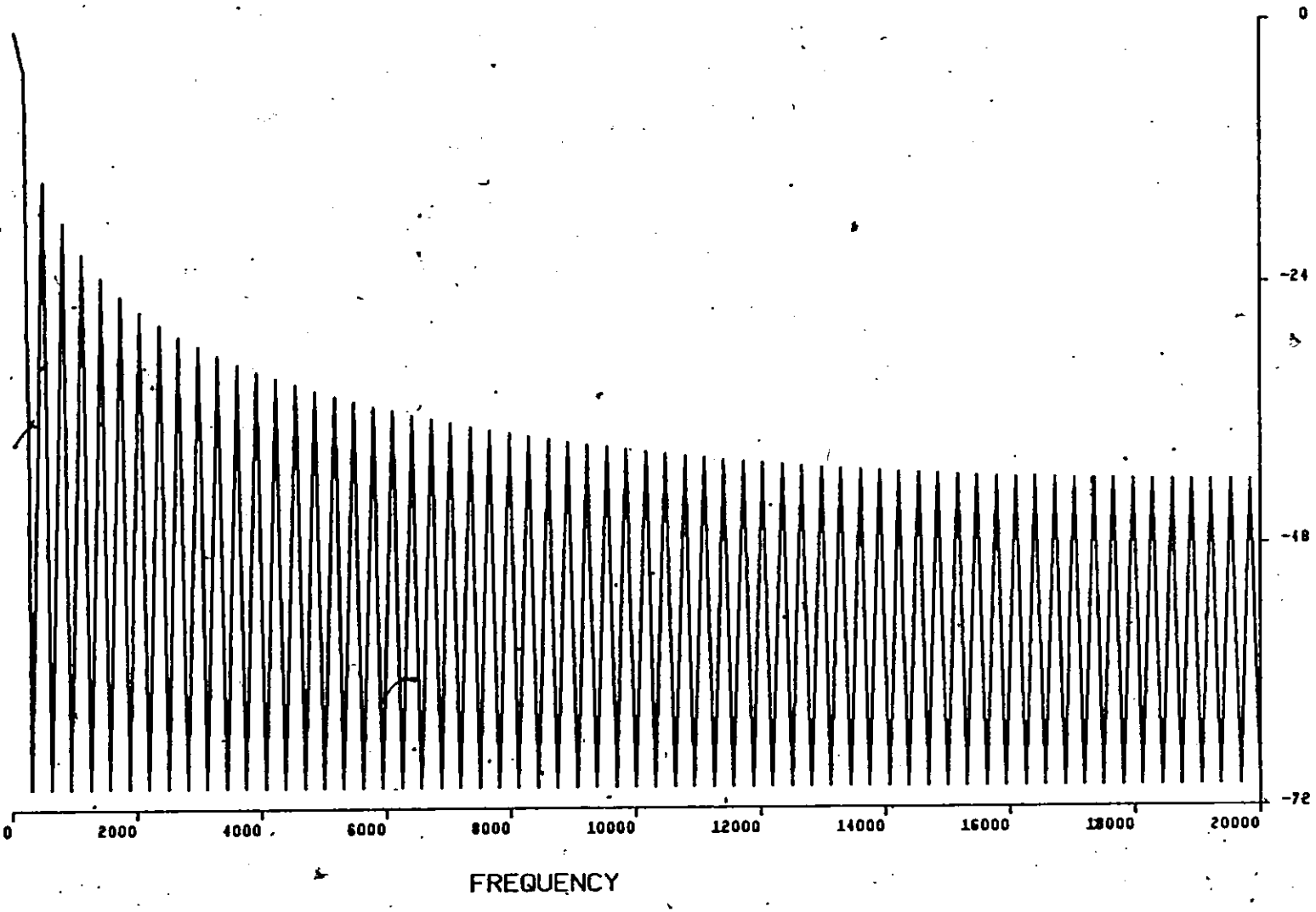

Fig. 3.4: Amplitude spectrum of baseband pulse.

spectrum where the curve has been normalized to the peak and the vertical scale is in decibels. Since the spectrum is symmetric about the point f=0, we plot the spectrum for positive frequencies only. This spectrum is in agreement with theory in so much as the spectral nulls occur at n/T Hz i.e. 312.5, 625, 937.5, ... Hz. However, the sidelobes appear to about 13.5 dB down from the main lobe instead of the expected 13 dB. We can explain this discrepancy by noting that the peak of the sidelobes do not occur midway between the spectral nulls which is where the odd numbered spectral points are evaluated. In fact, the FFT will be in agreement with the Fourier transform only in the limiting case when an infinite point FFT is performed.

The second type of signal we use to test the algorithm is an RF pulse. In this case we replace the central 128 samples of Fig. 3.3 with samples along a sinusoid. For simplicity we let the initial phase of the sinusoid be zero. Plots shown in Figs. 3.8, 3.9 and 3.10 represent the squared magnitude of the FFT (henceforth referred to as the amplitude spectrum) of the RF pulses shown in Figs. 3.5, 3.6 and 3.7. Since the spectrum is evaluated at the frequencies if_s/N where i is an integer, f_s is the sampling rate and N is the number of sample points used, it is simple to show that the spectral points occur at integer multiples of 156.25 Hz. This would imply that we can expect an accuracy of better than 78.125 Hz. At all three frequencies the accuracy is indeed better than this figure. The unexpected shapes of the spectra of pulses RF_1 and RF_3 are a result of the spectral points falling at neither the peaks of the sidebacks nor the nulls. When f_c is 10 KHz,

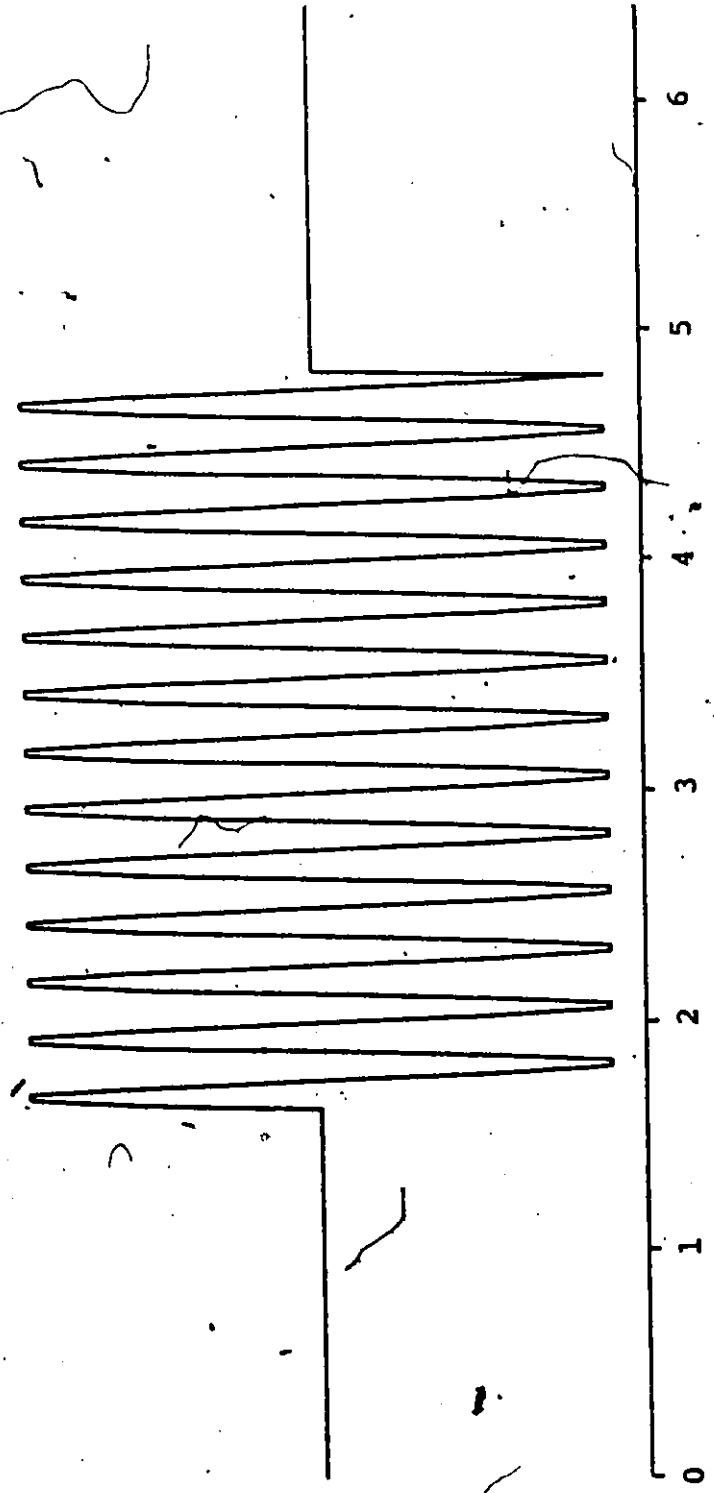

Fig. 3.5: RF pulse with f_c = 4 KHz.

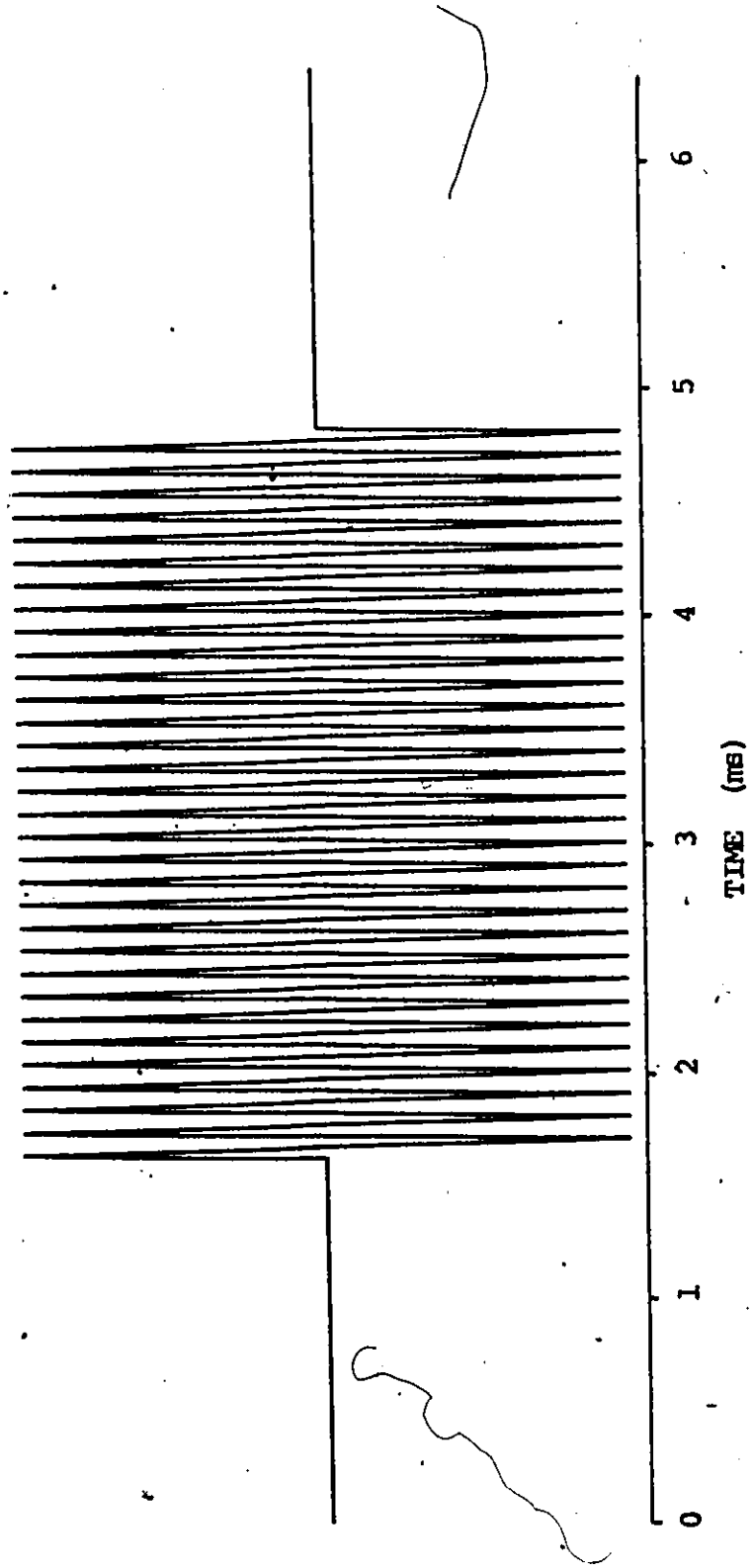

Fig. 3.6: RF pulse with f_c = 10 KHz.

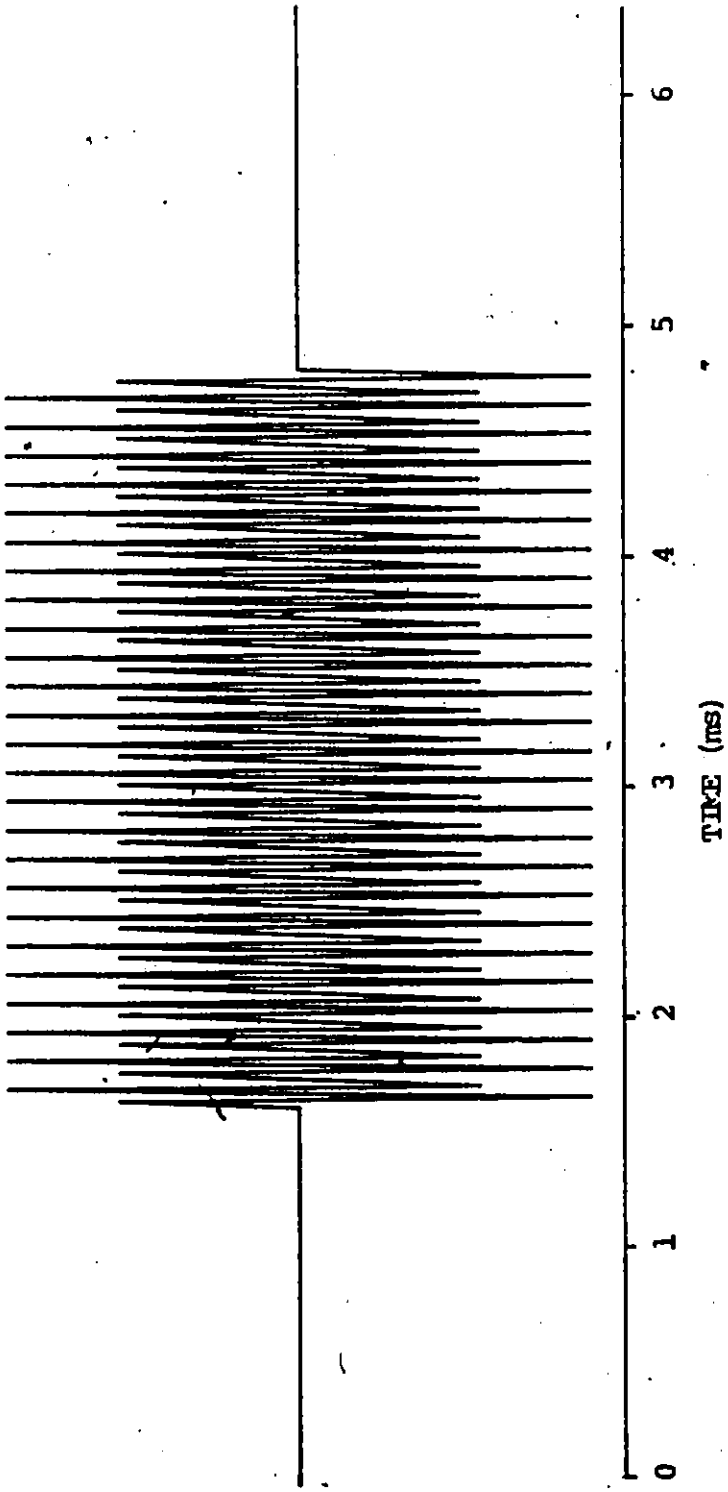

Fig. 3.7: RF pulse with f_c = 16 KHz.

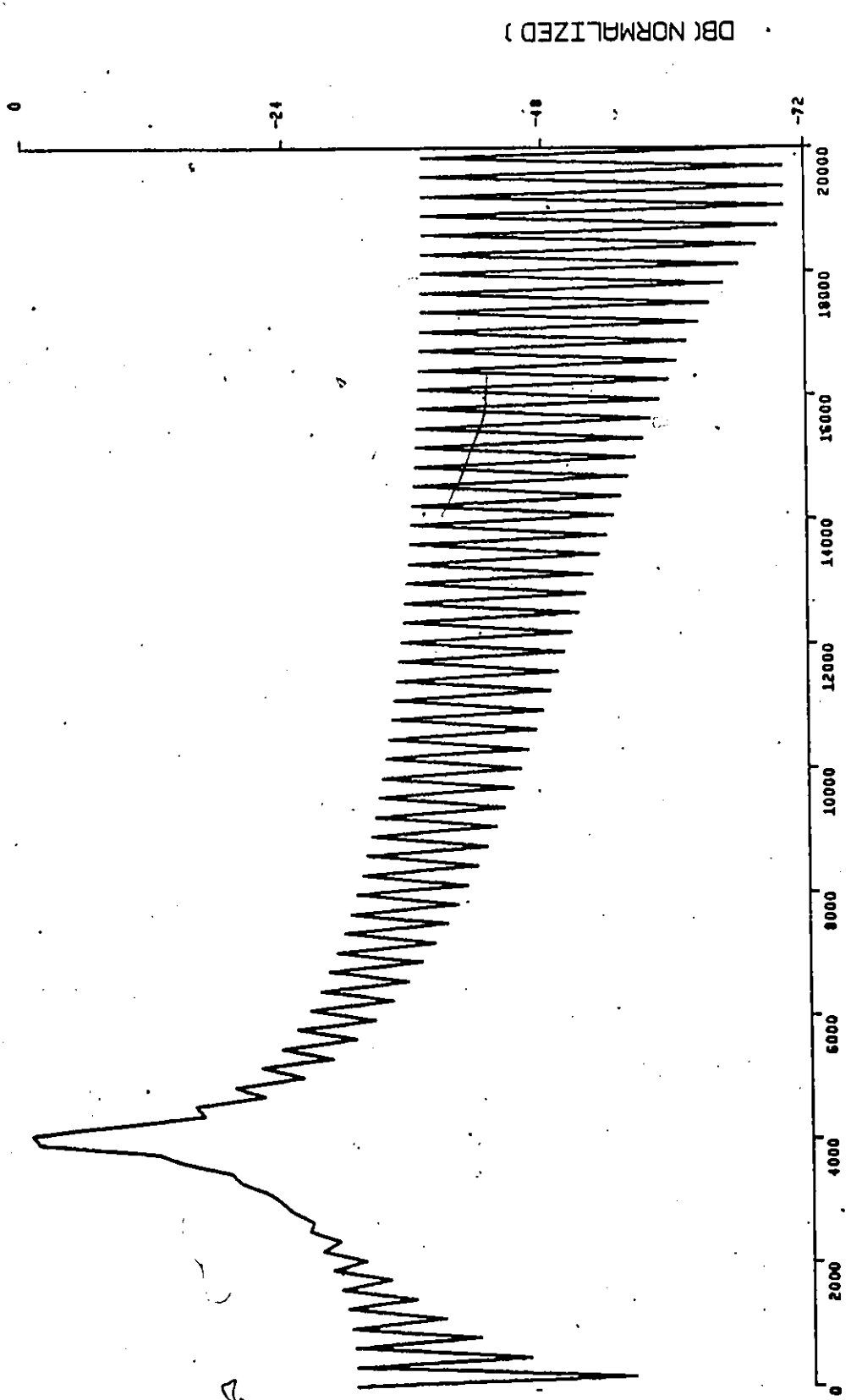

Fig. 3.8: Amplitude spectrum of RF pulse with f_c = 4 KHz.

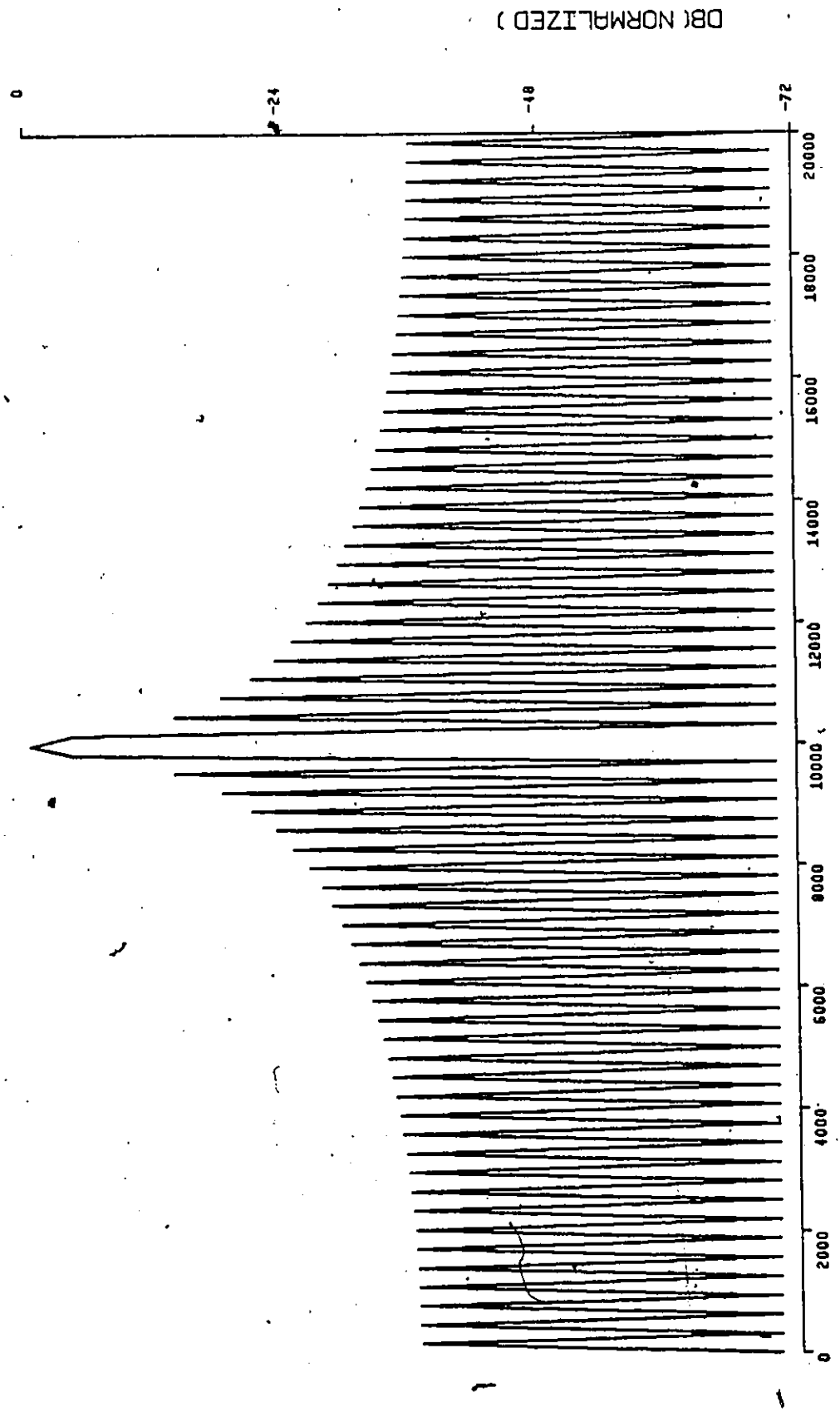

Fig. 3.9: Amplitude spectrum of RF pulse with f_c = 10 KHz.

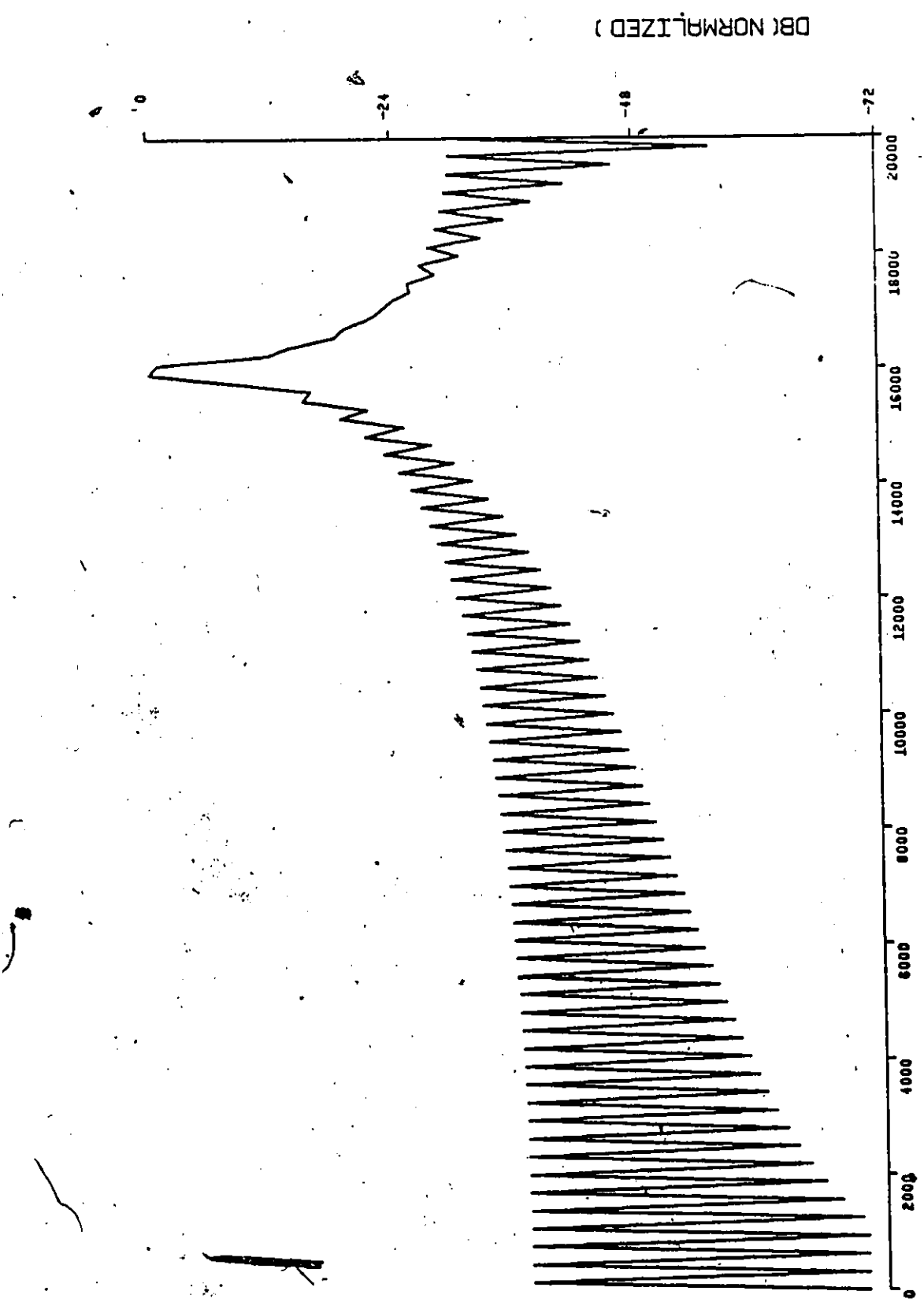

Fig. 3.10: Amplitude spectrum of RF pulse with f_c = 16 KHz.

every other point does indeed coincide with a null with the points in between being close to the peaks of the sidelobes.

Pulse RF_2 is processed at signal to noise ratios of 20 to -10 dB and the resulting amplitude spectra shown in Figs. A1.1 to A1.6. A comparison of these plots indicates that at values of SNR below 0 dB, detection of the main lobe becomes exceedingly difficult if not impossible.

In conclusion to this section we note that the FFT algorithm used performs as expected and that the results for two simple kinds of signals are in good agreement with theory. Having verified the FFT algorithm, we are now in a position to discuss the maximum entropy method and test the algorithm for the two simple types of signals.

3.3 The Maximum Entropy Method

The MEM is a signal processing method which has generated considerable interest in recent years, especially in the field of Geophysics, due to its excellent resolution capability. Although this method is adequately documented in the literature [4-7, 14-19], we present an outline here because the MEM is central to this dissertation.

Consider a zero-mean time series $\{x_t\}$, which can be complex in general, such that it satisfies the model

$$x_{t+1} = a_1 x_t + a_2 x_{t-1} + \ldots\ldots + a_m x_{t-m+1} + e_t \qquad (3.10)$$

Such a time series is said to be an autoregressive process of order m and is given the notation AR(m). If an estimate of the sample at time t+1 is obtained from the m previous samples by using a predictive

filter, Fig. 3.11, e_t can be viewed as the prediction error. The AR coefficients, a_i, can be obtained by minimizing the expectation of the square of the error term e_t. Once the coefficients and the prediction error power (P_M) are estimated, the spectral density can be found using

$$S(f) = \frac{P_M \, \Delta t}{\left| 1 + \sum_{n=1}^{M} a_n \exp(-j2\pi f n \Delta t) \right|^2} \qquad (3.11)$$

where

$\Delta t \equiv$ sampling interval

$P_M \equiv$ prediction error power which will be defined later.

This method of obtaining the spectral density by AR modelling is equivalent to the maximum entropy method. In order to use eq. (3.11) we need to know the AR coefficients a_n and the output power from the M^{th} order prediction error filter (PEF(M)) of Fig. 3.12. The implementation of the algorithm, to determine the coefficients, involves the design of a one step ahead predictive filter.

Consider the design of the predictive filter of Fig. 3.12. The desired response, at time t, is given by

$$d_t = x_{t+1} \qquad (3.12)$$

and its estimate is based on (regressed on) the present data value and m-1 preceeding data points such that

$$\hat{x}_{t+1} = a_1 x_t + a_2 x_{t-1} + \ldots + a_m x_{t-m+1} \qquad (3.13)$$

where $\hat{}$ indicates the estimated value. Such an estimate deviates from the desired output by an amount

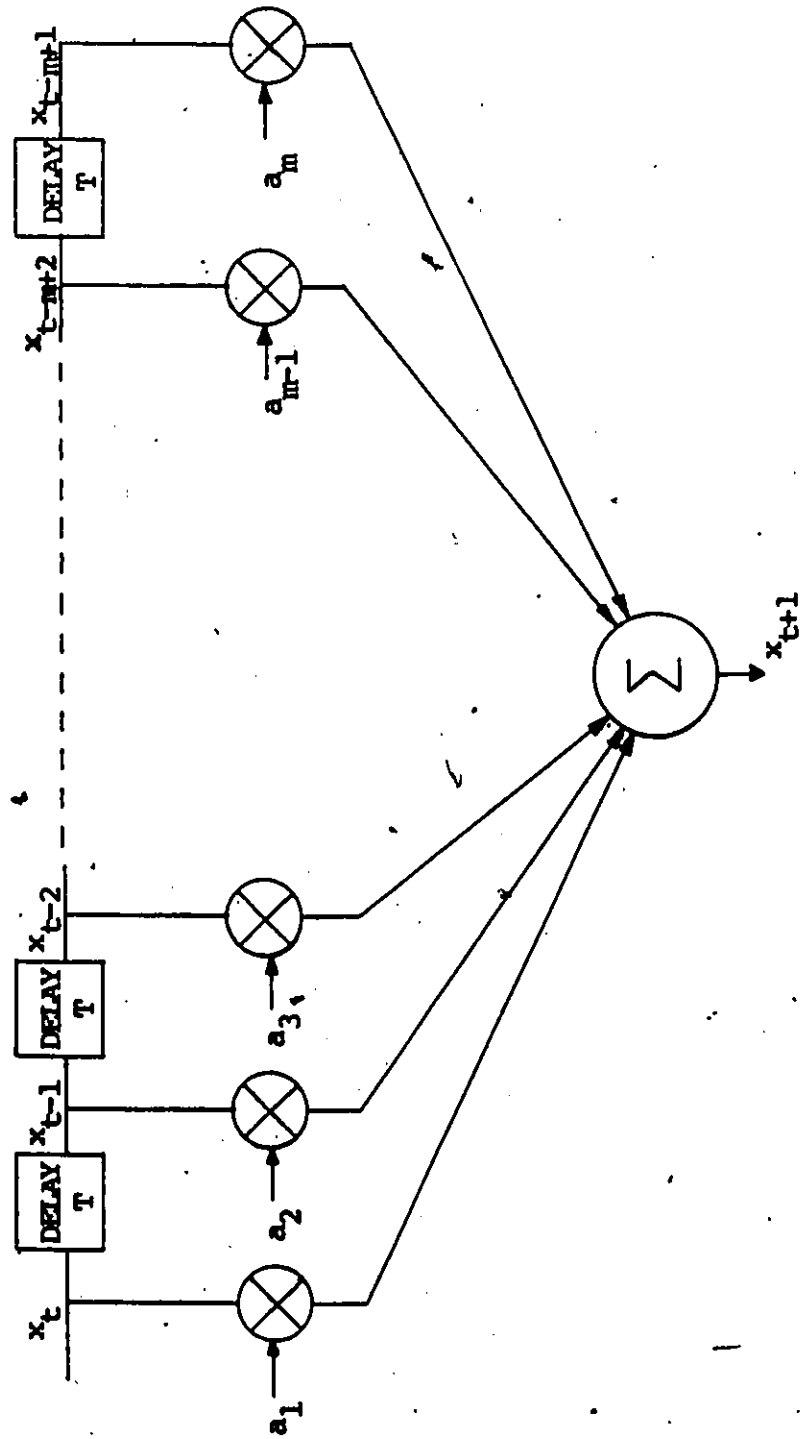

Fig. 3.11: A predictive filter of order m.

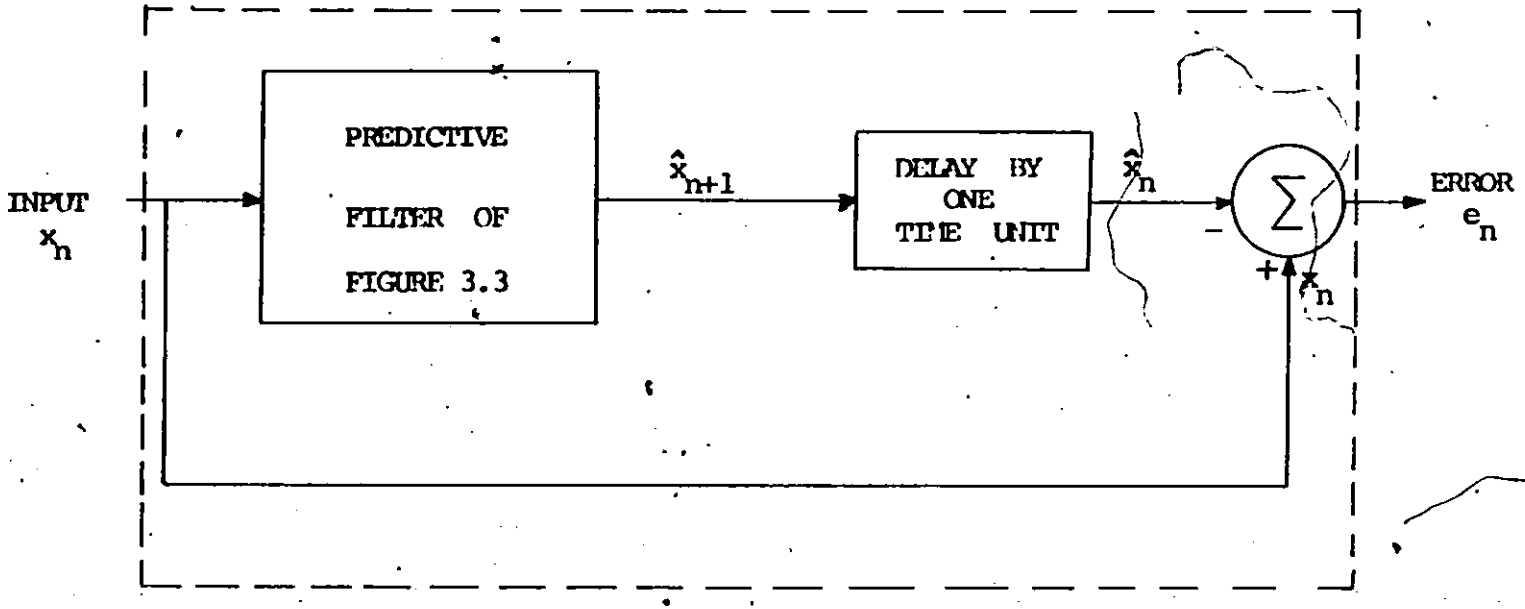

Fig. 3.12: Block diagram showing the relationship between the predictive filter of Fig. 3.11 and the prediction error filter.

$$e_t = x_{t+1} - \sum_{k=1}^{M} a_k \, x_{t-k+1} \tag{3.14}$$

We define the mean square error of the estimate as

$$E[e_t \, e_t^*] = E[(x_{t+1} - \sum_{k=1}^{M} a_k \, x_{t-k+1})(x_{t+1}^* - \sum_{k=1}^{M} a_k^* \, x_{t-k+1}^*)] \tag{3.15}$$

where

* denotes conjugation

E denotes expectation.

In an attempt to arrive at the optimum parameters $a_{o,k}$, we minimize the mean square error with respect to the a_k. It can be shown [5] that minimization of $E[e_t \, e_t^*]$ leads to the Yule Walker equations

$$\sum_{k=1}^{M} R_x(m-k) \, a_{o,k} = R_x(m) \quad m = 0, 1, \ldots, M-1 \tag{3.16}$$

where R_x denotes autocorrelation. By substituting the optimum coefficients ($a_{o,k}$) into eq. (3.15) we obtain a value for the minimum error power, which can be shown to be

$$P_{min} = \sum_{k=0}^{M} a_k \, R_x(-k) \tag{3.17}$$

where

$$a_k = \begin{cases} 1 & ; \; k = 0 \\ a_{0,k} & ; \; k = 1, 2, \ldots, M \end{cases}$$

Since eq. (3.14) represents the output from the prediction error filter of Fig. 3.12, it follows that P_{min} must represent the output power of the optimum PEF of order M. By manipulating eq. (3.16) to reduce the right side of the equations to zero and using

$$P_M = P_{min} = \sum_{k=0}^{M} a_k R_x(-k) \qquad (3.18)$$

to augment the system, we obtain the PEF equations

$$\begin{bmatrix} R_x(0) & R_x(-1) \cdots\cdots R_x(-M) \\ R_x(1) & R_x(0) \cdots\cdots R_x(1-M) \\ \vdots & \vdots \qquad\qquad \vdots \\ R_x(M-1) & R_x(M-2) \cdots\cdots R_x(-1) \\ R_x(M) & R_x(M-1) \cdots\cdots R_x(0) \end{bmatrix} \begin{bmatrix} 1 \\ a_1 \\ \vdots \\ a_{M-1} \\ a_M \end{bmatrix} = \begin{bmatrix} P_M \\ 0 \\ \vdots \\ 0 \\ 0 \end{bmatrix} \qquad (3.19)$$

A solution to eq. (3.19) yields the M+1 unknowns (a_1, a_2, ..., a_M, P_M) required to find the spectral density. This direct approach of solving the equations requires that we estimate the autocorrelation matrix. Since the available data is limited, we must make an assumption regarding data extensions (i.e. a zero extension). Such an assumption, however, is neither valid nor necessarily correct. Burg has devised a method (which we shall refer to as Burg's method) which obviates the requirement of obtaining an a priori estimate of the autocorrelation function. It is this method that we use in the implementation of the algorithm. Burg's scheme is a recursive technique that involves developing a PEF (n+1) from the PEF(n). The method is best described by carrying out a single recursion. Consider developing the prediction error filter of order n+1 (in what follows, the i^{th} coefficient of the PEF(J) is written as $a_{i,j}$. There are 4 basic steps involved:

1) Run the n+1 order filter over the data in both directions and find the average of the forward and backward error powers. (The reason

for including the backward error power, obtained by running the filter over the data in the reverse direction, will be given later). This results in the averaged power

$$P_{n+1} = \frac{1}{2[N-(n+1)]} \sum_{k=n+2}^{N} [|e_{f,n+1}|^2 + |e_{b,n+1}|^2] \tag{3.20}$$

where N ≡ number of samples and the forward and backward error powers are given by eqs. (3.20a) and (3.20b) respectively

$$e_{f,n+1} = \sum_{i=0}^{n+1} x_{k-i}\, a_{i,n+1} \tag{3.20a}$$

$$e_{b,n+1} = \sum_{i=0}^{n+1} x_{k-i}\, a^*_{n+1-i,n+1} \tag{3.20b}$$

2) Next we use the Levinson recursion, eq. (3.21), to replace the n coefficients $a_{i,n+1}$ $i = 0, 1, \ldots, n$ with the known coefficients $a_{i,n}$ $i = 0, 1, \ldots, n$ of the PEF of order n.

$$\begin{bmatrix} a_{0,n+1} \\ a_{1,n+1} \\ \vdots \\ a_{n,n+1} \\ a_{n+1,n+1} \end{bmatrix} = \begin{bmatrix} a_{0,n} \\ a_{1,n} \\ \vdots \\ a_{n,n} \\ 0 \end{bmatrix} + a_{n+1,n+1} \begin{bmatrix} 0 \\ a^*_{n,n} \\ \vdots \\ a^*_{1,n} \\ a^*_{0,n} \end{bmatrix} \tag{3.21}$$

This substitution reduces eq. (3.20) to an equation in one unknown, that being $a_{n+1,n+1}$.

3) Determine the reflection coefficient, $a_{n+1,n+1}$, by finding the solution to $\partial P_{n+1}/\partial a_{n+1,n+1} = 0$. The resulting value is given by

$$a_{n+1,n+1} = \frac{-2 \sum_{k=n+1}^{N} [e_{f,n}\, e^*_{b,n}]}{\sum_{k=n+2}^{N} [|e_{f,n}|^2 + |e_{b,n}|^2]} \qquad (3.22)$$

where

$$e_{f,n} = \sum_{i=0}^{n} x_{k-i}\, a_{i,n} \qquad (3.22a)$$

$$e_{b,n} = \sum_{i=0}^{n} x_{k-i}\, a^*_{n-1,n} \qquad (3.22b)$$

4) Use eq. (3.21) to find the coefficients of the PEF of order n+1 and find the prediction error power P_{n+1} given by

$$P_{n+1} = (1 - |a_{n+1,n+1}|^2)\, P_n \qquad (3.23)$$

It is evident from the foregoing that each recursion entails using eqs. (3.22), (3.21) and (3.23). For any PEF the first coefficient $a_{o,k}$ is always unity and hence the zeroth order PEF can be viewed as a straight piece of wire. Thus the recursion can be started using $a_o = 1$ and

$$P_o = \frac{1}{N} \sum_{i=1}^{N} x_i\, x_i^* \qquad (3.24)$$

In finding the error power of the filter we used the average of the foward and backward error powers. This was first suggested by Burg who noted that it ensured a stable filter. As we have already stated, Burg's method requires no unrealistic assumptions regarding data extensions as do methods such as the FFT. The question that still needs to be answered is how to choose the order of the AR process that should be fitted to the data.

Some of the available methods for determining the filter order are

[8] the Final Prediction-Error Criterion (FPE), the Information Theoretic Criterion (AIC) and the Autoregressive Transfer Function Criterion (CAT). These criteria have been derived on the assumption that the process being modelled is autoregressive. Since the signals we are processing, sinusoids in noise, are not autoregressive processes, the criteria yield rather poor results. Since our data is not autoregressive, the best we can do is to approximate it as an AR process. Empirically we have found that for a single sinusoid in noise, an order three AR process is a good approximation. Multiple signals in noise can be better approximated using higher orders and will be discussed in Chapter 5.

As was done with the FFT, we use the MEM to process baseband and RF pulses in order to ensure that our algorithm performs in an agreeable fashion.

3.3.1 Verification of the MEM

Before implementing the algorithm discussed in the previous section, it is of paramount importance that it performs as we would hope. The signals we use for this purpose have already been described in section 3.2.1 and hence in order to avoid repetition we shall merely reference the relevant figures.

Figure 3.13 shows the maximum entropy spectral estimate (MESE) of the baseband pulse of Fig. 3.3. One point that is worthy of note is the complete lack of sidelobes in the spectrum. This characteristic may be of considerable importance when the need arises to differentiate between

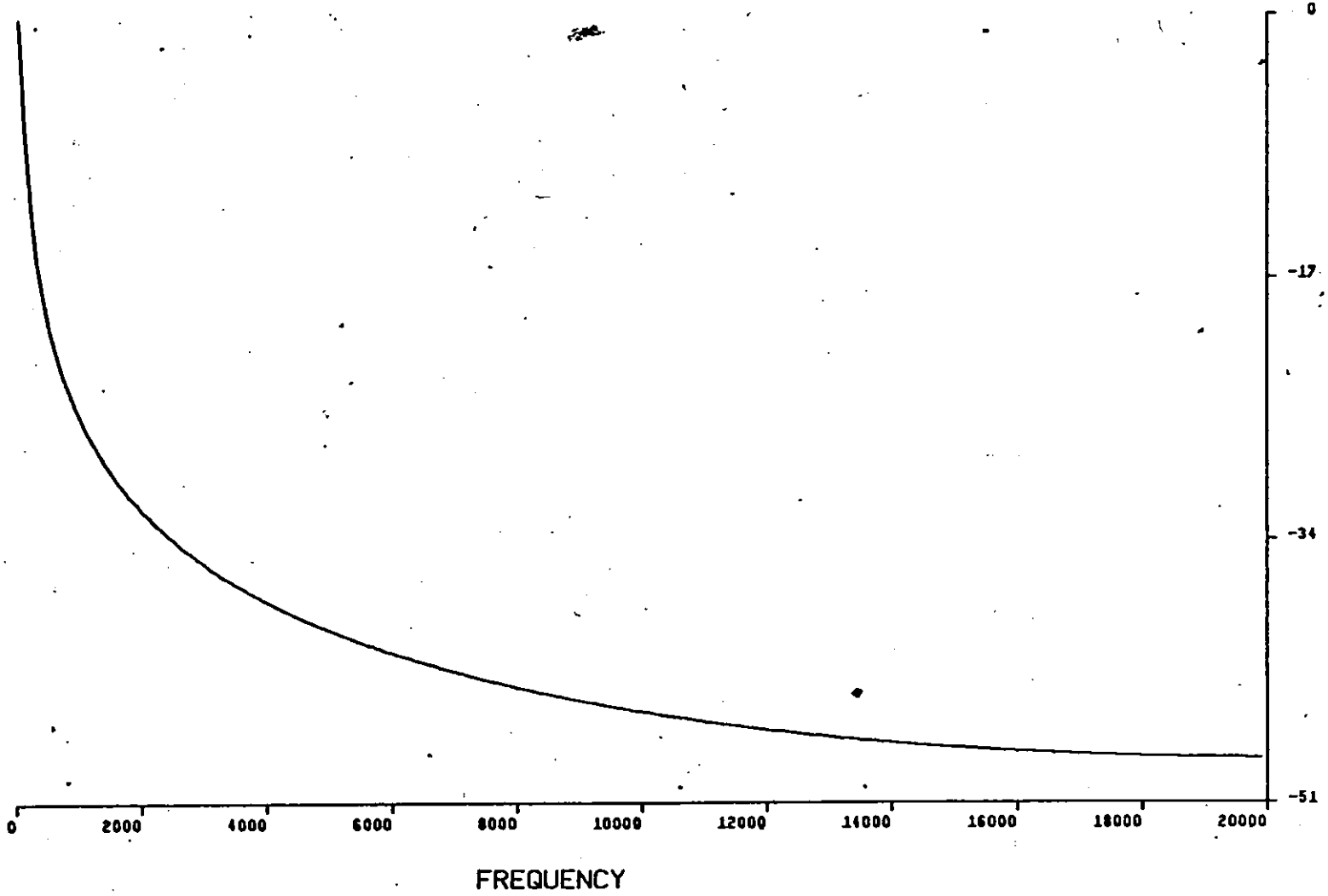

Fig. 3.13: ME spectrum of baseband pulse.

more than one frequency component. Processing the RF pulses of Figs. 3.5, 3.6 and 3.7 leads to the spectra of Figs. 3.14, 3.15 and 3.16. An expanded view of the peaks, by plotting the spectrum in the vicinity of the peak, is shown in Figs. 3.17, 3.18 and 3.19 respectively. These plots indicate that the greater resolution capability of the MEM results in better accuracy in comparison with the FFT.

Finally, we plot the ME spectra for pulse RF_2 at values of SNR from 20 dB to -10 dB in Figs. A2.1 to A2.7. At values of SNR below 0 dB, although it is still discernable, the peak becomes shifted substantially. A comparison of the results for the MEM and FFT indicates that the lack of sidelobes and the improved resolution capability of the MEM may offer significant advantages.

In the next section we examine the result of processing the autocorrelation of the signal using both the FFT and the MEM.

3.4 Processing the Autocorrelation of the Signal

We have already stated that the MEM is an adaptive method. Moreover, as previously indicated, our primary objective is to obtain an estimate of the carrier being modulated. In view of this, it is evident that the set of samples on either side of the sinusoid of the RF pulse will only hamper adaptation to the sinusoid itself. If we knew a-priori where the sine wave started, we could discard the irrelevant portion of the signal. On the other hand, without any such knowledge, ignoring any part of the set of samples may mean ignoring useful information. A possible alternative is outlined below.

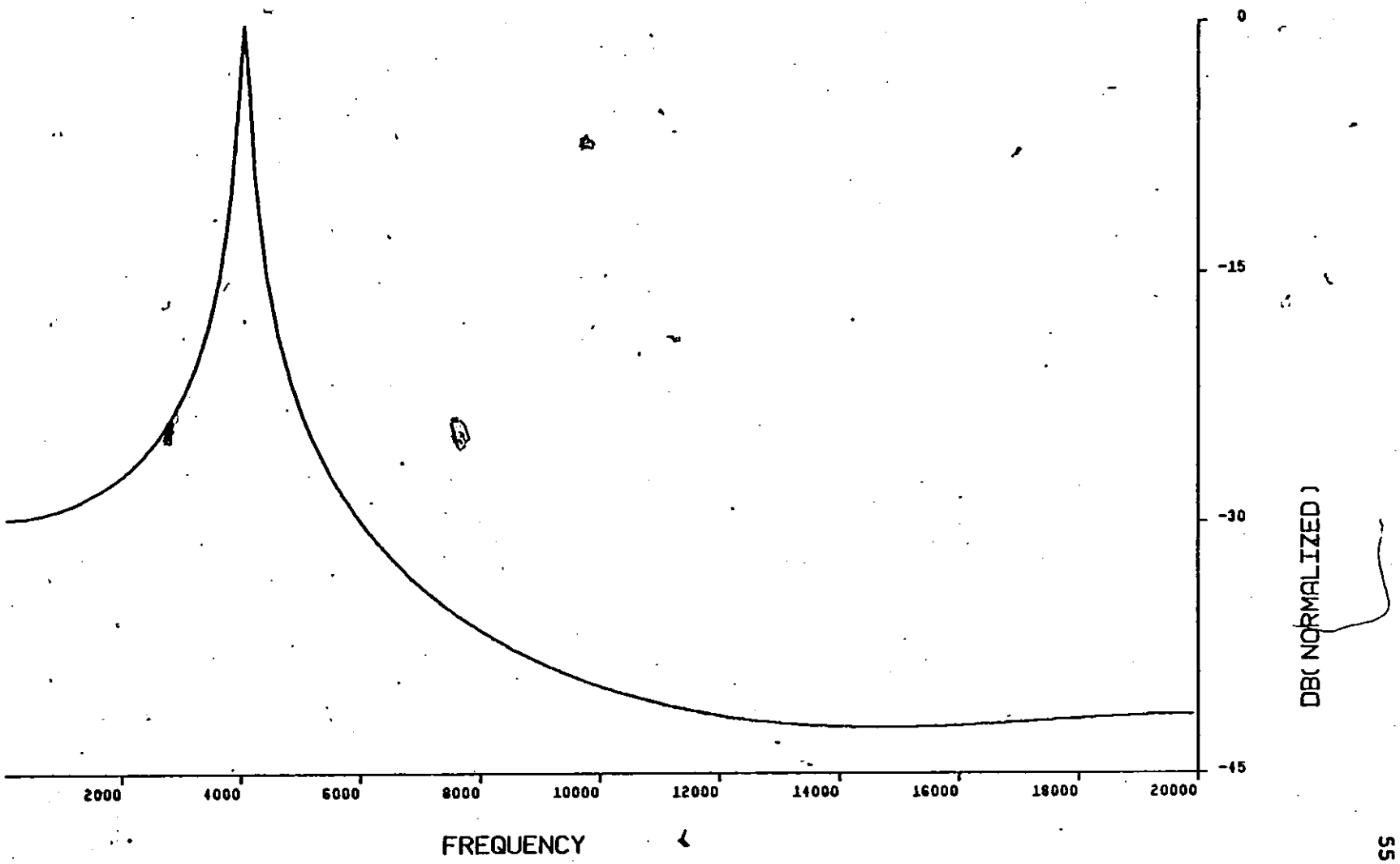

Fig. 3.14: ME spectrum of RF pulse with f_c = 4 KHz.

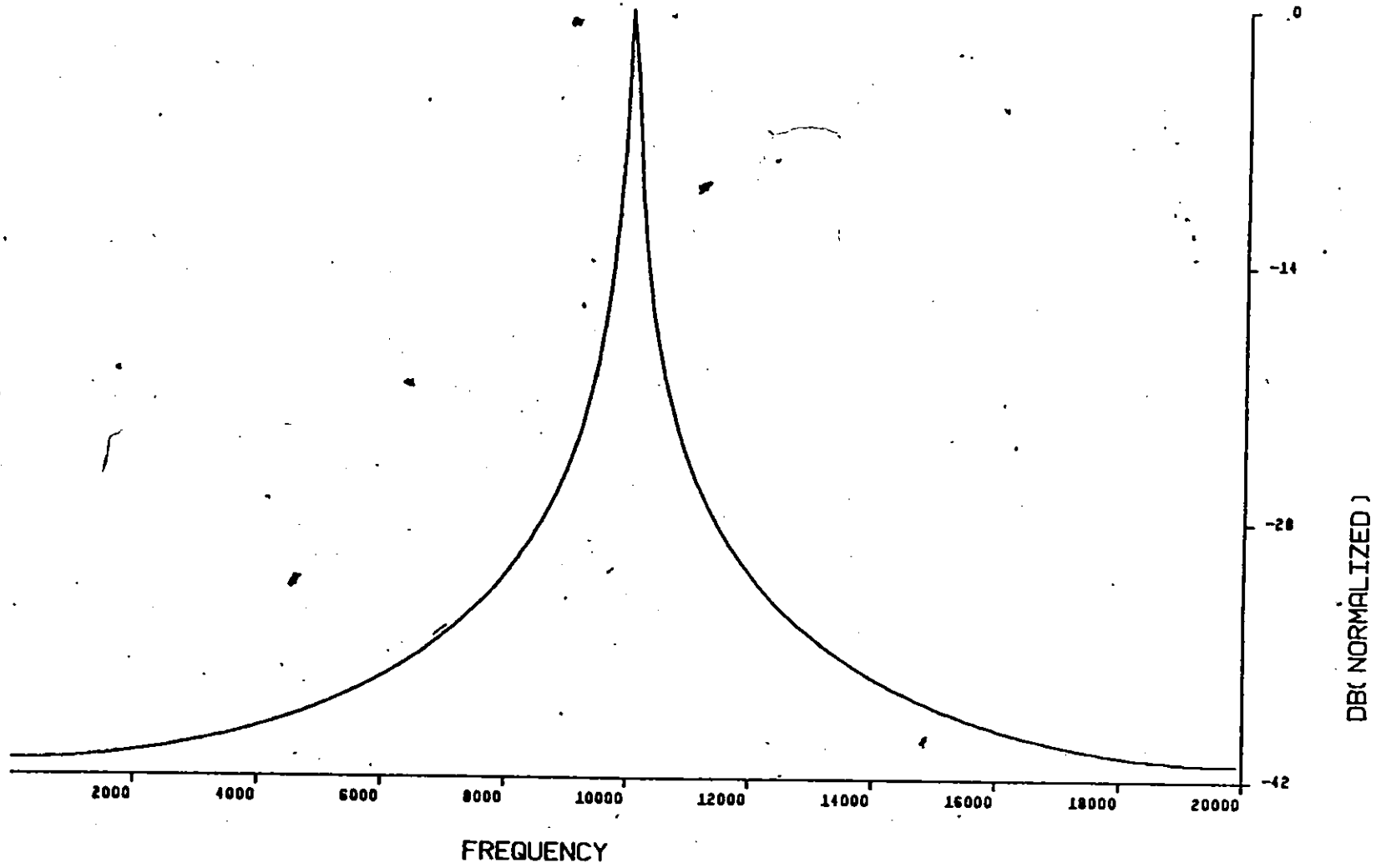

Fig. 3.15: ME spectrum of RF pulse with f_c = 10 KHz.

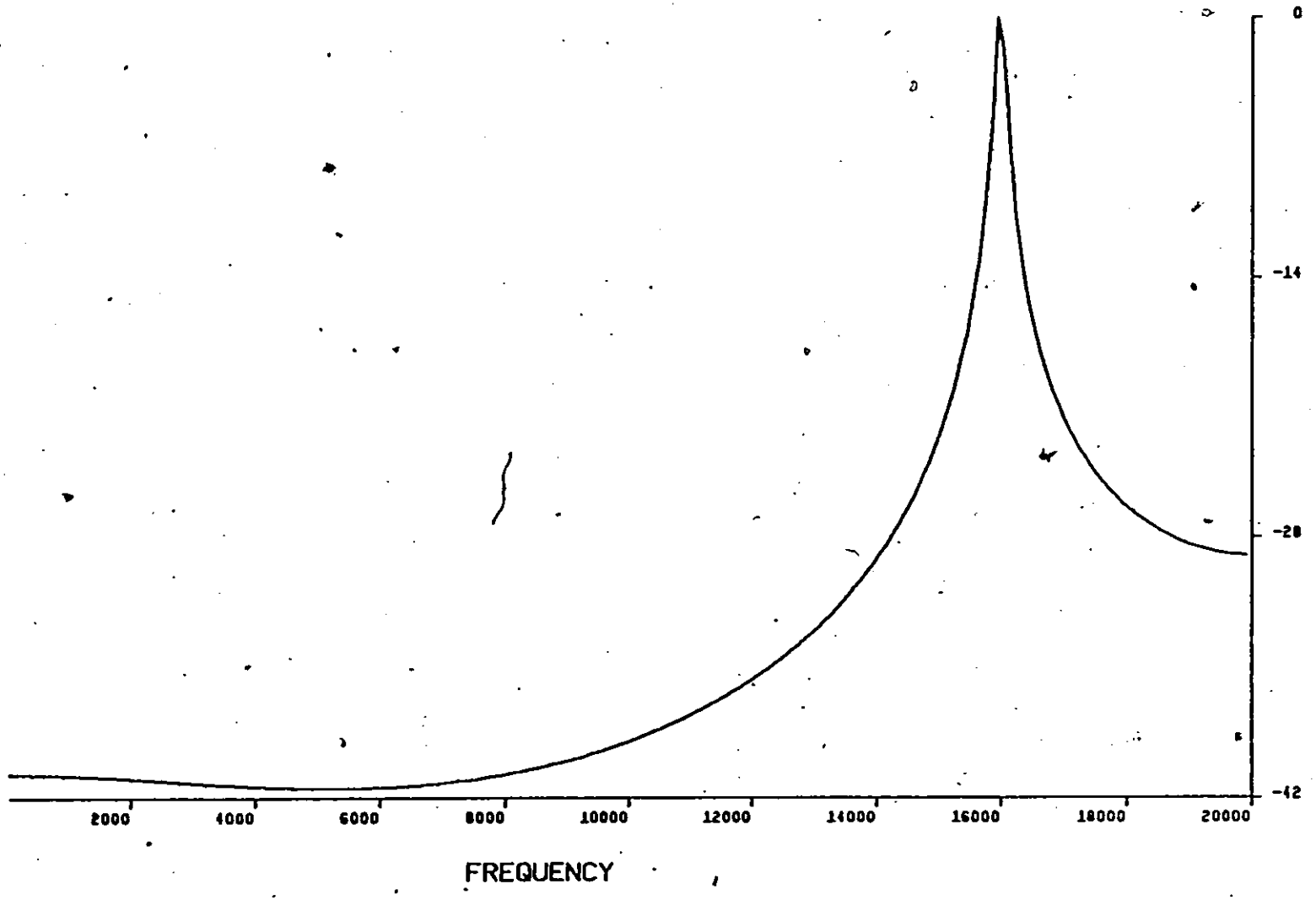

Fig. 3.16: ME spectrum of RF pulse with f_c = 16 KHz.

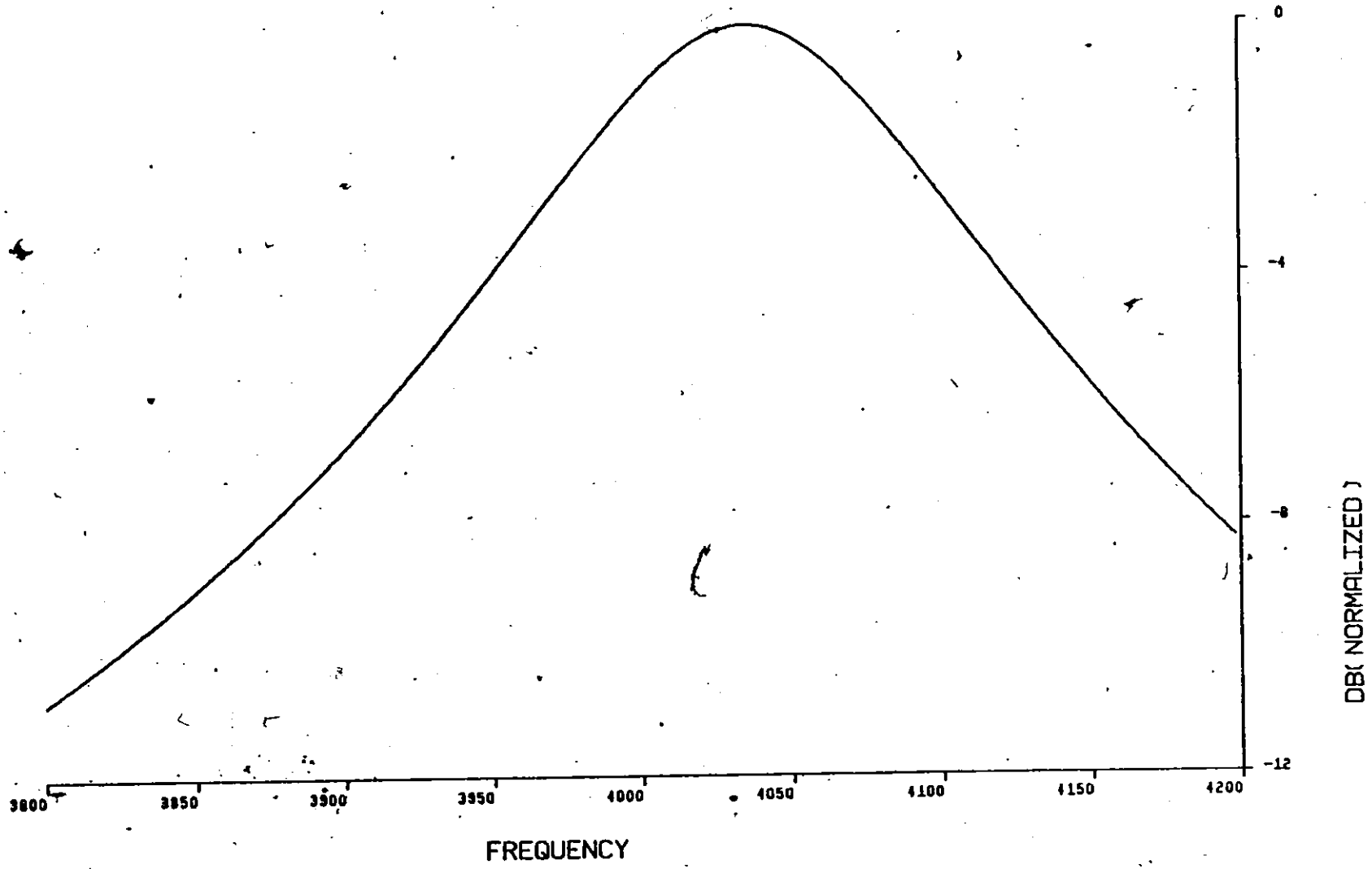

Fig. 3.17: Expansion of Fig. 3.14 in the vicinity of the peak.

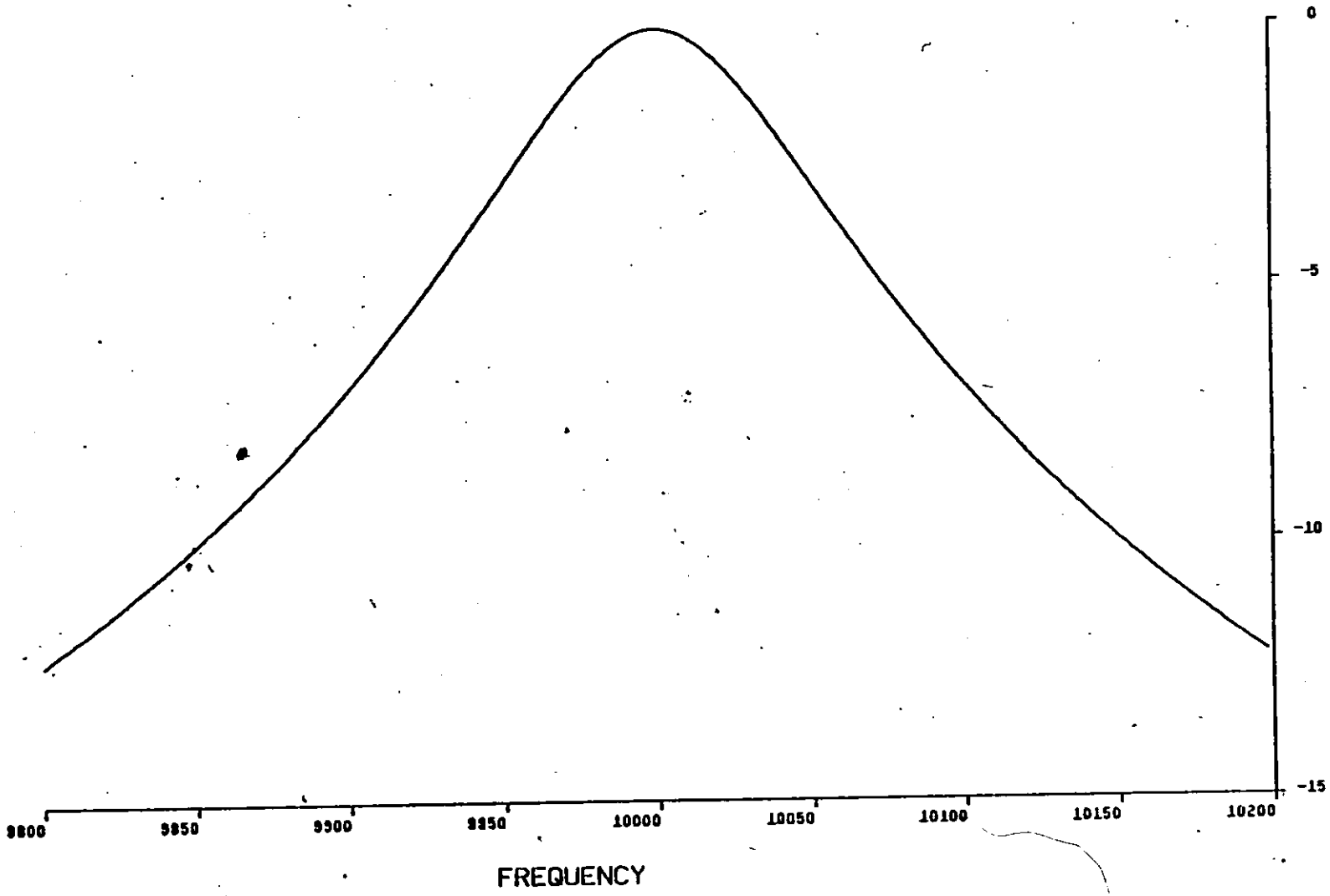

Fig. 3.18: Expansion of Fig. 3.15 in the vicinity of the peak.

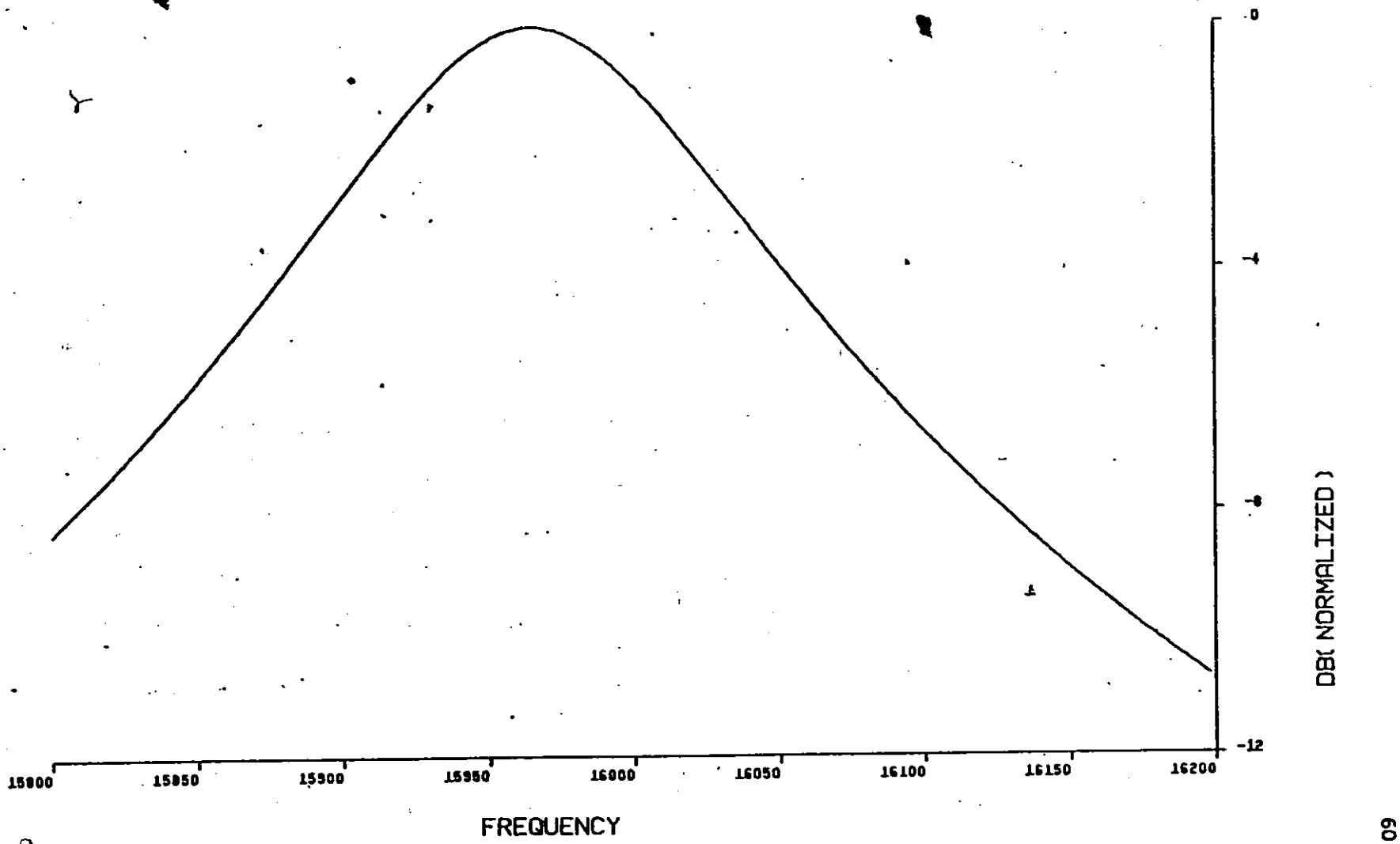

Fig. 3.19: Expansion of Fig. 3.16 in the vicinity of the peak.

Consider finding the autocorrelation of the signal

$$x(t) = \begin{cases} 0 & : \quad t < -T/2 \\ \sin \omega_c t & : -T/2 < t < T/2 \\ 0 & : \quad T/2 < t \end{cases} \tag{3.26}$$

which is a general form for the RF pulse. Since we are only considering a finite time interval, x(t) is clearly a finite energy signal and hence its autocorrelation is given by [8]

$$R_x(\tau) = \int_{-\infty}^{\infty} x(t)\, x(t-\tau)\, dt \tag{3.27}$$

where we have used the fact that x(t) is real. Substituting for x(t) in eq. (3.27) and using the property of symmetry, $R_x(\tau) = R_x(-\tau)$, we get

$$R_x(\tau) = \frac{1}{2} [T-|\tau|] \cos(\omega_c \tau) - \frac{1}{2\omega_c} \sin[\omega_c (T-|\tau|) \tag{3.28}$$

At the frequency of interest, in the region of 10 KHz, the second term in eq. (3.28) is negligible compared to the first and hence a good approximation is

$$R_x(\tau) = A [T-|\tau|] \cos(\omega_c \tau) \qquad -T < \tau < T \tag{3.29}$$

Two points to note in the autocorrelation are:

1) the carrier frequency remains unchanged

2) by processing the autocorrelation for lags within the interval [-T, T] we discard information not pertaining to the carrier frequency.

It is the second point that we hope will aid us in better exploiting the properties of the MEM.

Thus far, the autocorrelation has been found assuming zero noise. It is easily shown that if the signal is corrupted with additive

Gaussian noise, the effect is to introduce an additional term in the autocorrelation. This term takes the form

$$R_n(\tau) = \int_{-\infty}^{\infty} n(t)\, n(t-\tau)\, dt \qquad (3.30)$$

where n(t) is the Gaussian noise process. If the additive noise is white, eq. (3.30) reduces to

$$R_n(\tau) = \frac{N_o}{2}\, \delta(\tau) \qquad (3.31)$$

On the other hand, if the noise is filtered using an ideal low-pass filter the extra term in the autocorrelation is [8]

$$R_n(\tau) = N_o B \text{ sinc } (2B\tau) \qquad (3.32)$$

where B is the filter bandwidth. Equations (3.31) and (3.32) both indicate that autocorrelation has an effect of averaging out the noise.

It is a simple matter to show that the normalized Fourier transform of $R_x(\tau)$, given by eq. (3.29), is

$$S_x(f) = [\text{sinc } [(f - f_c)T]]^2 \qquad (3.33)$$

where $f > 0$ and $f_c T >> 1$. On the other hand, the normalized squared magnitude of the Fourier transform (the energy density spectrum) is also given by [8]

$$|G(f)|^2 = [\text{sinc } [(f - f_c)\, T]]^2 \qquad (3.34)$$

and the two methods are equivalent. This being the case we shall no longer consider the Fourier transform of the autocorrelation. Earlier in this section we postulated why the performance of the MEM may be improved by pre-processing via the autocorrelation. In the next section we investigate this method for an RF pulse.

3.4.1 Processing the Autocorrelation using MESA

In forming the estimate of the autocorrelation, we are faced with the choice of deciding whether to use a biased or unbiased estimate (eqs. (3.35) or (3.36) respectively) [13].

$$R(m) = \frac{1}{N} \sum_{n=0}^{N-1-m} x(n)\, x(m+n) \qquad 0 \leq m \leq N-1 \tag{3.35}$$

$$R(m) = \frac{1}{N-m} \sum_{n=0}^{N-1-m} x(n)\, x(m+n) \qquad 0 \leq m \leq N-1 \tag{3.36}$$

Our estimate will be based on eq. (3.35) which places less confidence on the higher lags. The reason for this choice is that estimates of higher lags are based on fewer samples and hence less reliable. Moreover, since the duration of the sinusoid is N/2, we shall limit the lags to the range $0 \leq m \leq N/2 - 1$. Figure 3.20 shows our estimate of the autocorrelation of the pulse in Fig. 3.9 for positive and negative lags m.

Figures 3.21, 3.22 and 3.23 show the results of processing the autocorrelation of the three RF pulses (Fig. 3.8, 3.9 and 3.10) using the MEM. For brevity, we shall henceforth refer to this form of processing by the abbreviation MEMCOR. An expanded view of the three spectra is provided in Figs. 3.24, 3.25 and 3.26. A comparison of these results with those for the MEM indicates a dramatic improvement in resolution while maintaining a filter order of 3. Further, there is no degradation in the accuracy of the location of the peak.

In order to see the effect of noise, the pulse of Fig. 3.9 with additive noise has been processed using MEMCOR. Results for values of SNR in the range 20 dB to -10 dB are given in Figs. A3.1 to A3.9. Once

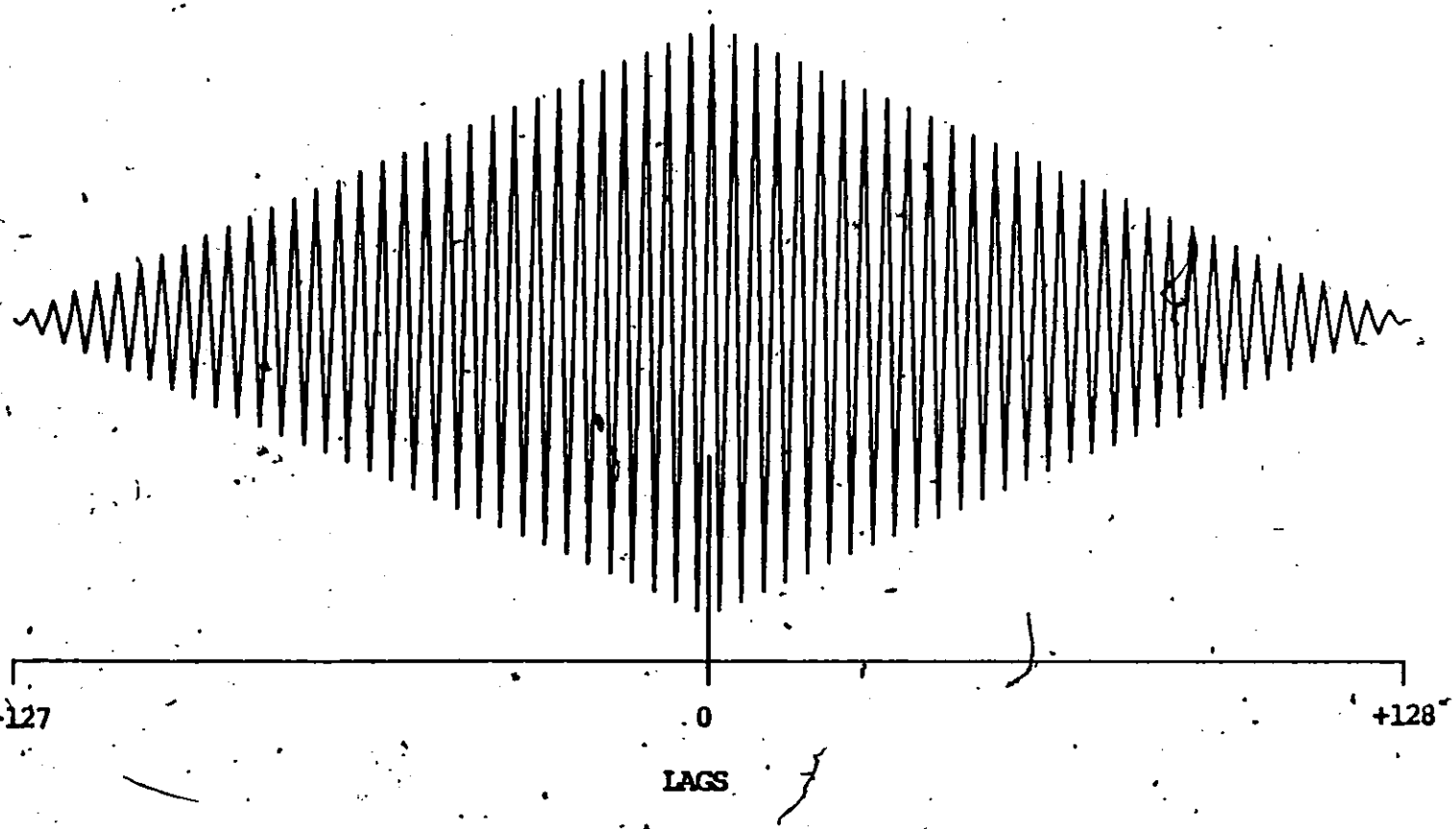

Fig. 3.20: Autocorrelation of an RF pulse with f_c = 10 KHz.

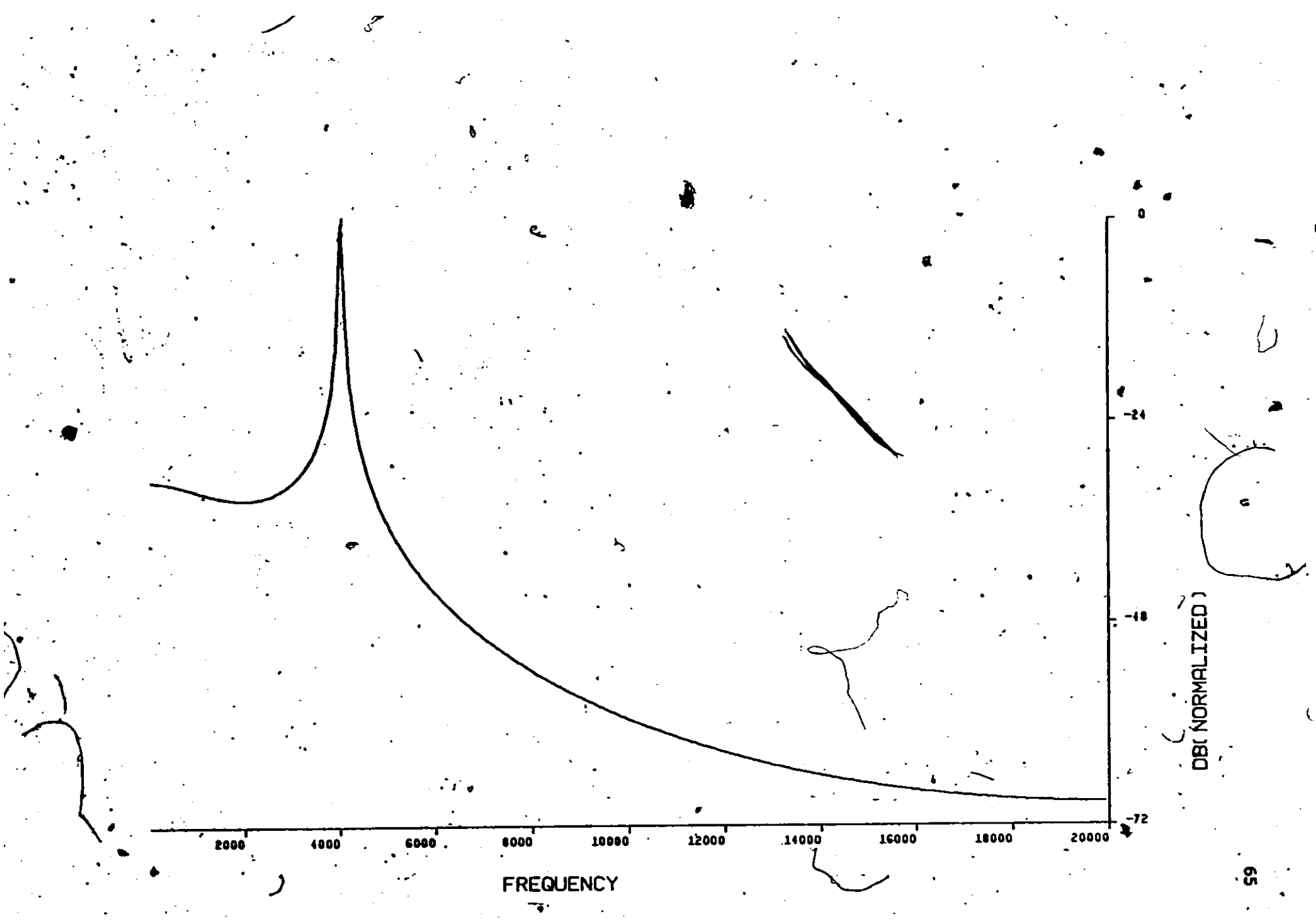

Fig. 3.21: MEM of the autocorrelation of an RF pulse with f_e = 4 KHz.

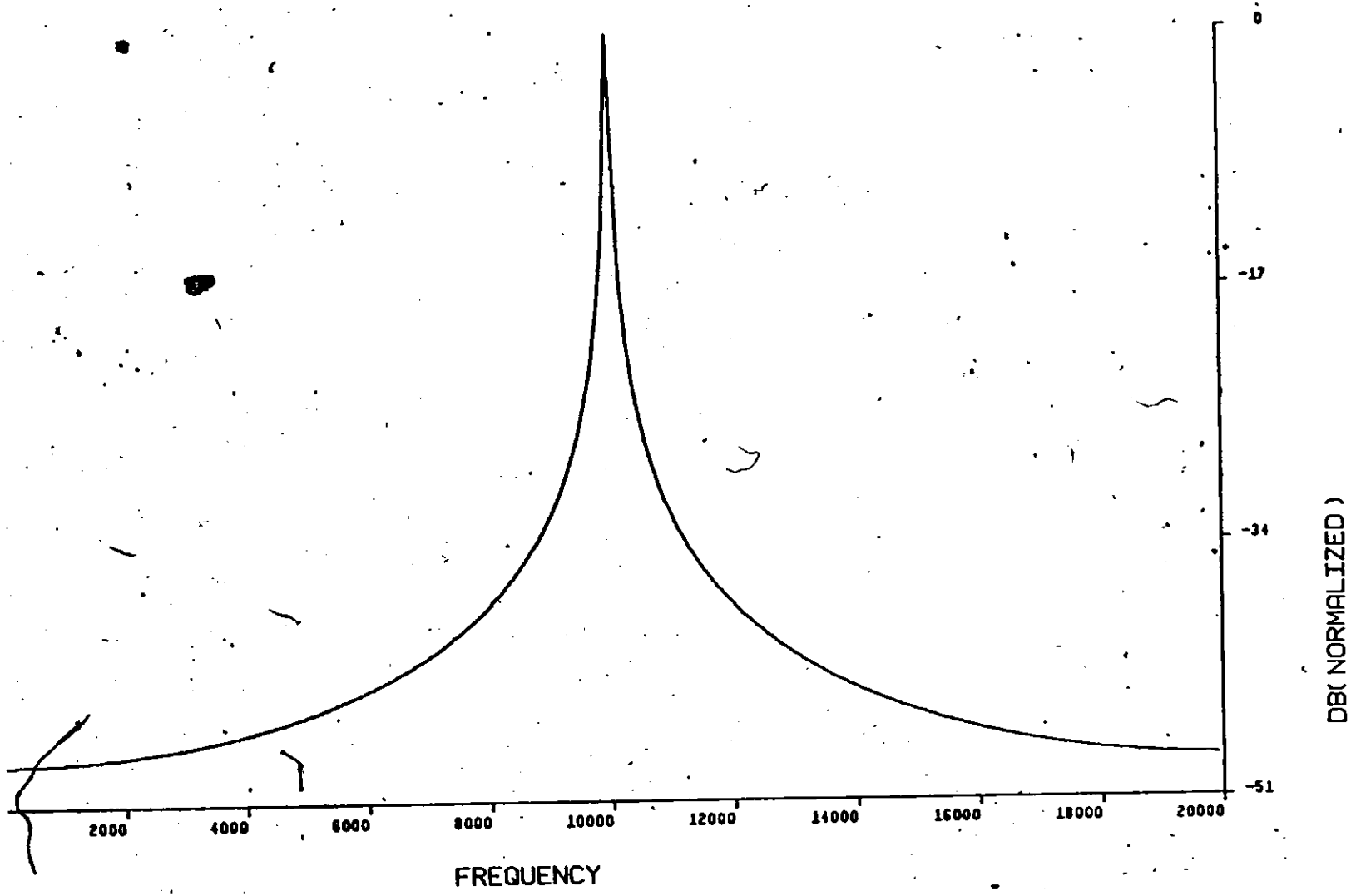

Fig. 3.22: MEM of the autocorrelation of an RF pulse with f_c = 10 KHz.

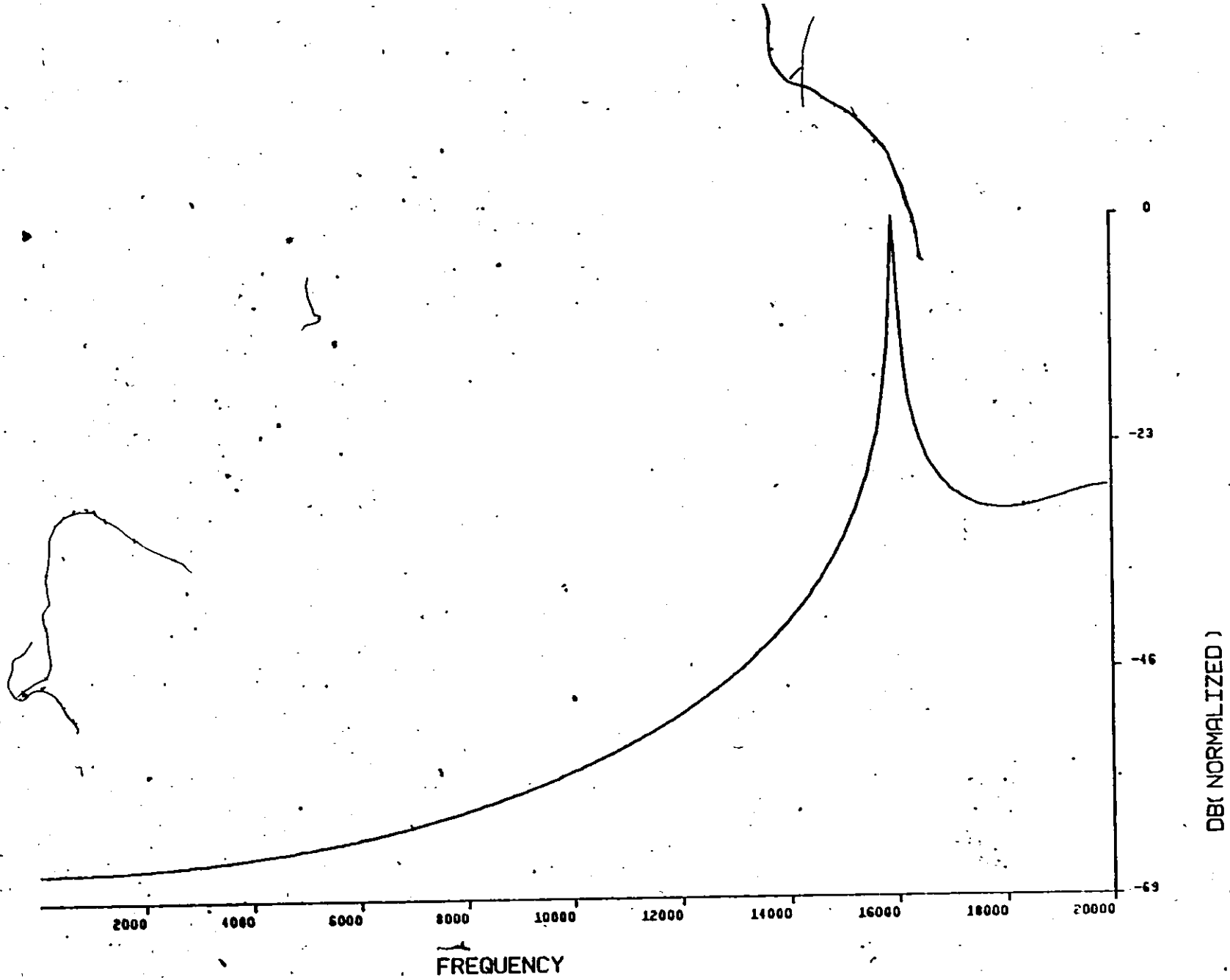

Fig. 3.23: MEM of the autocorrelation of an RF pulse with f_c = 16 KHz.

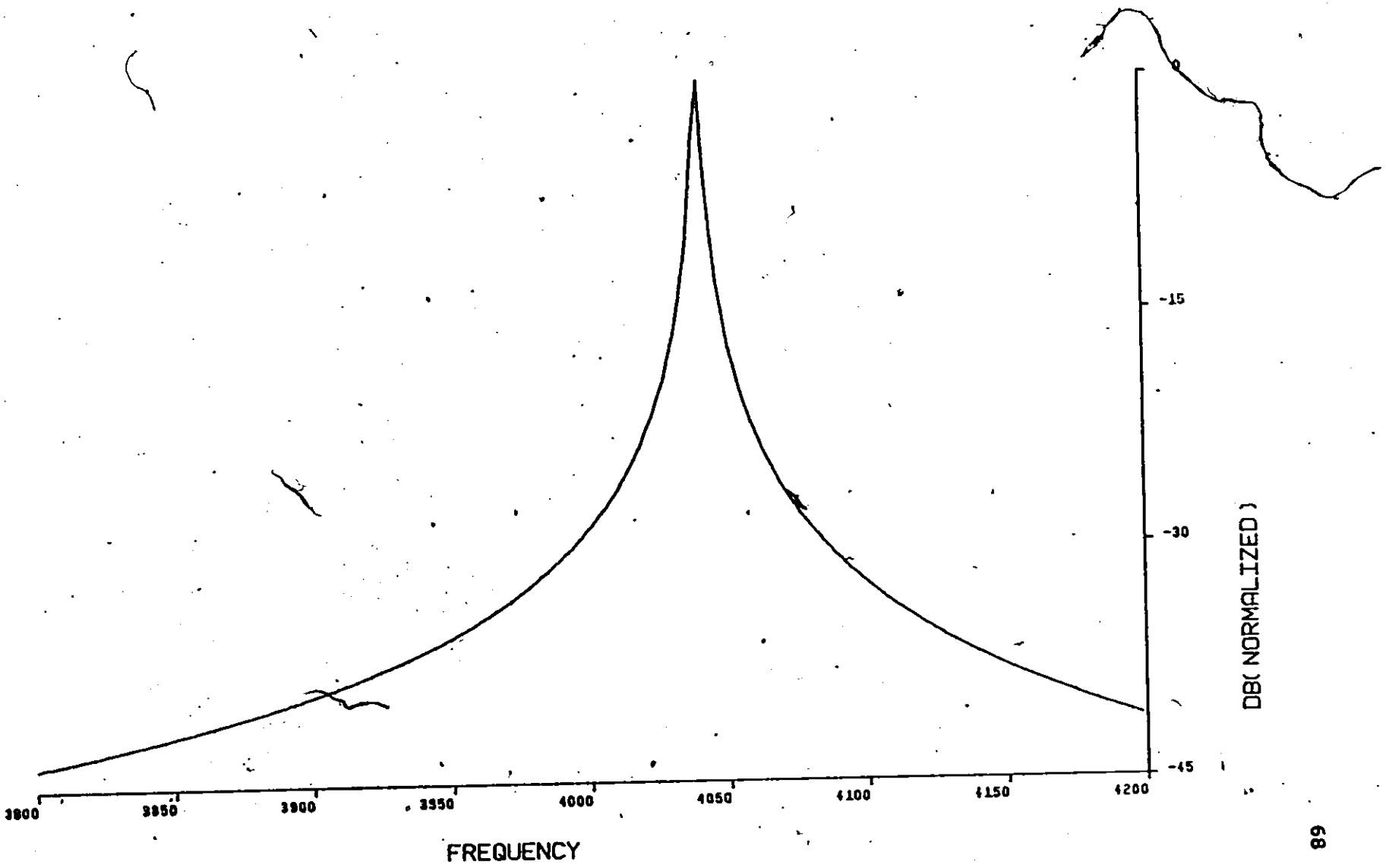

Fig. 3.24: Expansion of Fig. 3.21 in the vicinity of the peak.

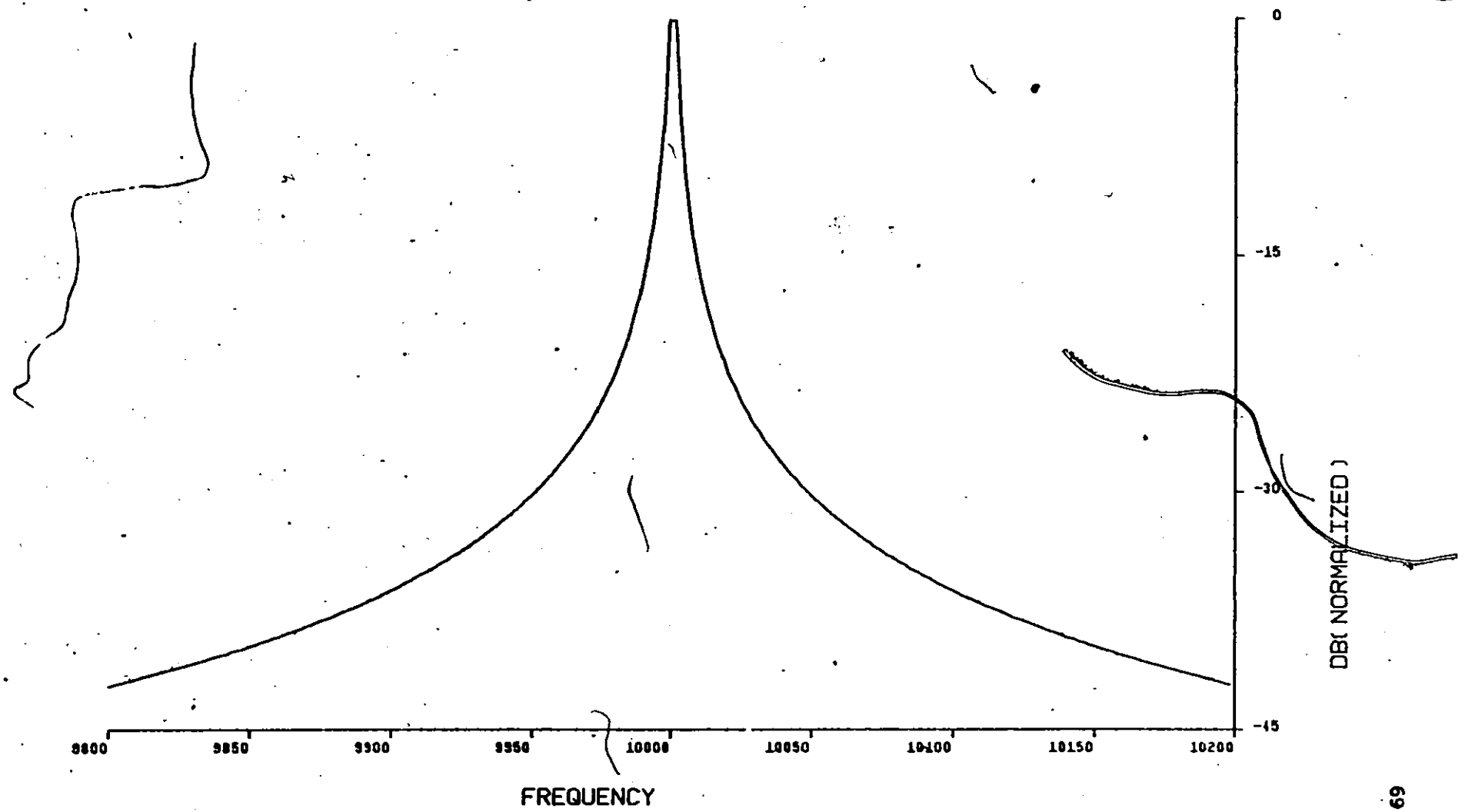

Fig. 3.25: Expansion of Fig. 3.22 in the vicinity of the peak.

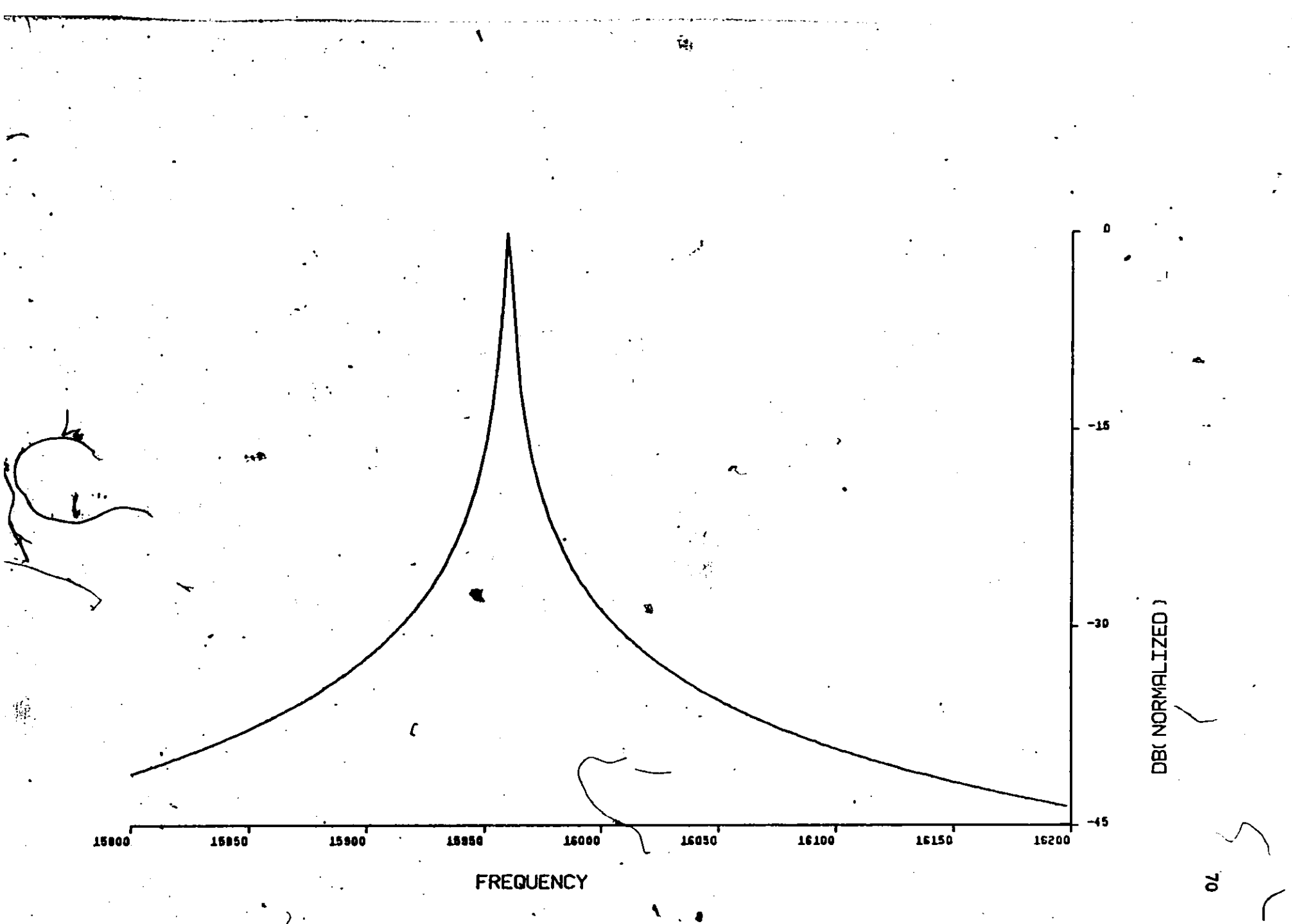

Fig. 3.26: Expansion of Fig. 3.23 in the vicinity of the peak.

again a comparison with the straightforward MEM indicates the far superior resolution of the MEMCOR. Even at an SNR of OdB, the MEMCOR provides very good resolution. As before, in all cases the filter order has been maintained at 3, and the accuracy of the location of the peak has been found to be no worse than the MEM.

In this Chapter we have provided a detailed description of three methods of signal processing with the third method being a slight variation of the MEM. We have attempted to provide some insight into the expected results for each method by processing a well known signal, namely the RF pulse. Furthermore, in presenting these results we have verified that the algorithm for each method performs appropriately. In Chapter 4 we gauge the performance of each method for ideal ELT signals.

CHAPTER 4

PROCESSING SINGLE ELT SIGNALS

So far we have considered the effect of processing RF pulses with the aim of verifying that the algorithms used do indeed perform in an acceptable fashion. One fact we noted was that abrupt changes in the signal envelope, as with an RF pulse, tend to hamper detection by the MEM by broadening the main lobe. We showed that a possible method of combating this situation is to remove the abrupt changes by forming the autocorrelation. Since many ELT units transmit a signal which employs pulse modulation with varying duration, it is expected that by similar pre-processing we can improve the performance of the MEM.

We begin this Chapter by providing an explanation of our choice of sampling rate. Following this we examine the processing results for the FFT, the MEM and the MEM with autocorrelation. Since the number of plots to be included is quite large, wherever feasible we have tried to put multiple curves on a single plot. For ease in viewing these plots, the hoirzontal axis has been set so as to coincide with all curves on a particular plot. Each curve has been separately normalized to its peak with the vertical scale in decibels, thus the peak of each curve is the 0 dB point for that curve. Subsequent curves on a single plot have been shifted vertically for clarity. A vertical distance representing a 10 dB difference is marked on each plot. This reference scale is common to all curves on a single plot.

4.1 Signal Sampling and Overall Spectral Plots

We noted earlier that the Doppler spread is approximately ±3 KHz. Furthermore, the expected variation in frequency of the oscillators used in ELT units is ±3 KHz. Because this is a long term instability, the variation over the course of a single satellite pass for any given ELT is negligible. However, the Doppler coupled with the expected oscillator frequency variation implies that after mixing down to an intermediate frequency the carrier component will lie in a region ±6 KHz about the IF centre frequency. For the simulation we chose an IF of 10 KHz which results in a carrier within the interval 4 KHz to 16 KHz. The Nyquist criterion requires a sampling rate of at least twice the highest frequency component in the signal. By choosing a sampling rate of 40 KHz (twice the Nyquist rate of the intermediate frequency) we satisfy the Nyquist requirement since 40 KHz is approximately 1.5 times the Nyquist rate of the upper frequency of interest, namely, 16 KHz.

4.2 Block Processing the Received Signal

Given that the duration of a single modulation sweep is a quarter of a second, a sampling rate of 40 KHz results in 10,000 samples over a single sweep. In the simulation, the received signal is sectioned into blocks of 256 samples and the processing performed on a per block basis. Since the modulation is repetitive and there is a non integer number of blocks over a single modulation sweep, the position of the blocks relative to the start of the modulation sweep is of no consequence. In view of this, we shall henceforth section the signal so that the first

sample of the first block coincides with the start of a modulation sweep. Moreover, unless otherwise specified we shall assume the carrier has a phase of zero at the start of the modulation.

Figure 4.1 shows blocks 3, 14, 27 and 38 (arbitrarily selected) of an ELT signal at an SNR of 30 dB with a square modulation and a linear frequency sweep. The duty cycle of the modulating pulses is 0.4. A comparison of the various blocks indicates quite clearly the increase in pulse duration as a result of the linearly decreasing frequency sweep from which we determine the rise and fall times of the pulses. Since we would also like to process the ELT signal by applying the MEM to the autocorrelation of the signal, we include in Fig. 4.2 a plot of the normalized autocorrelation of the blocks of Fig. 4.1. Our calculation of the autocorrelation is again based on the biased estimate of eq. (3.35). Moreover, for reasons given in Chapter 3, we restrict the estimate to lags in the range $0 \leq |m| \leq N/2 - 1$. A point worthy of note is the large reduction in null time brought about by taking the autocorrelation. As was the case with an RF pulse we would expect this reduction in null time to improve the MEM results. Blocks 3, 14, 27 and 38 of an ELT signal employing a sinusoidal modulation with a linear frequency sweep are shown in Fig. 4.3. Parameters relevant to this signal are the modulation factor and the SNR which have been set at 1.0 and 30 dB respectively. The autocorrelation (normalized) of the blocks of Fig. 4.3 are shown in the plots of Fig. 4.4. Before discussing the results of processing these sets of signals we point out that the carrier frequency is arbitrarily selected to be 9378 Hz for

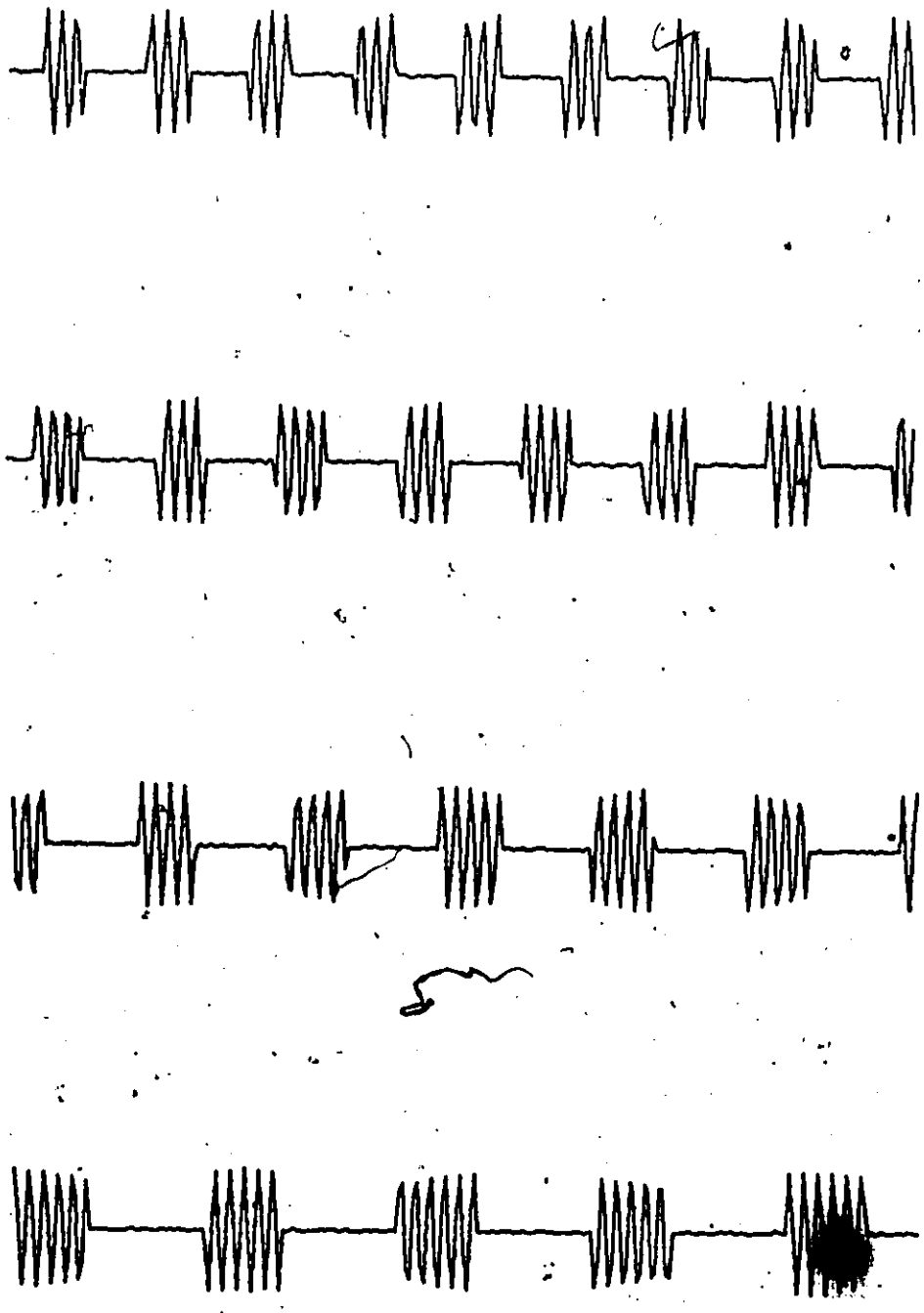

Fig. 4.1: Blocks 3, 14, 27 and 38 of an ELT signal employing square modulation with a linear frequency sweep. SNR = 30 dB, duty cycle = 0.4.

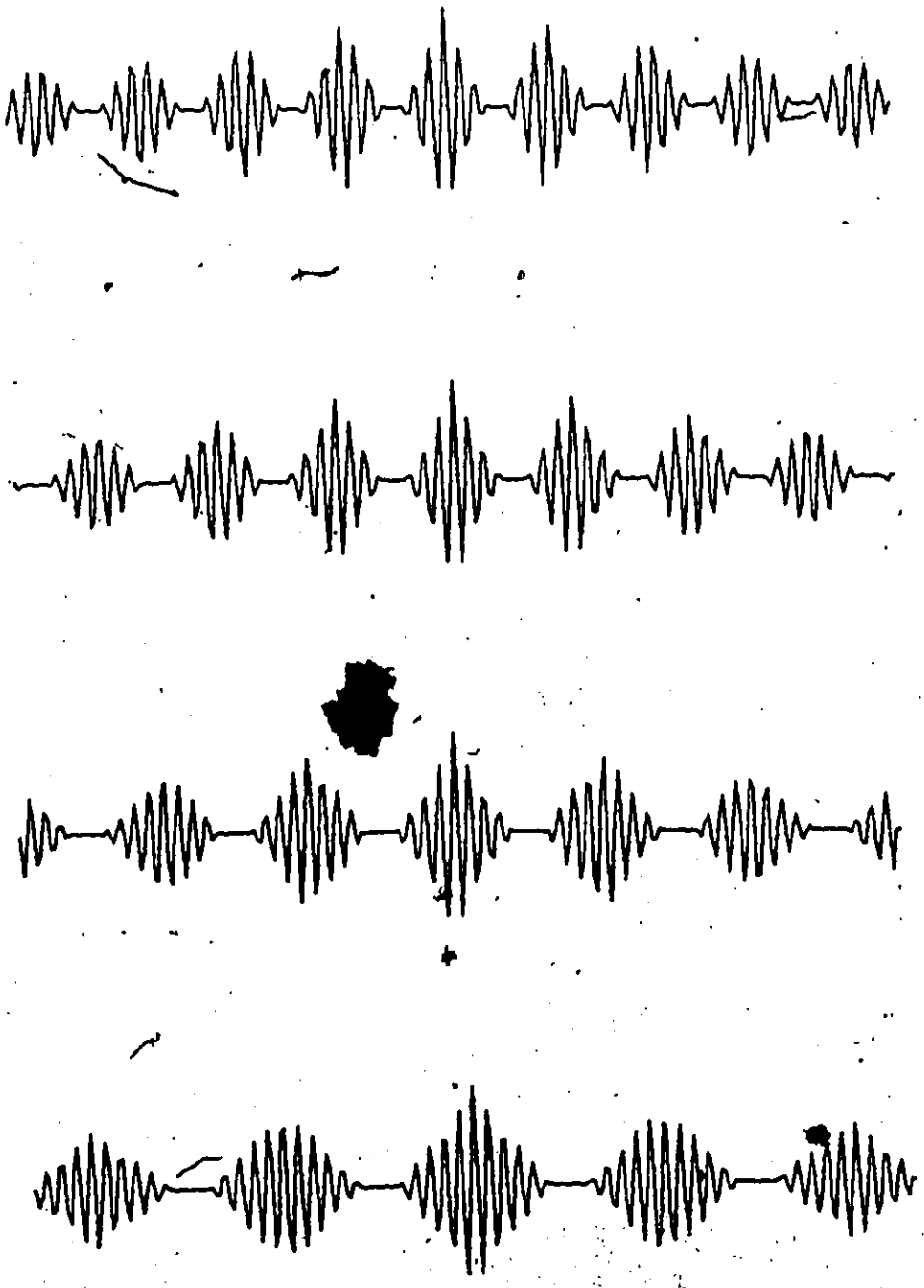

Fig. 4.2: Normalized autocorrelations of the blocks in Fig. 4.1.

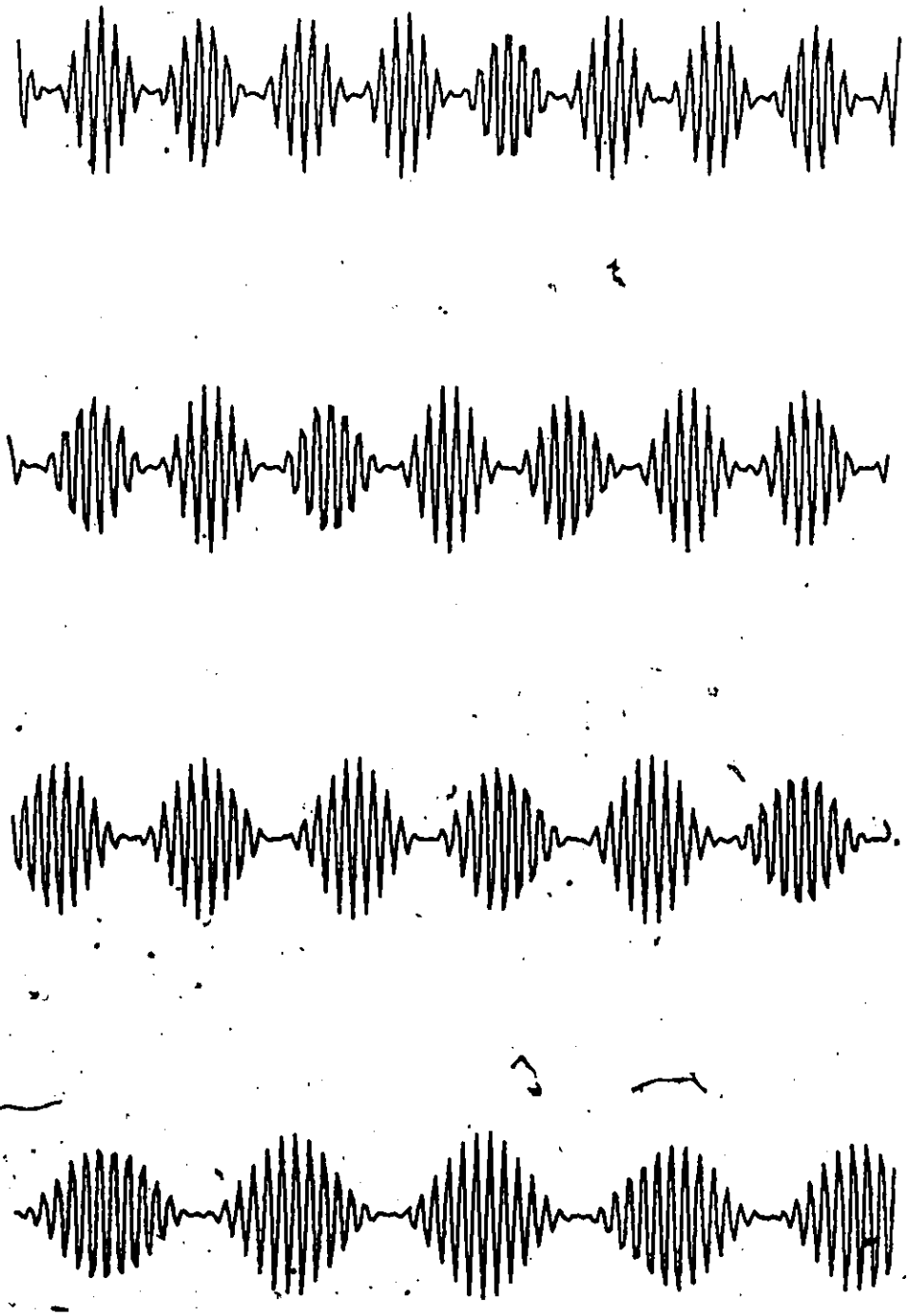

Fig. 4.3: Blocks 3, 14, 27 and 38 of an ELT signal employing a sinusoidal modulation with a linear frequency sweep. SNR = 30 dB, modulation index = 1.0.

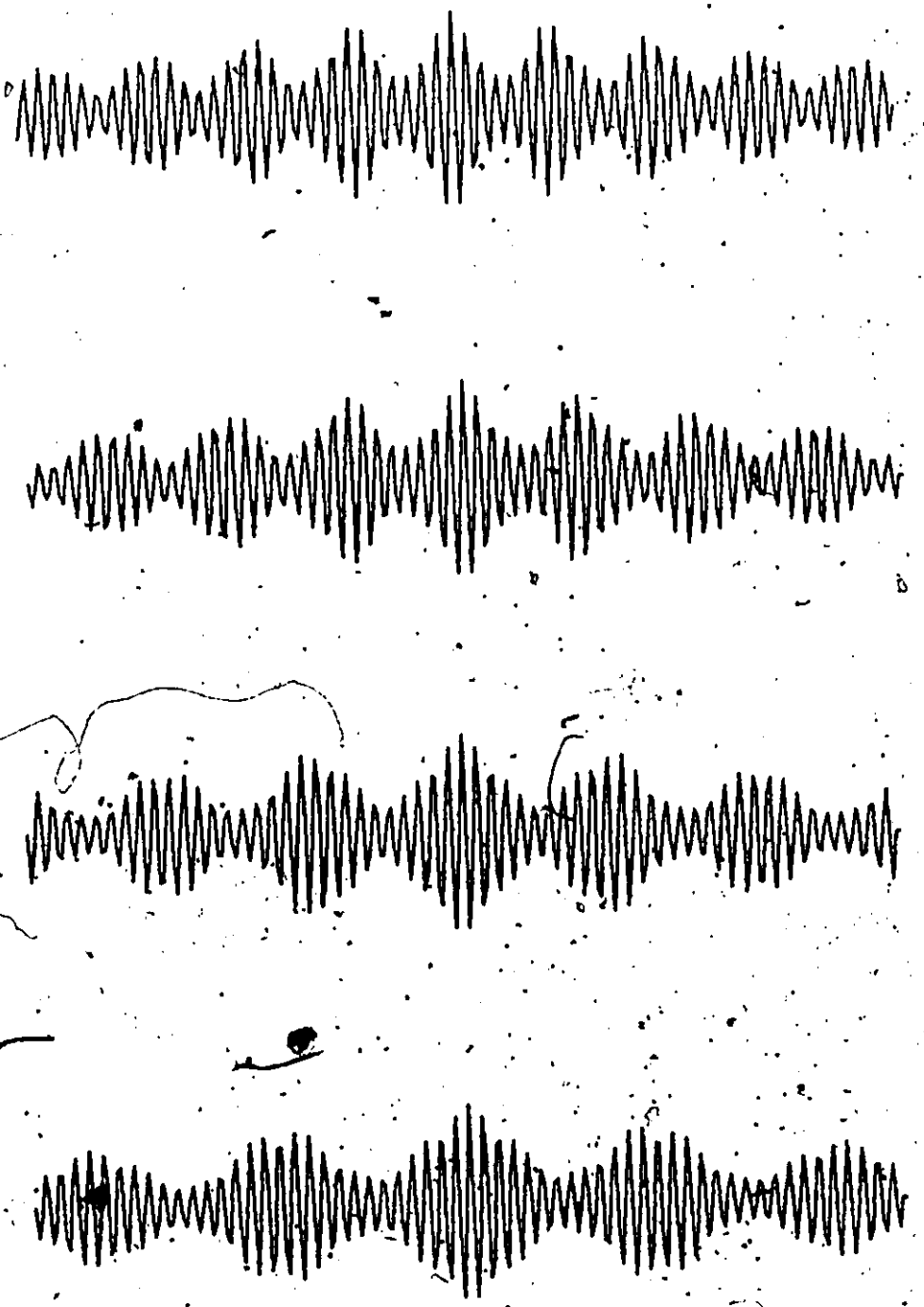

Fig. 4.4: Normalized autocorrelations of the blocks of Fig. 4.3.

both Fig. 4.1 and Fig. 4.3.

Results of processing the blocks of Fig. 4.1 using the FFT, the MEM and the MEMCOR are shown in Figs. 4.5, 4.6 and 4.7, respectively. Each curve is labelled to indicate the corresponding data block. A comparison of the FFT spectra indicates a shift in the sidelobes, in the direction of the main lobe, as we process blocks that appear later along a given modulation sweep. This is as we would expect as a result of an increase in pulse duration along a modulation cycle. The sidelobes are approximately 4 dB down from the main lobe which could impose a severe limitation in detecting multiple signals.

Figures 4.6 and 4.7 indicate that the MEM offers advantages over the FFT since it does not suffer from the sidelobe problems we noted above. A problem with the MEM is the rather broad main lobe that results from processing a pulse modulated signal (Fig. 4.6). Figure 4.7 shows that a significant sharpening of the spectra can be achieved by processing the autocorrelation of the signal. By forming the autocorrelation, we modify the signal so that we average the information pertaining to the carrier frequency over a larger interval of the processed data as can be seen by comparing Figs. 4.1 and 4.2. As explained in Chapter 3 this modification has the effect of reducing the duration of the nulls between the RF pulses and hence enhancing adaptation in the MEM.

In order to compare results for the two kinds of modulation, we process blocks 3, 14, 27 and 38 of a sinusoidal modulated signal (shown in Fig. 4.3) using the three methods. Figures 4.8, 4.9 and 4.10 show

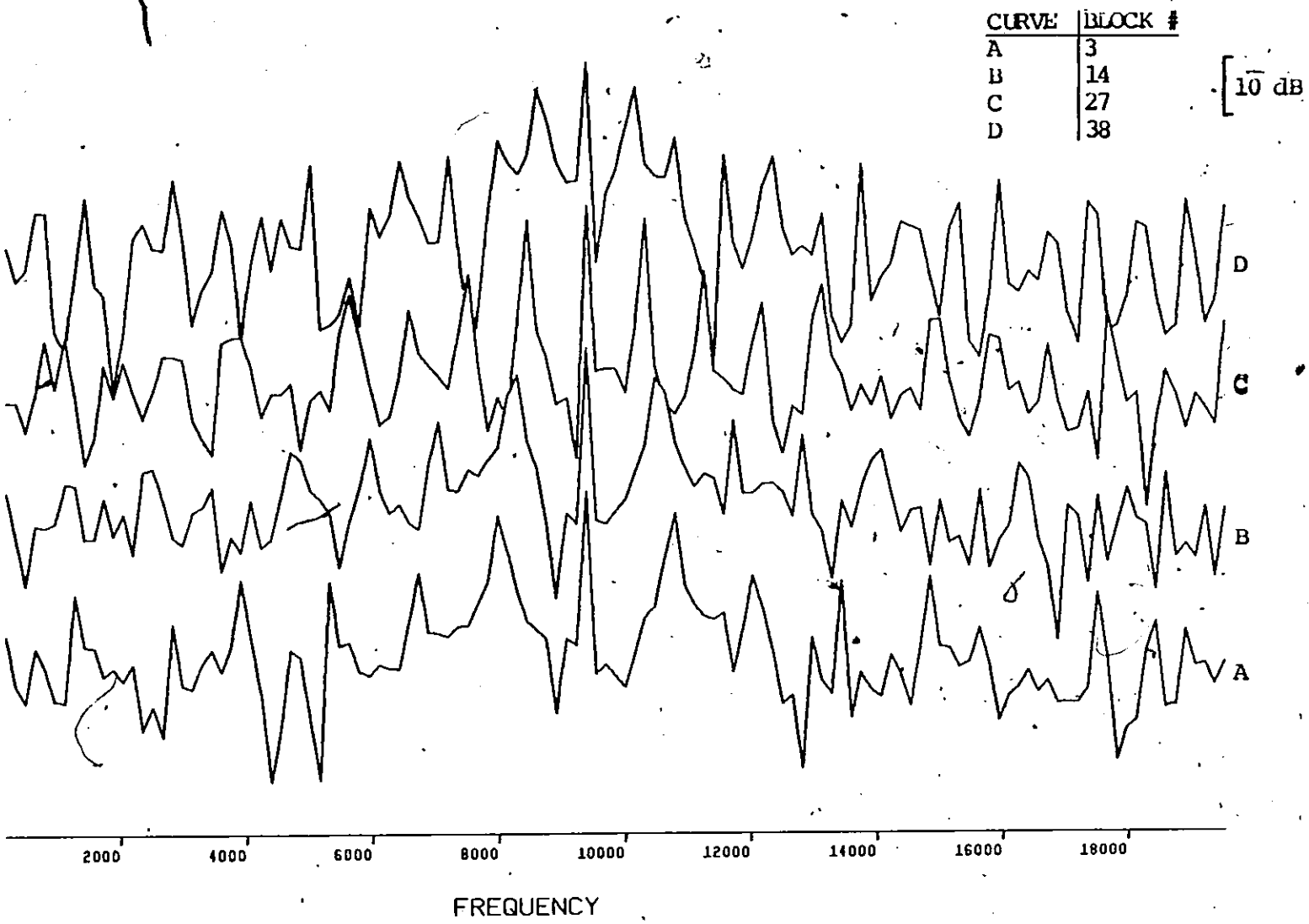

Fig. 4.5: Amplitude spectra of the blocks of Fig. 4.1.

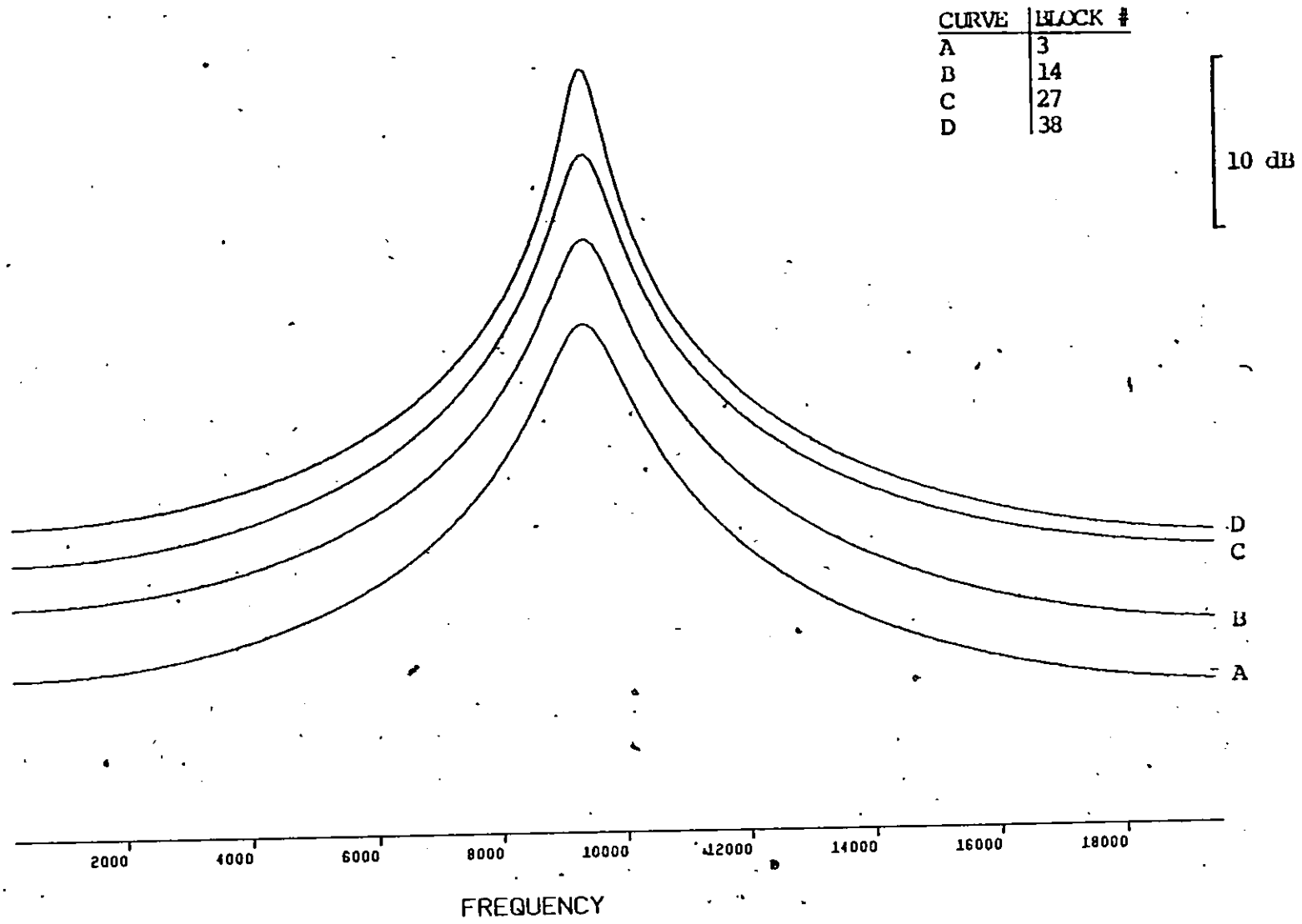

Fig. 4.6: ME spectra of the blocks of Fig. 4.1.

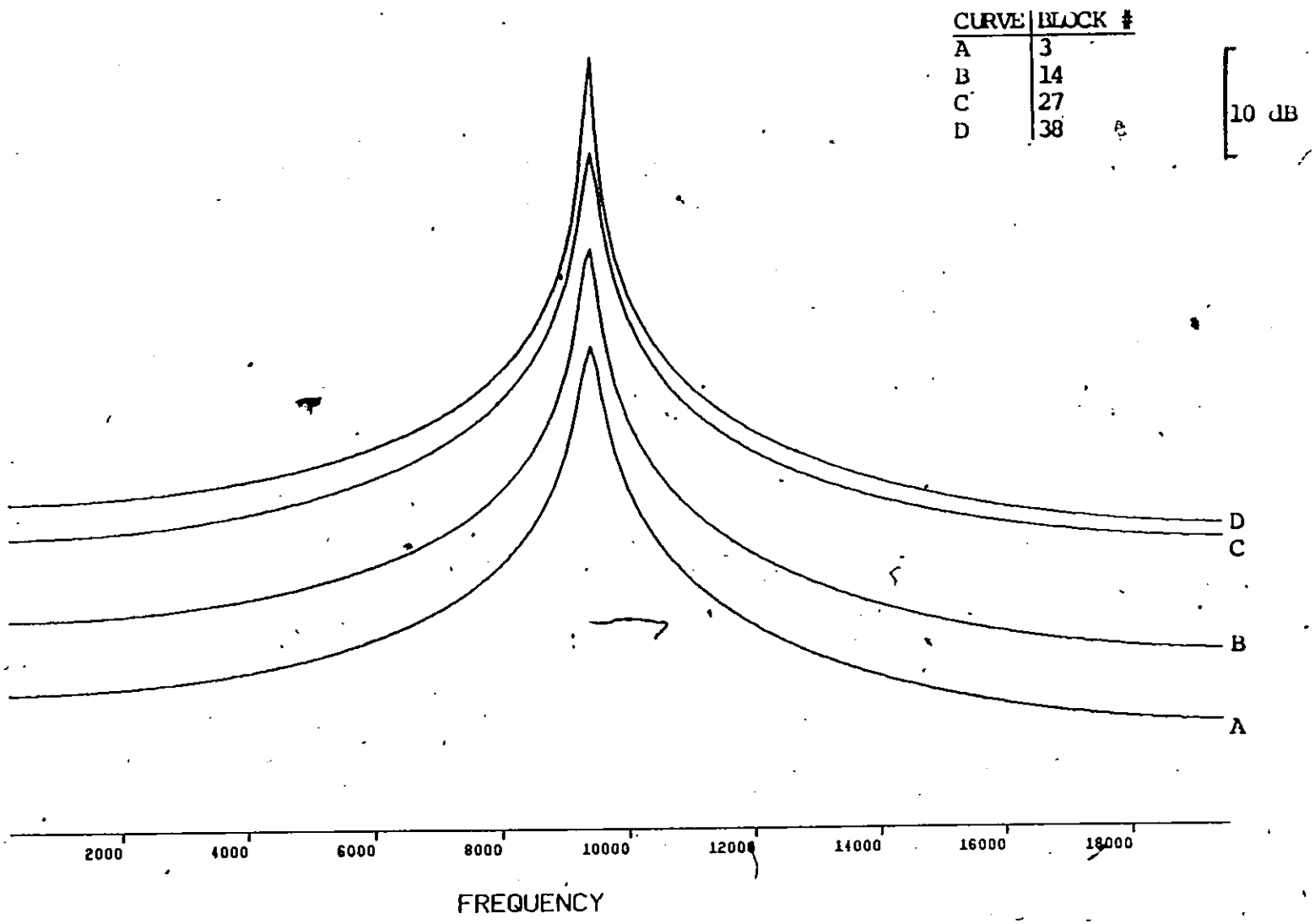

Fig. 4.7: ME spectra of the autocorrelations of the blocks of Fig. 4.1.

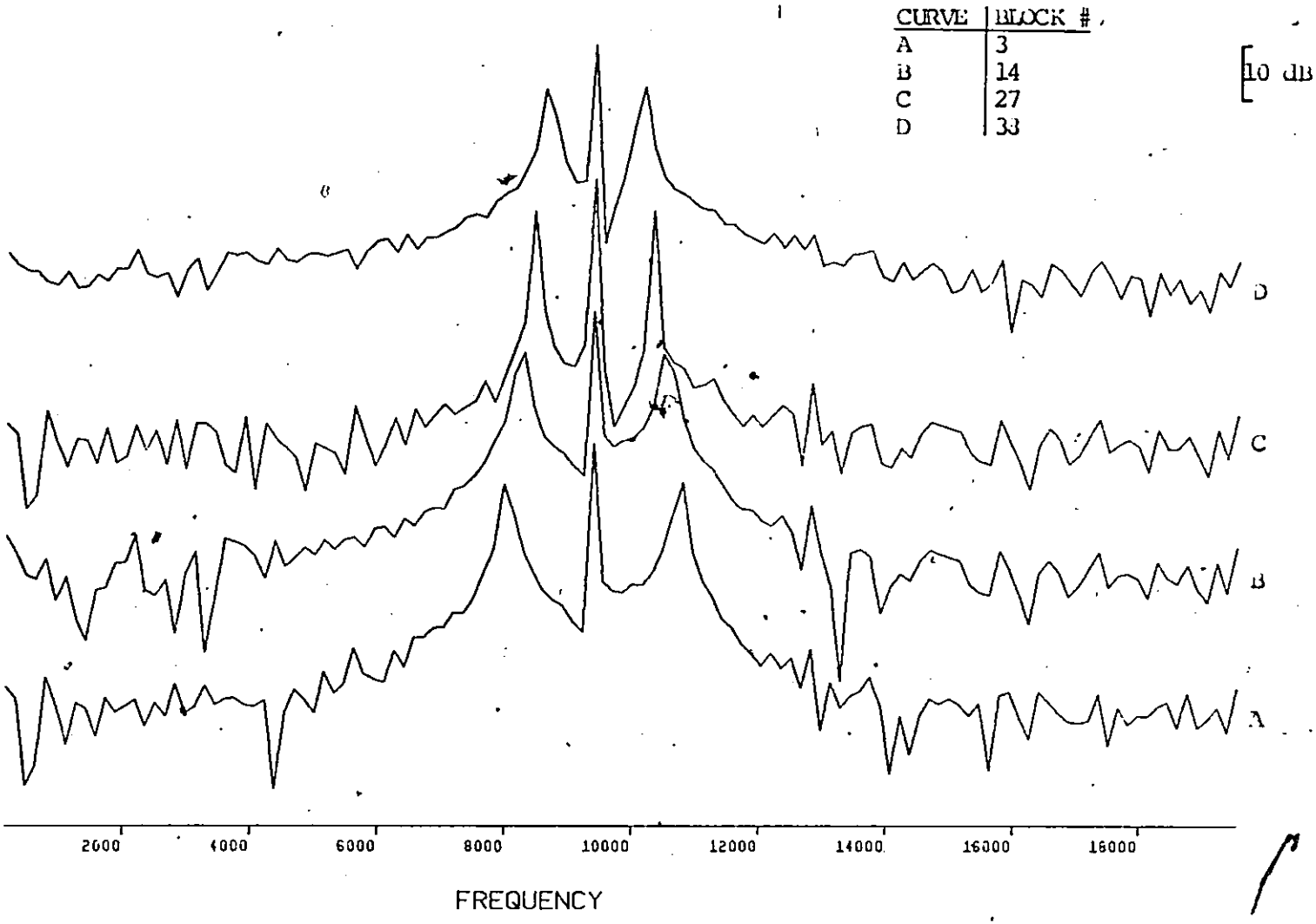

Fig. 4.8: Amplitude spectra of the blocks of Fig. 4.3.

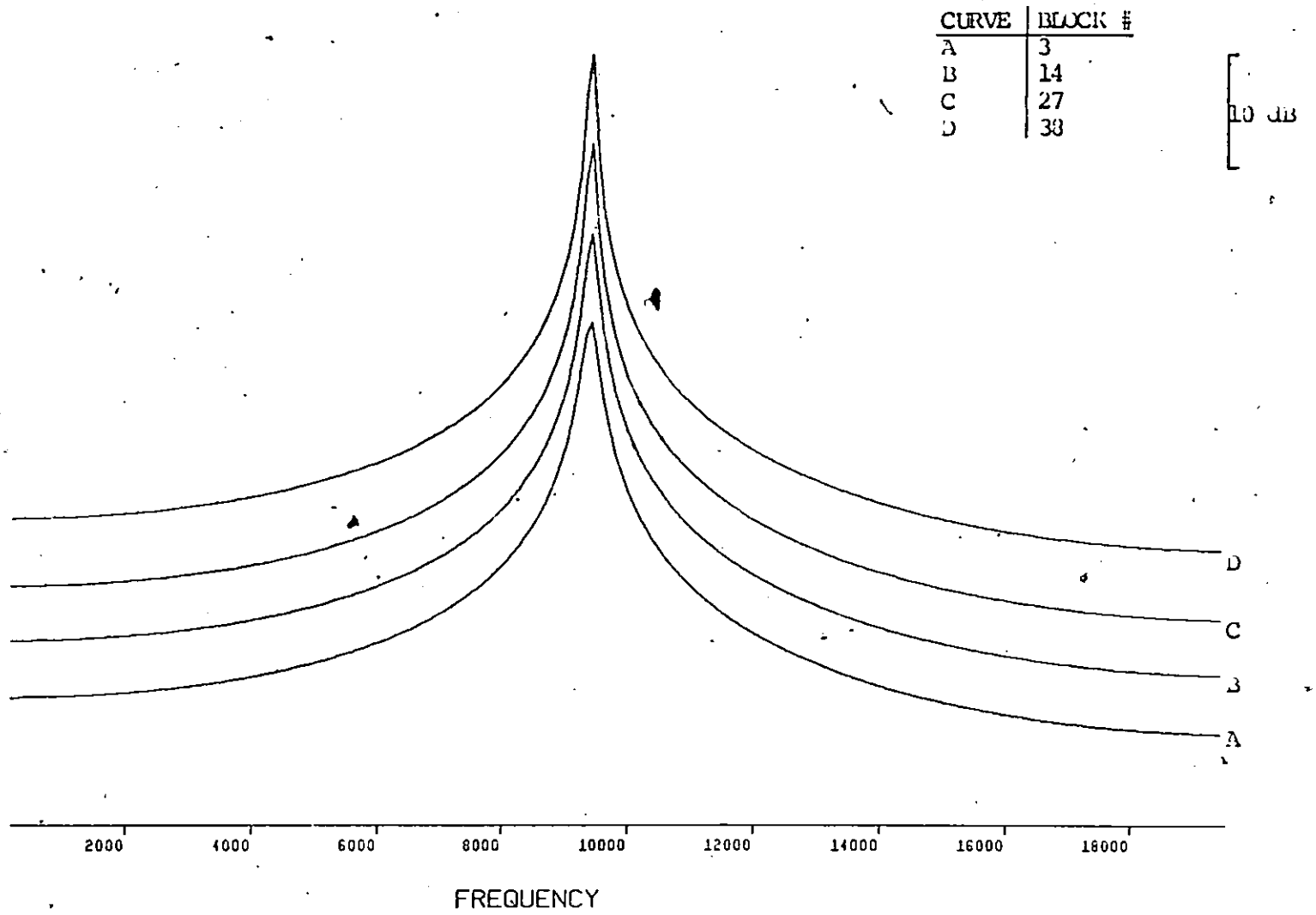

Fig. 4.9: ME spectra of the blocks of Fig. 4.3.

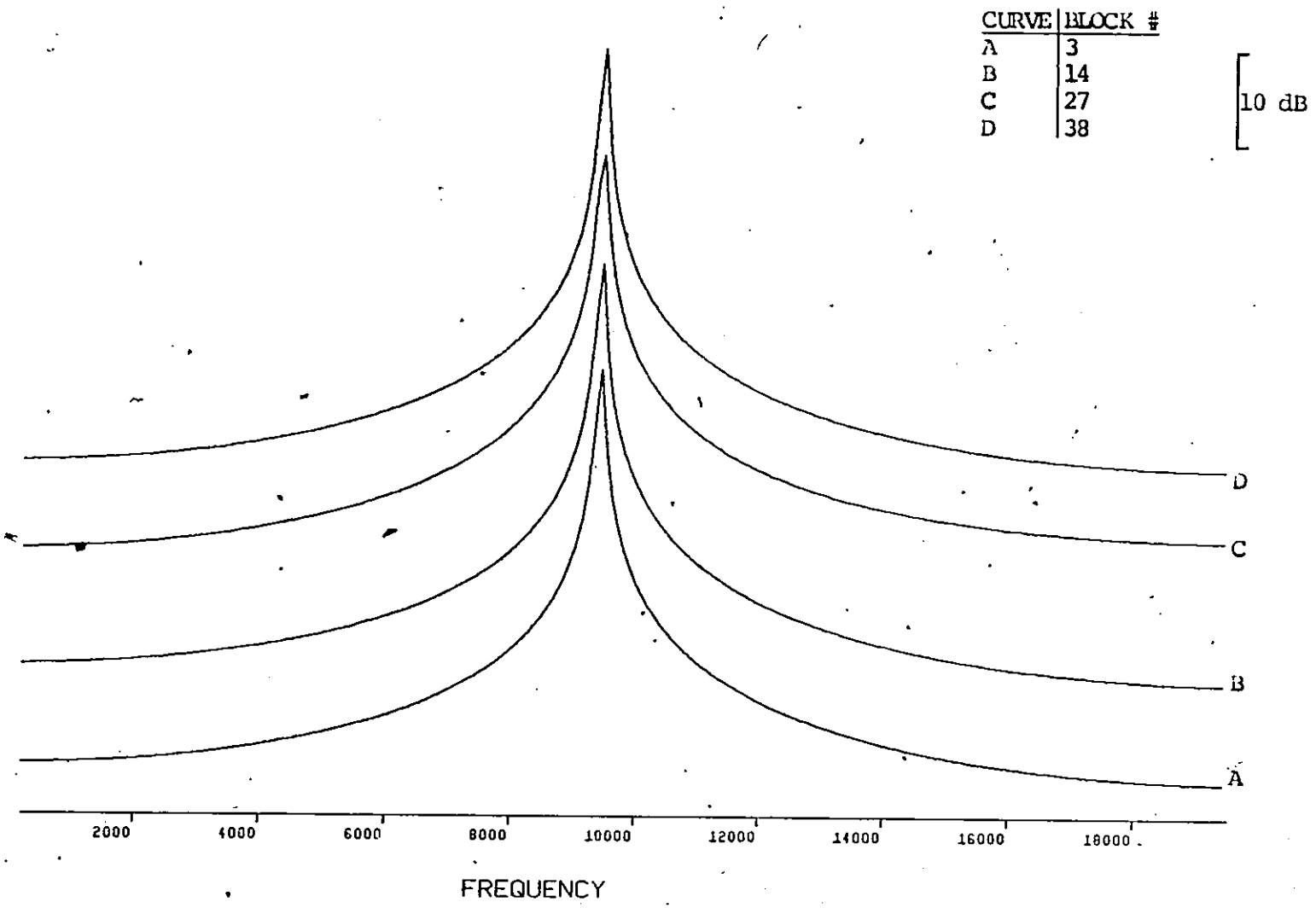

Fig. 4.10: ME spectra of the autocorrelations of the blocks of Fig. 4.3.

results for the FFT, the MEM and the MEMCOR respectively. The FFT spectrum now has its main lobe centered at the carrier frequency and sidelobes located at points corresponding to the sum and difference frequencies of the carrier and the sinusoidal modulation. Consider, for example, the data block of Fig. 4.3(a). The average instantaneous modulation frequency for this block is approximately 1355 Hz which is consistent with the sidelobes appearing at frequencies around 9378 Hz + 1355 Hz and 9378 Hz - 1355 Hz. Sidelobe problems are less severe for this type of signal as they are roughly 6.5 dB below the main lobe.

Figures 4.9 and 4.10, which show results for the MEM and the MEMCOR respectively, indicate that the MEM offers advantages over the FFT since it does not give rise to sidelobe problems. Comparing results for the MEM and the MEMCOR we note that no significant benefit is obtained by processing the autocorrelation of a sinusoidal modulated signal as opposed to the pulse modulated case where processing the autocorrelation lead to a significant improvement. One other major difference between the two basic types of ELT signals is, when processing different blocks of a sinusoidal modulated signal, the difference between spectra of blocks at the start of a modulation and at the end of a modulation is not as large as for a pulse modulated signal. From the foregoing, it is apparent that in a sense, the pulse modulated ELT signal offers the worst case from a detection viewpoint regardless of whether processing is performed by way of the MEM or the FFT.

4.3 Spectral Comparison with Variations in Modulation

Although the ELT signals can take on any of a variety of different formats, they can be separated into two broad categories depending on whether the modulation is sinusoidal or square. This section is devoted entirely to determining the effect of processing signals of different formats. Based on these results we choose a format which is, in a sense, representative of the worst case and limit further study in this Chapter to that particular format. Furthermore, since the effect of variations in signal to noise ratio is investigated later in the Chapter we shall limit present study to the case of high SNR (30 dB). For ease of reference we restate some of the equations defining the ELT signal and indicate the bounds on some of the parameters. The transmitted signal is defined by

$$S(t) = A_c\,[1 + m(t)] \sin \omega_c t \tag{4.1}$$

where, for a sinusoidal modulation, m(t) is given by eq. (4.2).

$$m(t) = \mu \sin[\theta_i(t)] \tag{4.2}$$

In eq. (4.2), μ is the modulation factor and $\theta_i(t)$ is the instantaneous phase given by eq. (2.3). Recall from Chapter 2 that $\theta_i(t)$ is dependent only on the type of frequency sweep used (linear or quadratic) and the modulation index is in the range $0.85 \leq \mu \leq 1.0$. A square modulation is defined by the train of pulses of Fig. 2.1 with the rise and fall times (t_j and p_j) of the j^{th} pulse found by solving the equations

$$\frac{1}{2\pi}\,[\theta_i(t = t_j) - \theta_i(t = 0)] = j-1 \tag{4.3}$$

$$\frac{1}{2\pi}\,[\theta_i\,(t = P_j) - \theta_i(t = 0)] = j-1+d \tag{4.4}$$

where $\theta_i(t)$ is defined by eq. (2.3). The duty cycle (d) lies in the range $0.3 \leq d \leq 0.5$ and is related to the rise and fall times through eq. (4.5)

$$d = (p_j - t_j)/(t_{j+1} - t_j) \qquad (4.5)$$

Having re-acquainted ourselves with the ELT signal we examine some of the processing results.

Figures 4.11, 4.12 and 4.13 show results of processing square modulated signals with modulations derived from two kinds of frequency sweeps (linear and quadratic). The FFT indicates very little difference in the results with the sidelobes being at approximately the same levels for both types of signals (Fig. 4.11). Results for the MEM are also comparable. As indicated in Fig. 4.13, although a difference in frequency sweep has very little effect on the MEMCOR, there is a noticeable improvement to be gained by applying the MEM to the autocorrelation rather than applying it directly to the set of samples. Again this supports the conclusions reached from previous results.

Plots of Figs. 4.14, 4.15 and 4.16 pertain to a sinusoidal modulated ELT signal. Contrasting these curves with those of Figs. 4.11, 4.12 and 4.13 indicates that the major difference occurs not from the choice of frequency sweep but by changing from a square modulation to a sinusoidal modulation. A sinusoidal modulated ELT signal yields a much sharper spectrum. Comparing Figs. 4.15 and 4.16 we find that taking the autocorrelation of a sinusoidal modulated signal prior to applying the MEM leads to very slight improvement.

To complete our investigation of variations in modulation we need

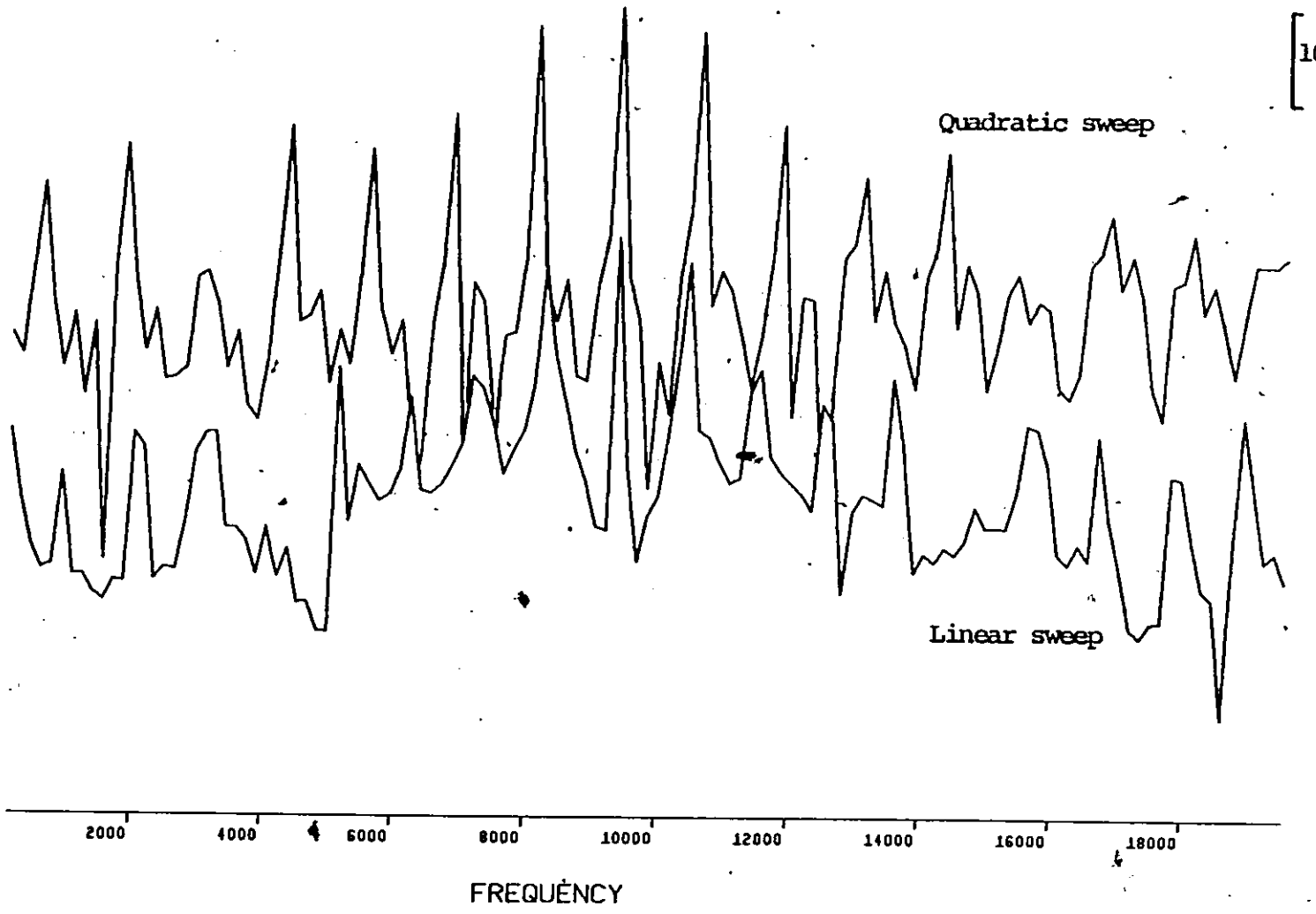

Fig. 4.11: Amplitude spectra of a square modulated ELT signal with two types of frequency sweep. Block number = 20, SNR = 30 dB and f_c = 9.378 KHz.

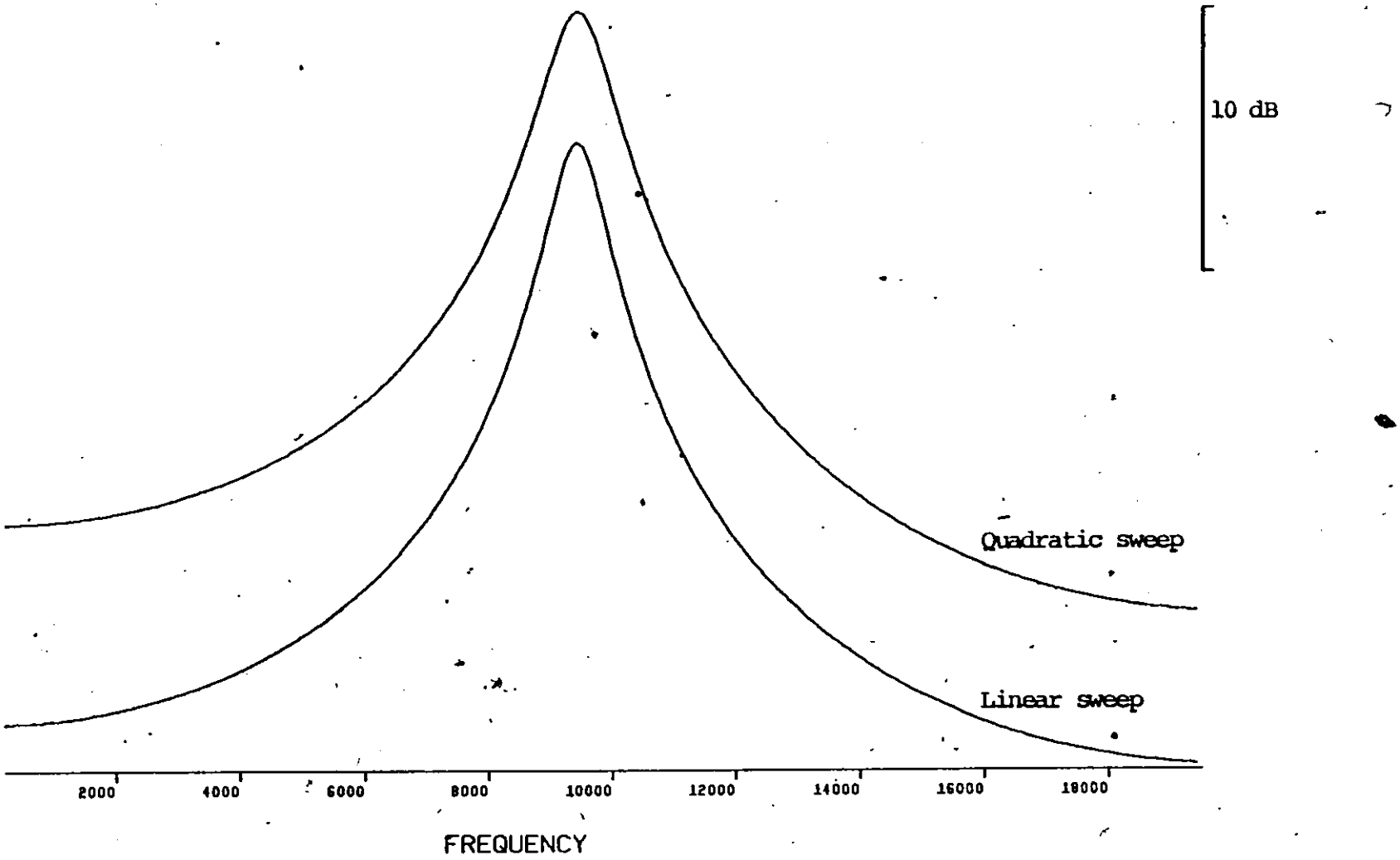

Fig. 4.12: ME spectra of a square modulated ELT signal with two types of frequency sweep. Block number = 20, SNR = 30 dB and f_c = 9.378 KHz.

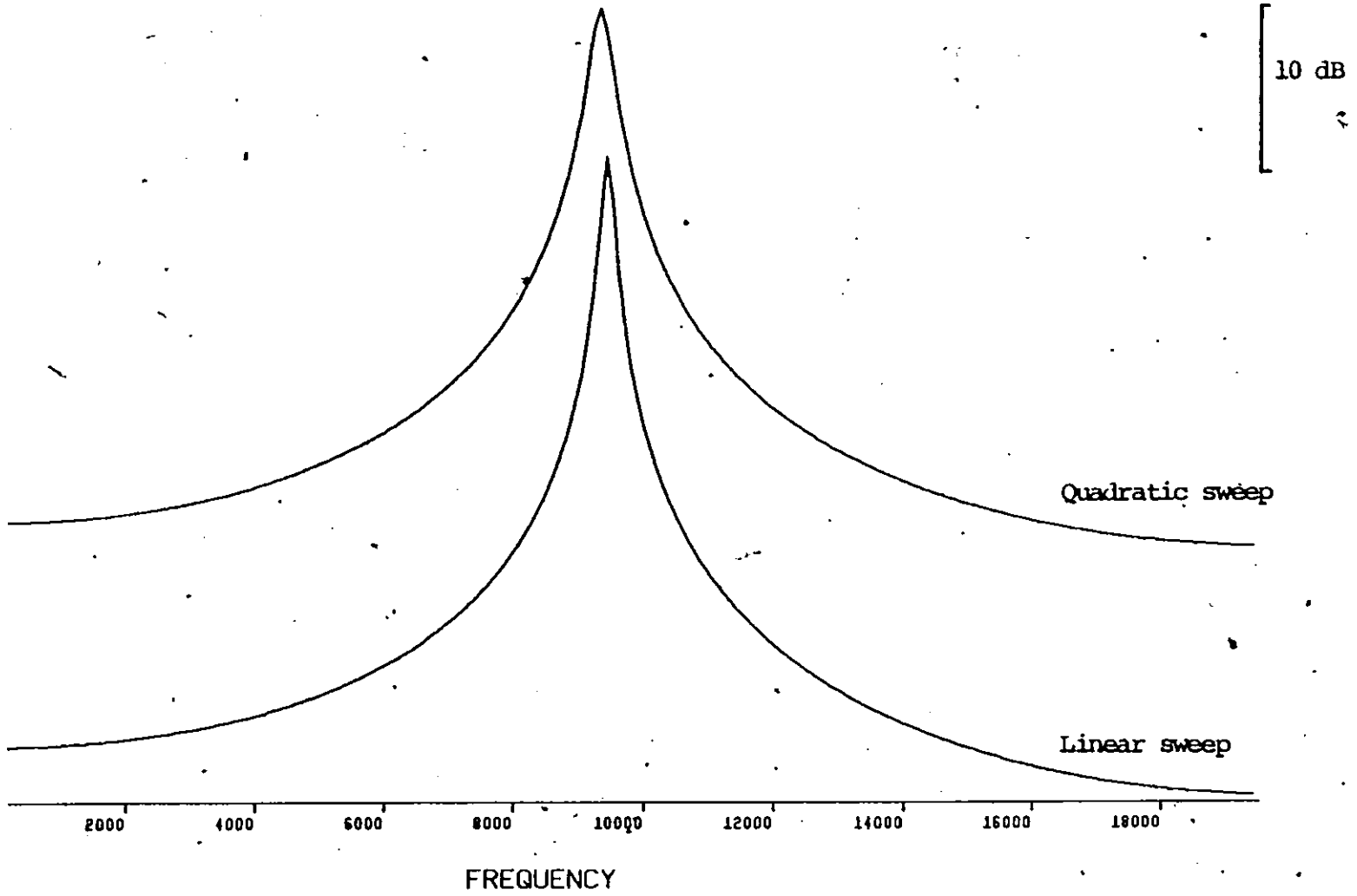

Fig. 4.13: ME spectra of the autocorrelation of a square modulated ELT signal with two types of frequency sweep. Block number = 20, SNR = 30 dB and f_c = 9.378 KHz.

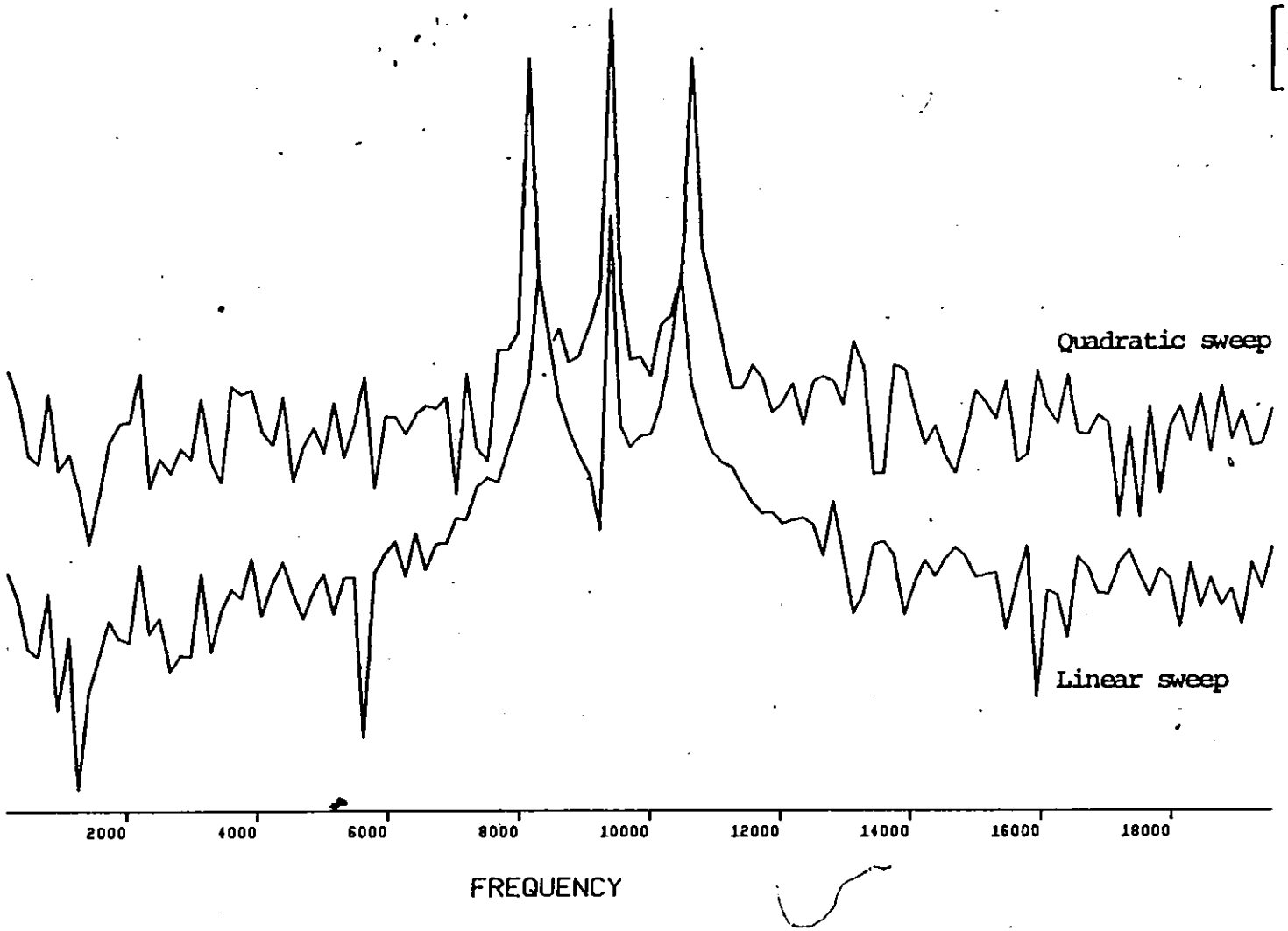

Fig. 4.14: Amplitude spectra of a sinusoidal modulated ELT signal with two types of frequency sweeps. Block number = 20, SNR = 30 dB and f_c = 9.378 KHz.

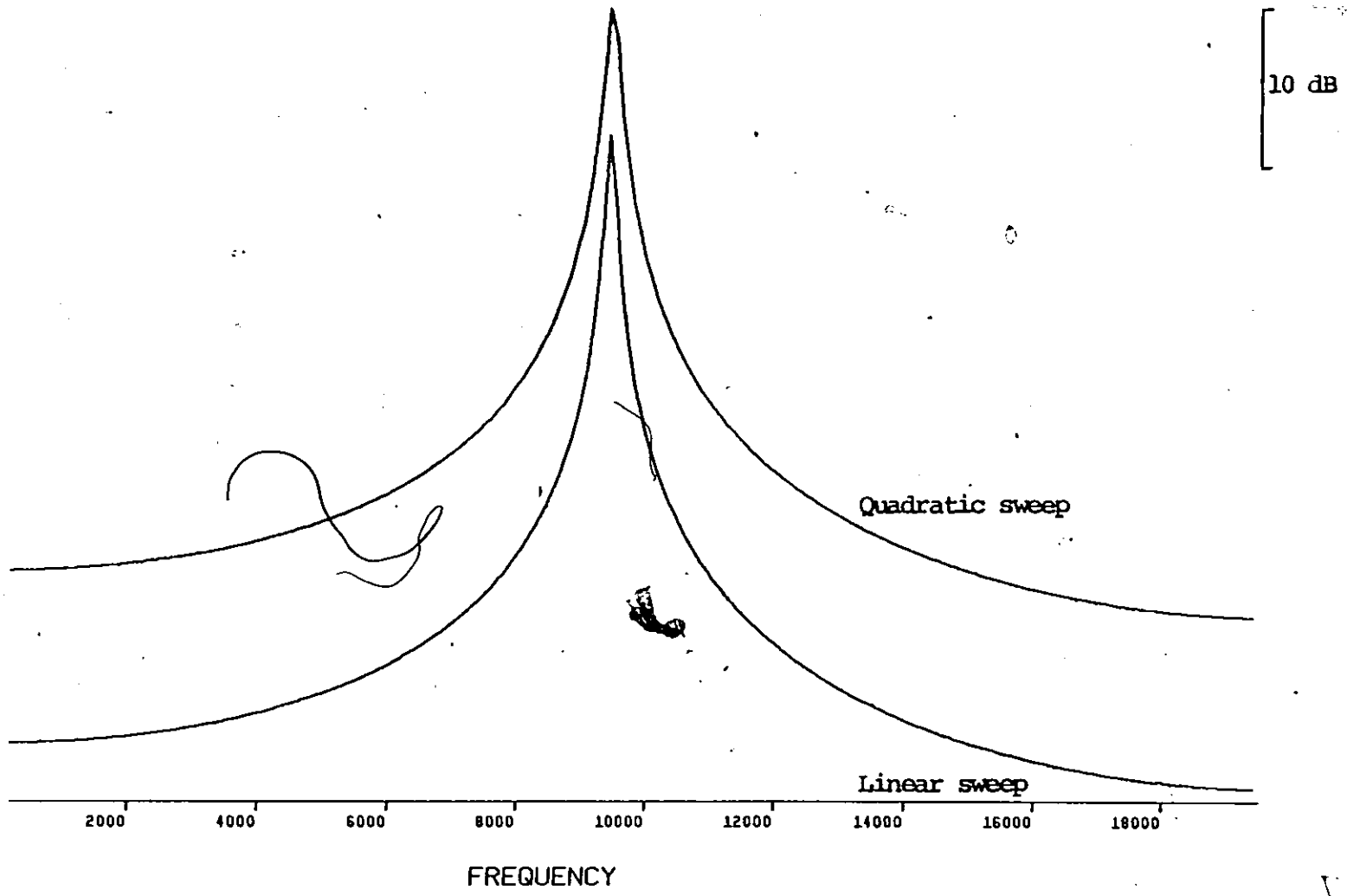

Fig. 4.15: ME spectra of a sinusoidal modulated ELT signal with two types of frequency sweeps. Block number = 20, SNR = 30 dB and f_c = 9.378 KHz.

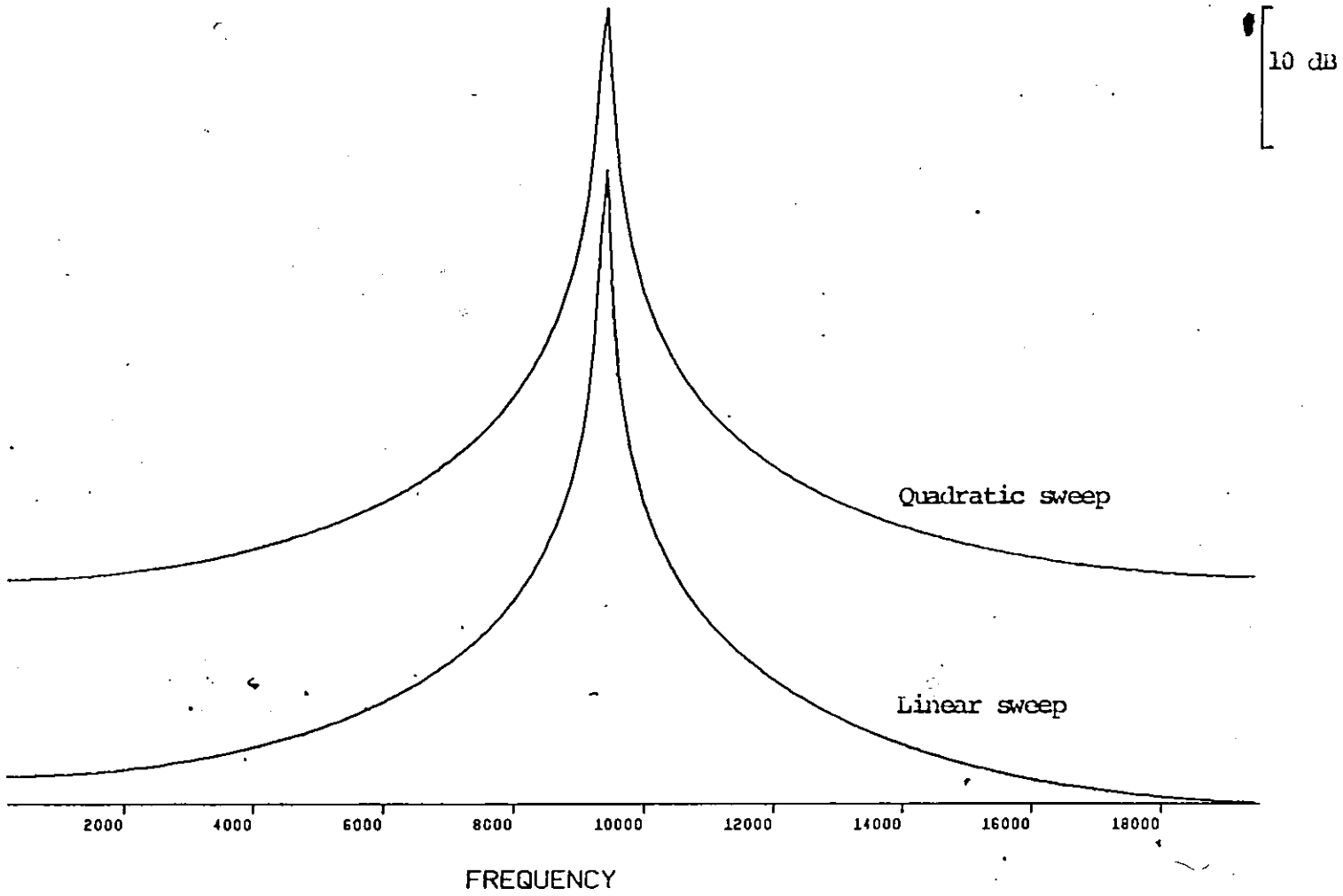

Fig. 4.16: MEMCOR of a sinusoidal modulated ELT signal with two types of frequency sweeps. Block number = 20, SNR = 30 dB and f_c = 9.378 KHz.

to consider two further parameters, namely, the modulation index, μ, and the duty factor, d. A comparison of results for different values of modulation index of a sinusoidal modulation indicates that there is very little change in the spectrum regardless of the method of processing. Of the three methods, the largest change is noted in the FFT spectrum with the sidelobes decreasing by about 2dB in response to a decrease in μ from 1.0 to 0.85. Because of the fact that there is very little change in the spectra with the specified changes in μ, we have not included these results. In contrast, as the duty cycle of a square modulation is changed from 0.35 to 0.5, the ME spectrum becomes significantly sharper (Fig. 4.18). We would expect this since increasing the duty cycle decreases the nulls in the signal and therefore enhances the adaptation process in the MEM. The MEM of the autocorrelation, on the other hand, does not show quite as dramatic an improvement as shown by Fig. 4.19. Fig. 4.17 indicates a decrease in the FFT sidelobes (relative to the mainlobe) as the duty cycle is increased. This is consistent with the fact that increasing the duty cycle has the effect of increasing the power at the carrier frequency relative to the power at the modulation frequency.

In summarizing this section we note that of the two major types of signals, the square modulated signal can be considered the worst case. Moreover, since the difference in results for signals with linear and quadratic sweeps is small and the linear sweep is more popular of the two, we limit further work in this Chapter to square modulated signals with modulations employing a frequency sweep that is a linear function

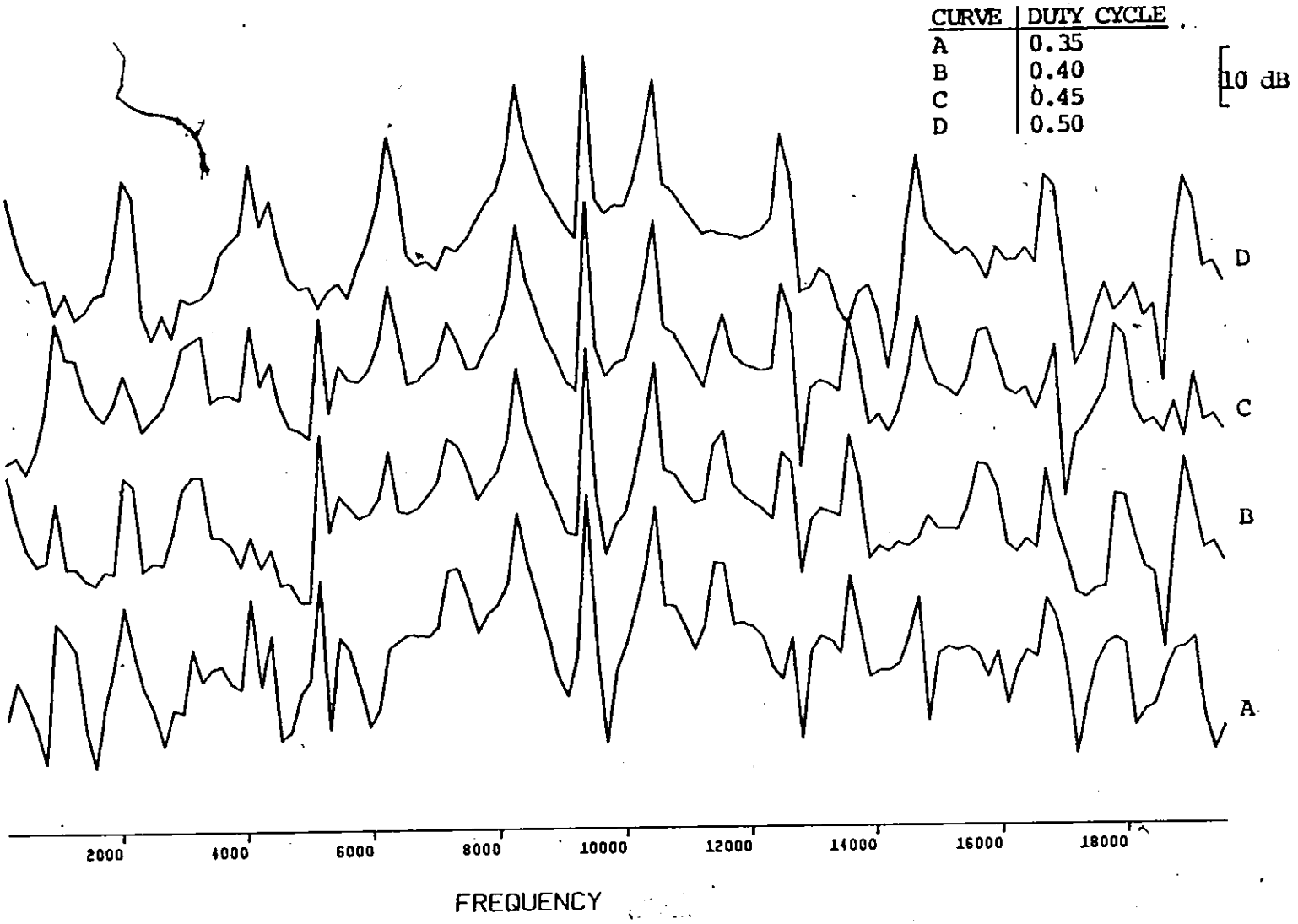

Fig. 4.17: Amplitude spectra of a square modulated ELT signal for various values of duty cycle. Block number = 20, SNR = 30 dB and f_c = 9.378 KHz.

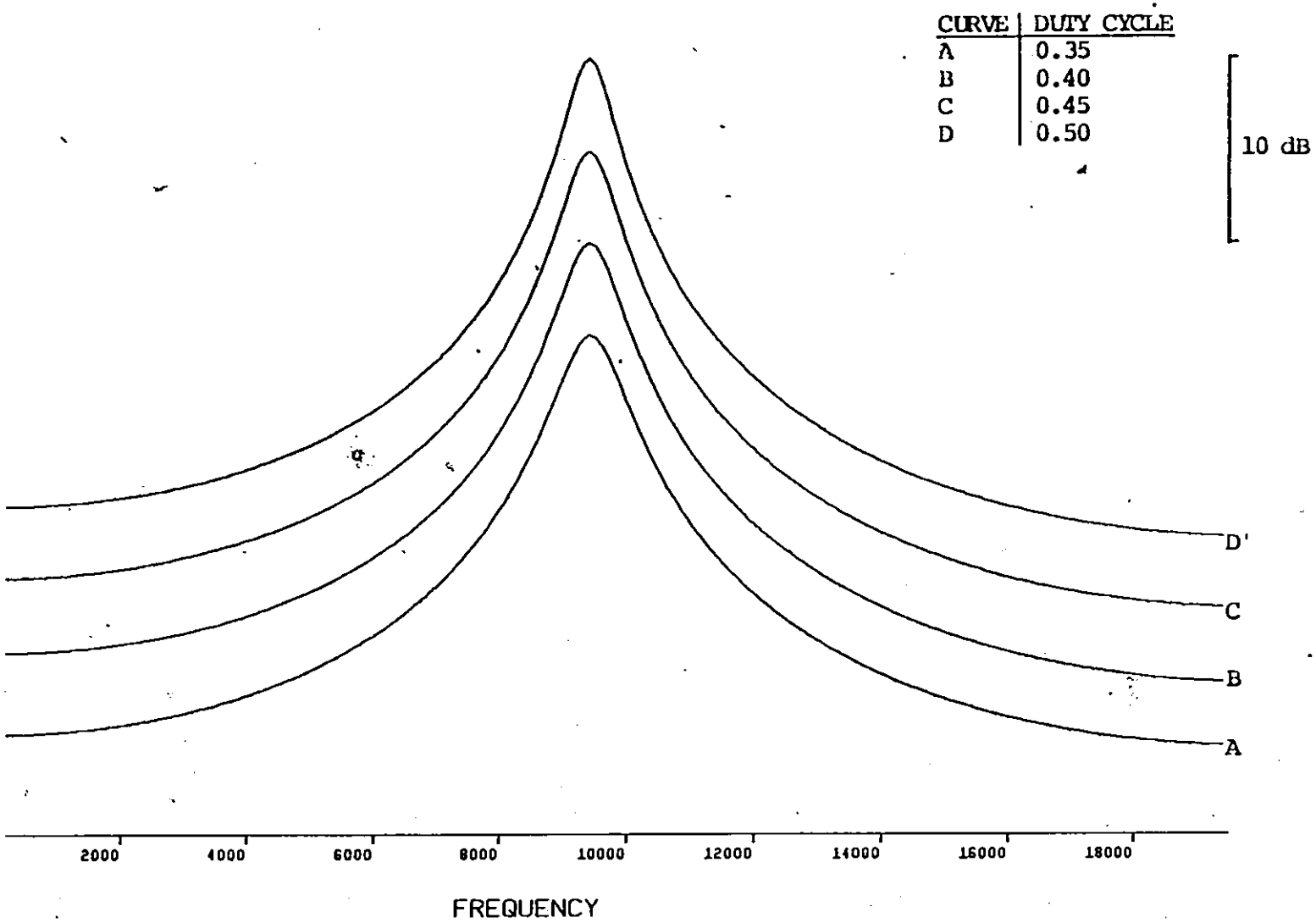

Fig. 4.18: ME spectra of a square modulated ELT signal for various values of duty cycle. Block number = 20, SNR = 30 dB and f_c = 9.378 KHz.

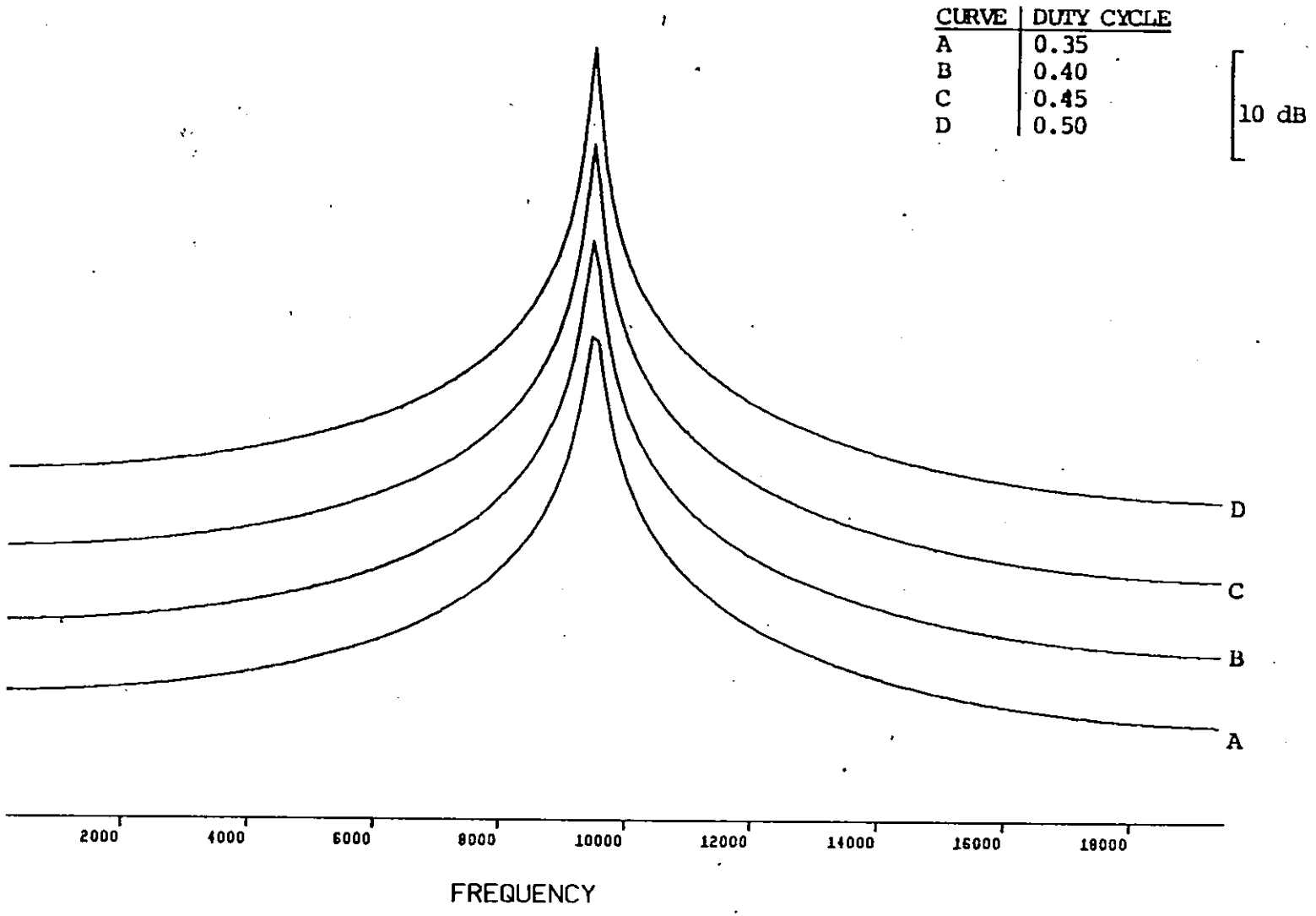

Fig. 4.19: MEMCOR of a square modulated ELT signal for various values of duty cycle. Block number = 20, SNR = 30 dB and f_c = 9.378 KHz.

of time. The only other parameter we need to specify to define the modulation completely is the duty cycle. We set its value at 0.4 since this is approximately midway within the allowable range. The final three sections of this Chapter explore the effects of changes in signal to noise ratio, processing types of signals referred to in Chapter 2 as "phase randomized signals" and processing 406 MHz ELT signals.

4.4 Spectral Comparison with Variations in SNR

In Chapter 2 we provided an explanation for modelling the received signal in terms of the Doppler shifted ELT signal in additive Gaussian noise. We also derived an equation for the signal to noise ratio which is used to gauge the performance of the processing method when the signal is embedded in different noise levels. Thus far, in view of the fact that our aim has been to determine the effect of variations in other parameters, we have used a high value of SNR. The effect of values of SNR in the medium to very low range is of great interest since it provides us with an indication of the robustness of the processor.

Figures 4.20, 4.21 and 4.22 show processing results of a square modulated ELT signal for the three methods being discussed. Each figure shows curves for SNR's of 15, 10, 5, 0 and -5 dB. To enable a useful comparison, the same set of noise samples has been used at all values of SNR and the standard deviation of the samples has been adjusted to arrive at the required noise level. Relative to results for high SNR, the FFT performs in a comparable manner for noise figures down to 10 dB. At values around 5 dB and less the sidelobes begin to mask out the main

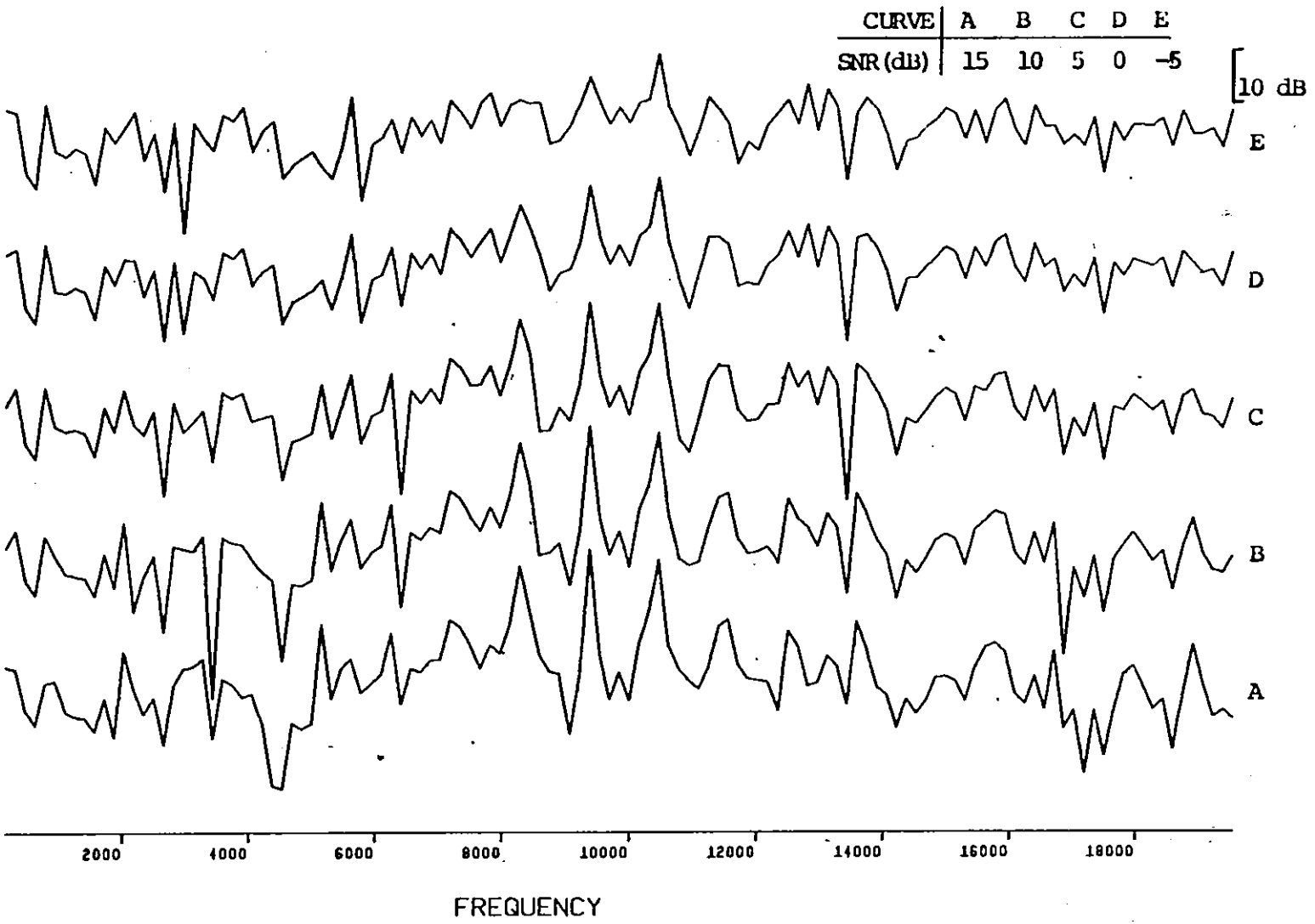

Fig. 4.20: Amplitude spectra of a square modulted ELT signal for various SNR's. Block number = 20 and f_c = 9.378 KHz.

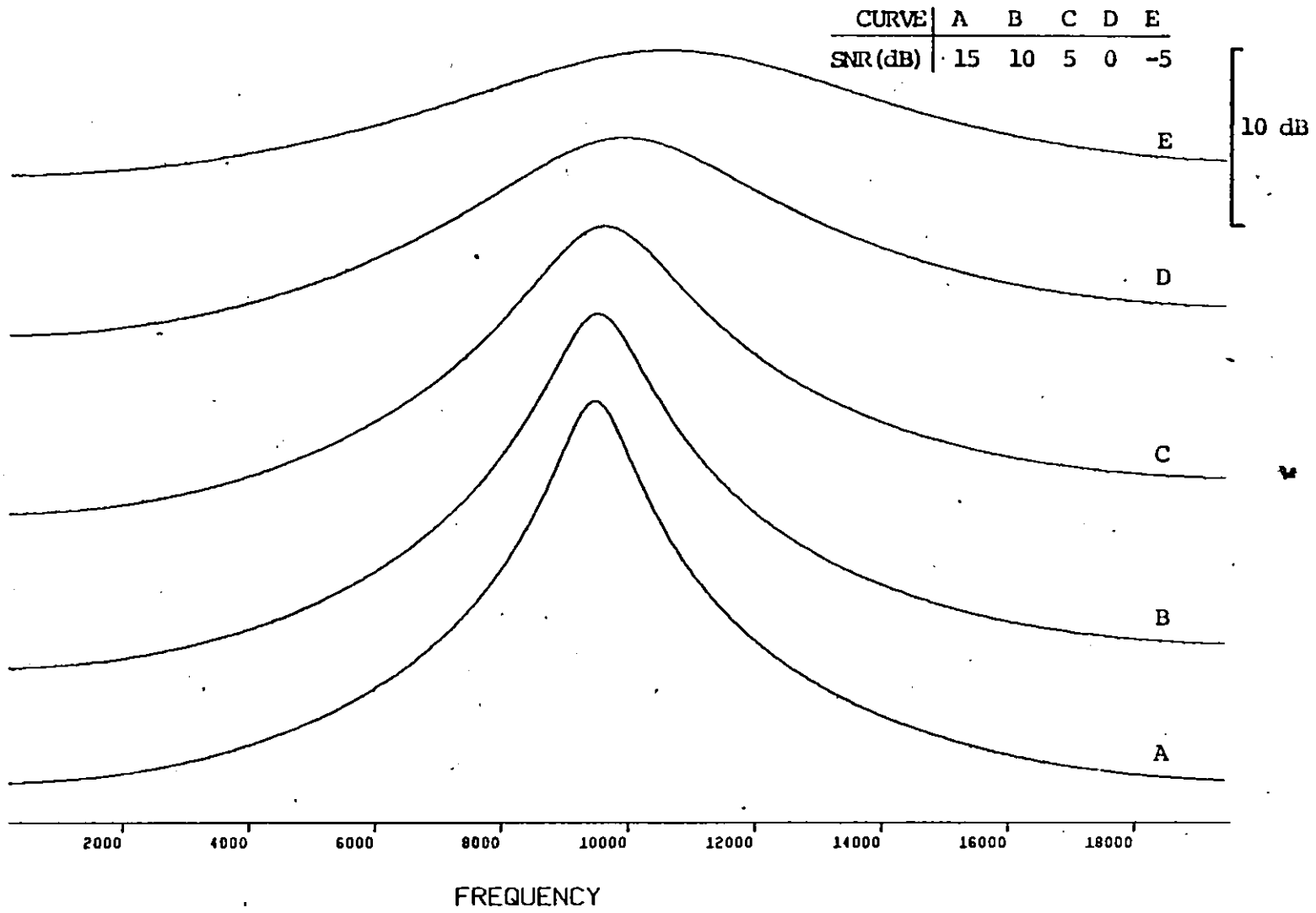

Fig. 4.21: ME spectra of a square modulated ELT signal for various SNR's. Block number = 20 and f_c = 9.378 KHz.

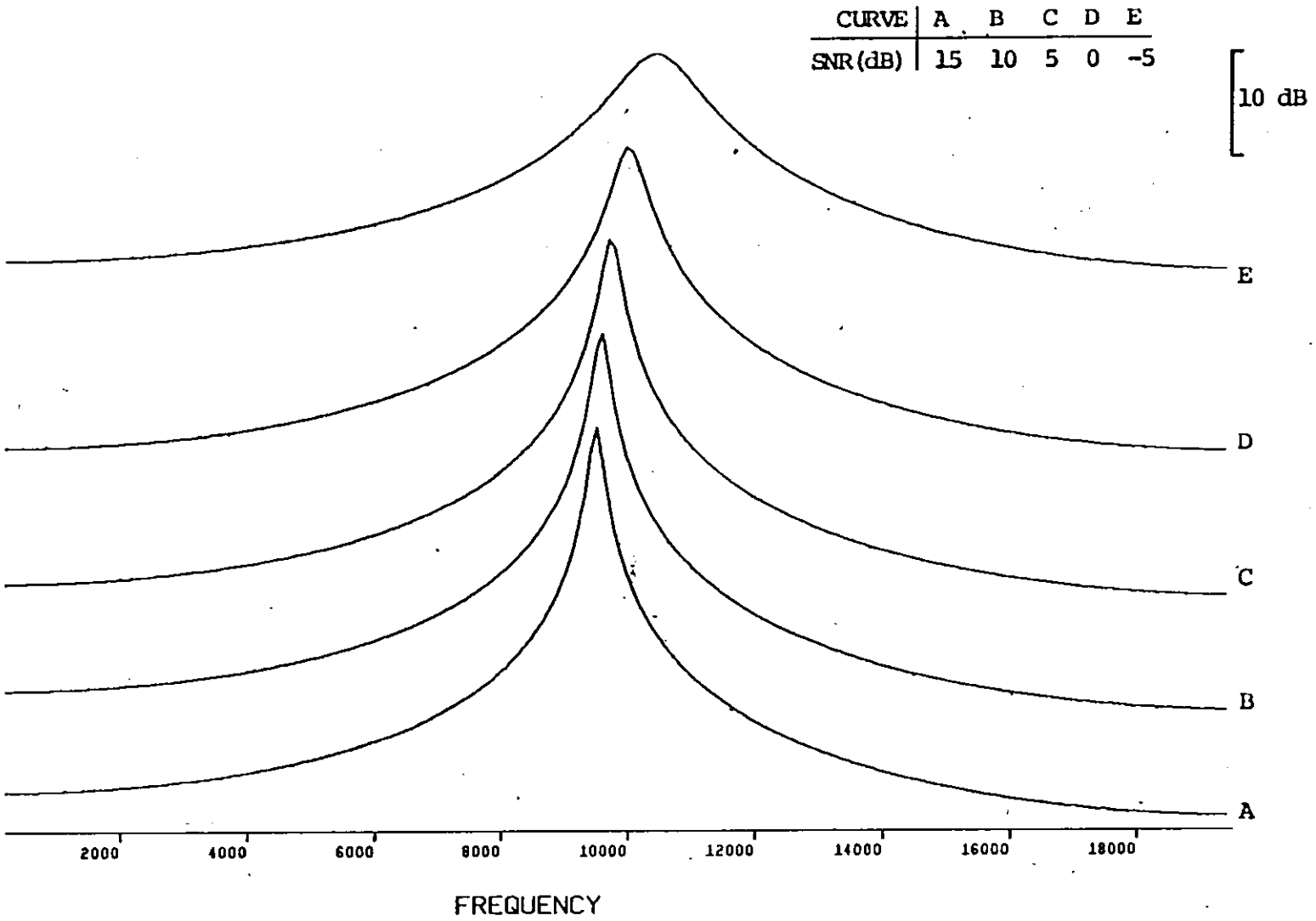

Fig. 4.22: MEMCOR of a square modulated ELT signal for various SNR's. Block number = 20 and f_c = 9.378 KHz.

lobe and detection is no longer possible. With the MEM (Fig. 4.21), the peak is discernible down to an SNR of 0 dB, but the accuracy in locating the carrier component degrades quite rapidly. At a signal to noise ratio of 5 dB, the peak is shifted by about 200 Hz. Figure 4.22, which shows results for the MEMCOR, indicates that the additional processing yields a well defined peak even when the SNR is 0 dB. The detection error, for the MEMCOR, is larger than that for the MEM with errors of approximately 100 Hz and 300 Hz at signal to noise ratios of 15 dB and 5 dB, respectively. Moreover, changing the filter order (PEFO) does not improve the estimate in any sense. However, of the three methods, the MEMCOR gives the best defined peak at all values of SNR.

4.5 Processing Results for Phase Randomized Signals

In our description of the ELT signals (Chapter 2) we showed that "phase randomized signals" arise as a result of using the train of pulses to switch the oscillator. The effect of this is to introduce a random phase at the start of each RF pulse.

Figures 4.23, 4.24 and 4.25 each show results of processing continuous phase and phase randomized signals. Both the MEM and MEMCOR indicate very little difference in results for the two types of signals whereas the FFT spectrum degrades quite considerably as a result of phase randomizing. Figure 4.23 shows the extent to which the FFT spectrum degrades. Note in particular the significant reduction in resolution as a result of introducing a random phase.

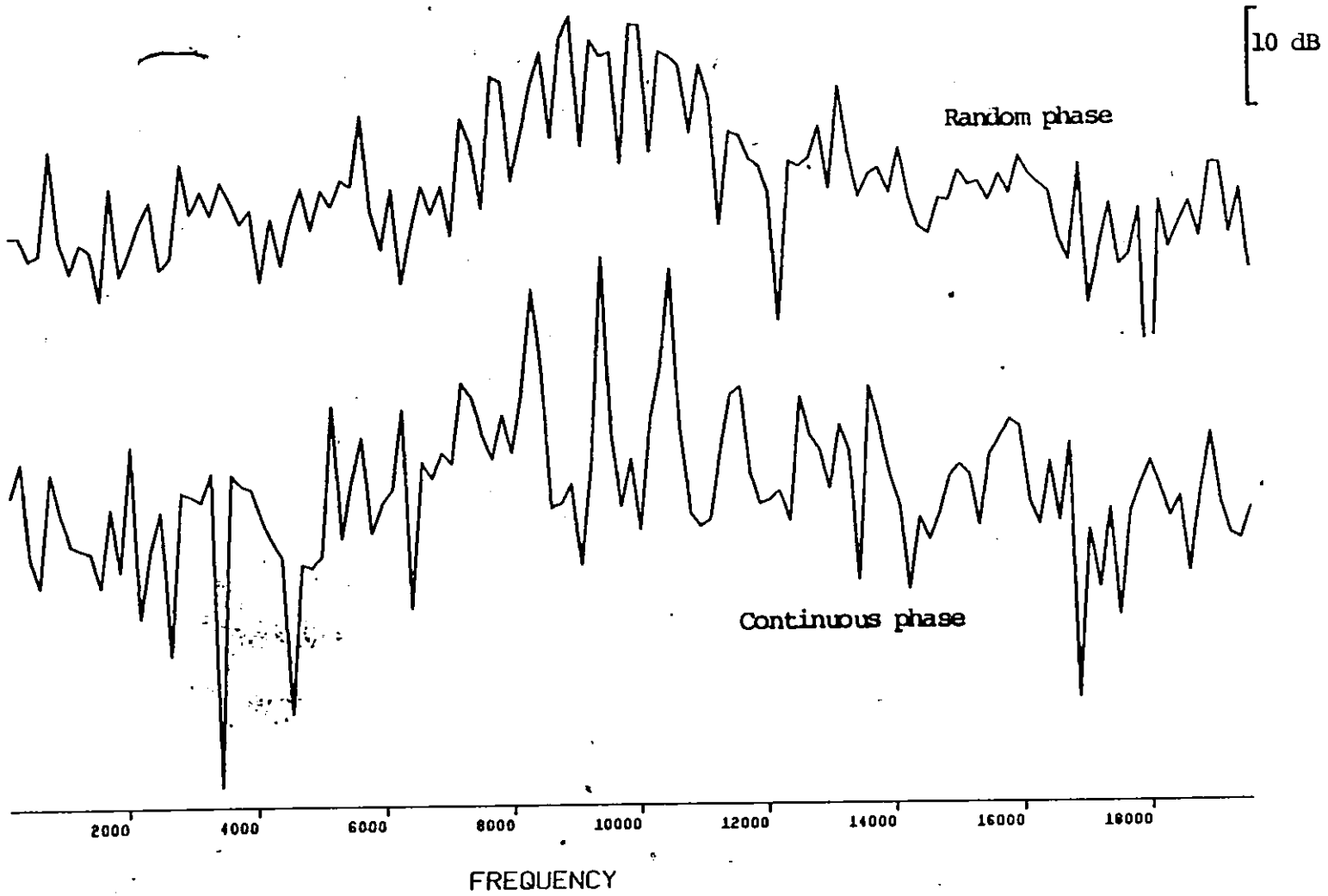

Fig. 4.23: Amplitude spectra of a square modulated ELT signal with continuous and random phase. Block number = 20, SNR = 10 dB and f_c = 9.378 KHz.

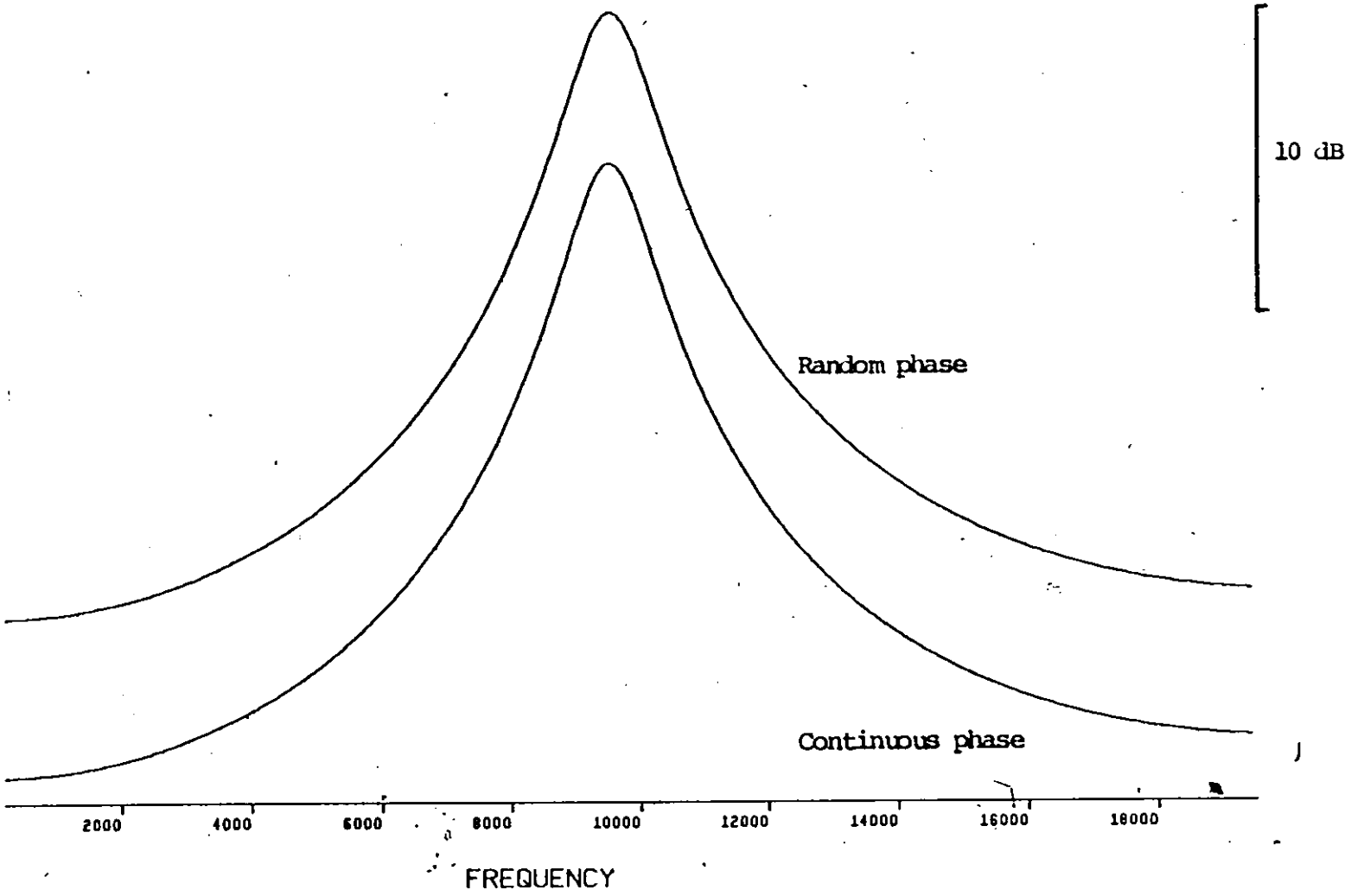

Fig. 4.24: ME spectra of a square modulated ELT signal with continuous and random phase. Block number = 20, SNR = 10 dB and f_c = 9.378 KHz.

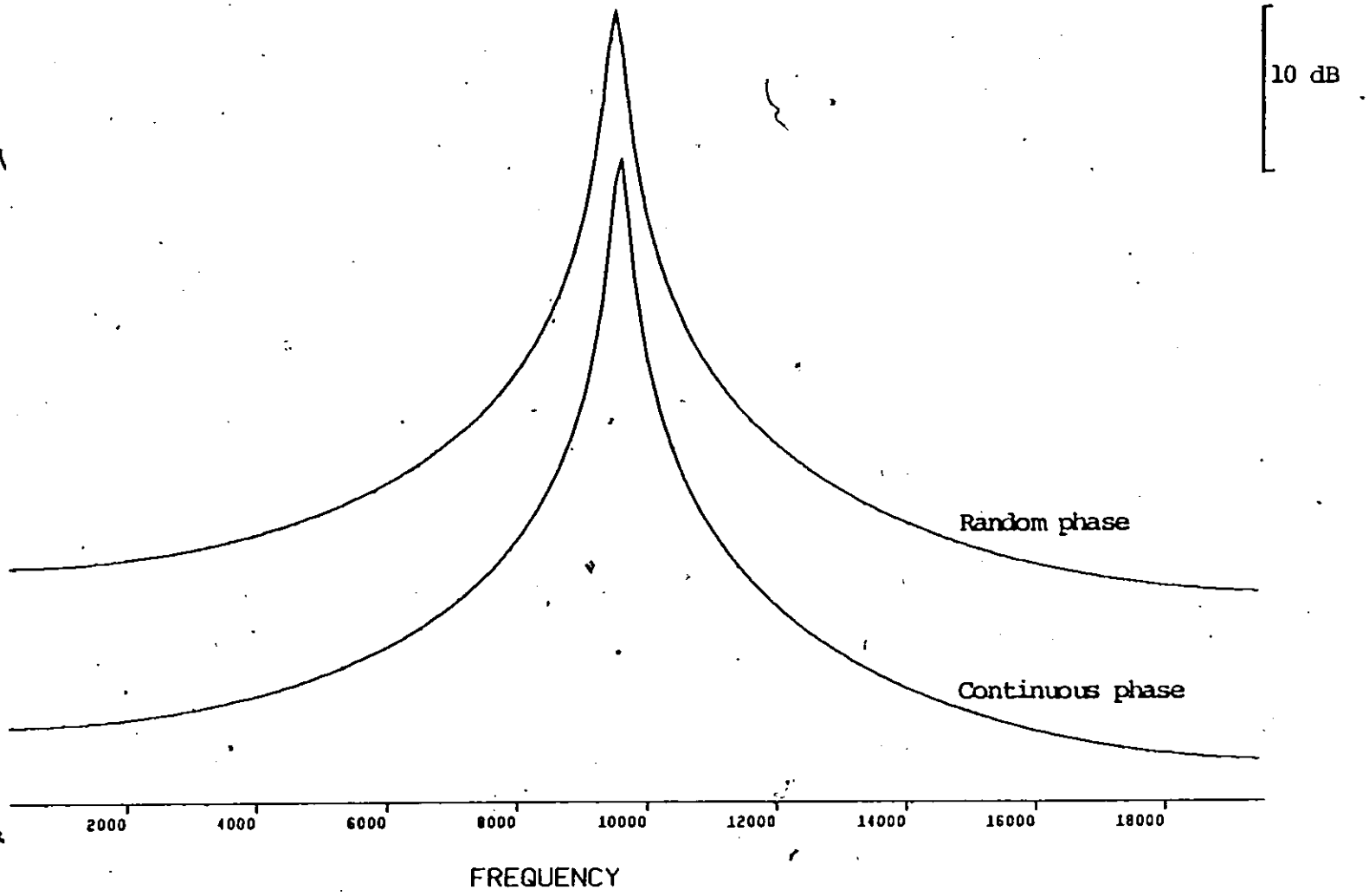

Fig. 4.25: MEMCOR of a square modulated ELT signal with continuous and random phase. Block number = 20, SNR = 10 dB and f_c = 9.378 KHz.

4.6 Processing 406 MHz ELT Transmissions

Transmission from 406 MHz ELT's consists of phase modulated data and a continuous sinusoid as described by Fig. 2.6. Although this type of ELT is in its experimental stages, for brevity, we include processing results for the 406 MHz signal. As we would expect, this form of signal results in much sharper spectra (Figs. 4.26, 4.27 and 4.28). The MEM and FFT are comparable at an SNR of 20 dB, but when the SNR is 10 dB or less the FFT yields much better results. From Figs. 4.26 and 4.27 we note that at signal to noise ratios of 0 dB and less the MEM is quite unacceptable whereas the FFT performs reasonably down to 0 dB SNR. As compared to both these methods, the MEMCOR performs admirably at noise figures down to 0 dB and provides a satisfactory estimate at an SNR of -5 dB (Fig. 4.28).

In summary, we note that detection of signals employing a square modulation is more problematic because of high FFT sidelobes and broad MEM spectra. Modification of the data by way of autocorrelation results in a much sharper MEM spectrum. Moreover, processing the autocorrelation of the data results in a decrease in sensitivity to variations in the parameters which specify the signal format. Both the MEM and the FFT results deteriorate quite rapidly as the SNR is reduced below 10 dB. With the FFT, the problem lies in the rapidly increasing sidelobe levels whereas with the MEM a broadening of the main lobe hampers the detection process. Although the MEMCOR results in much sharper spectra, especially at low SNR, the error in the frequency estimate is no better than that obtained using the MEM. We find that

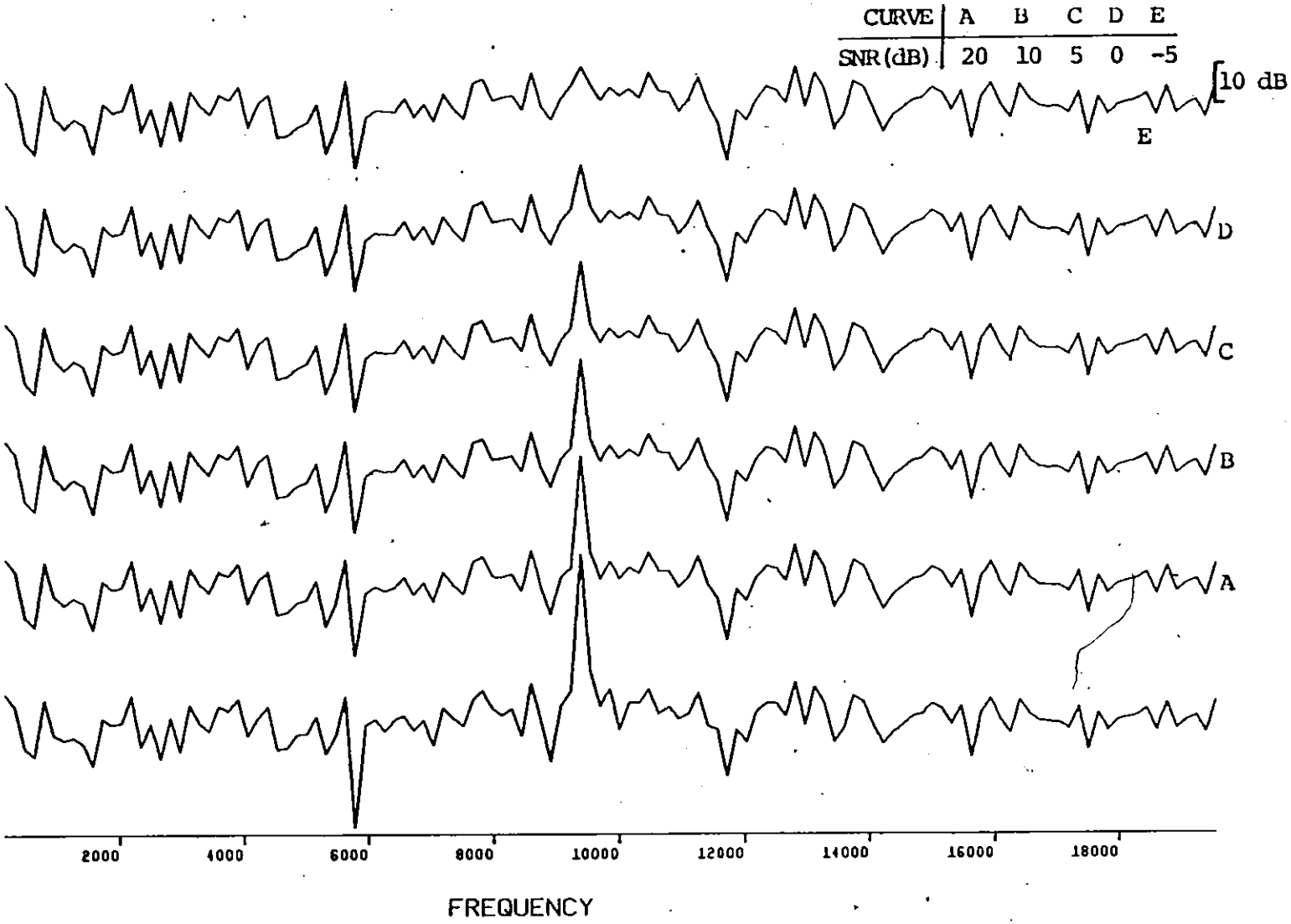

Fig. 4.26: Amplitude spectra of a continuous sinusoid with f_c = 9.378 KHz and signal to noise ratios as indicated on the plot.

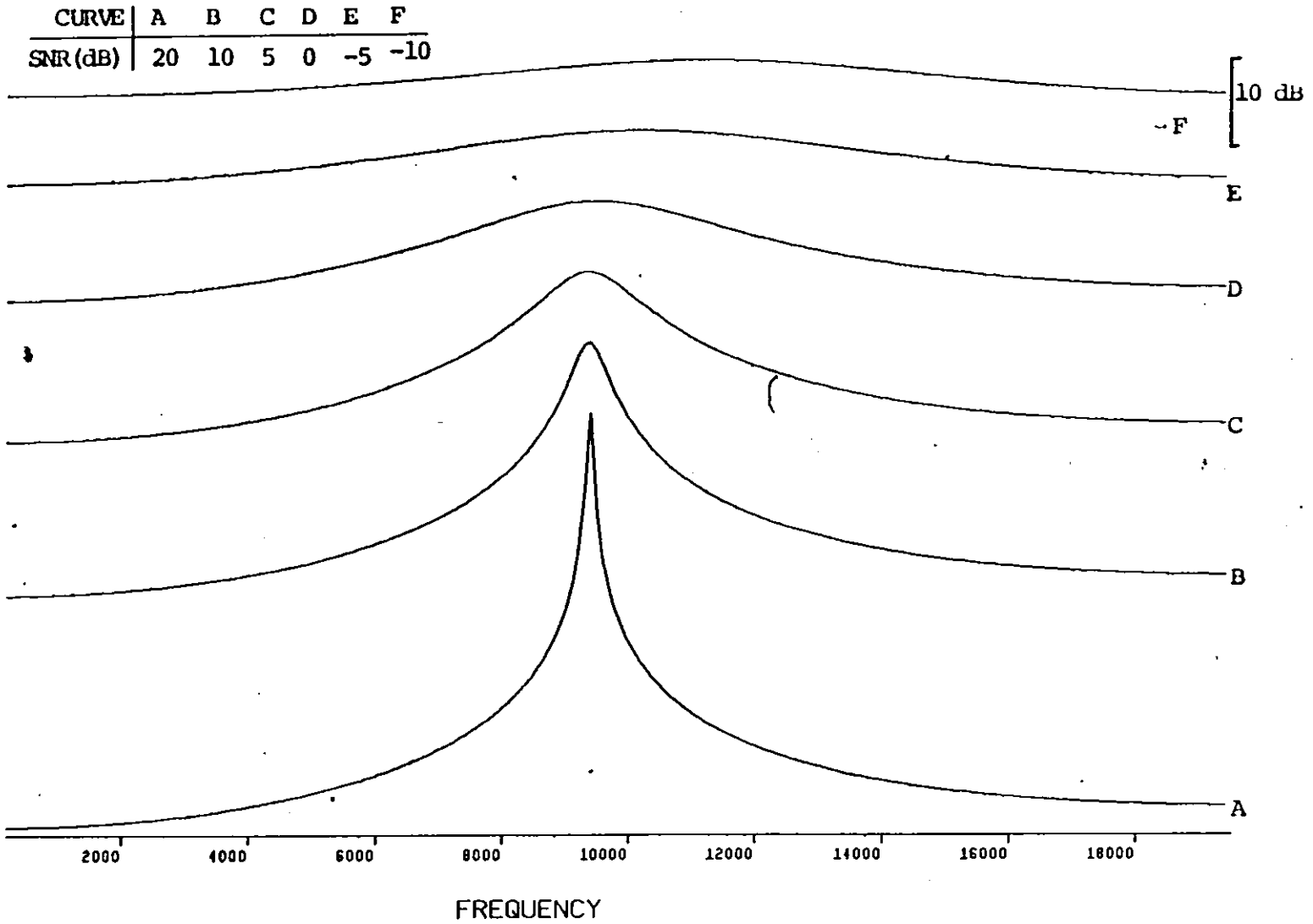

Fig. 4.27: ME spectra of a continuous sinusoid with f_c = 9.378 KHz and signal to noise ratios as indicated on the plot.

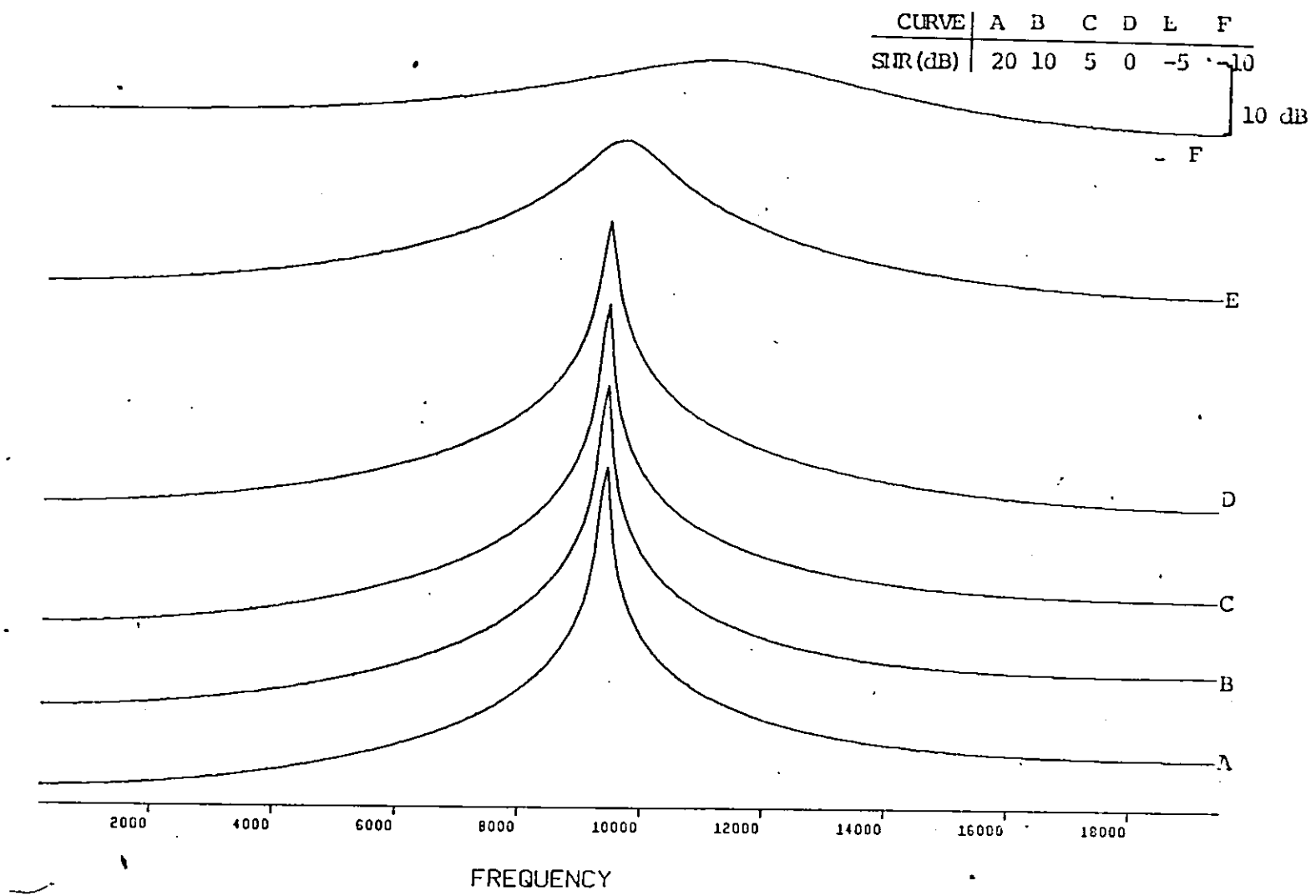

Fig. 4.28: MEMCOR of a continuous sinusoid with f_c = 9.378 KHz and signal to noise ratios as indicated on the plot.

phase randomization has a substantially greater effect on the FFT than the MEM. In particular, with the FFT the spectrum broadens to the point where the main lobe and the main sidelobes become encompassed in a single lobe. In contrast, the MEM and MEMCOR are relatively immune to phase randomization. The final section in this chapter involved processing a continuous sinusoid of the type transmitted by 406 MHz ELT's. Results of processing this signal are, as one would expect, far better than those of processing modulated signals. In particular, we find the performance of the MEM with prior autocorrelation to be very good even at very low SNR. As pointed out in this chapter we have restricted our research to the case of single signals. In order to obtain a good comparison of the methods used, it is necessary to compare results for two or more signals received simultaneously. Chapter 5 is devoted entirely to the problem of processing multiple signals.

CHAPTER 5

PROCESSING MULTIPLE ELT SIGNALS

Should the situation arise whereby more than one platform is in distress, the received signal could comprise more than one ELT signal. A necessary and sufficient condition for this scenario is that the ELT units be close enough in distance to be visible to the satellite simultaneously. Although the probability of this situation occurring is small, the fact that it is not impossible (directional antennas notwithstanding) necessitates its consideration. This chapter is devoted entirely to processing multiple signals. Although we try to include results for a large variety of signal parameter combination, we have to impose some limitations. For this reason we consider only those parameters which have a relatively large influence on the results. Furthermore, we limit research to the case of two signals.

$$y(t) = S_1(t) + S_1(t + t_{of}) + n(t) \qquad (5.1)$$

Equation (5.1) depicts the case when the received signal consists of two ELT transmissions in noise. In specifying the signal to noise ratio we will quote two values, one for each of the signals in noise (n(t)) separately, i.e. SNR_1 will pertain to signal $S_1(t)$ in noise n(t) and SNR_2 will pertain to $S_2(t + t_{of})$ in the same noise n(t). The parameter t_{of}, in eq. (5.1), is the offset time of one ELT transmission relative to the other. Perhaps this is best described with the aid of a diagram (Fig. 5.1). As can be seen, the offset is defined as the time difference between the start of the modulations of the two signals. Since the modulation is repetitive with a repetition time of Tr, the

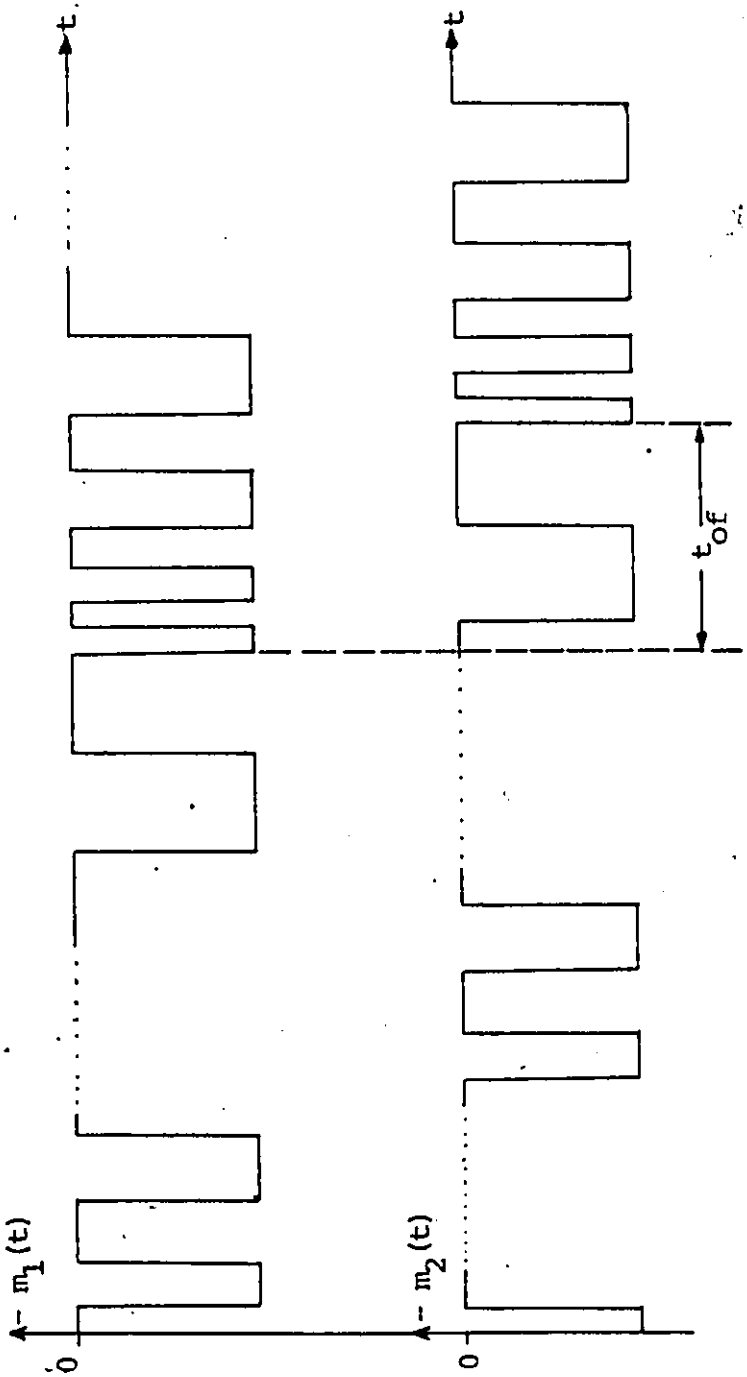

Fig. 5.1: The offset time as a function of the starting times of the two modulation cycles where t_{s_1} and t_{s_2} indicate the beginning of the modulation cycles.

offset need only be specified modulo T_r. Keeping in mind the two additional parameters we have defined (to completely specify a multiple signal) we proceed to the analysis of the processing results.

5.1 Processing Multiple Signals of Different Combinations

Our aim in this section is to compare results for the three possible different signal combinations. Since we devote a separate section to effects of variations in the ratio SNR_1/SNR_2 and the parameter t_{of}, present considerations are limited to signals of equal power, infinite SNR and an offset such that the string of RF pulses of one signal appears in the nulls between the RF pulses of the second signal. For each pair of signal combinations we shall include on a single plot results for different carrier frequency differences ($fc_1 - fc_2$). In particular, the carrier frequency of the first signal will be held constant at fc_1 = 11.2 KHz whereas the carrier frequency of the second signal (fc_2) will be varied. Values of fc_2 for the five curves on each plot (starting with the bottom most curve) are 10, 9, 8, 7 and 6 KHz. This will allow us to determine the ability of each method to resolve the peaks at the two carriers (for each pair of signal combinations) as a function of the separation between carrier frequencies. The block of data we process lies approximately midway in the modulation sweep and starts at time 0.1408 seconds relative to the beginning of the modulation sweep of the first signal.

5.1.1 Two Pulse Modulated Signals

Figures 5.2, 5.3 and 5.4 show results for the MEM, the MEMCOR and the FFT. Before proceeding to comparisons we point out that the

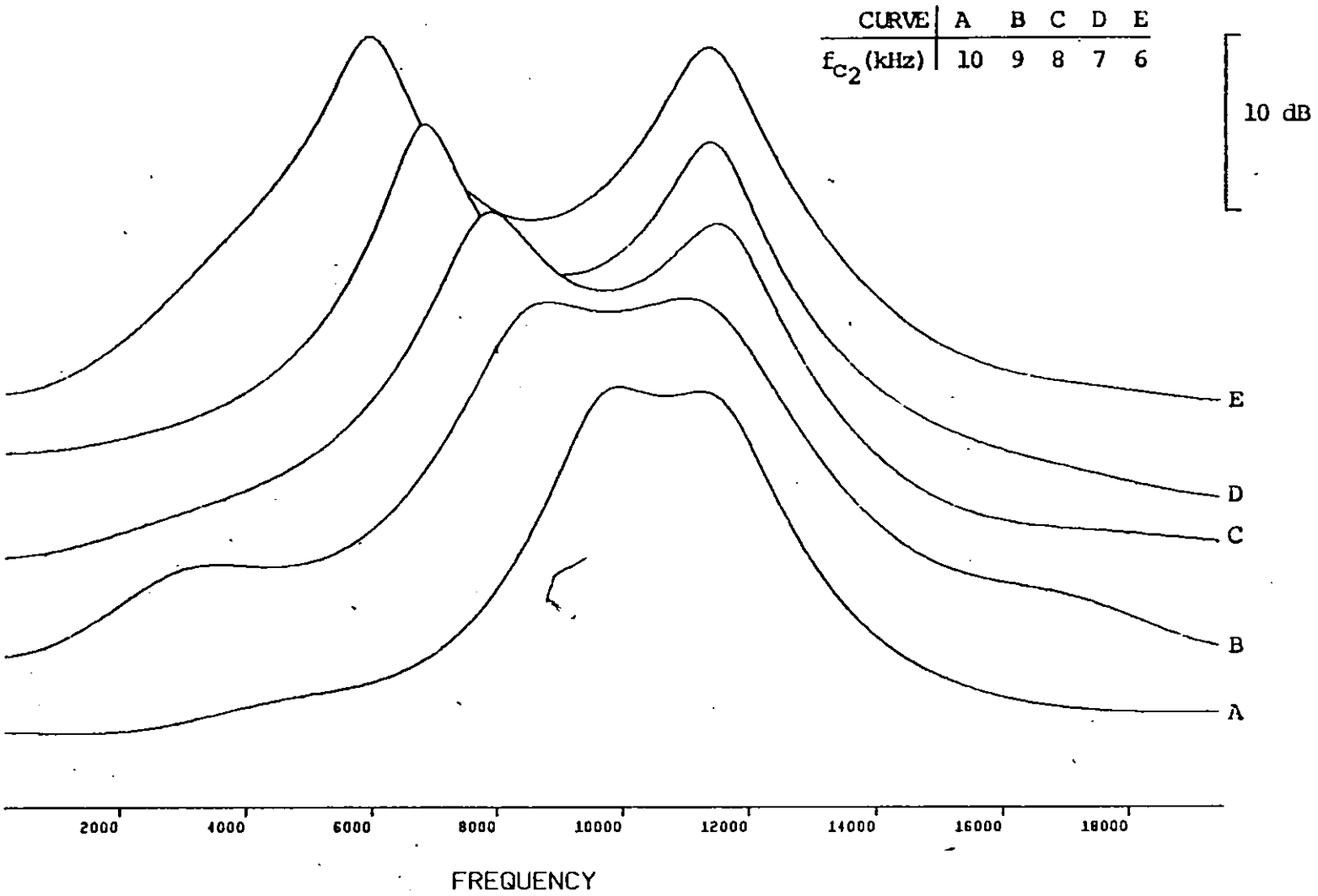

Fig. 5.2: ME spectra of two square modulated ELT signals with f_{c_1} = 11.2 KHz, $SNR_1 = SNR_2 = \infty$, PEFO = 10 and f_{c_2} as specified on the plot.

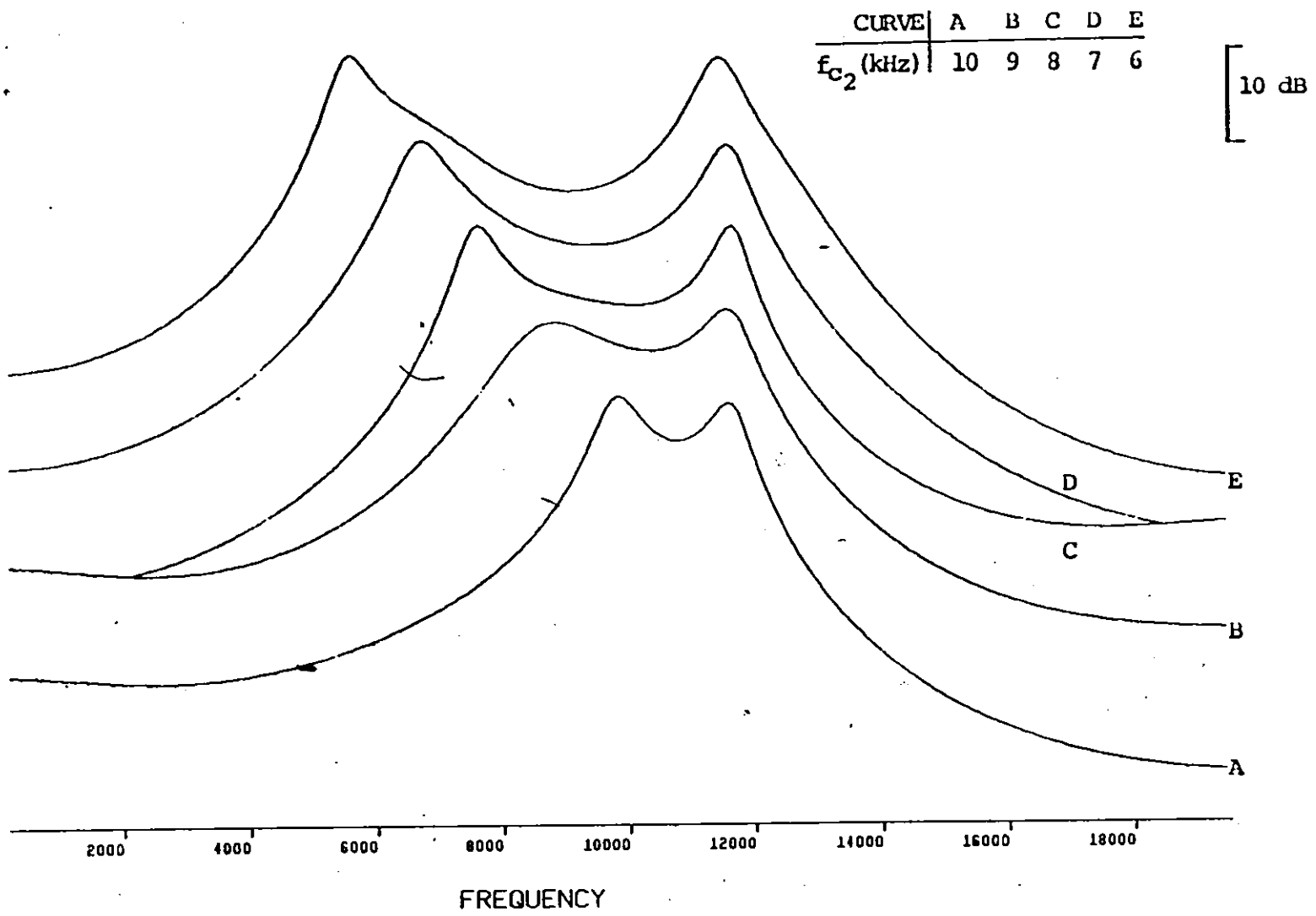

Fig. 5.3: MEMCOR of two square modulated ELT signals with f_{c_1} = 11.2 KHz, $SNR_1 = SNR_2 = \infty$, PEFO = 8 and f_{c_2} as specified on the plot.

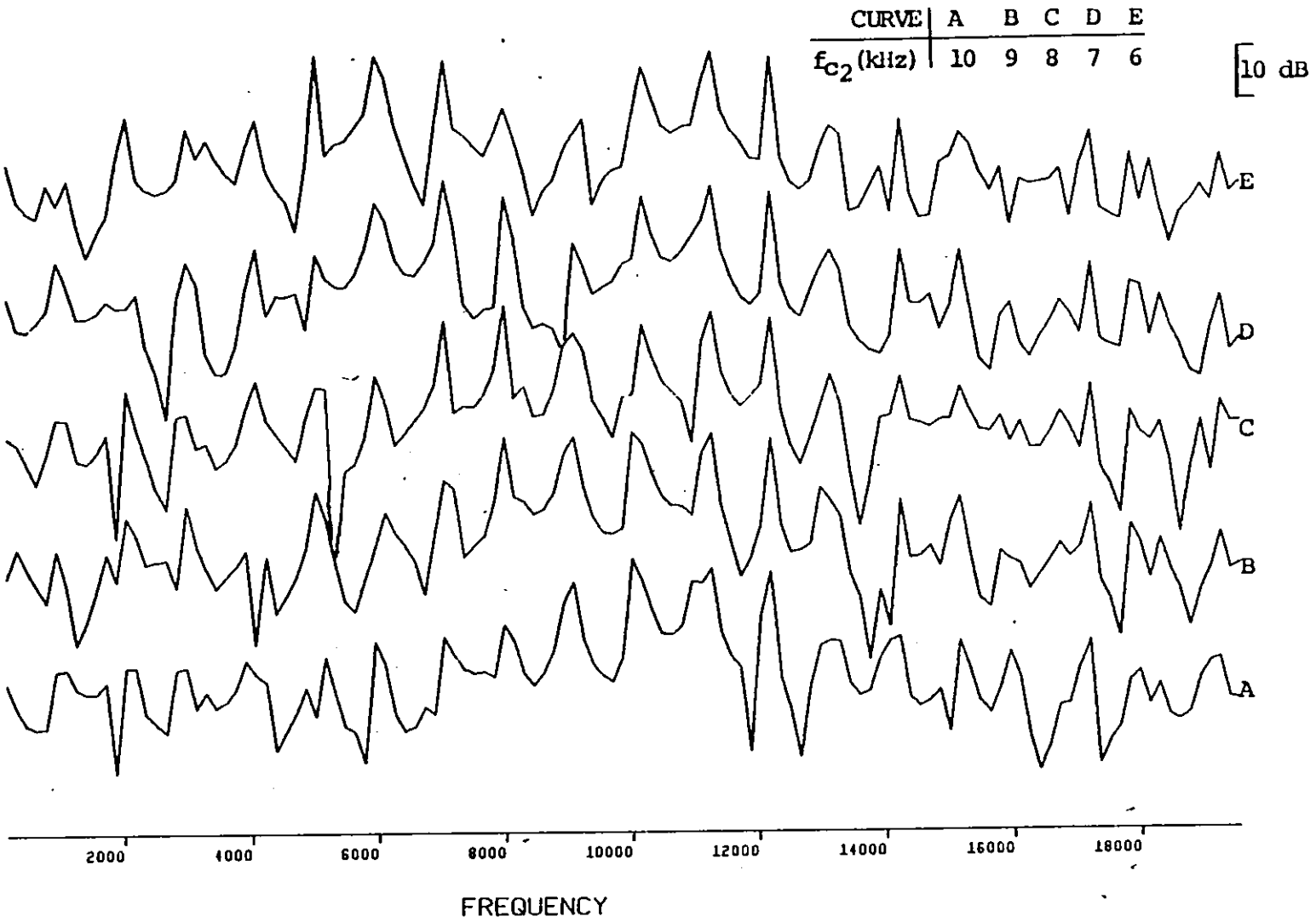

Fig. 5.4: Amplitude spectra of two square modulated ELT signals with f_{c_1} = 11.2 KHz, $SNR_1 = SNR_2 = \infty$ and f_{c_2} as specified on the plot.

prediction error filter orders quoted below each plot yield the best results for detection purposes. The effect of processing (with the MEM) using lower or higher orders together with a discussion on the accuracy of the location of the peaks are included at the end of the section. Comparing the results we find that both the MEM and the MEMCOR give superior results for detection purposes since any peak detection method applied to the results (within the band of interest, i.e. 4–16 KHz) yields the required peaks. results for the FFT show that detection is extremely difficult (if not impossible in some cases) since the sidelobe structure appears at levels comparable to the peaks of interest and in some cases the sidelobes are higher than the main lobes and would lead to erroneous results. As shown by Fig. 5.3, processing the autocorrelation of the data by using the MEM results in a considerably sharper spectrum and enhances detection. In brief, we note that for the specified carrier frequency separations both MEM based methods perform adequately.

5.1.2 Two Sinusoidal Modulated ELT Signals

Results for two sinusoidal modulated signals are shown in Figs. 5.5, 5.6 and 5.7. All three methods show an improvement in results for sinusoidal modulated signals as compared to the case of pulse modulated signals. The MEM gives the sharpest spectrum with extremely well defined peaks. As compared to the MEM, the MEMCOR peaks are significantly more rounded although the results are still quite acceptable. Figure 5.7 shows that the FFT performance is greatly improved compared to the results for two pulse modulated signals. However, despite the fact that the number of interfering sidelobes (in

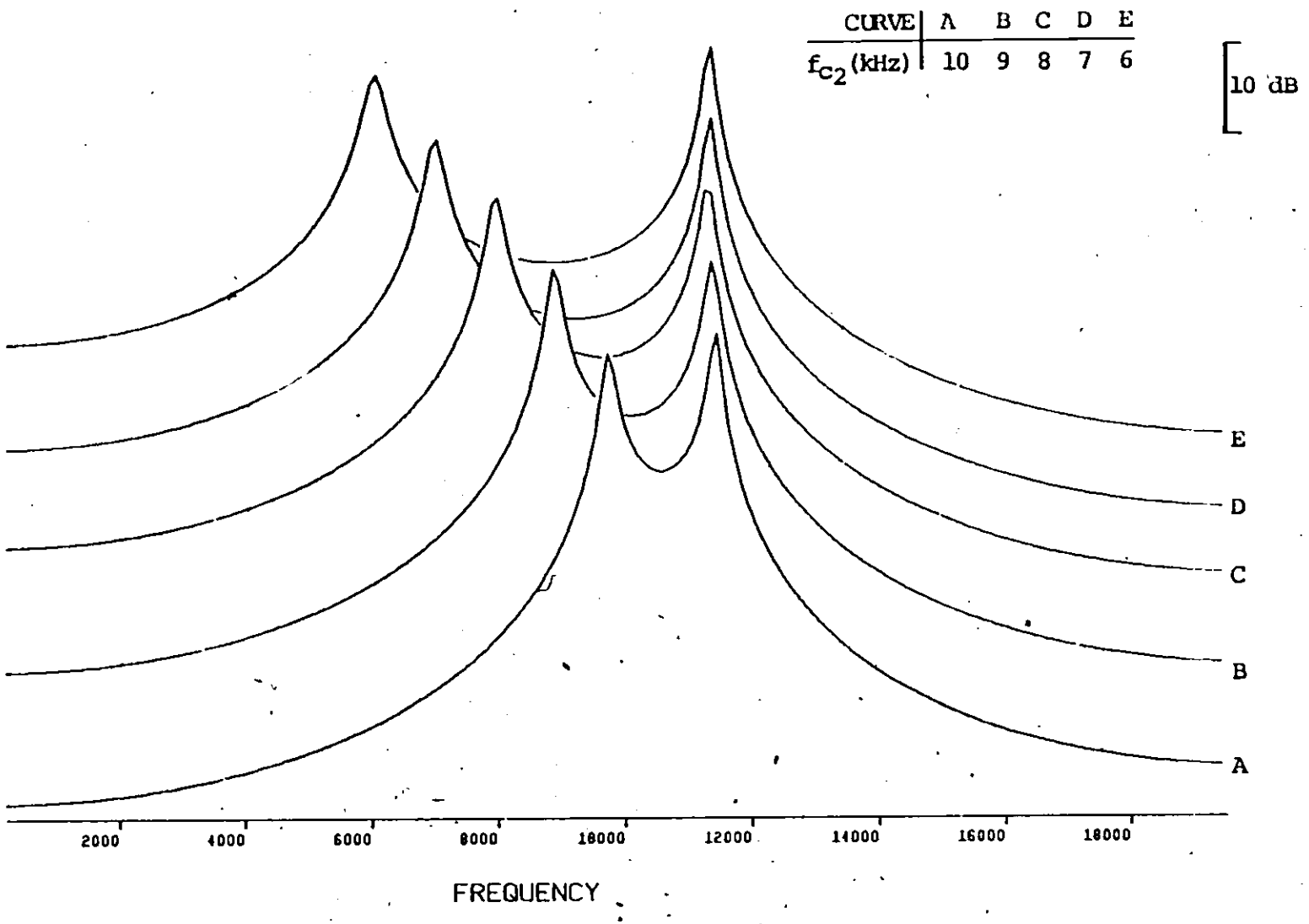

Fig. 5.5: ME spectra of two sinusoidal modulated ELT signals with f_{c_1} = 11.2 KHz, $SNR_1 = SNR_2 = \infty$, PEFO = 5 and f_{c_2} as specified on the plot.

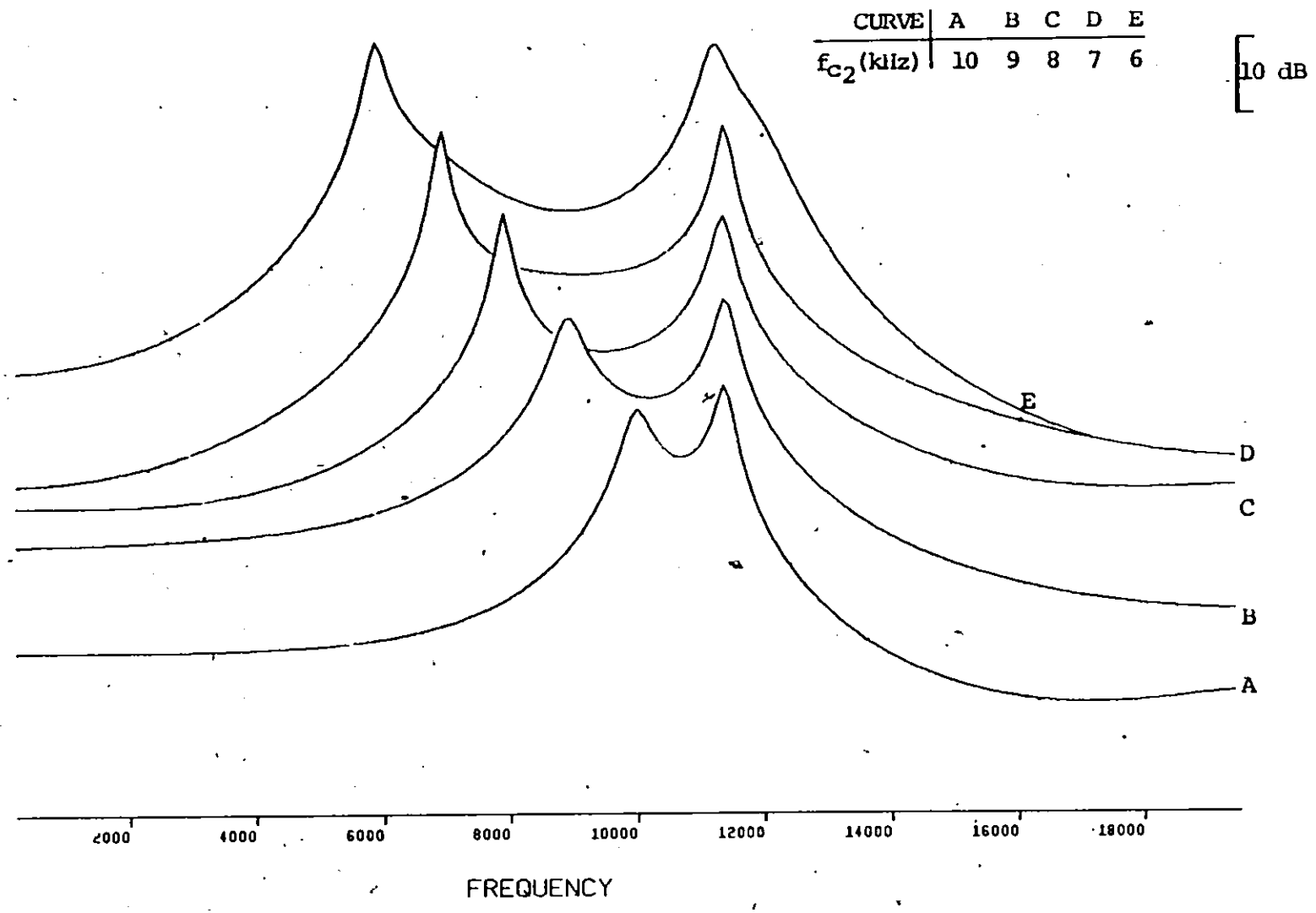

Fig. 5.6: MEMCOR of two sinusoidal modulated ELT signals with f_{c_1} = 11.2 KHz, SNR_1 = SNR_2 = ∞, PEFO = 8 and f_{c_2} as specified on the plot.

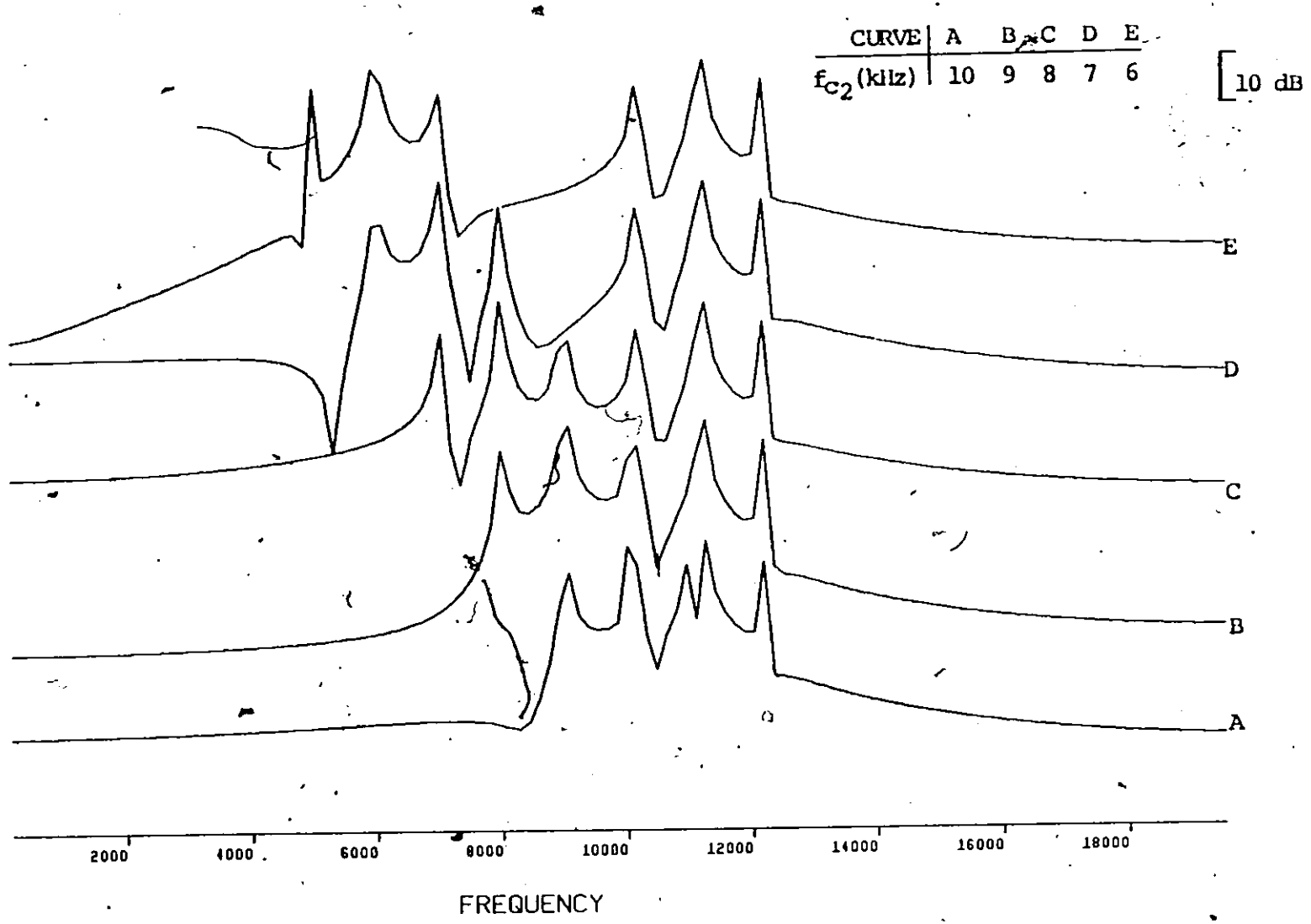

Fig. 5.7: Amplitude spectra of two sinusoidal modulated ELT signals with f_{c_1} = 11.2 KHz, $SNR_1 = SNR_2 = \infty$ and f_{c_2} as specified on the plot.

the FFT) is greatly reduced and the two predominant peaks are the peaks of interest, the major sidelobes are still only about 3-4 dB down from the main peaks and could quite eaily trigger a false alarm. Again we note the superior performance of the MEM and MEMCOR over the FFT since they result in easily detectable and well defined peaks.

5.1.3 Pulse and Sinusoidal Modulated ELT Signals

We noted in Chapter 4 that results for a sinusoidal modulated signal were significantly better than those for a pulse modulated signal. Figures 5.8, 5.9 and 5.10 show that when we process a combination of pulse and sinusoidal modulated signals all three methods yield a more prominant peak at the carrier frequency associated with the sinusoidal modulated signal. The MEM and MEMCOR both provide good detection capability whereas the FFT does not offer any hope of detecting the peak at the carrier of the pulse modulated signal. Although results for the MEM and MEMCOR are good, we find these methods are not failsafe as indicated by their inability to resolve the peak at 11.2 KHz when fc_2 is 9 KHz. Increasing the prediction error filter order is found to overcome this difficulty.

In Chapter 4, we found the MEM based methods performed satisfactorily for single ELT signals when the order was set constant at 3. However, for multiple signals, the filter order which results in the best performance is subject to variation from one case to another. Using filter orders that are too low results in a failure to resolve the peaks whereas too high an order results in the appearance of erroneous peaks.

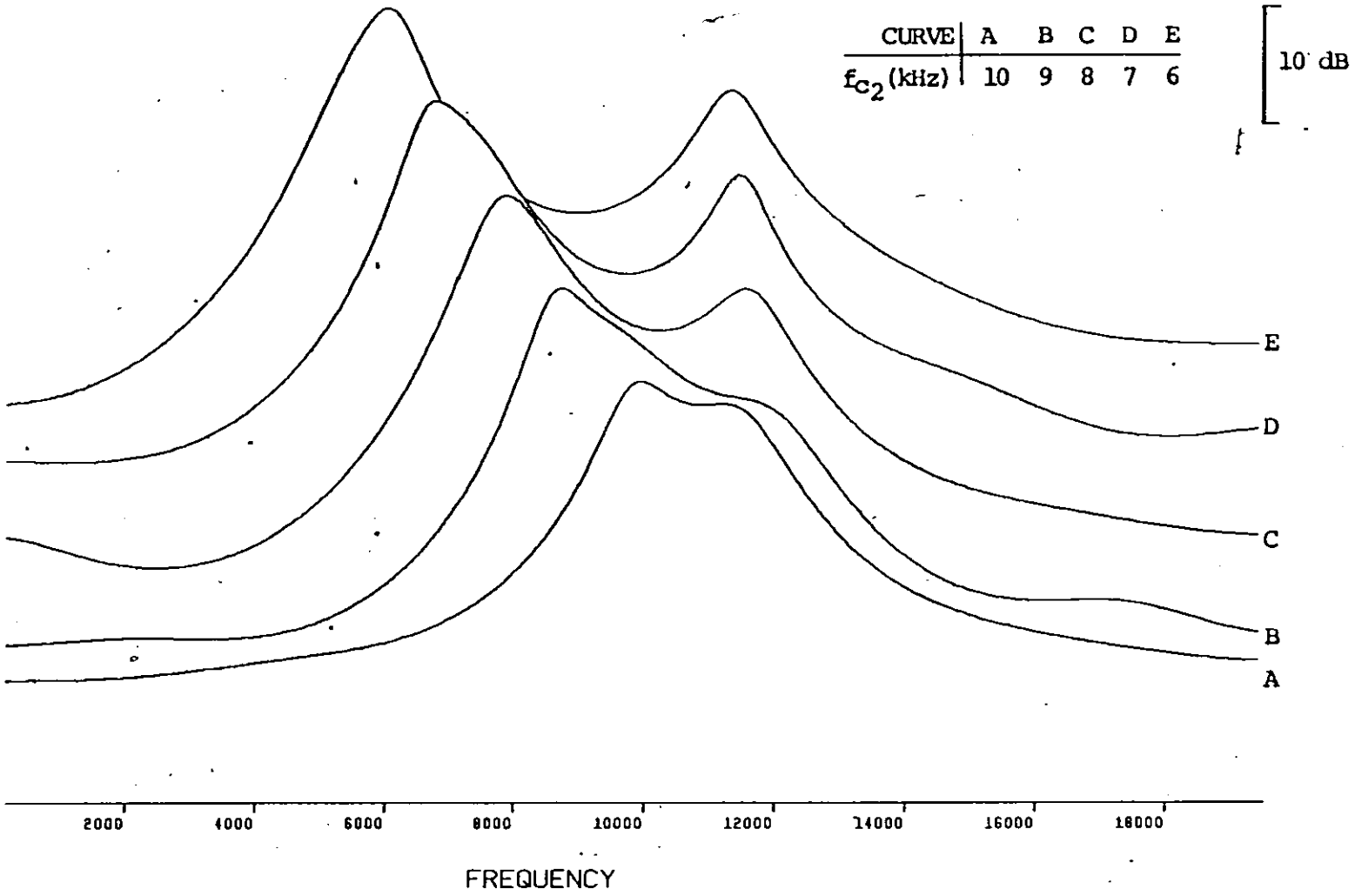

Fig. 5.8: ME spectra of the combination of square and sinusoidal modulated ELT signals with f_{c_1} = 11.2 KHz, SNR_1 = SNR_2 = ∞, PEFO = 10 and f_{c_2} as specified on the plot.

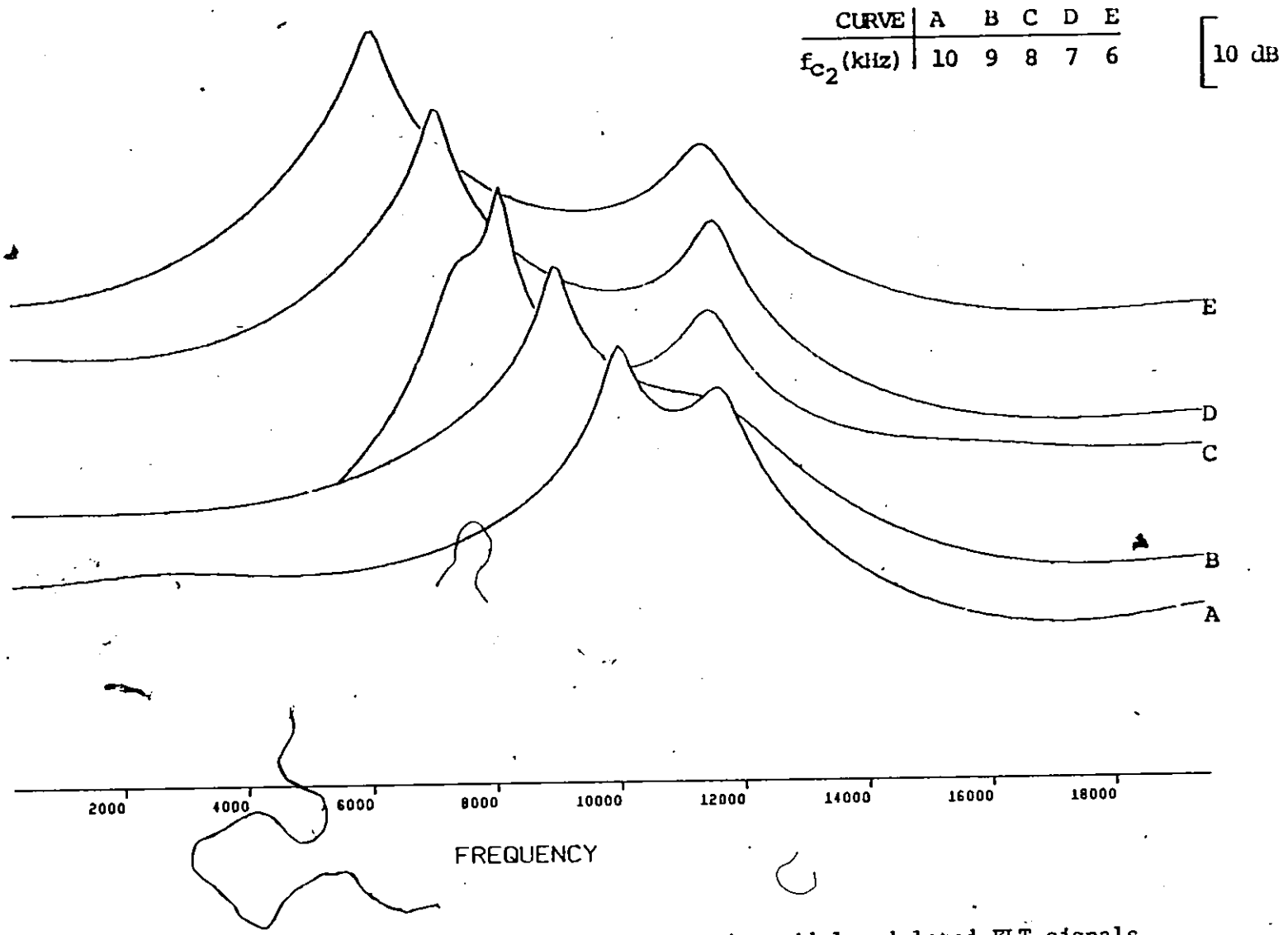

Fig. 5.9: MEMCOR of the combination of square and sinusoidal modulated ELT signals with f_{c_1} = 11.2 KHz, SNR_1 = SNR_2 = ∞, PEFO = 10 and f_{c_2} as specified on the plot.

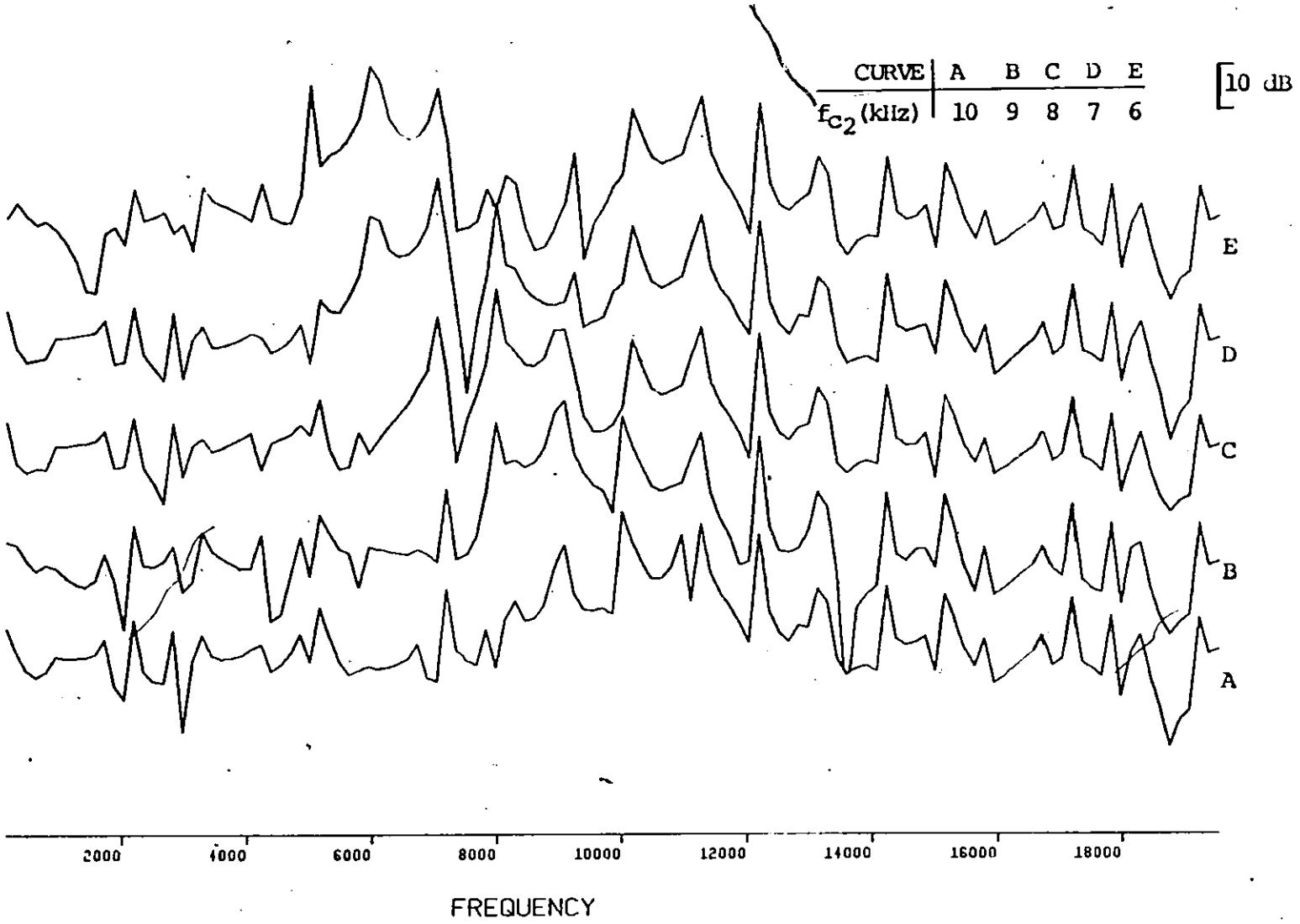

Fig. 5.10: Amplitude spectra of the combination of square and sinusoidal modulated ELT signals with f_{c_1} = 11.2 KHz, $SNR_1 = SNR_2 = \infty$ and f_{c_2} as specified on the plot.

5.4 The Effect of Variations in SNR

The capability of each processor to detect ELT signals in noise is an important characteristic in gauging its performance. As pointed out in the previous section, the remainder of this chapter limits consideration to the particular case of a combination of pulse modulated and sinusoidal modulated ELT signals. Values of the parameters pertaining to each plot are specified below that plot. Parameters set constant are the offset, which is set equal to the duration of a single pulse of the modulating pulse train, and the carrier frequencies associated with the pulse modulated and sinusoidal modulated signals, fc_1 and fc_2 (11.2 KHz and 8 KHz respectively). Consideration is given to cases of equal as well as unequal SNR's.

5.2.1 Processing Signals of Equal SNR

Figures 5.11, 5.12 and 5.13 depict results for the MEM, the MEMCOR and the FFT as the SNR is varied from 20 dB to 0 dB in steps of 5 dB. The signal to noise ratios of both signals are equal for any particular curve and are given by the values quoted on the plot.

Both the MEM and MEMCOR indicate that detection of the two peaks is not a problem even when the signal to noise ratio is in the vicinity of 0 dB. At relatively low values of SNR (less than 10 dB) we find the accuracy of the location of the peak at fc_1, associated with the pulse modulated signal, degrades quite rapidly and is in error by about 800 Hz at 0 dB. On the other hand, the FFT results in a spectrum from which it is not possible to detect the peak at fc_1 since it is masked by the sidelobe structure.

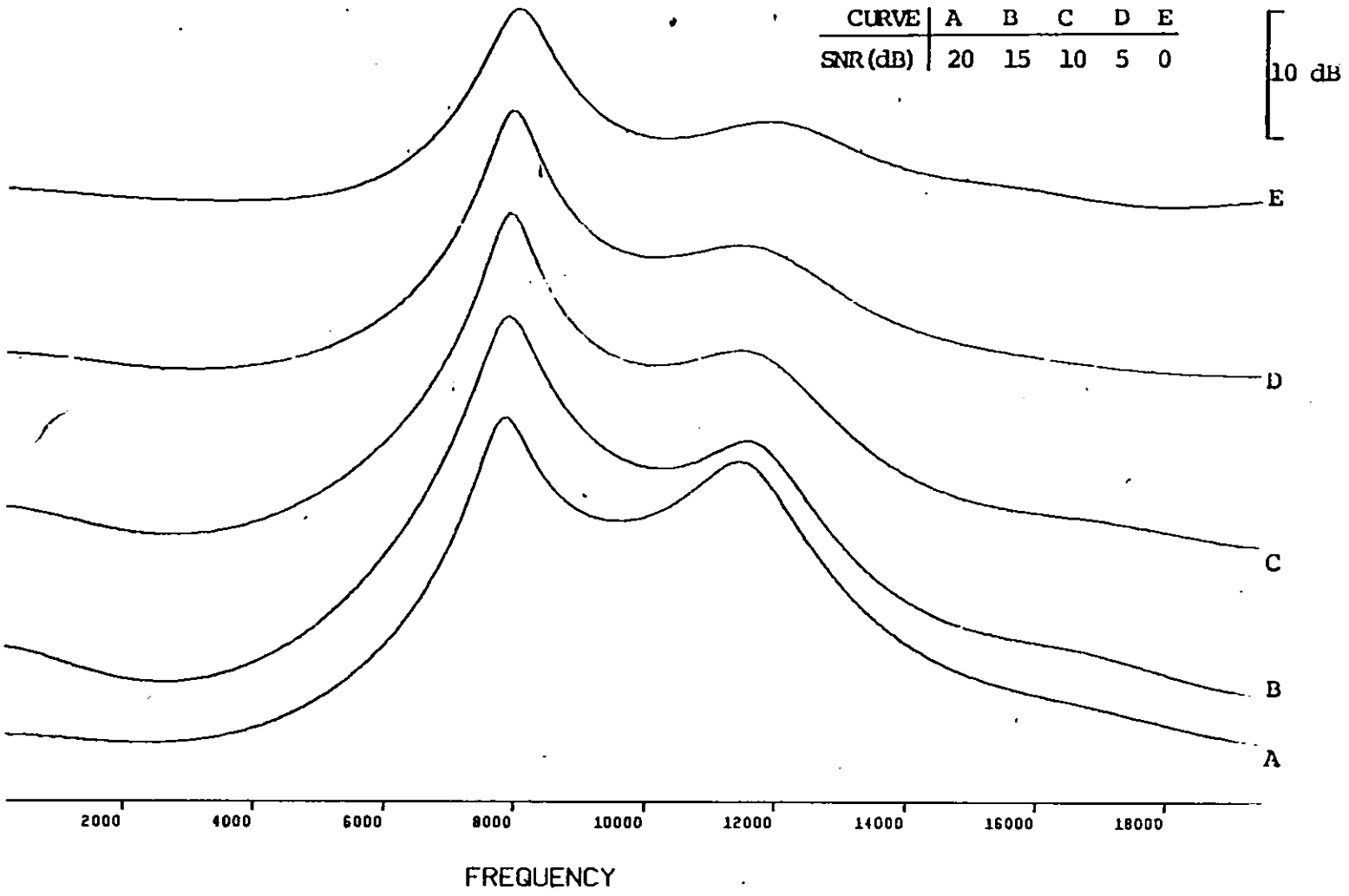

Fig. 5.11: ME spectra of the combination of square and sinusoidal modulated ELT signals with f_{c_1} = 11.2 KHz, f_{c_2} = 8 KHz, PEFO = 10 and SNR_1 = SNR_2 (specified on the plot.

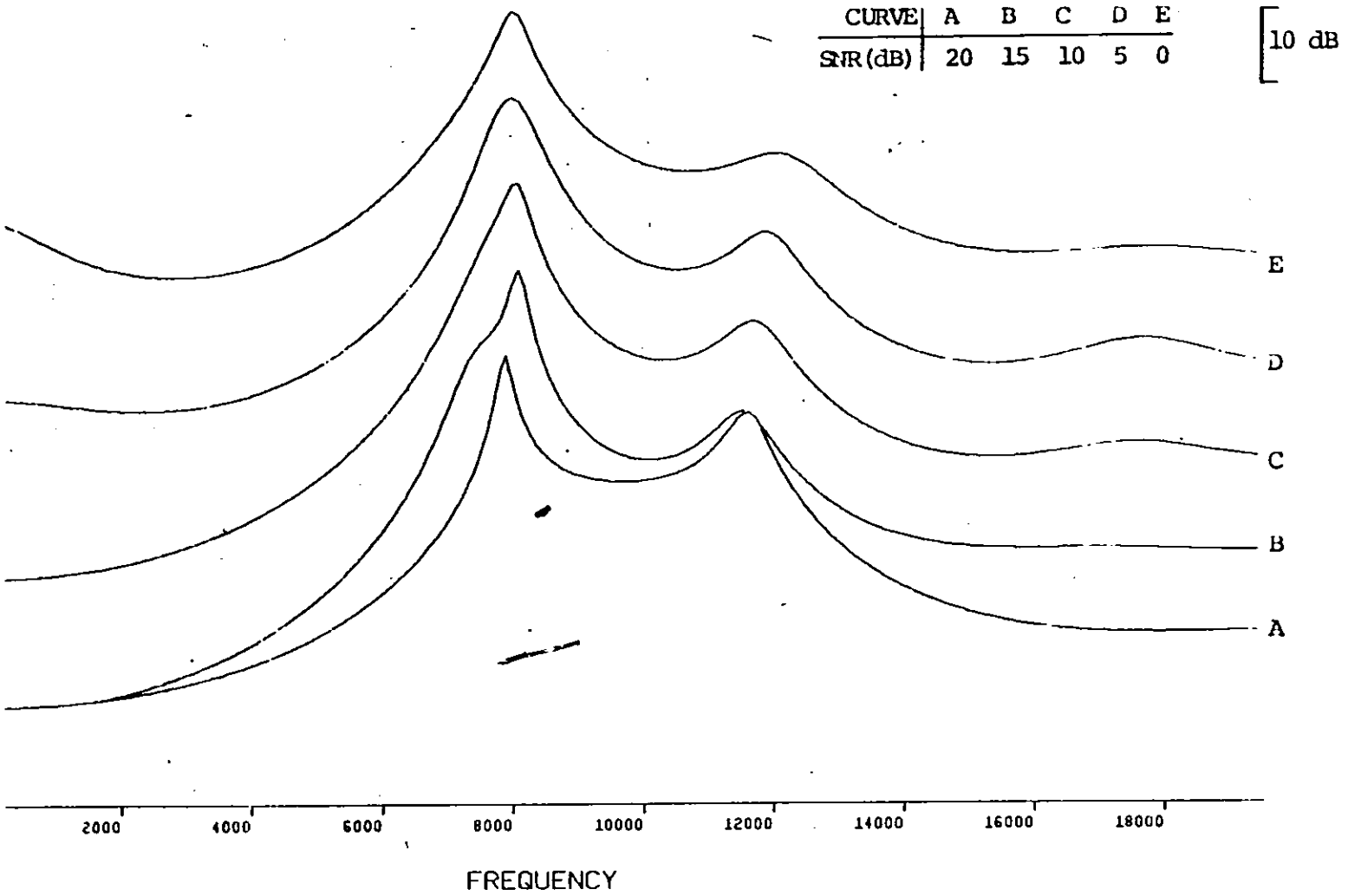

Fig. 5.12: MEMCOR of the combination of square and sinusoidal modulated ELT signals with f_{c_1} = 11.2 KHz, f_{c_2} = 8 KHz, PEFO = 9 and SNR_1 = SNR_2 (specified on the plot.

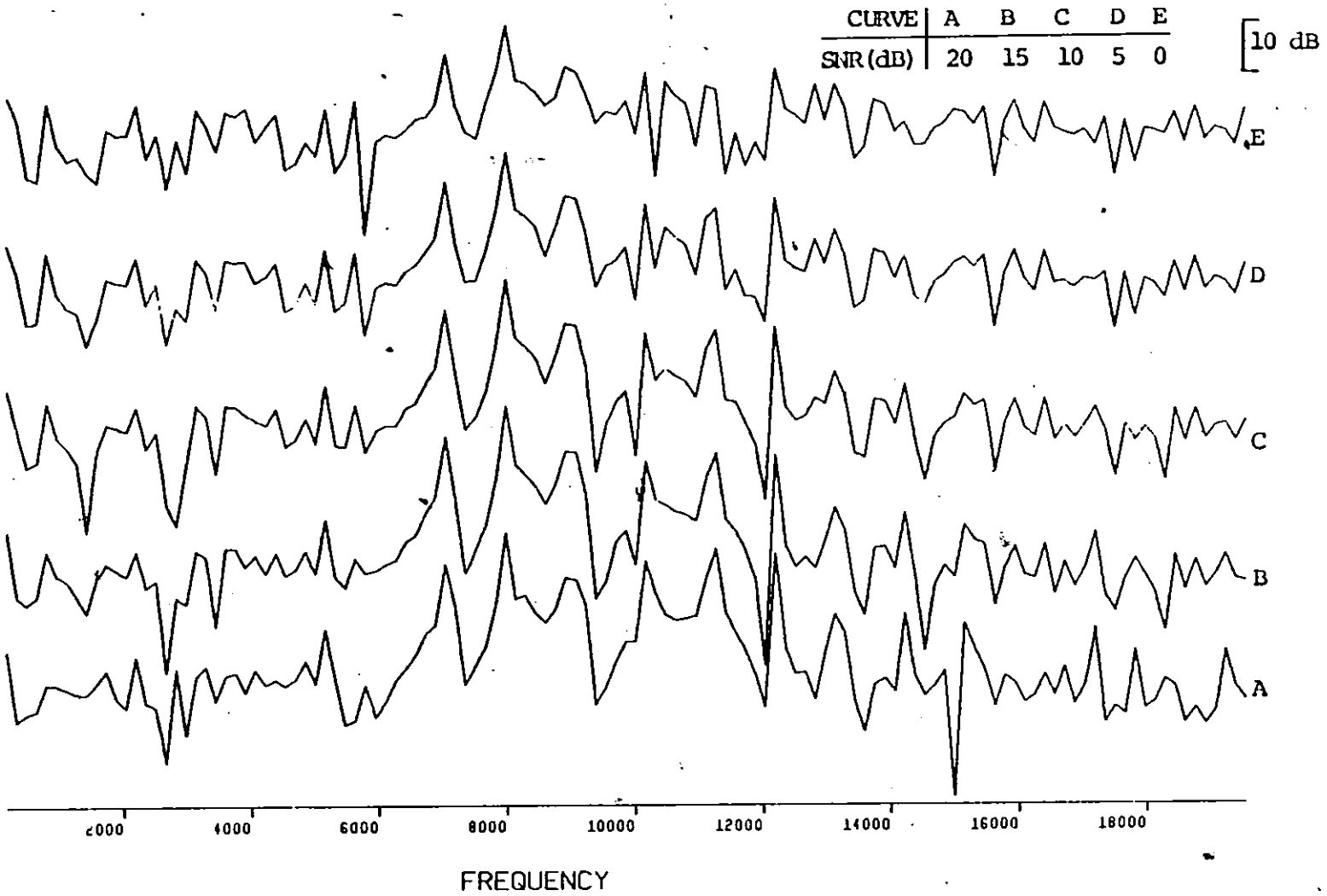

Fig. 5.13: Amplitude spectra of the combination of square and sinusoidal modulated ELT signals with f_{c_1} = 11.2 KHz, f_{c_2} = 8 KHz and SNR_1 = SNR_2 (as specified on the plot.

5.2.2 Processing Results for Unequal SNR's

The situation of unequal SNR's or unequal signal powers can be thought of as arising due to the two transmitters being at different distances from the satellite or alternatively because the power source of one of the transmitters is failing. In order to extract useful information regarding the effect of unequal values of SNR (for the two signals) we divide the results up into two sets. The first set (Figs. 5.14, 5.15 and 5.16) show the effect of maintaining SNR_2 (for the sinusoidal modulated signal) at 10 dB while varying SNR_1 through the range 20 to 0 dB in steps of 5 dB. In contrast, Figs. 5.17, 5.18 and 5.19 correspond to the situation where SNR_1 is maintained at 10 dB while SNR_2 is varied from 20 dB to 0 dB in steps of 5 dB. Consider the case of SNR_2 constant while the SNR of the pulse modulated signal is varied (Figs. 5.14, 5.15 and 5.16). The FFT provides a good estimate of fc_2 but the problem of detecting the peak at fc_1 exists at all values of SNR_1. A comparison of the MEM and the MEMCOR shows that the MEM is a lot less sensitive to differences in SNR. In particular, we find the MEM performs adequately to the point where both SNR"s are 10 dB. The above comments are also applicable to the case of SNR_1 equal to 10 dB and SNR varied (Figs. 5.17, 5.18 and 5.19). An interesting point to note is that results for the MEM (Fig. 5.17) are now considerably better. It would appear, from Figs. 5.14 and 5.17, that as long as the SNR of the pulse modulated signal is in the region of 10 dB or more, the MEM can be used to detect the peaks at the carrier frequencies even when SNR_2 is 0 dB. On the other hand when the SNR of the pulse modulated signal is less than 10 dB, detection is possible even when the SNR's are 0 dB only if the two signals are of approximately equal powers.

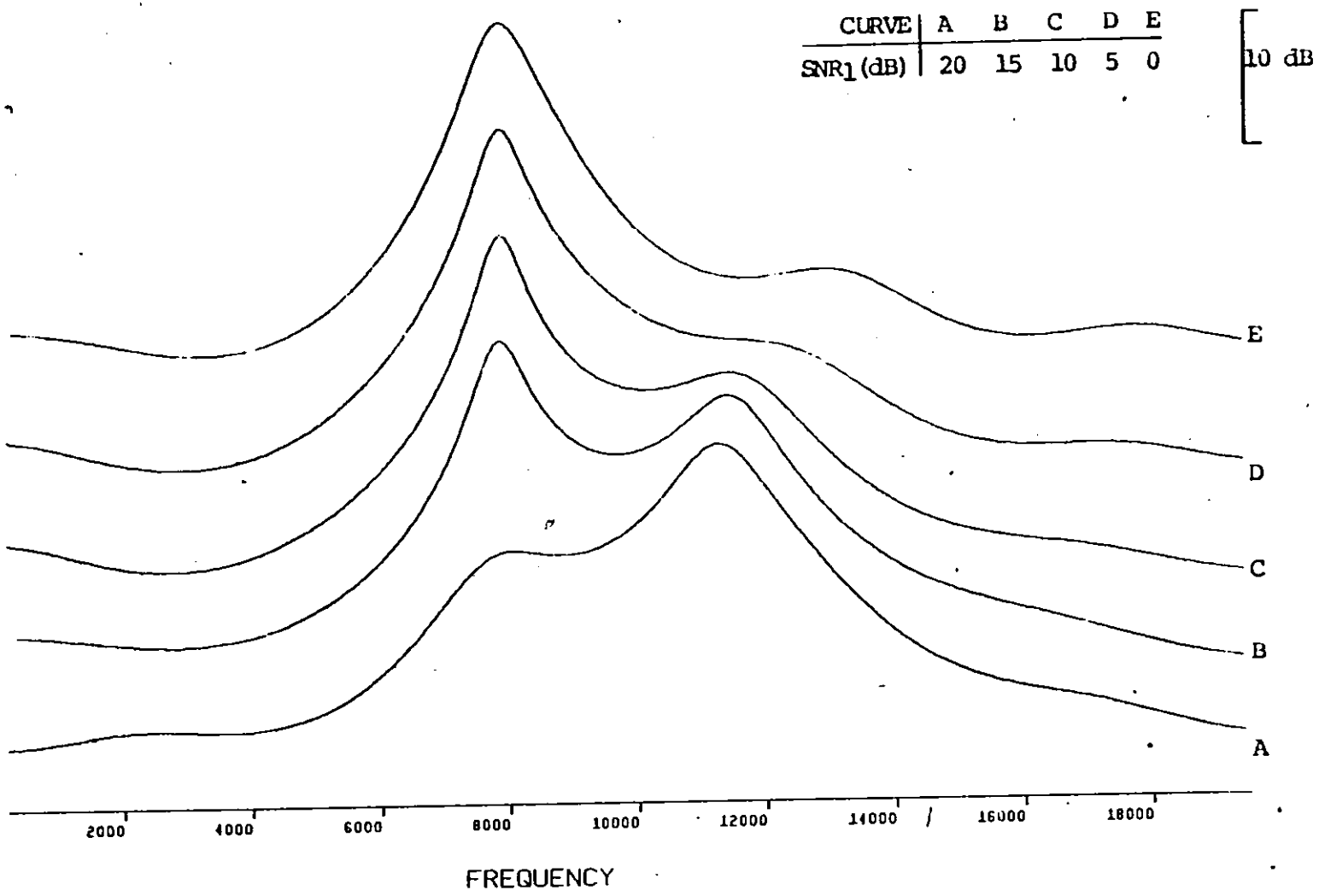

Fig. 5.14: ME spectra of the combination of square and sinusoidal modulated ELT signals with f_{c_1} = 11.2 KHz, f_{c_2} = 8 KHz, PEFO = 10, SNR_2 = 10 dB and SNR_1 as specified on the plot.

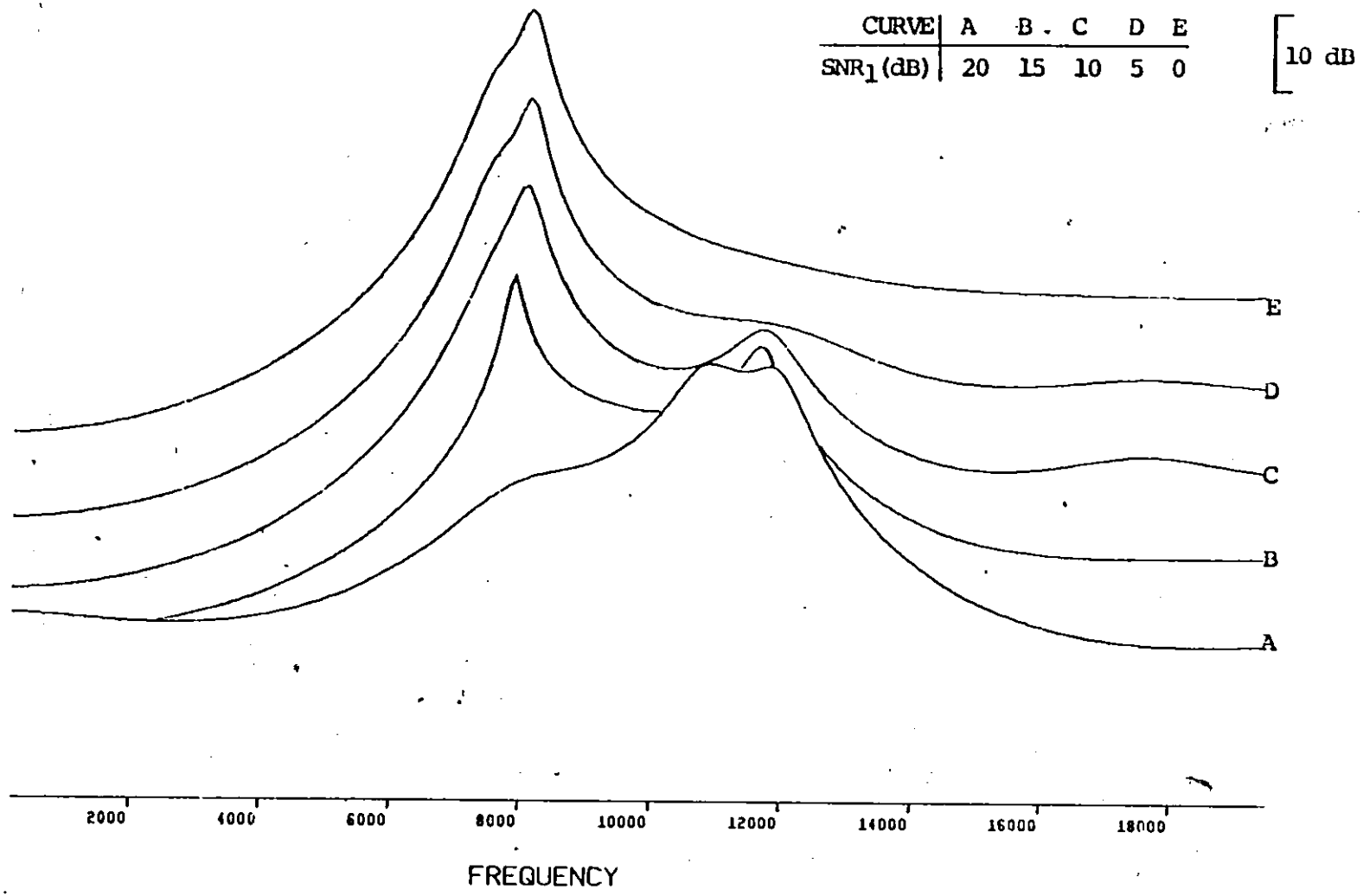

Fig. 5.15: MEMCOR of the combination of square and sinusoidal modulated ELT signals with f_{c_1} = 11.2 KHz, f_{c_2} = 8 KHz, PEFO = 9, SNR_2 = 10 dB and SNR_1 as specified on the plot.

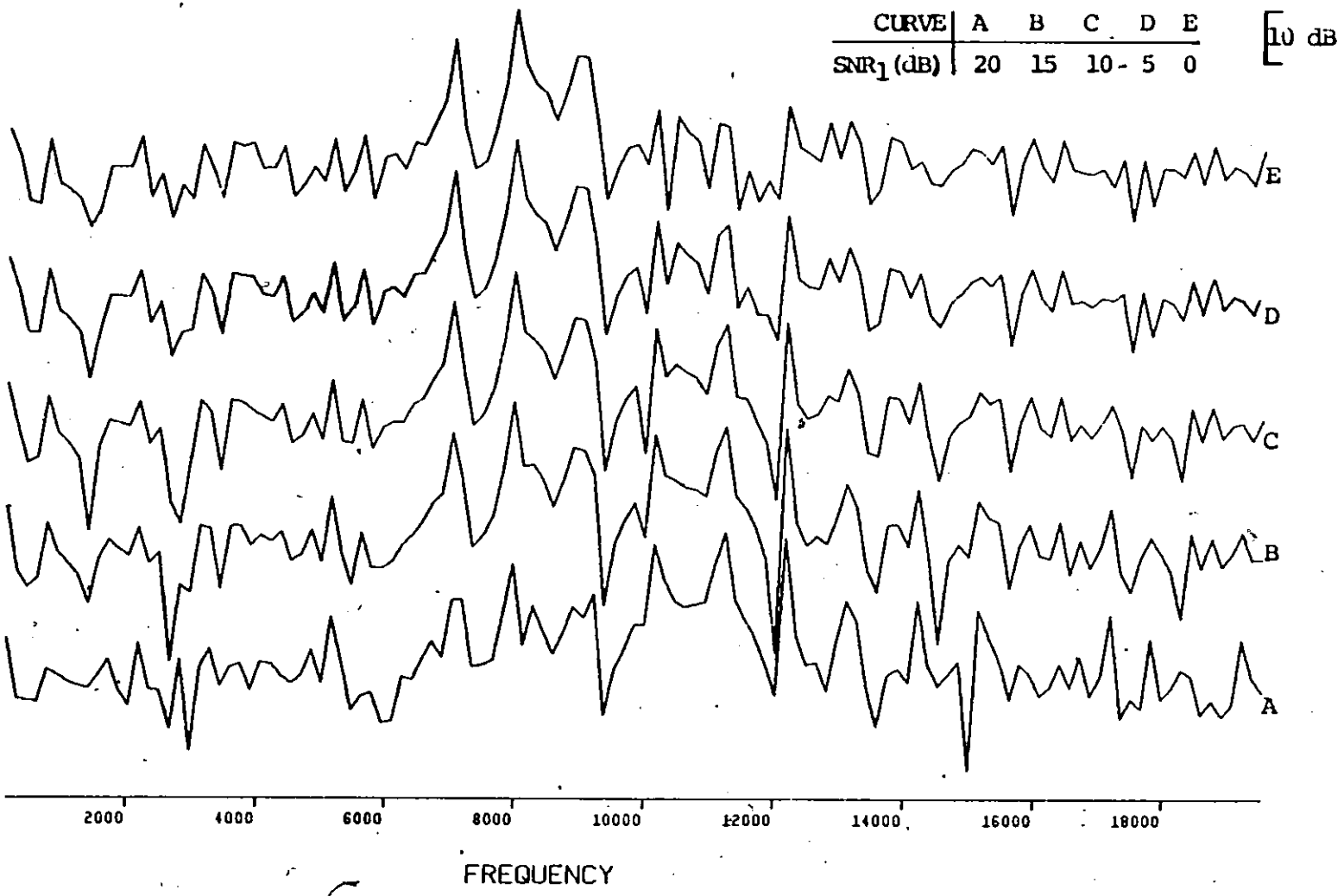

Fig. 5.16: Amplitude spectra of the combination of square and sinusoidal modulated ELT signals with f_{c_1} = 11.2 KHz, f_{c_2} = 8 KHz, SNR_2 = 10 dB and SNR_1 as specified on the plot.

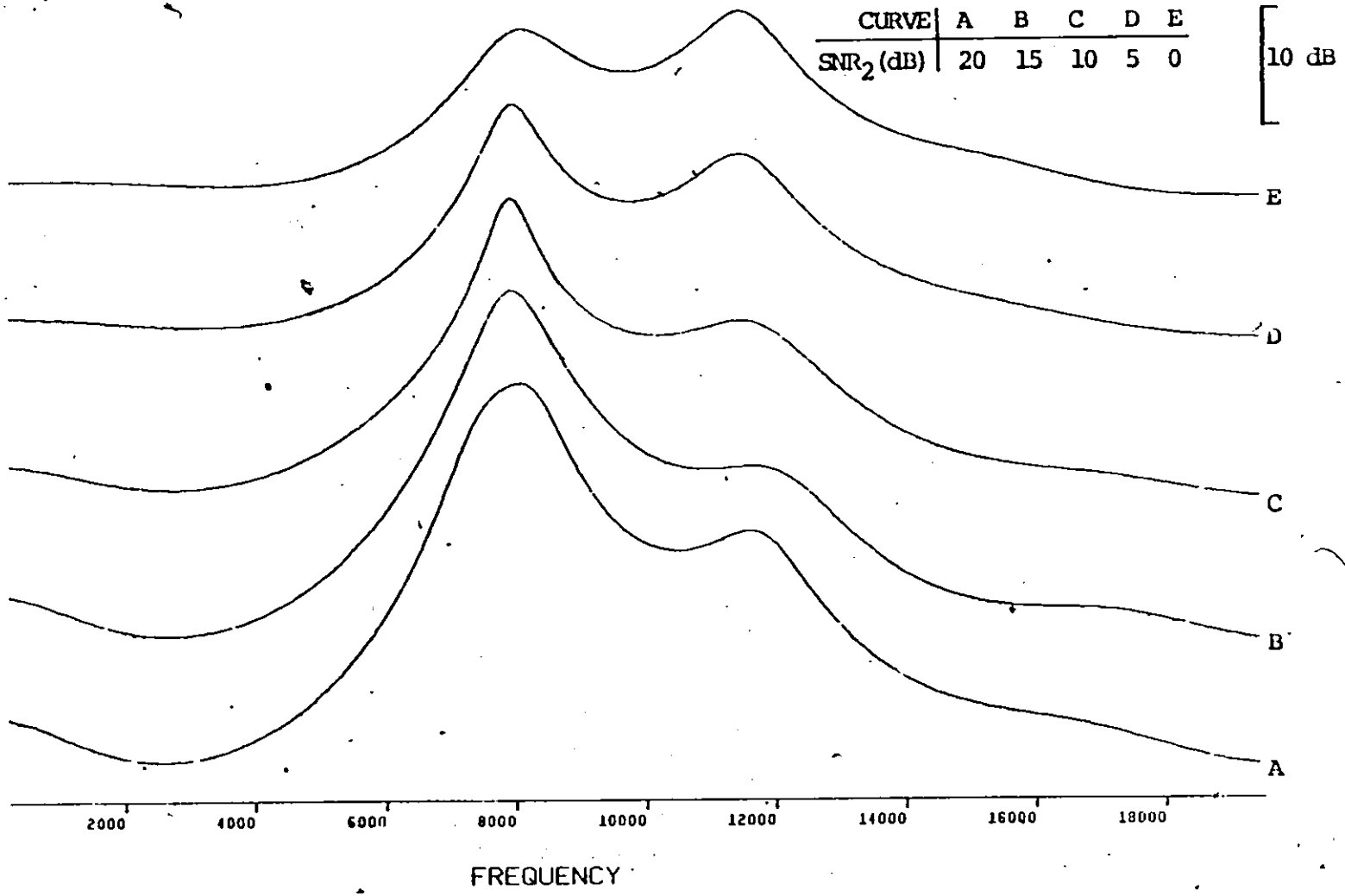

Fig. 5.17: ME spectra of the combination of square and sinusoidal modulated ELT signals with f_{c_1} = 11.2 KHz, f_{c_2} = 8 KHz, PEFO = 10, SNR_1 = 10 dB and SNR_2 as specified on the plot.

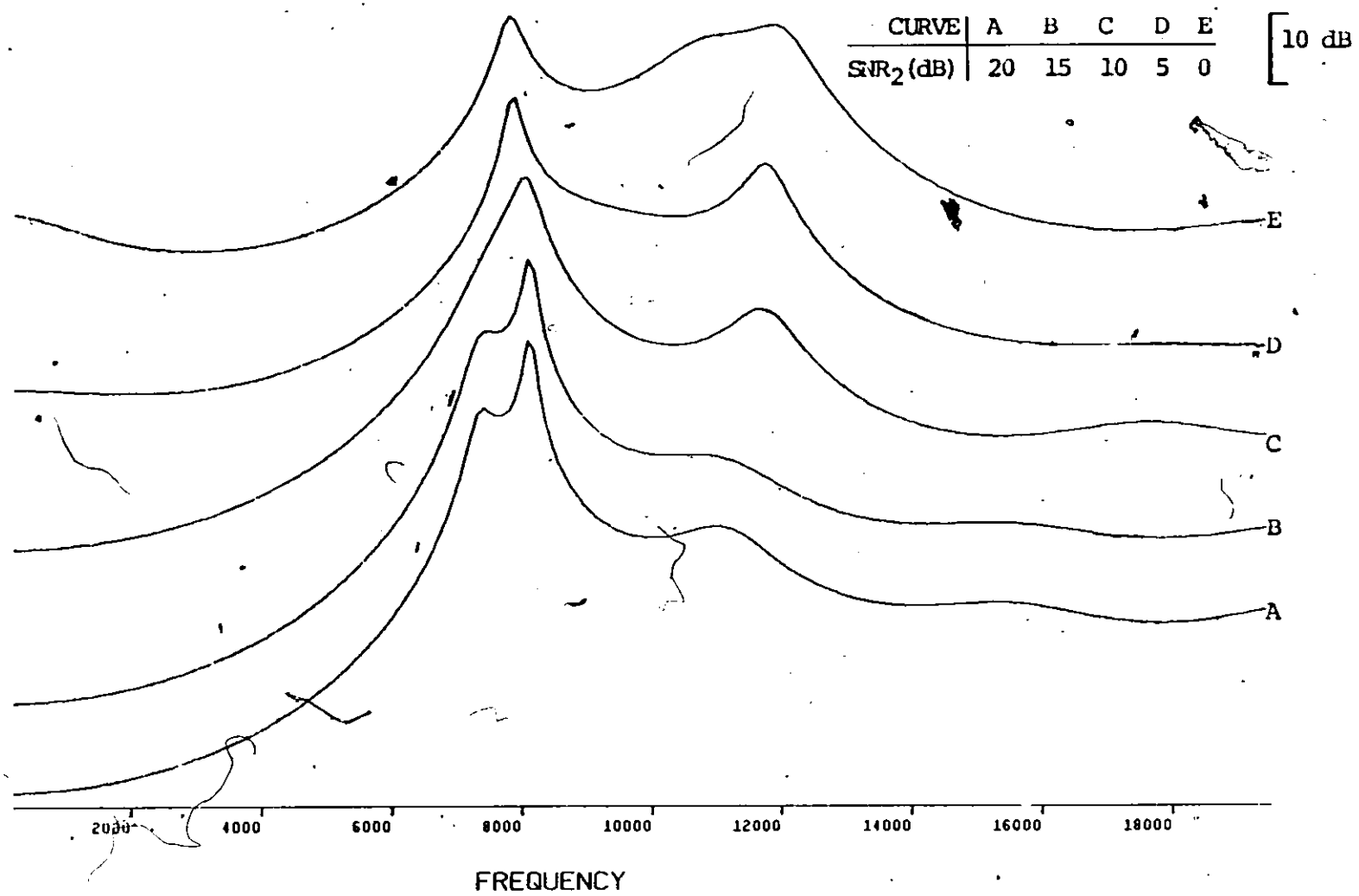

Fig. 5.18: MEMCOR of the combination of square and sinusoidal modulated ELT signals with f_{c_1} = 11.2 KHz, f_{c_2} = 8 KHz, PEFO = 9, SNR_1 = 10 dB and SNR_2 as specified on the plot.

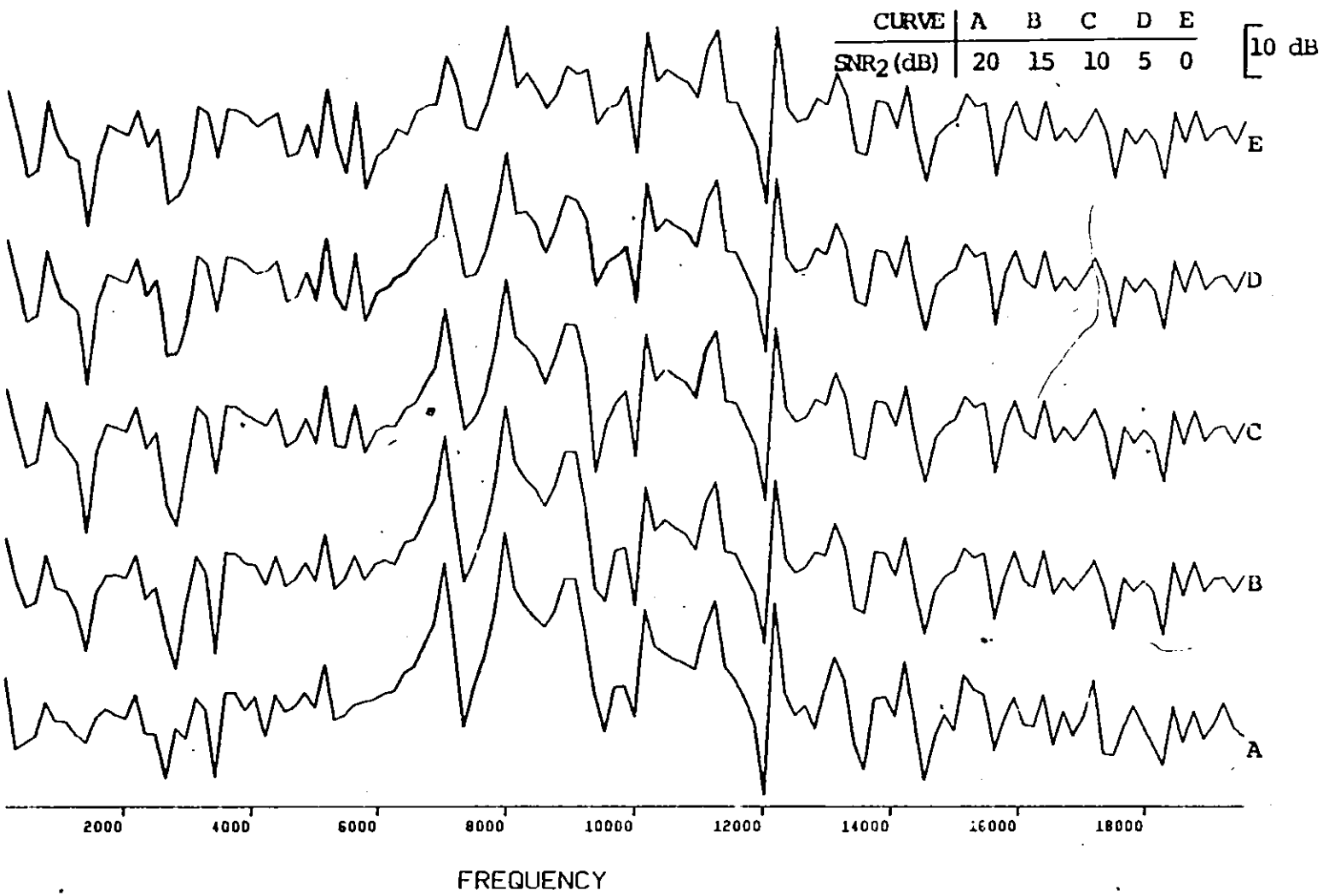

Fig. 5.19: Amplitude spectra of the combination of square and sinusoidal modulated ELT signals with f_{c_1} = 11.2 KHz, f_{c_2} = 8 KHz, SNR_1 = 10 dB and SNR_2 as specified on the plot.

5.3 Variation of the Offset Between the Signals

In varying the offset (t_{of}) we set the other variables constant. The values of these variables are $SNR_1 = SNR_2 = 10$ dB, $fc_1 = 11.2$ KHz and $fc_2 = 8$ KHz where again the indicies 1 and 2 refer to the pulse modulated and sinusoidal modulated signals respectively. Figs. 5.20, 5.21 and 5.22 show results for the MEM, the MEMCOR and the FFT. The offset time for each subsequent curve on a single plot is increased by a time of approximately one quarter the duration of a single pulse of the train of modulating pulses with zero offset for the first curve. We note that a time shift is equivalent to multiplying by an exponential term in the frequency domain. As we would expect, the effect of varying the offset is a very slight change in the FFT spectrum (Fig. 5.22). Moreover, it is satisfying to note that the MEM and MEMCOR are also not effected to any significant extent by this variation.

5.4 A Phase Randomized Signal

In order to investigate the detection performance of each method when the pulse modulated signal is phase randomized we include the plots of Figs. 5.23, 5.24 and 5.25. The values of the variables used are $SNR_1 = SNR = 10$ dB, $fc_1 = 11.2$ KHz and the time offset is equal to the duration of a single pulse of the pulse modulation. For the five curves on each plot, the values of fc_2 are 10, 9, 8, 7 and 6 KHz in that order. The effect of phase randomization of the pulse modulated signal is quite apparent from Fig. 5.25 which shows a severe rounding of the peak and sidelobe structure corresponding to the pulse modulated signal. Again we see that detection of the peak at 11.2 KHz is not possible when using the FFT. Figure 5.24 indicates that the MEMCOR is not without its

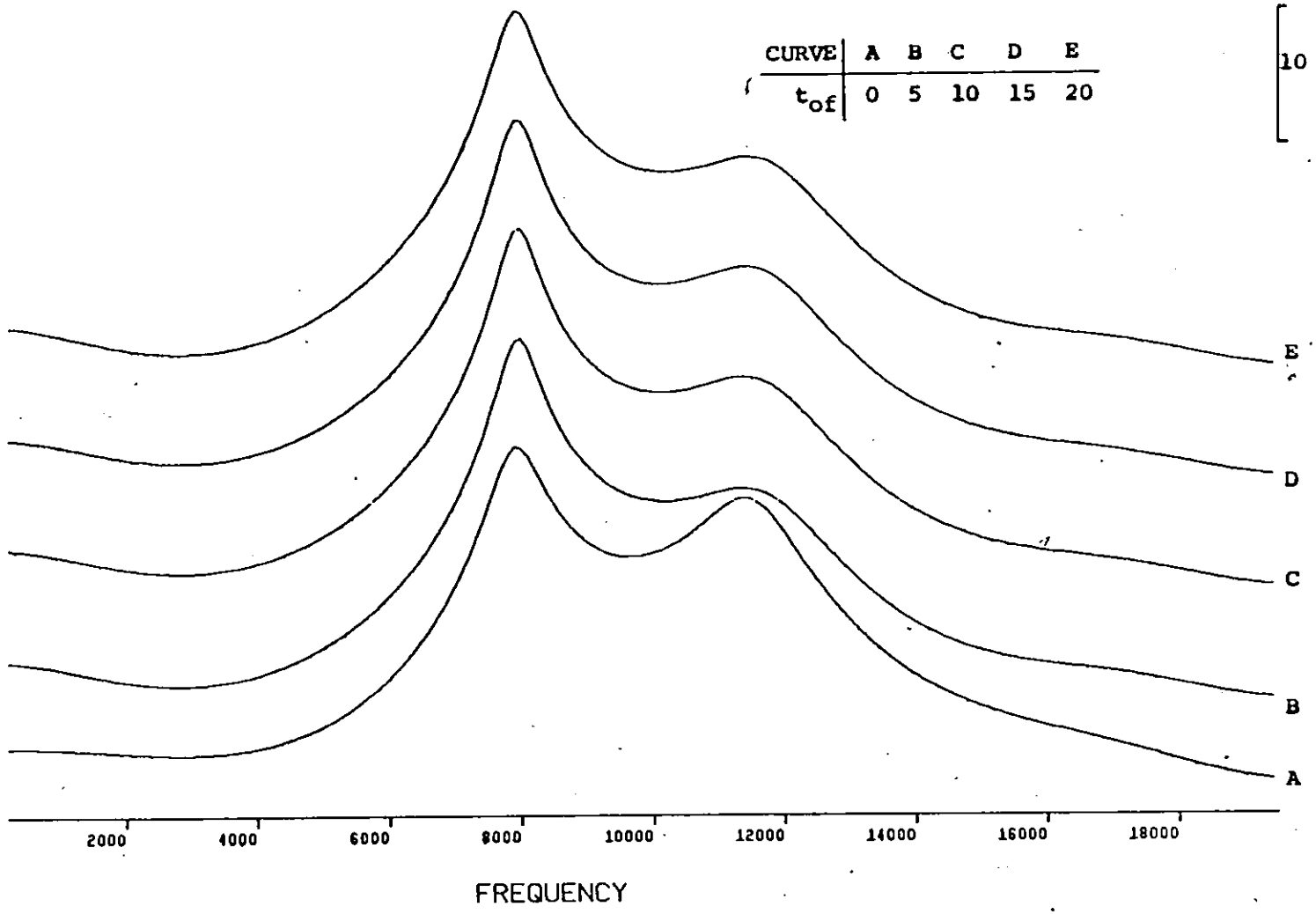

Fig. 5.20: MEM of the combination of square and sinusoidal modulated ELT signals with f_{c_1} = 11.2 KHz, f_{c_2} = 8 KHz, PEFO = 10, SNR_1 = SNR_2 = 10 dB and the offset time (t_{of}) as specified.

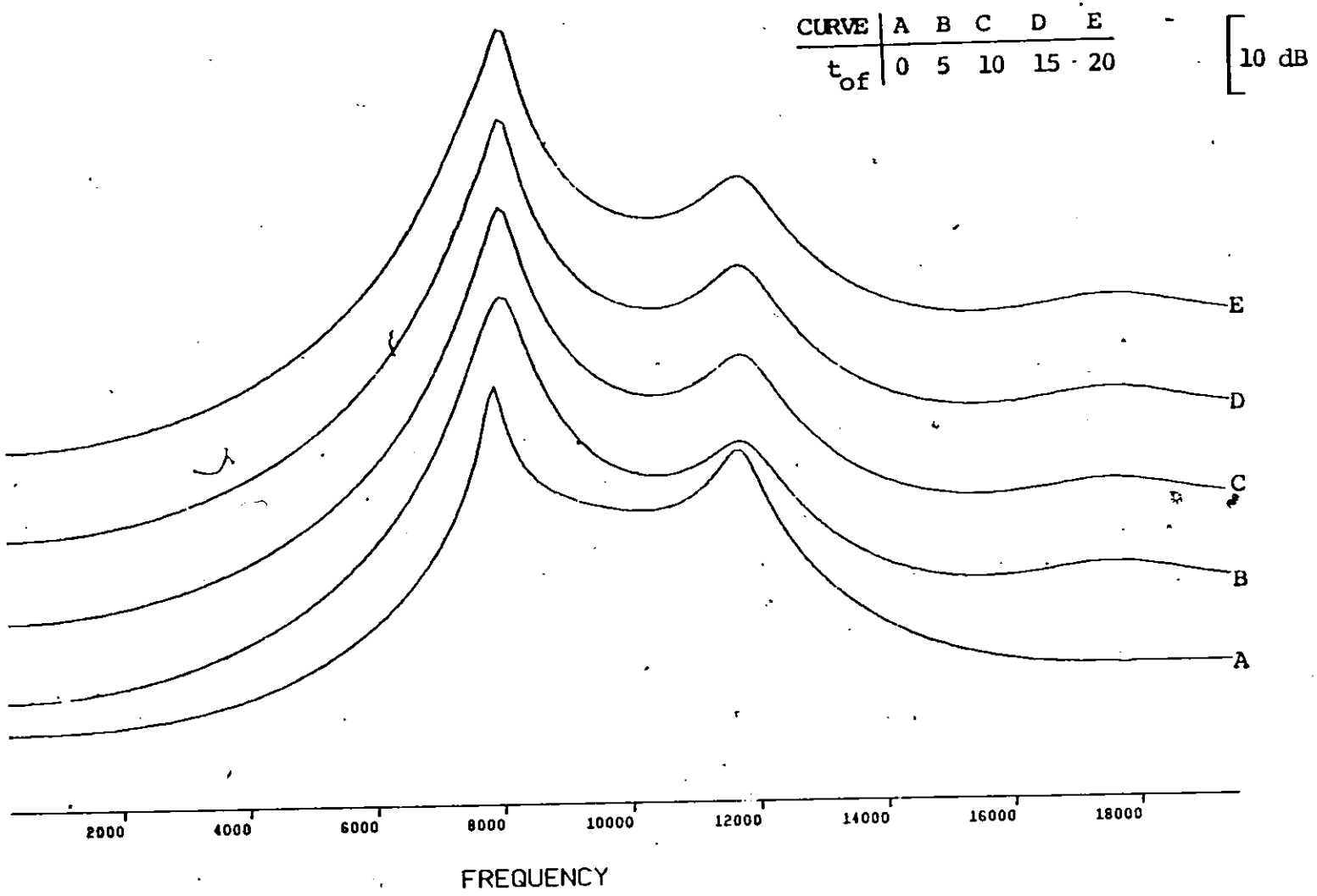

Fig. 5.21: MEMCOR of the combination of square and sinusoidal modulated ELT signals with f_{c_1} = 11.2 KHz, f_{c_2} = 8 KHz, PEFO = 9., $SNR_1 = SNR_2$ = 10 dB and the offset time (t_{of}) as specified on the plot.

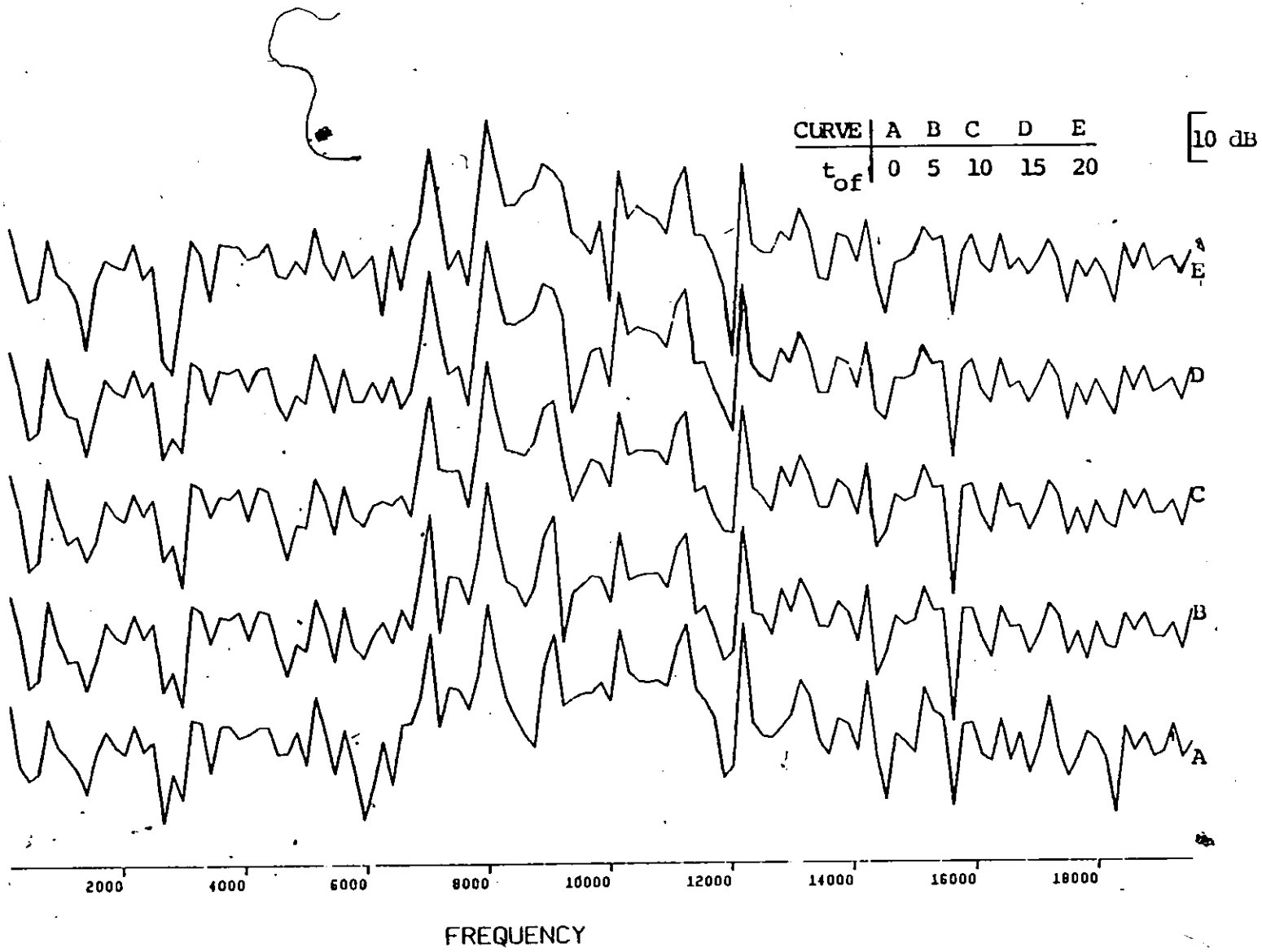

Fig. 5.22: Amplitude spectra of the combination of square and sinusoidal modulated ELT signals with f_{c_1} = 11.2 KHz, f_{c_2} = 8 KHz, SNR_1 = SNR_2 = 10 dB and t_{of} as specified on the plot.

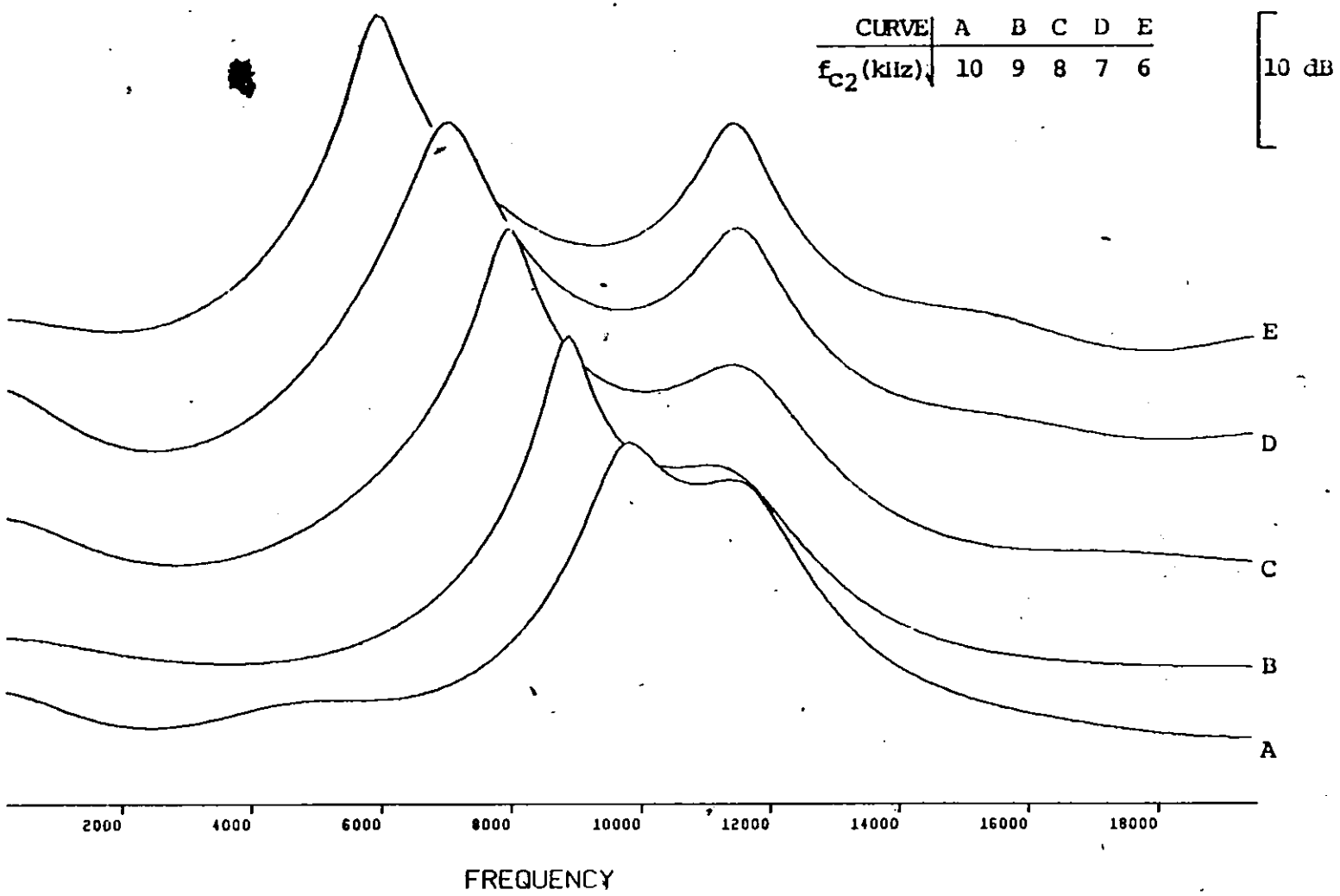

Fig. 5.23: ME spectra of the combination of square and sinusoidal modulated ELT signals with f_{c_1} = 11.2 KHz, PEFO = 10, SNR_1 = SNR_2 = 10 dB and f_{c_2} as specified on the plot. The square modulated signal is phase randomized.

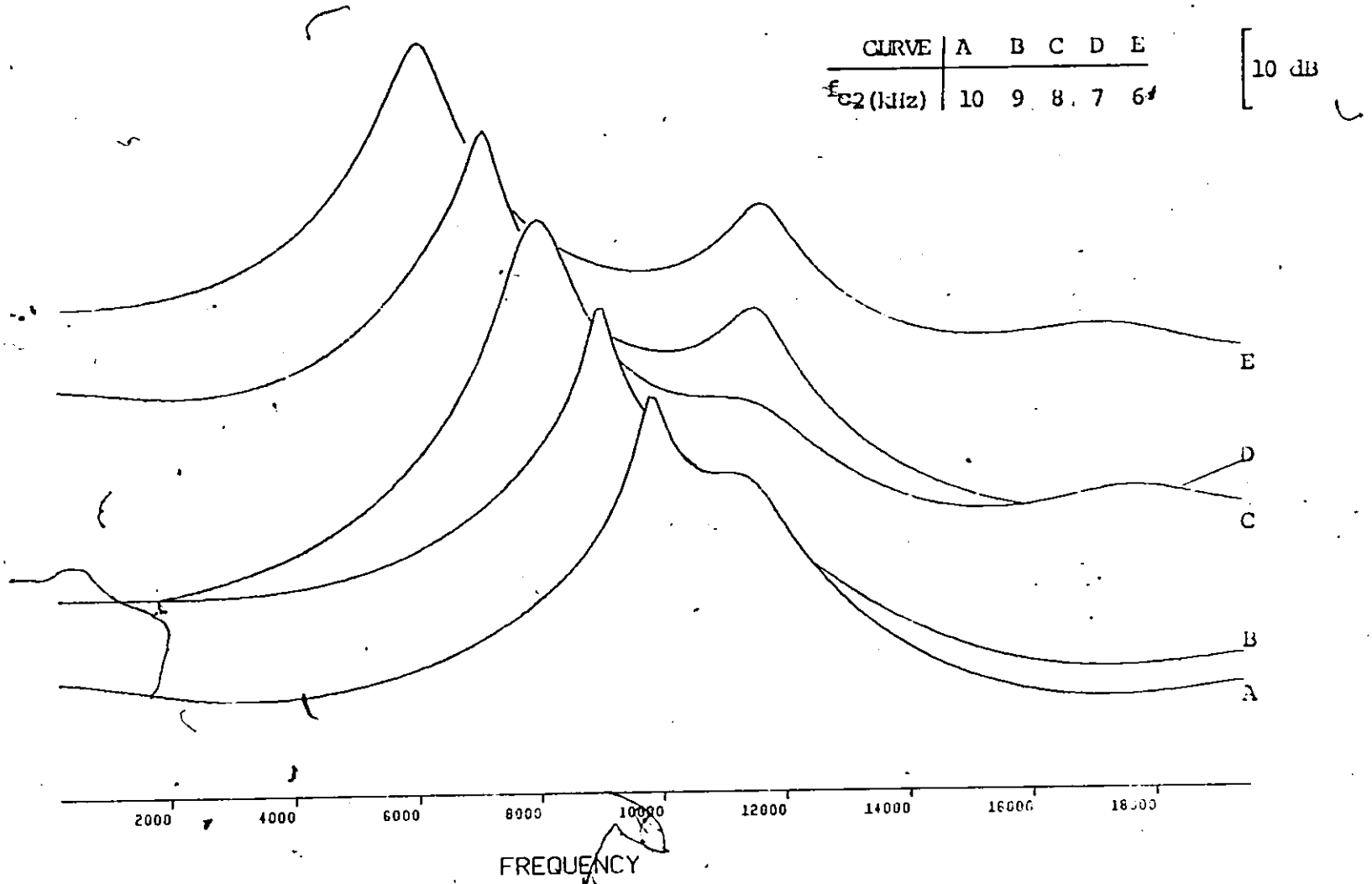

Fig. 5.24: MEMCOR of the combination of square and sinusoidal modulated ELT signals with f_{c_1} = 11.2 KHz, SNR_1 = SNR_2 = 10 dB and f_{c_2} as specified on the plot. The square modulated signal is phase randomized.

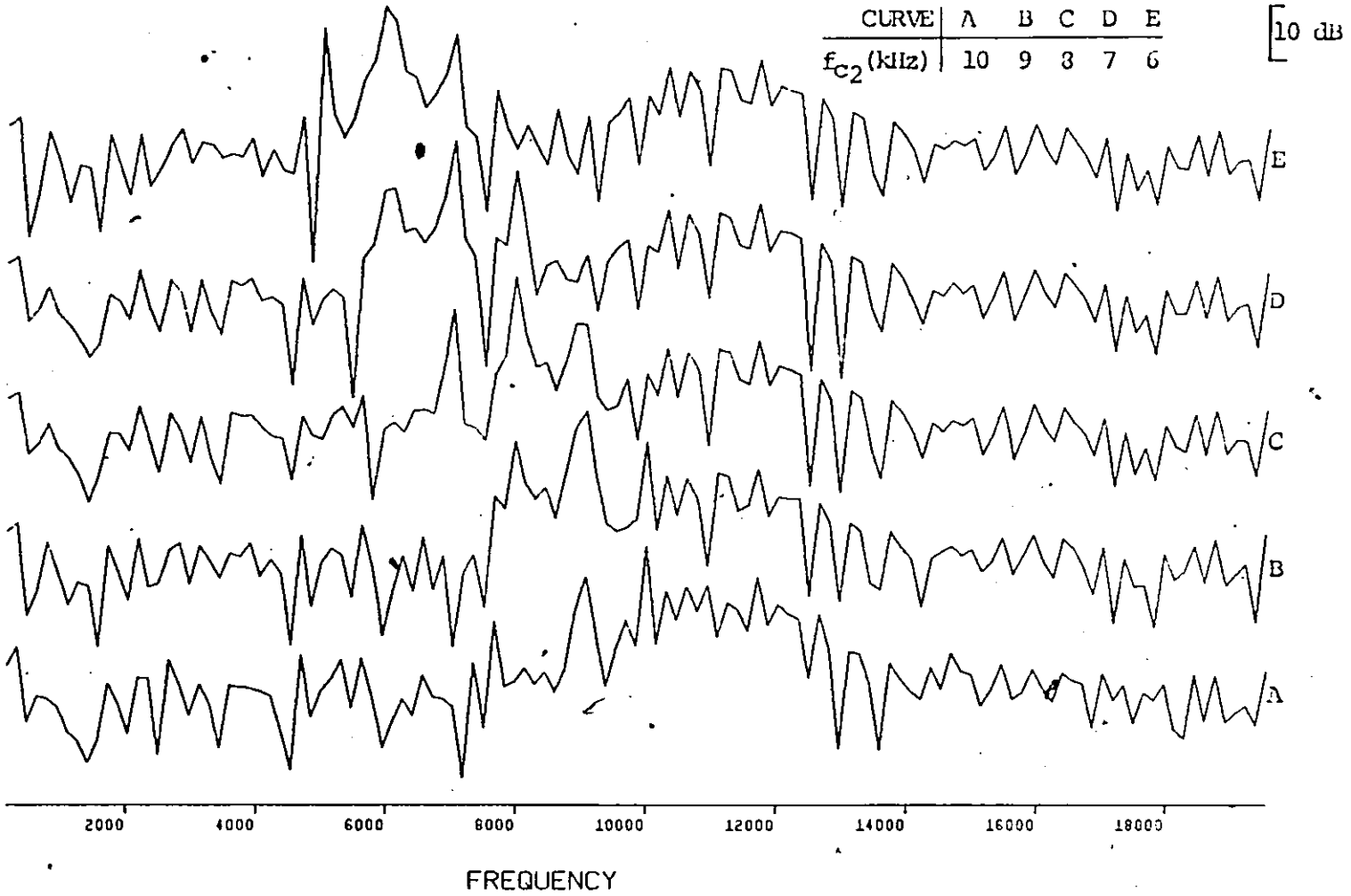

Fig. 5.25: Amplitude spectra of the combination of square and sinusoidal modulated ELT signals with f_{c_1} = 11.2 KHz, SNR_1 = SNR_2 = 10 dB and f_{c_2} as specified on the plot. The square modulated signal is phase randomized.

problems as is evidenced by its inability to resolve the peak at 11.2 KHz consistantly. The superior performance of the MEM as compared to the other two methods is shown in Fig. 5.23. Although the error in the location of the peak associated with the 11.2 KHz carrier is not negligible (≈ 400 Hz), the MEM certainly enables detection of the two ELT signals.

Although we have had to limit the investigation in this chapter, the problems and advantages of each method have surfaced through the analysis. Comments related to these attributes together with concluding remarks and suggestions for further work are presented in Chapter 6.

CHAPTER 6

CONCLUSIONS AND SUGGESTIONS FOR FUTURE WORK

6.1 Conclusions

This work has explored the feasibility of using the MEM for processing emergency locator transmitter signals. In order to gauge its performance the results for the MEM have been compared with those for the signal processing method used presently, namely the FFT. A description of the nature of ELT signals has shown the diversity of 121.5 and 243 MHz signal formats and indicated the complexity of using matched filtering to detect these signals. Moreover, we have outlined some of the problems associated with the FFT. In Chapter 3 we described the mechanics of the MEM and pointed out the equations necessary to determine the prediction filter coefficients recursively. Three methods of terminating this recursive procedure have been tried and found to be unsuitable for the signals being processed. In light of this, the signals were processed using various filter orders and the ideal filter order chosen for each particular case.

As the main body of this thesis differentiated between results for a single ELT signal and for a combination of two ELT signals, the conclusions are also divided into two sections.

6.1.1 Single ELT Signals

1) Upon processing ELT signals employing the two distinct types of

modulation we found detection of the carrier component to be considerably more difficult when the signal employs square modulation. In light of this, further work in the chapter was limited to square modulated signals.

2) A change in the duty cycle of a square modulated signal (an increase) was noted to increase the detection capability of all methods considered. This is as we would expect since the effect of this change is to increase the power at the carrier frequency relative to the power at the modulation.

3) As the SNR is decreased we find the degradation in performance is more rapid with the FFT then the MEM. With the MEM we found that the peak was discernible at SNR's down to about 0 dB although it is shifted. Pre-processing by way of forming the autocorrelation results in increased peak definition (in the MEM) at all SNR's but at the expense of a shift in this peak.

4) Perhaps the most dramatic difference between the MEM and the FFT appears when we process phase randomized signals. Whereas the MEM appears to be relatively immune to phase randomization, the FFT shows a significant degradation and in fact one would have to apply some form of smoothing function to extract useful information from the FFT.

6.1.2 Multiple ELT Signals

1. Results of processing a combination of two ELT signals showed that the particular combination of square modulated and sinusoidal

modulated signals presented the most severe problems. We found when processing single ELT signals that a sinusoidal modulated signal resulted in much sharper spectra than square modulated signals. For multiple signals the FFT results showed that the sidelobes associated with the peak relevant to the sinusoidal modulated signal masked out the peak at the carrier frequency of the square modulated signal. In light of this, further work in the chapter was restricted to this particular combination of signals.

2. The performance of the FFT was found to be unacceptable for all values of SNR since the results did not allow detection of the carrier frequency associated with the square modulated signal. When the signals are of equal power, the MEM performs adequately (with or without prior autocorrelation) at SNR's as low as 0 dB. Pre-processing, however, results in severe degradation when the signals are of unequal power. Use of the MEM is not completely free of detection problems as is evident from Fig. 5.14. When the SNR of the square modulated signal is about 5 dB or less, and the power in the sinusoidal modulated signal is greater by a factor of approximately three, detection of the carrier associated with the square modulated signal becomes a problem. A comparison of the methods being investigated in processing multiple signals in noise has indicated the robustness of the MEM.

6.2 Suggestions for Future Work

This research has established the viability of the MEM as a SARSAT

signal processor. The performance of the MEM has been demonstrated to be superior to that of the FFT in a number of situations. It is suggested that implementation of the MEM algorithm within the SARSAT system would require evaluation of the following details:

1) Develop a strategy for determining the optimum prediction filter order for processing a particular ELT data sequence.
2) Examine the effects of narrowband digital filtering (to subdivide the doppler bandwidth into a number of smaller bandwidths) on ME spectral estimation of ELT signals.
3) Determine the maximum number of ELT signals which can be separated over the 20 KHz bandwidth, assuming no limit to MEM filter order.
4) Calculate the signal to noise ratio with and without digital filtering.
5) Study the enhancement when averaging over MEM spectral records and compare this with the advantage of increasing the length of the data record processed.
6) Evaluate the ultimate capabilities of the MEM processor (for ELT signals) taking doppler shift, signal length (as a fraction of a complete satellite pass) and spectral resolution into account.
7) Study the effects of non-linear amplification on the MEM.
8) Examine methods of processing using a combined "autoregressive - moving average" (ARMA) model.

REFERENCES

1. Mundo, C., Tami, L. and Larson, G., "Program plan for search and rescue electronics alerting and locating system", Transportation systems center, Cambridge, Massachusetts, Rept. No. DOT-TSC-OST-73-42, February, 1974.

2. Lambert, J.D. and Winter, A.E., "A Search and Rescue Satellite System (SARSAT) Experiment", COmmunications '76 Conf., 8-11 June, 1976, Brighton, England.

3. Winter, A.E., Lambert, J.D., Pearce, J.L. and Werstiuk, H.L., "Satellite-Aided Search and Rescue", IEEE Conference, Montreal, Canada, 20-22 October, 1976.

4. Burg, J.P., "Maximum Entropy Spectral Analysis", Ph.D. Thesis, Stanford University, Stanford, CA, May, 1975.

5. Haykin, S. (Editor), "Nonlinear Methods of Spectral Analysis", Springer-Verlag, 1978.

6. Anderson, N., "On the Calculation of Filter Coefficients for Maximum Entropy Spectral Analysis", Geophysics, Vol. 39, No. 1, February 1974, pp. 69-72.

7. Chen, W.Y. and Stegen, G.R., "Experiments with Maximum Entropy Power Spectra of Sinusoids", J. Geophys. Res., Vol. 79, pp. 3019-3022, July 10, 1974.

8. Haykin, S., "Communication Systems", pp. 250-253 (John Wiley and Sons, 1978).

9. "COSPAS/SARSAT Implementation Plan (CSIP)", Joint CANADA, FRANCE, U.S., U.S.S.R. demonstration project, 22 May 1980. Co-authors: Communications Research Centre (CRC), Dept. of Communications, Ottawa, Ontario, Canada, K2H 8S2, et al.

10. Wozencraft, J.M. and Jacobs, I.M., "Principles of Communication Engineering", pp. 234-237 (John Wiley and Sons, 1965).

11. Bergland, G.D., "A Guided Tour of the Fast Fourier Transform", IEEE Spectrum, Vol. 6, No. 7, pp. 41-51, July 1969.

12. Brigham, E.O., "The Fast Fourier Transform", (Prentice-Hall Inc., 1974).

13. Rabiner, L.R. and Gold, B., "Theory and Application of Digital Signal Processing", pp. 356-434 (Prentice-Hall Inc., 1975).

14. Burg, J.P., "A New Analysis Technique for Time Series Data", NATO Adv. Study Inst. Signal Processing, Enschede, Netherlands (1968).

15. Ulrych, T.J., Smylie, D.E., Jensen, O.G. and Clarke, G.K., "Predictive Filtering and Smoothing of Short Records by using Maximum Entropy", J. Geophys. Res., Vol. 78, No. 23, pp. 4959-4964.

16. Radoski, H.R., Fougere, P.F. and Zawalick, E.J., "A Comparison of Power Spectral Estimates and Applications of the MEM", J. Geophys. Res., Vol. 80, No. 4, pp. 619-625, Feb. 1, 1975.

17. Box, G.P. and Jenkins, G.M., "Time Series Analysis - Forecasting and Control", Holden-Day Inc., San Francisco, 1976, pp. 53-66.

18. Chan, H.C. and Haykin, S., "Applications of the MEM in Radar Signal Processing", Comm. Res. Lab., McMaster Univ., Hamilton, Canada, Rept. No. CRL-62, March 1979.

19. Akaike, H., "Fitting Autoregressive Models for Prediction", Ann. Inst. Statist. Math., 21, pp. 243-247, 1969a.

20. Akaike, H., "Statistical Predictor Identification", Ann. Inst. Statist. Math., 22, pp. 203-217, 1970.

APPENDIX A1

PROCESSING RESULTS FOR AN RF PULSE IN NOISE USING THE FFT

Figures A1.1 to A1.6 show the amplitude spectra of an RF pulse with f_c = 10 KHz and signal to noise ratios of 20 dB to -10 dB. As before, we find at high SNR (20 dB) the major sidelobes are 13 dB down from the main lobe. In fact, the sidelobe structure provides little to no hindrence in detecting the peak at the carrier frequency for signal to noise ratios as low as 0 dB. At values of SNR around -5 dB the sidelobe structure begins to attain significant levels compared to the main lobe (approximately 4 to 5 dB down from the main lobe). However, it is not until the signal to noise ratio is below -5 dB that detection becomes severely impaired (Fig. A1.6). It is evident from the results that the FFT performs quite adequately as a method of detecting the peak at the carrier frequency when the signal under consideration is an RF pulse and the signal to noise ratio is approximately 0 dB or greater.

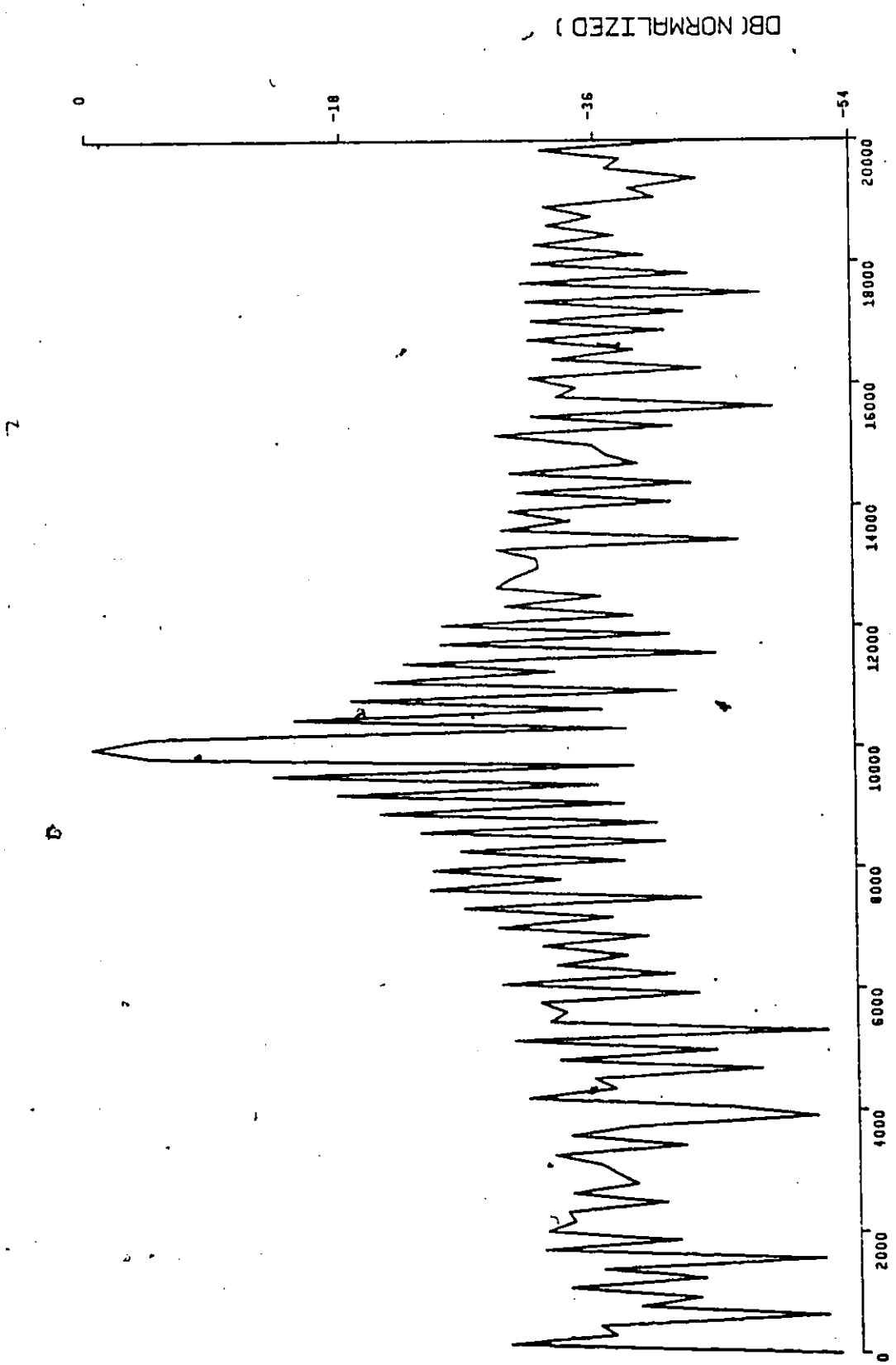

Fig. A1.1 Amplitude spectrum of an RF pulse with f_c = 10 KHz and SNR = 20 dB.

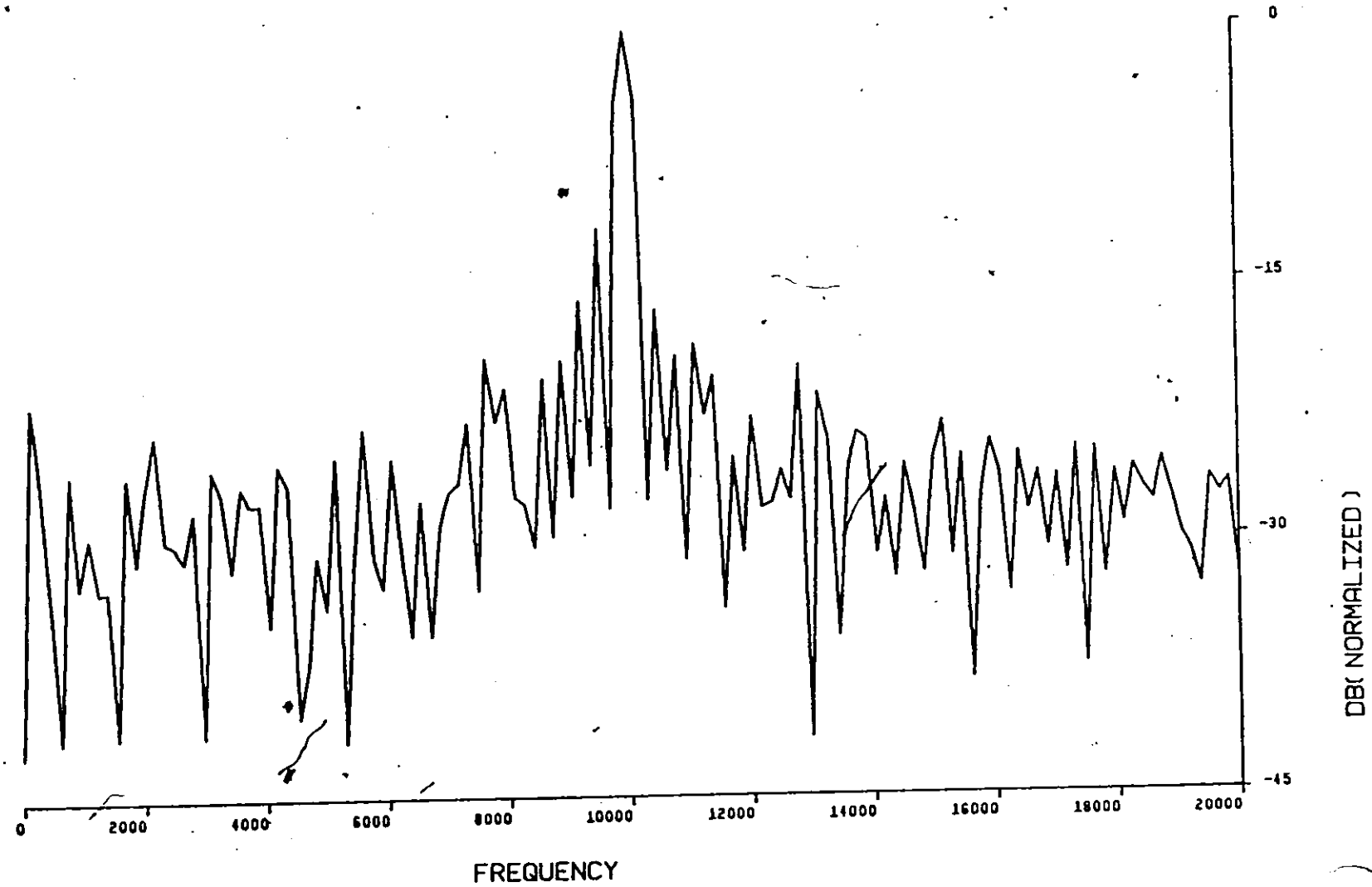

Fig. A1.2: Amplitude spectrum of an RF pulse with f_c = 10 KHz and SNR = 10 dB.

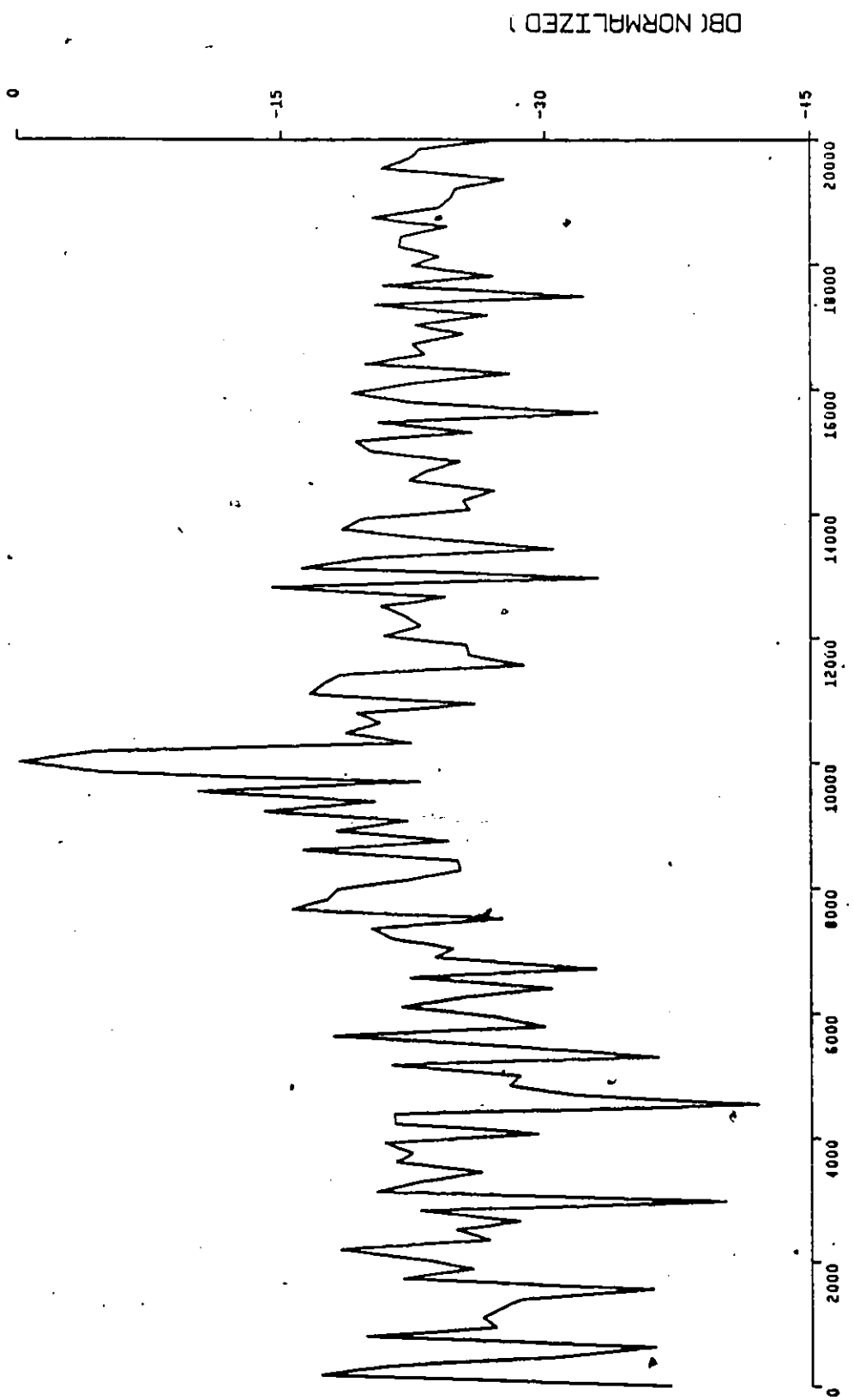

Fig. A1.3: Amplitude spectrum of an RF pulse with f_c = 10 KHz and SNR = 5 dB.

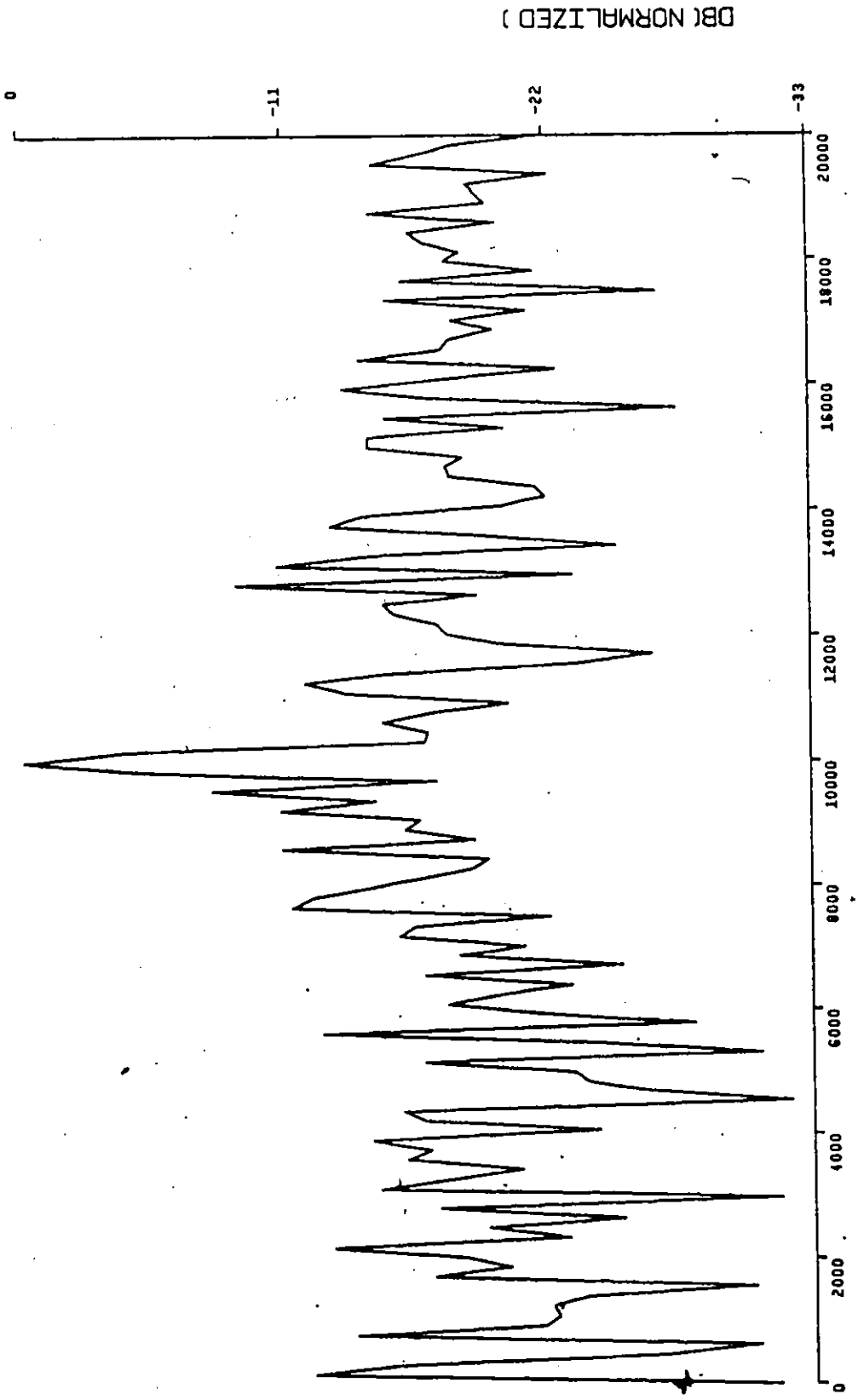

Fig. A1.4: Amplitude spectrum of an RF pulse with f_c = 10 KHz and SNR = 0 dB.

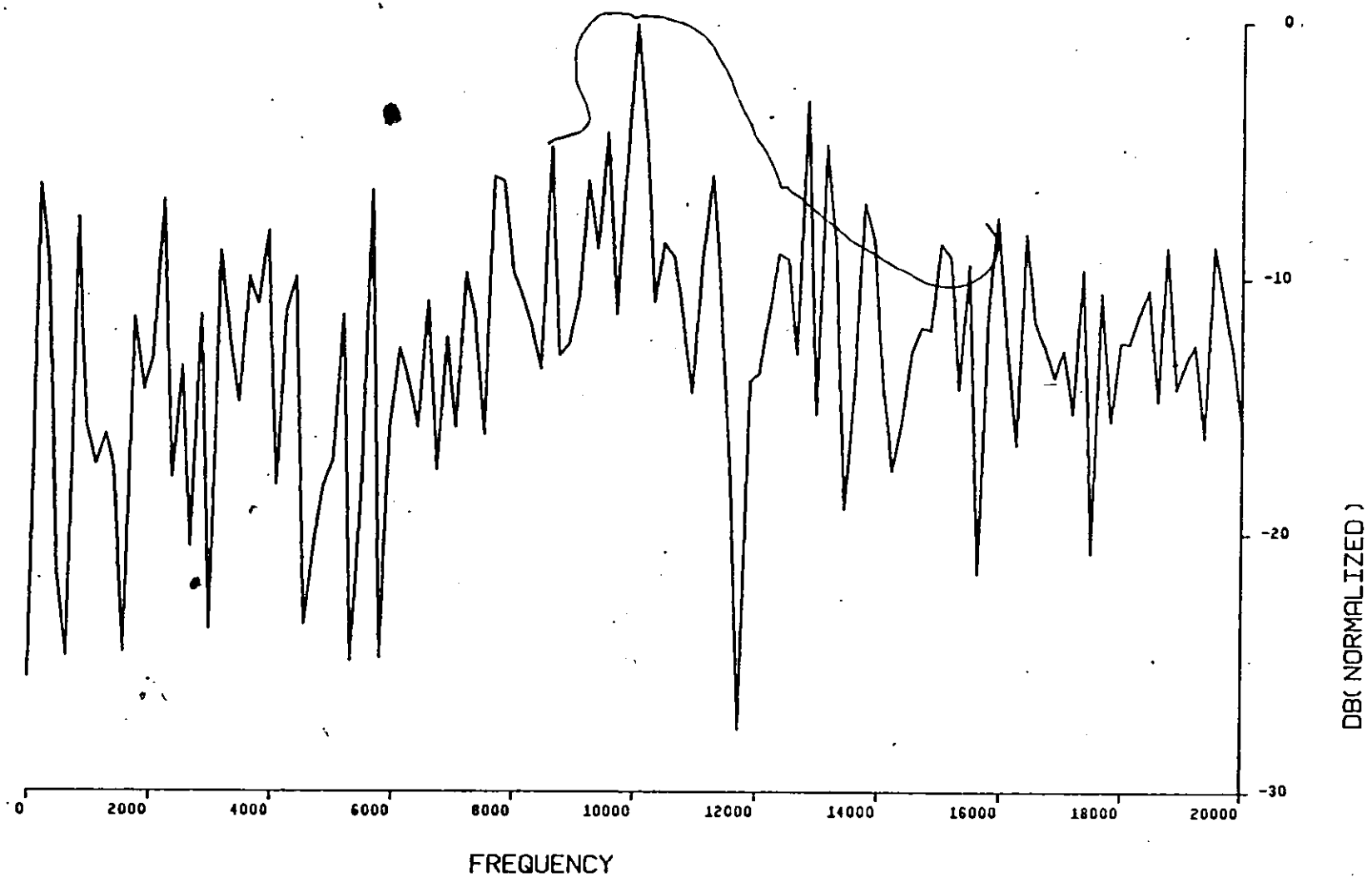

Fig. A1.5: Amplitude spectrum of an RF pulse with f_c = 10 KHz and SNR = -5 dB.

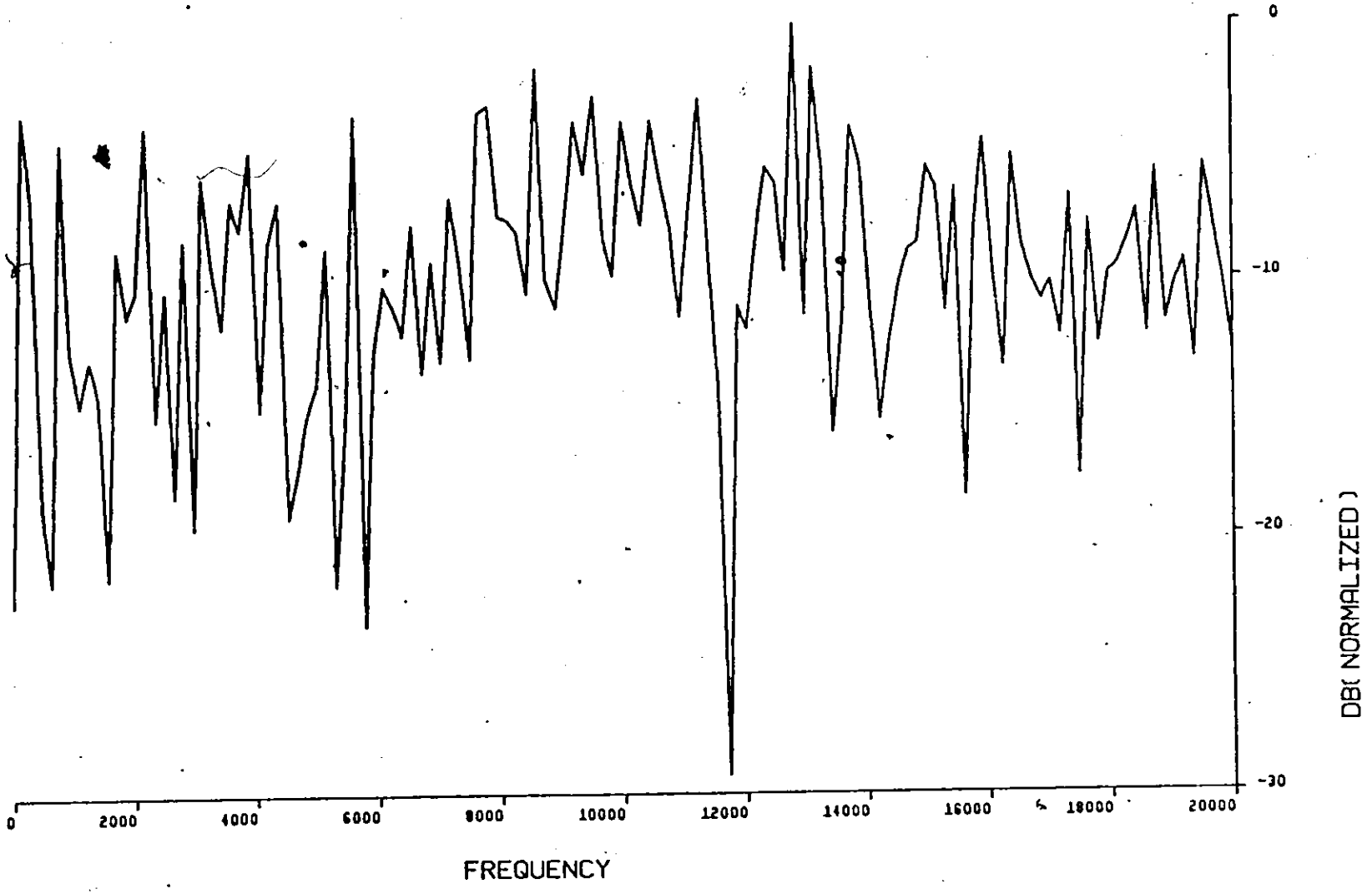

Fig. A1.6: Amplitude spectrum of an RF pulse with f_c = 10 KHz and SNR = -10 dB.

APPENDIX A2

PROCESSING RESULTS FOR AN RF PULSE IN NOISE USING THE MEM

Results of processing an RF pulse using the MEM are given in Figs. A2.1 to A2.7. In those instances when the peak is extremely well defined, an expanded view is included to show the finer detail (if indeed there is any) in the vicinity of the peak. The plots indicate that at values of SNR of approximately 10 dB and less the peak corresponding to the carrier frequency begins to round off significantly. Despite this fact the peak is adequately defined even at SNR's of 5 dB. For values of SNR below approximately 5 dB, the frequency estimate begins to suffer considerably although detection is possible even at SNR's of -10 dB. Comparing these results with the amplitude spectra of Figs. A1.1 to A1.6 we see that for detection purposes the MEM offers some advantages over the FFT since it does not suffer from sidelobe problems.

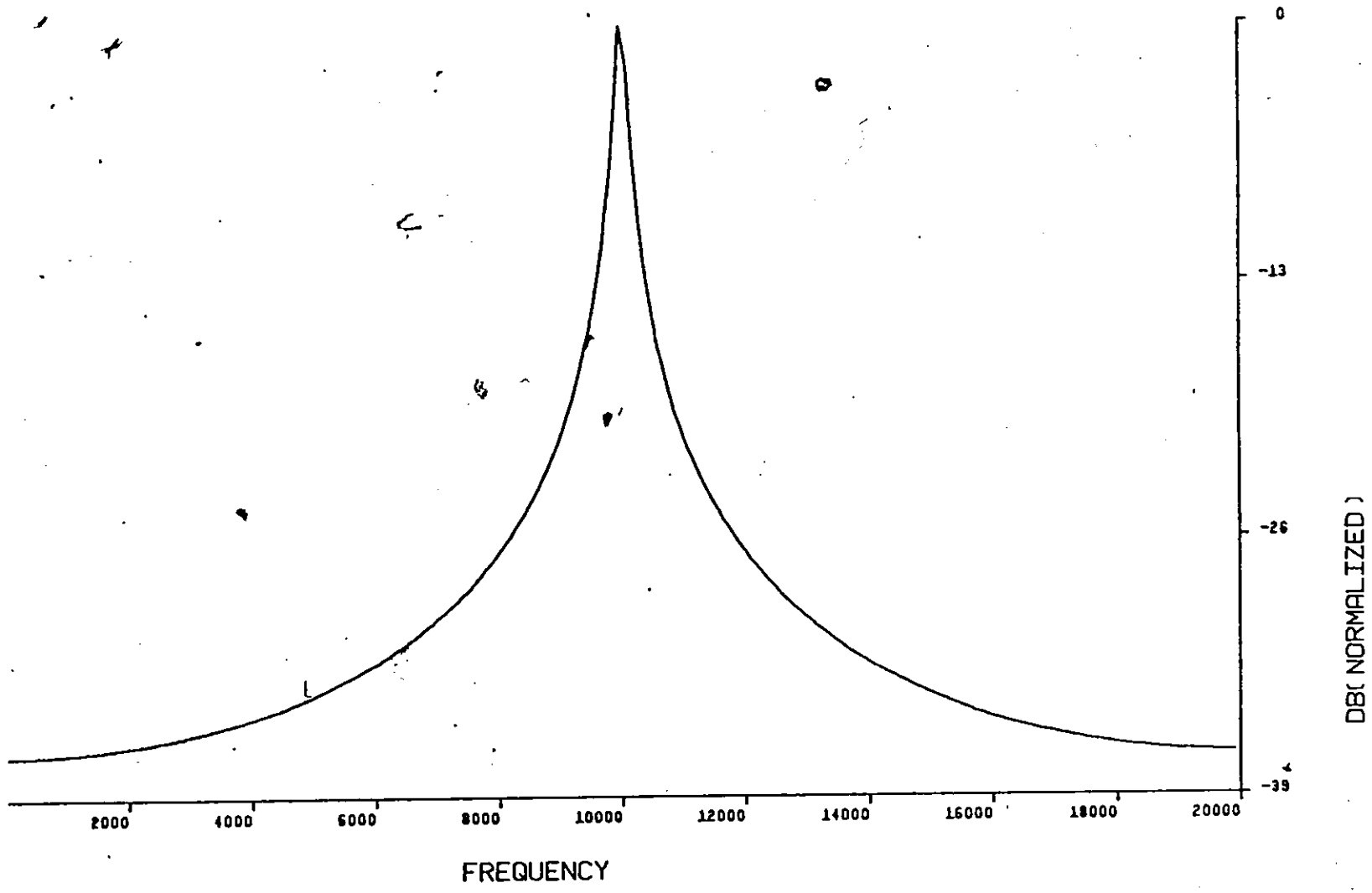

Fig. A2.1: ME spectrum of an RF pulse with f_c = 10 KHz and SNR = 20 dB.

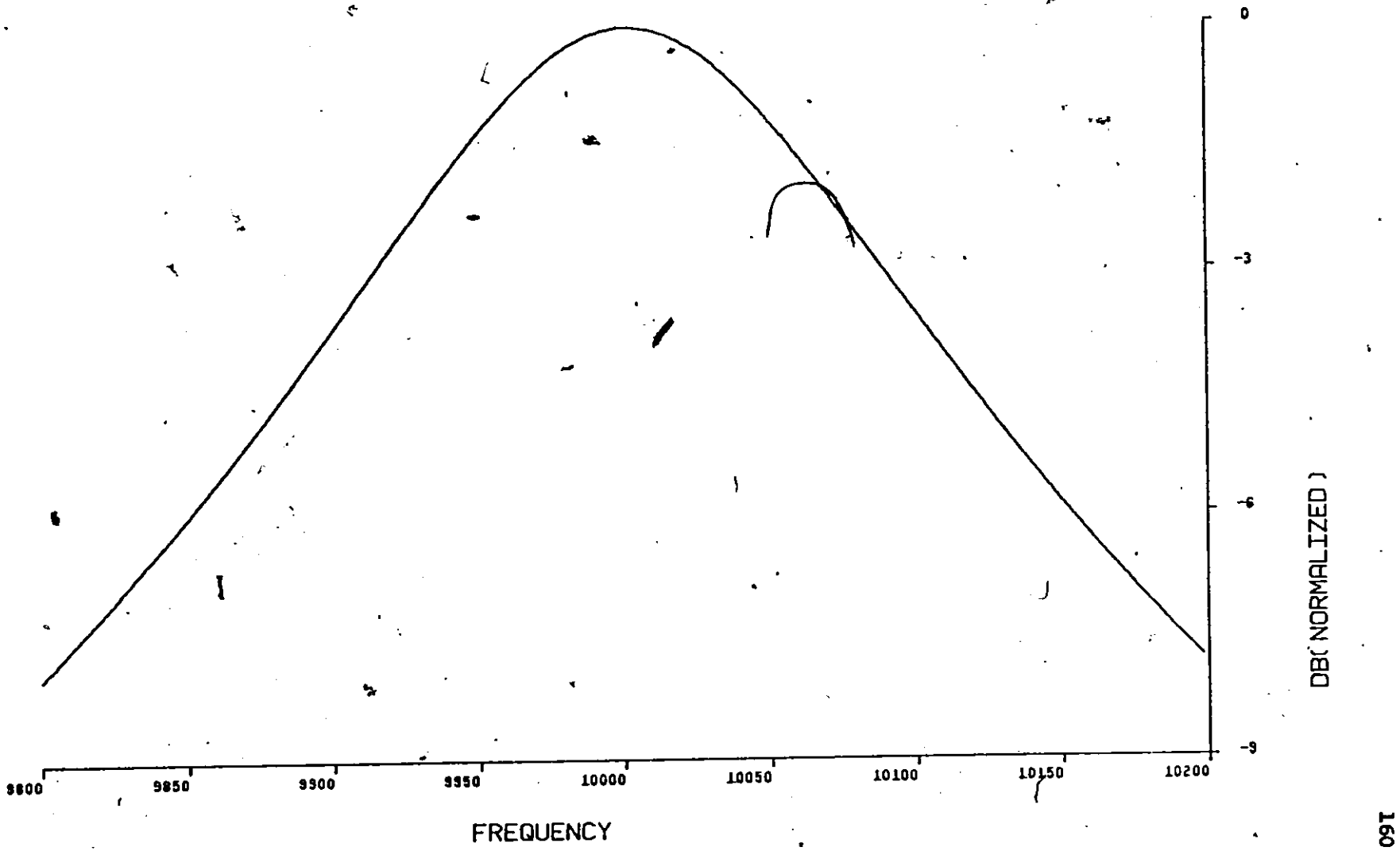

Fig. A2.2: Expansion of Fig. A2.1 in the vicinity of the peak.

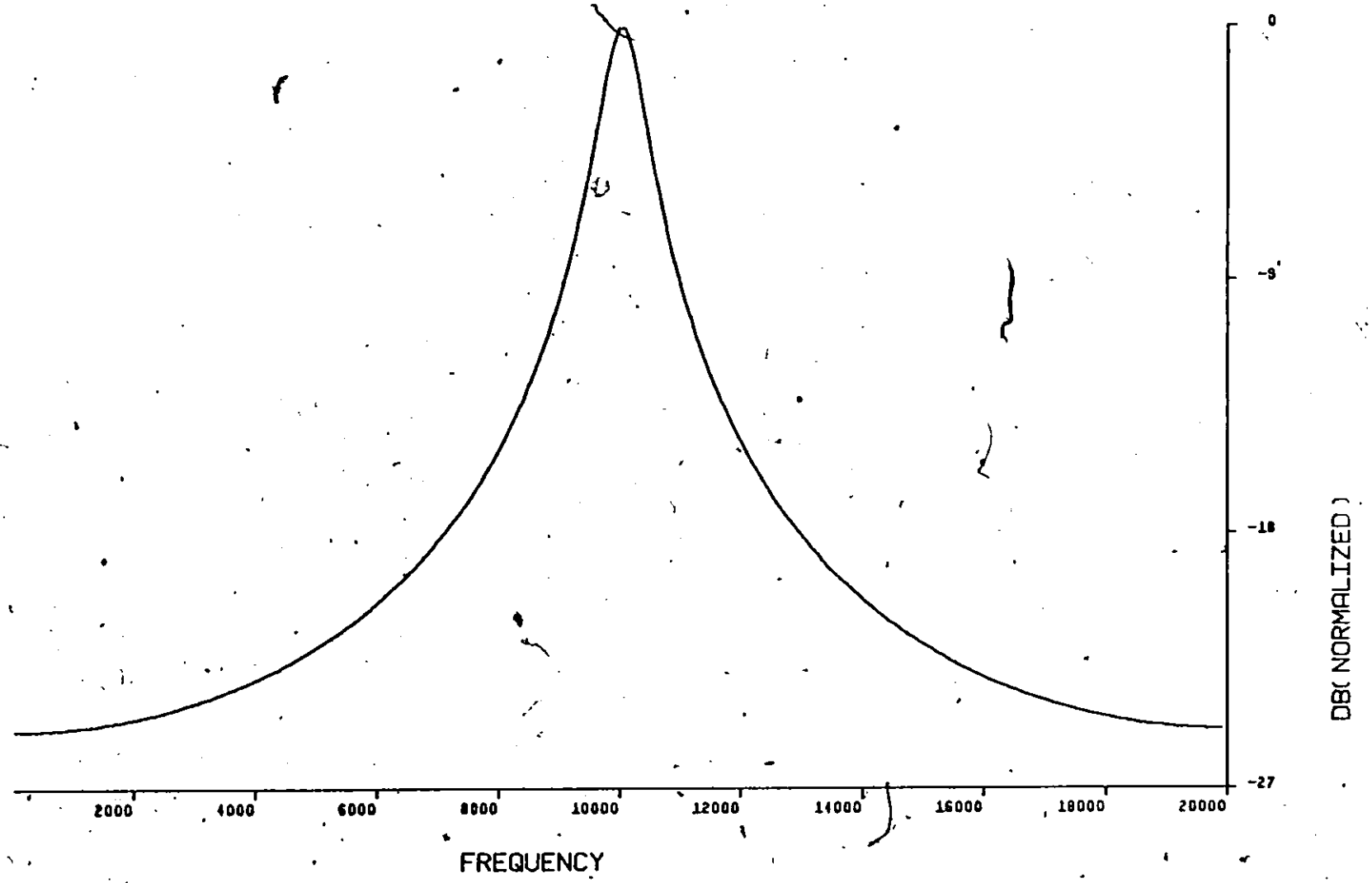

Fig. A2.3: ME spectrum of an RF pulse with f_c = 10 KHz and SNR = 10 dB.

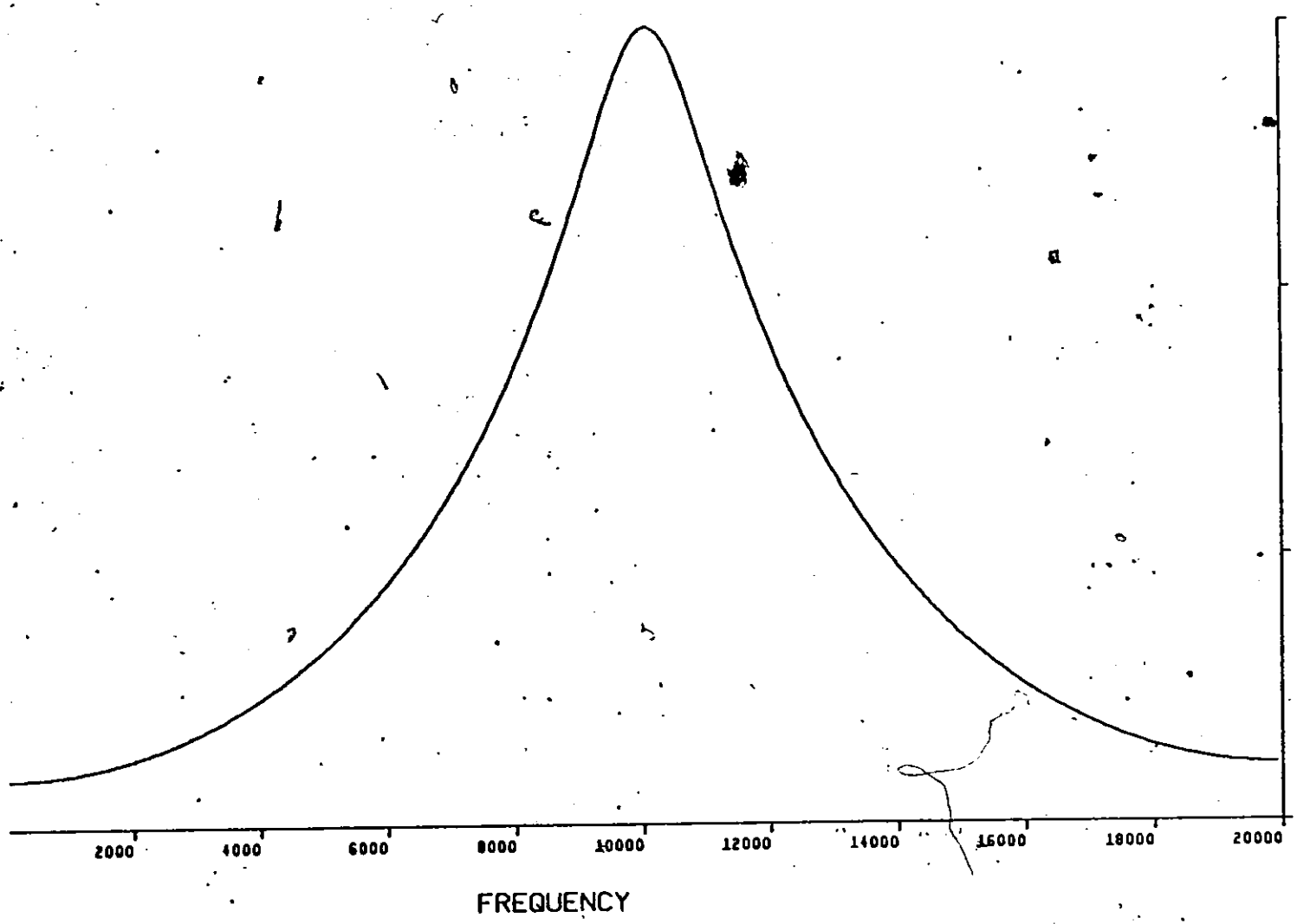

Fig. A2.4: ME spectrum of an RF pulse with f_c = 10 KHz and SNR = 5 dB.

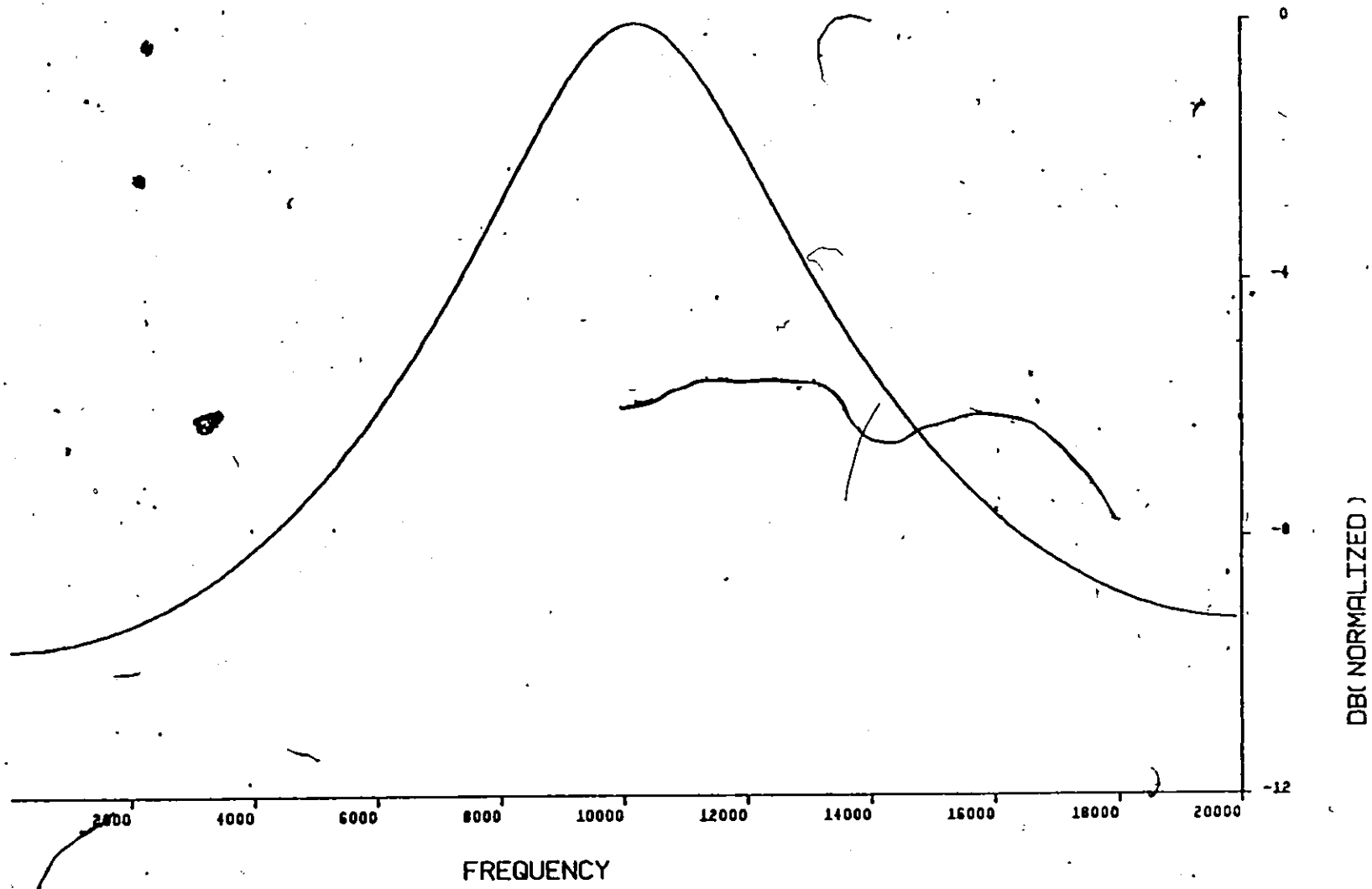

Fig. A2.5: ME spectrum of an RF pulse with f_c = 10 KHz and SNR = 0 dB.

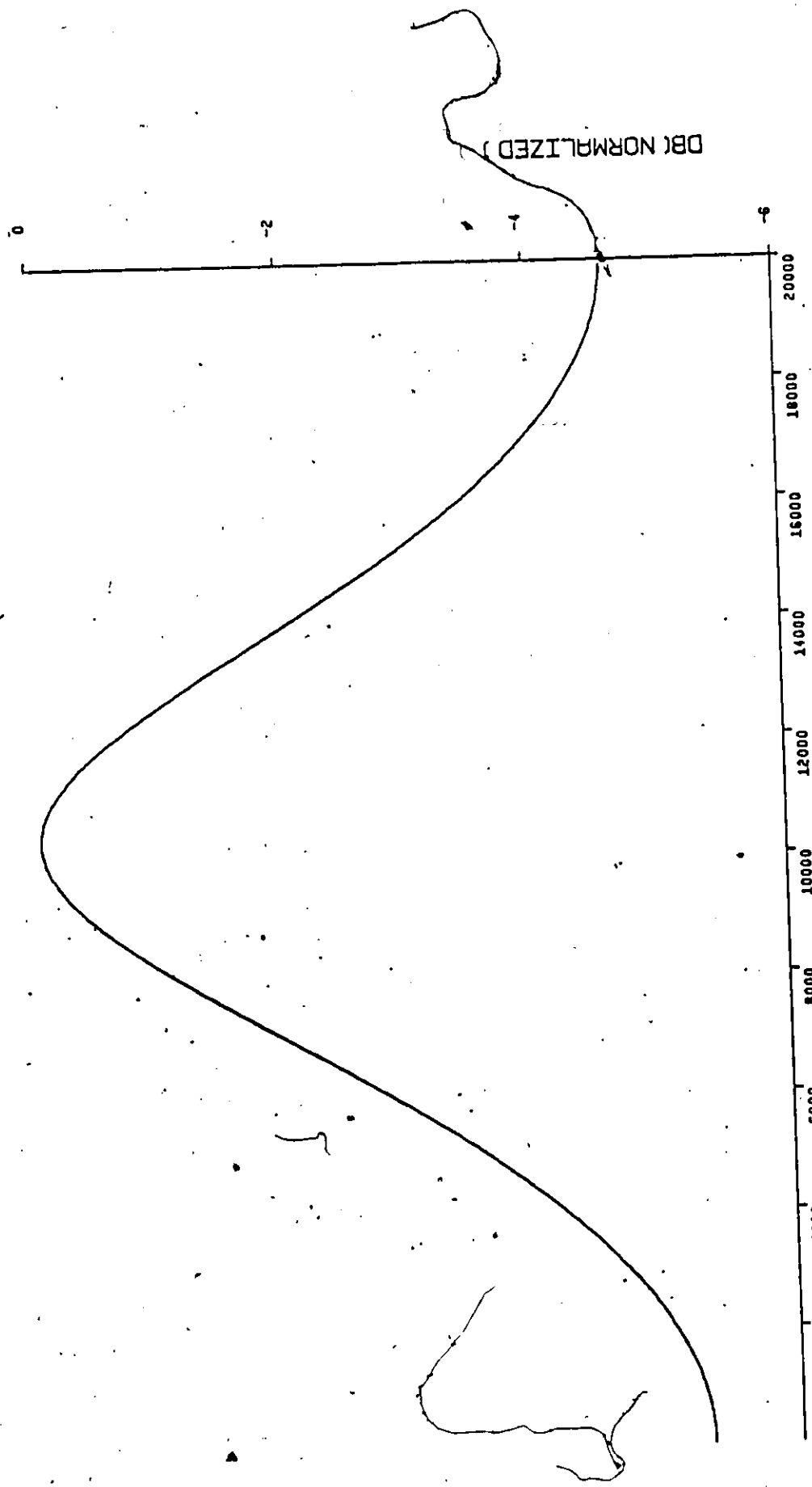

Fig. A2.6: ME spectrum of an RF pulse with f_c = 10 KHz and SNR = -5 dB.

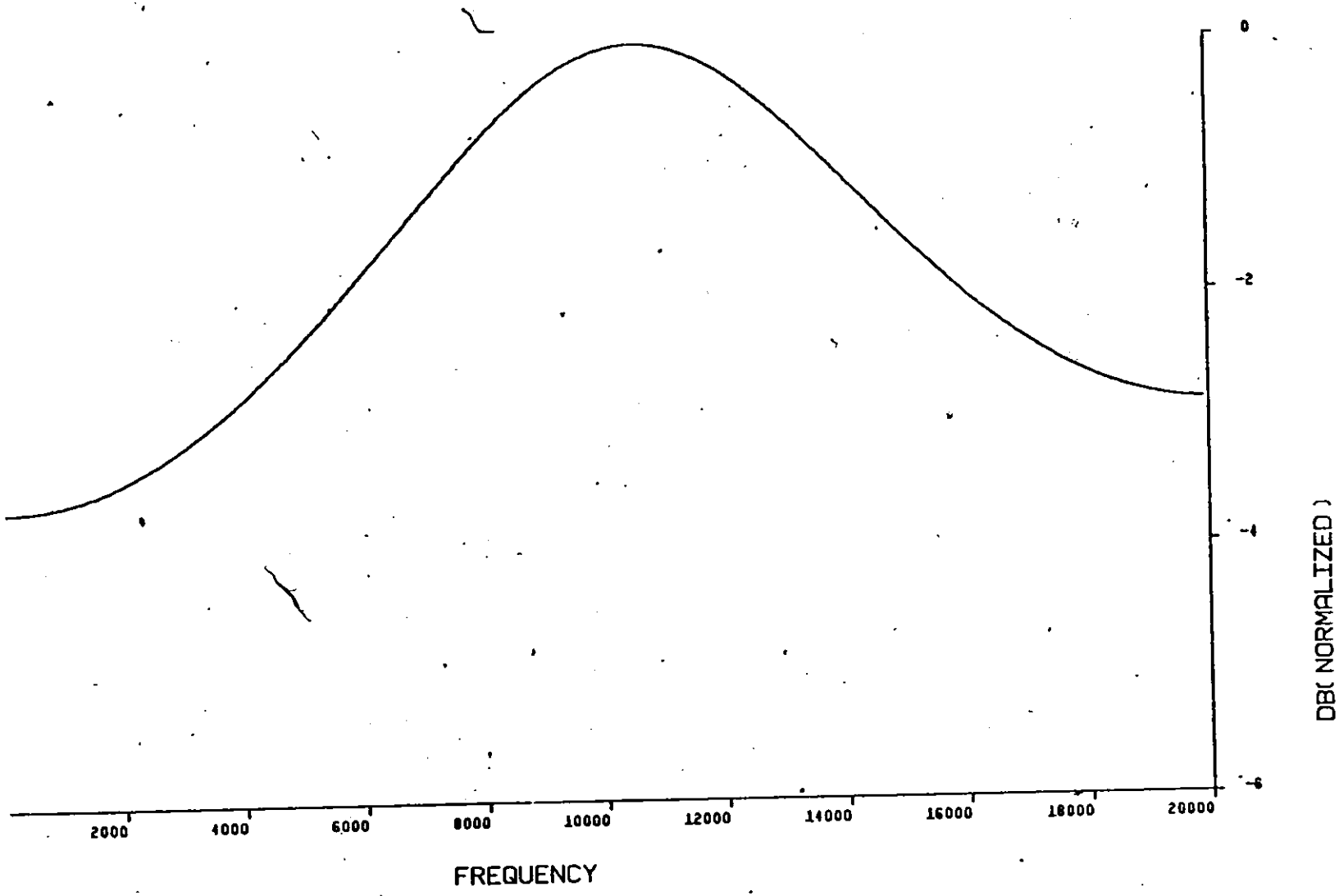

Fig. A2.7: ME spectrum of an RF pulse with f_c = 10 KHz and SNR = -10 dB.

APPENDIX A3

PROCESSING RESULTS FOR AN RF PULSE IN NOISE USING THE MEMCOR

A comparison of Figs. A2.1 to A2.7 (the MEM) and Figs. A3.1 to A3.9 (the MEM with autocorrelation) shows a significant improvement as a result of prior autocorrelation. Perhaps the extent of the improvement can best be seen by comparing the expanded views of Figs. A2.2 and A3.2 which show the MEM and MEMCOR results at SNR's of 20 dB. Figure A3.7 shows that the performance of the MEMCOR is better then satisfactory at SNR's around 0 dB but that further reductions in SNR to around -5 dB result in degradation in the frequency estimate.

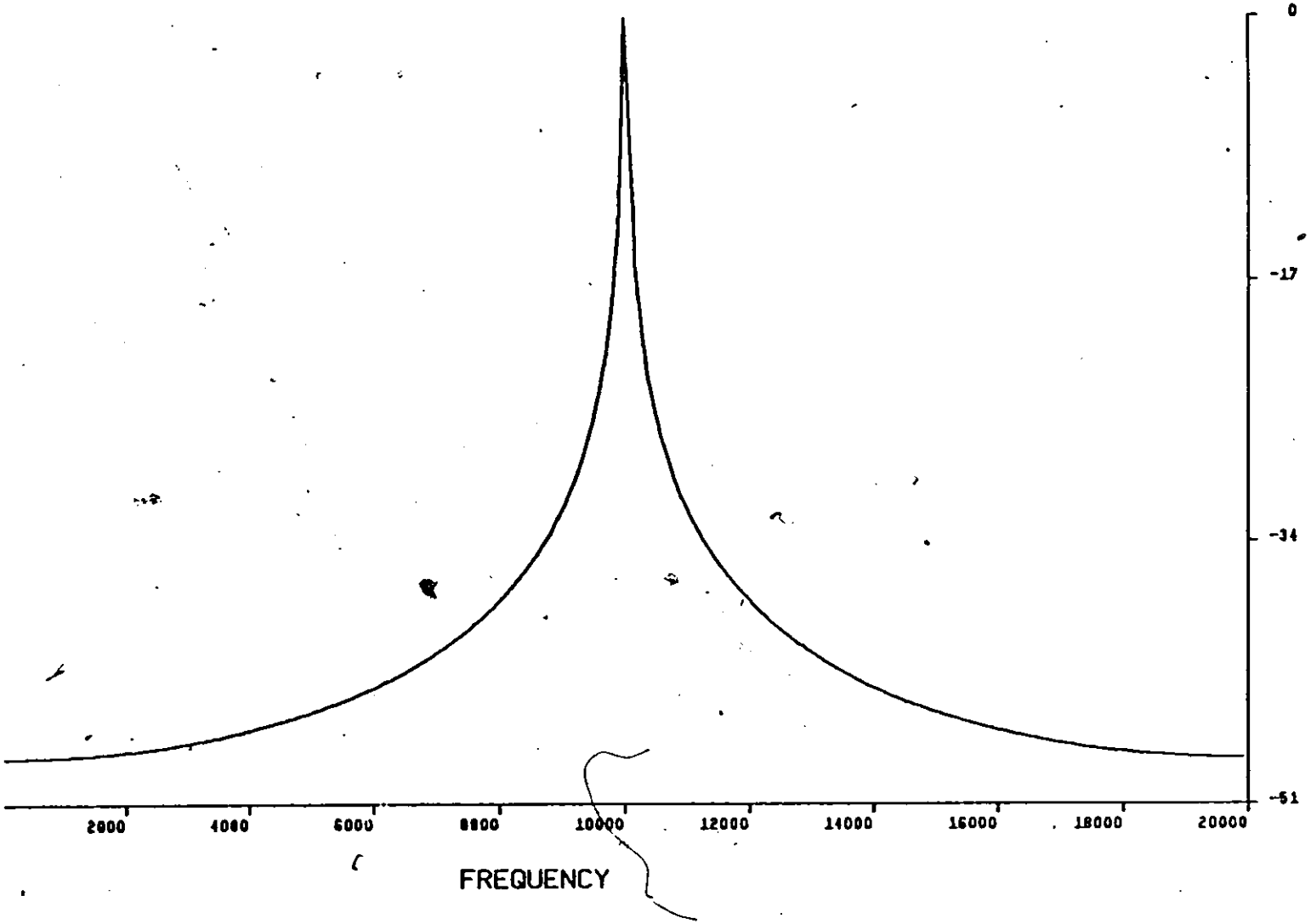

Fig. A3.1: MEMCOR of RF pulse with f_c = 10 KHz and SNR = 20 dB.

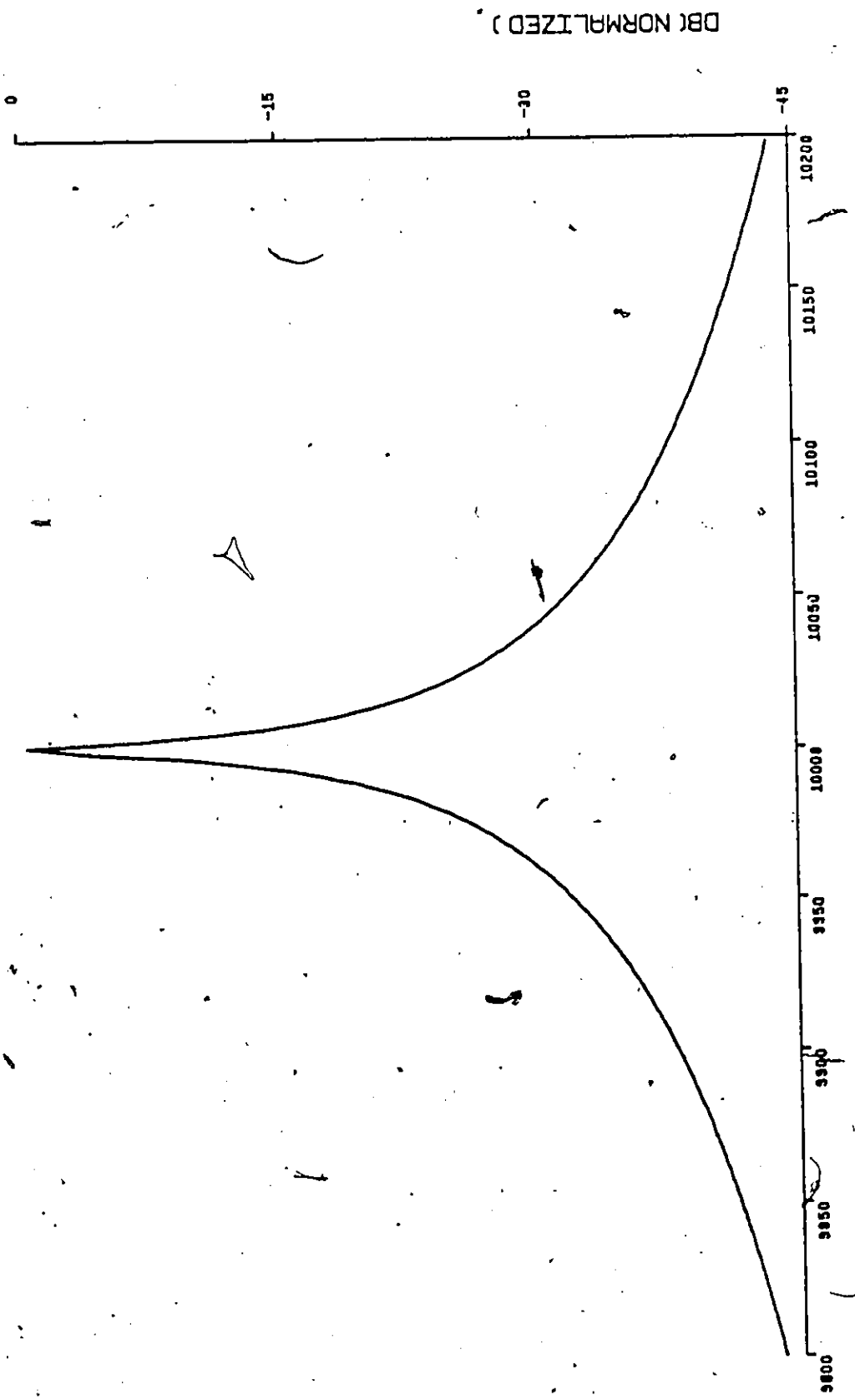

Fig. A3.2: Expansion of Fig. A3.1 in the vicinity of the peak.

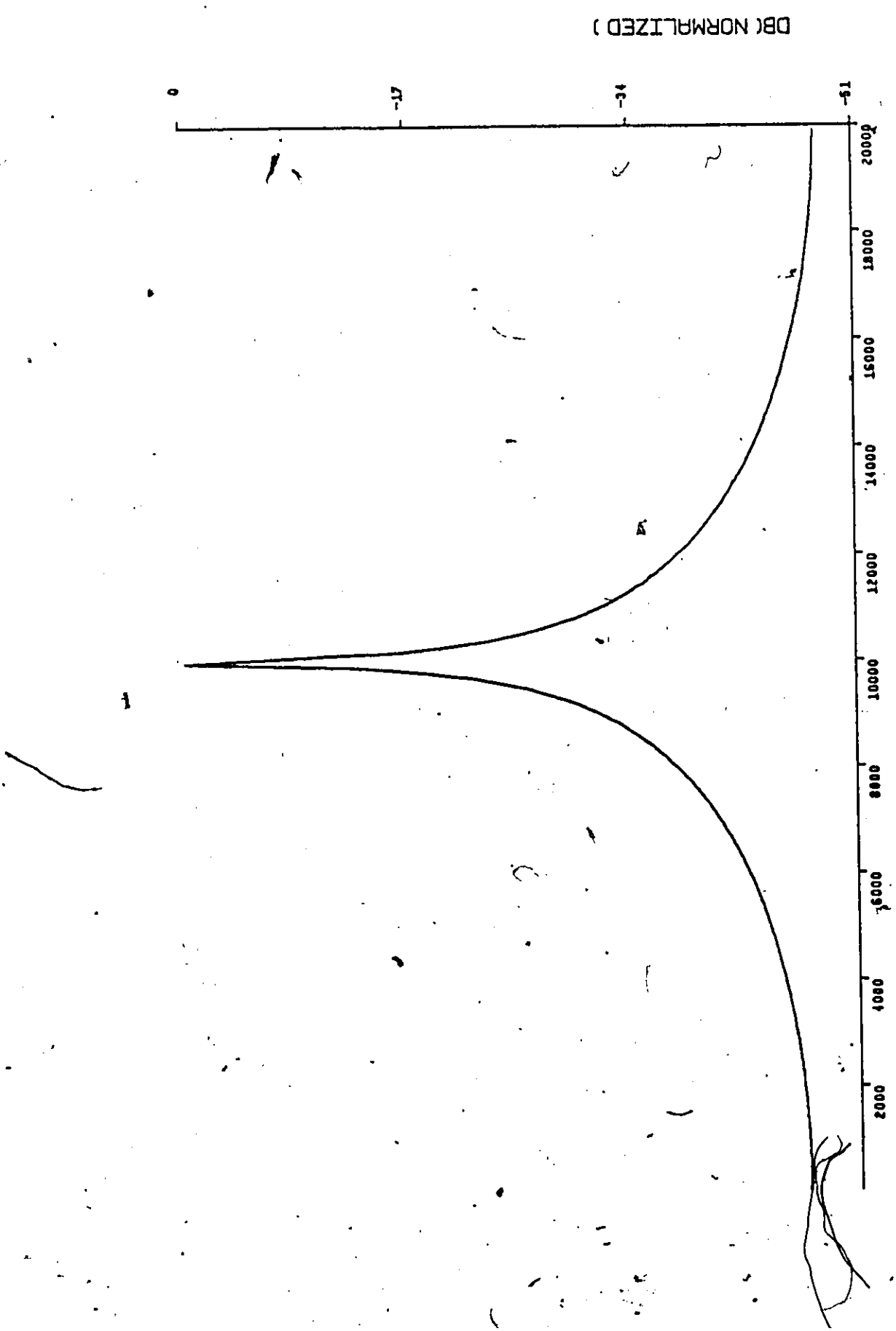

Fig. A3.3: MEMCOR of RF pulse with RF pulse with f_c = 10 KHz and SNR = 10dB.

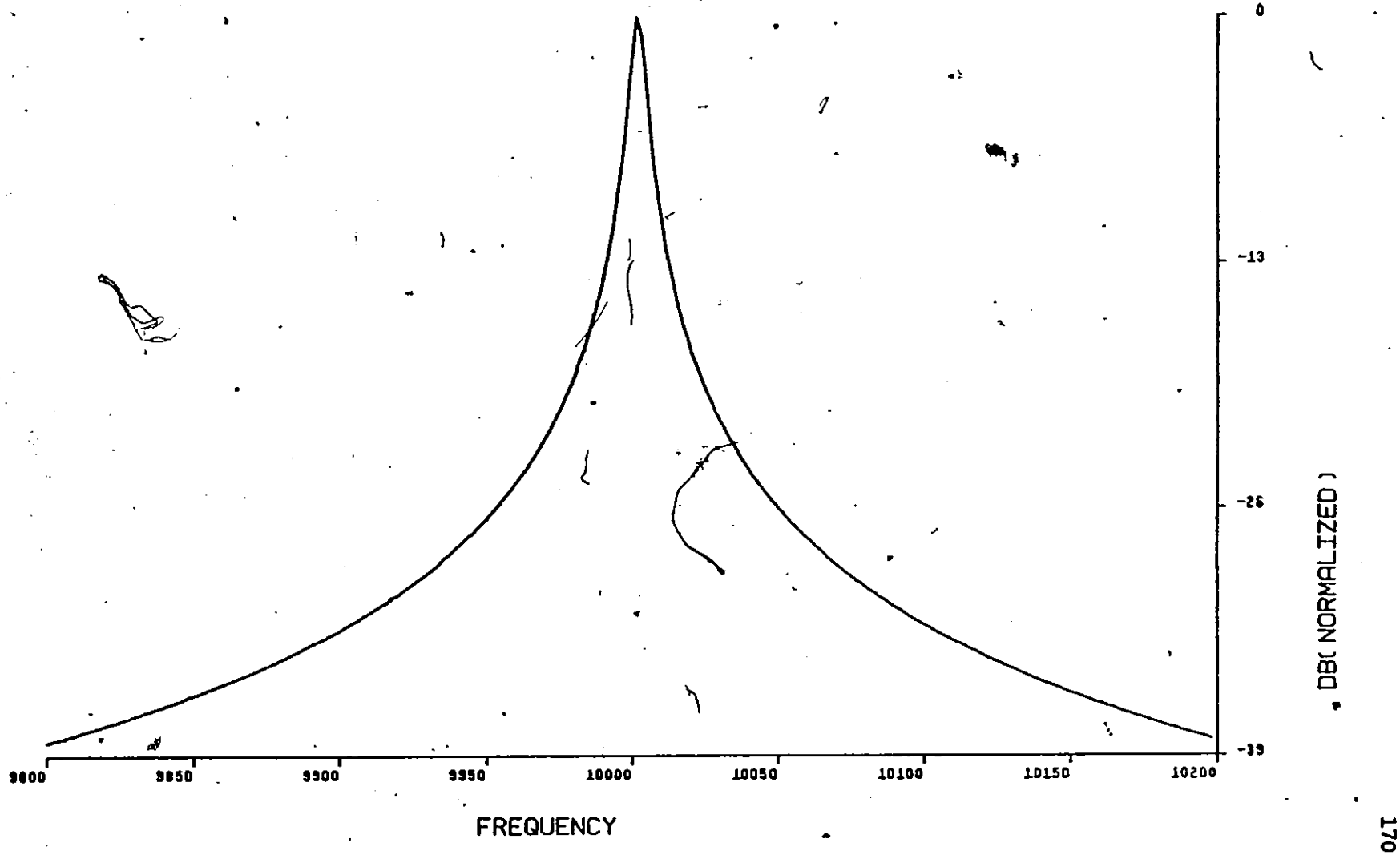

Fig. A3.4: Expansion of Fig. A3.3 in the vicinity of the peak.

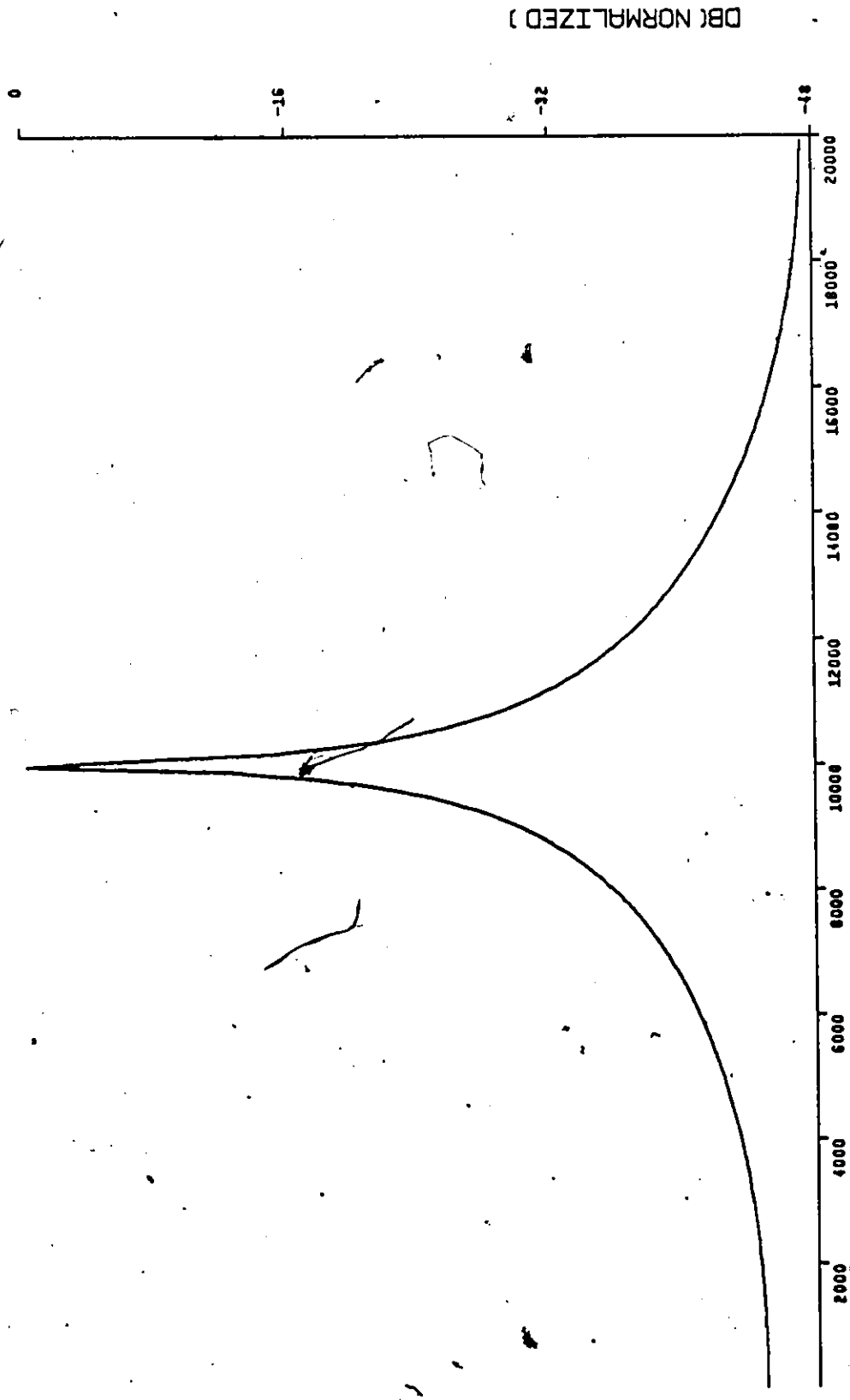

Fig. A3.5: MEMCOR of RF pulse with f_c = 10 KHz and SNR = 5 dB.

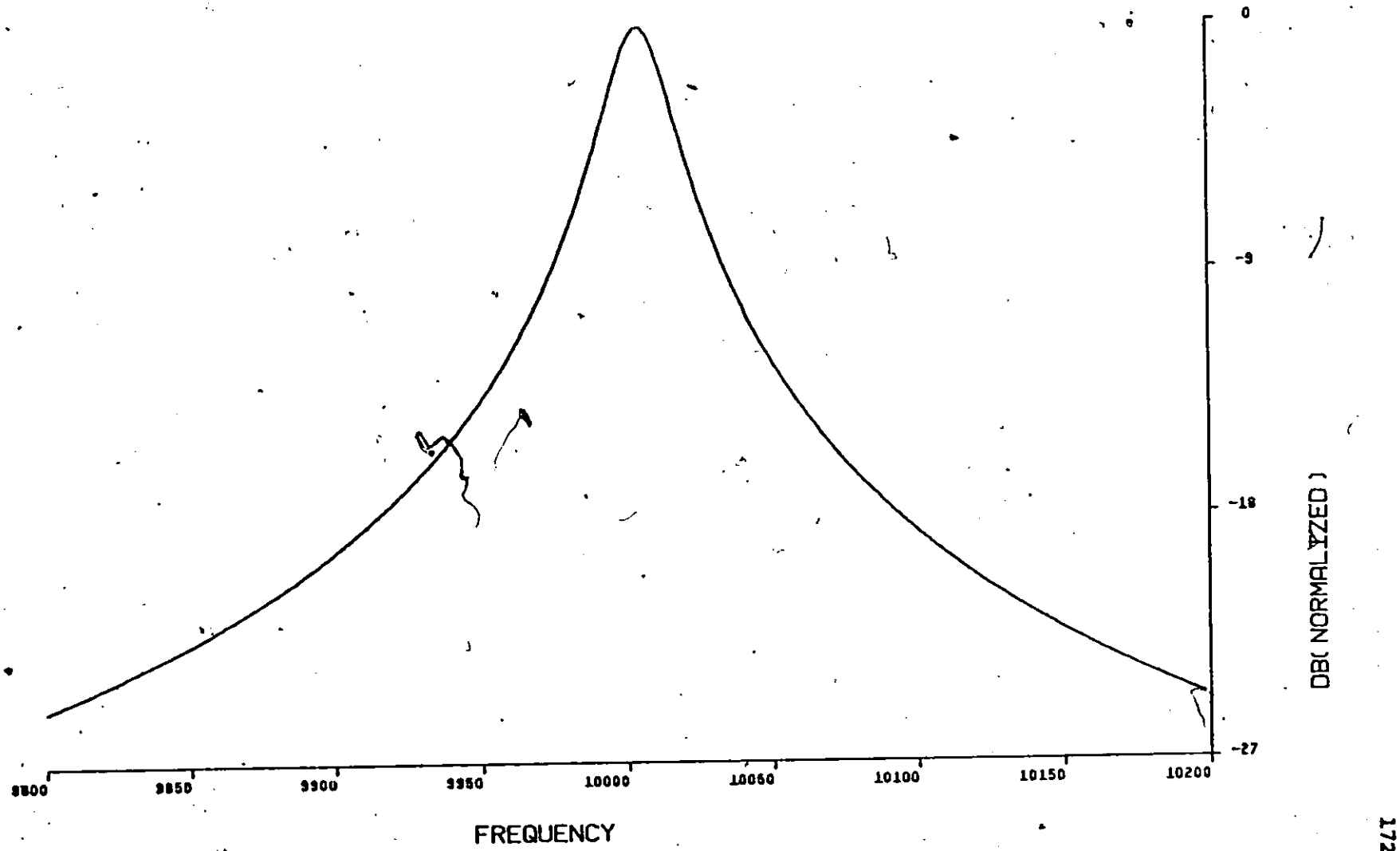

Fig. A3.6: Expansion of Fig. A3.5 in the vicinity of the peak.

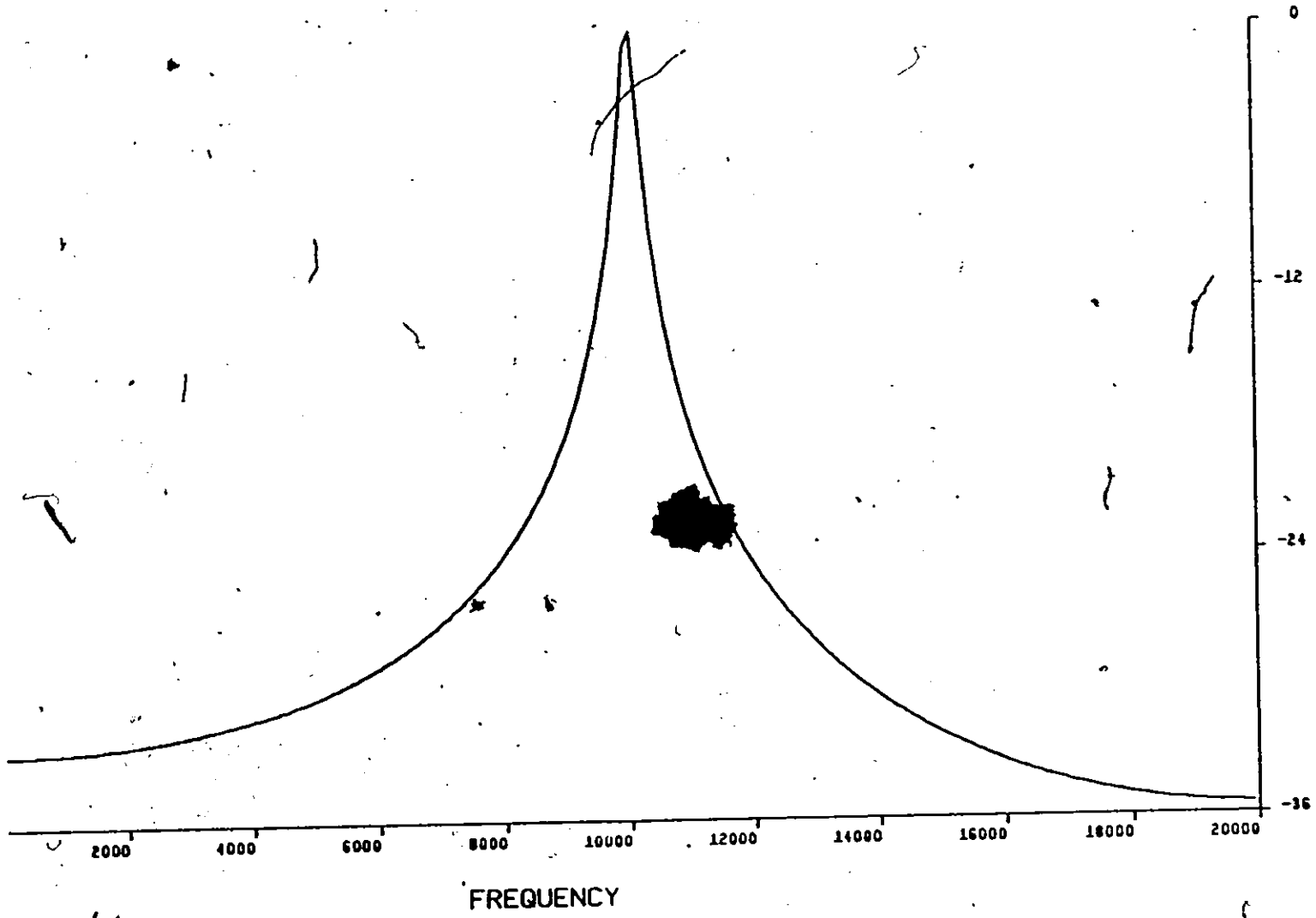

Fig. A3.7: MEMCOR of RF pulse with f_c = 10 KHz and SNR = 0 dB.

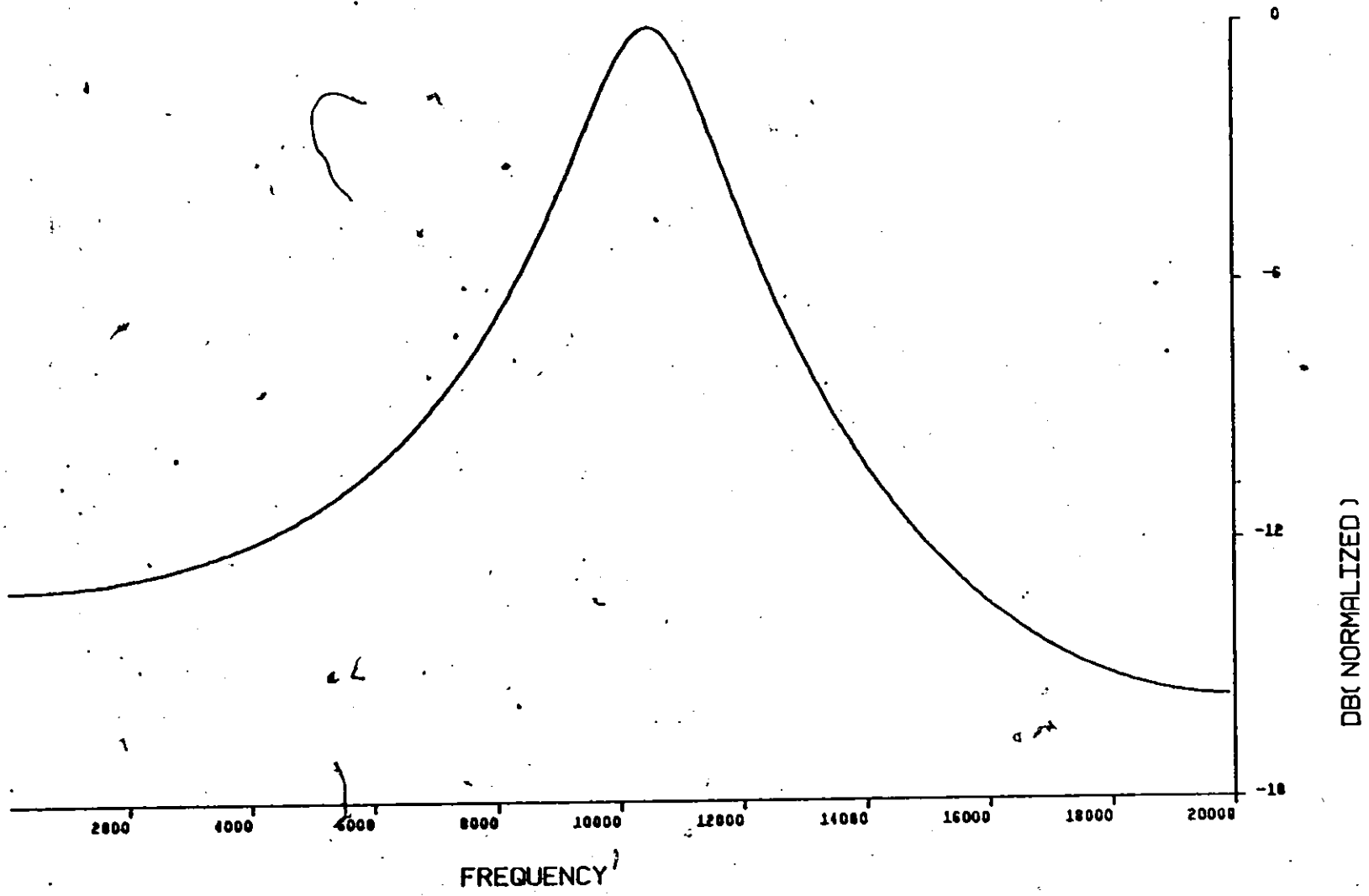

Fig. A3.8: MEMCOR of RF pulse with f_c = 10 KHz and SNR = -5 dB.

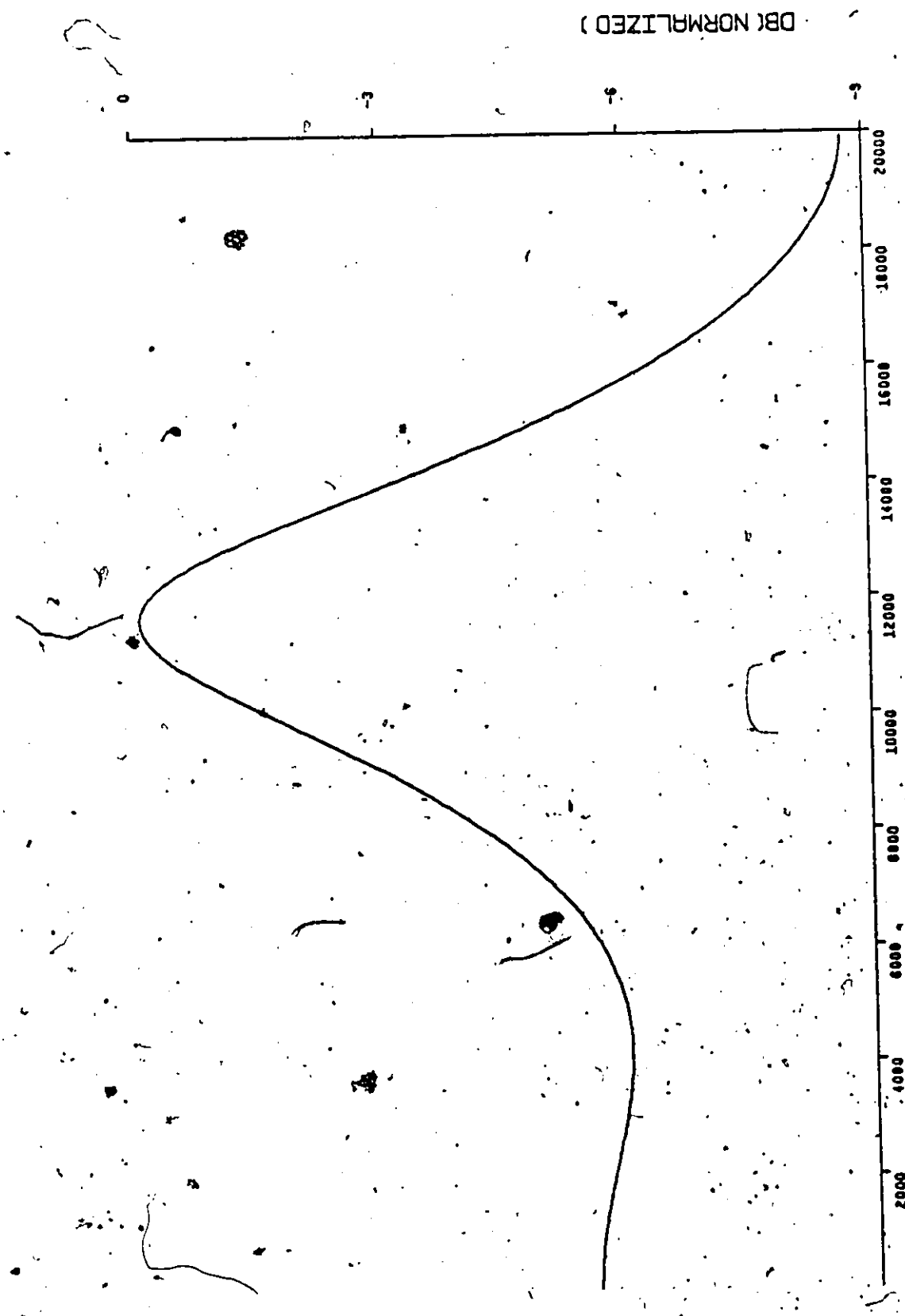

Fig. A3.9: MEMCOR of RF pulse with f_c = 10 KHz and SNR = -10 dB.